



GPO PRICE \$ _____
CFSTI PRICE(S) \$ _____
Hard copy (HC) 5.00
Microfiche (MF) 1.50

653 July 65

FACILITY FORM 502

N68-17557
(ACCESSION NUMBER) (THRU)
1
(PAGES) (CODE)
1
(NASA CR OR TMX OR AD NUMBER) (CATEGORY)

CR-72374

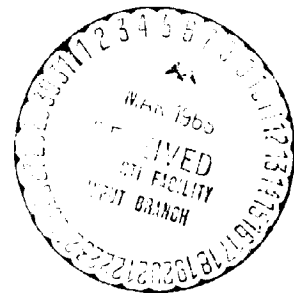
Copy No. 71

Report No. 1111-1

COMPUTER PROGRAM FOR THE ANALYSIS
OF ANNULAR COMBUSTORS

VOLUME I: CALCULATION PROCEDURES

Prepared for the
National Aeronautics and Space Administration
Air Breathing Engine Division
Lewis Research Center
Cleveland, Ohio
(Contract No. NAS3-9402)



NORTHERN RESEARCH AND ENGINEERING CORPORATION
219 Vassar Street
Cambridge, Massachusetts 02139

January 29, 1968

This work was performed under the direction of Dr. D. M. Dix. The initial portion was carried out by M. R. Bewsher, R. G. Croissant, P. N. Hoggett, and J. A. Monahan. The final portion, consisting of obtaining satisfactory operation of the computer program and revising the final report, was carried out by W. L. Brassert and Dr. P. L. Duffield.

Dr. A. D. Carmichael, Professor A. H. Lefebvre, I. N. Montchiloff, and Professor D. B. Spalding contributed in a consulting capacity.

TABLE OF CONTENTS

SUMMARY	1
INTRODUCTION	2
Background	2
Overall Objectives of Present Program	5
Arrangement of Report	5
OVERALL APPROACH	6
Introduction	6
Major Assumptions	6
Combustor Geometry and Nomenclature	8
Input to the Computer Program	10
Overall Structure of Computer Program	13
Control Subprogram	13
Diffuser Subprogram	17
Air-Flow Subprogram	20
Heat-Transfer Subprogram	22
Output of the Computer Program	25
DIFFUSER SUBPROGRAM - ANALYTICAL METHODS AND PROGRAM DEVELOPMENT. . .	31
Introduction	31
Major Assumptions	31
Definition of Terms	34
Alternative Analysis Procedures Available in the Subprogram	38
Empirical-Data Method	38
Streamtube Method	43

Mixing-Equation Method	55
Description of the Calculation Procedure for the Entire Diffuser	58
Structure of the Subprogram	59
AIR-FLOW SUBPROGRAM - ANALYTICAL METHODS AND PROGRAM DEVELOPMENT . .	70
Introduction	70
Assumptions	71
Calculation Procedure - Outline	72
Primary Zone of Flame Tube	77
Flow in the Annulus	81
Introduction to Jet Flow and Mixing	87
Characteristics of Penetration Jets	88
Characteristics of Wall Jets	93
Jet-Mixing Models	95
Aerodynamic Treatment of Porous Walls	98
Flow and Heat Addition in the Flame Tube	99
Structure of the Subprogram	103
HEAT-TRANSFER SUBPROGRAM - ANALYTICAL METHODS AND PROGRAM DEVELOPMENT	104
Introduction	104
Heat Balance in Flame Tube	104
Calculation Options and Assumptions	105
Radiation From the Flame to the Flame-Tube Wall - One- Dimensional Model	108
Radiation From the Flame to the Flame-Tube Wall - Two- Dimensional Model	111
Radiation From the Flame-Tube Wall to the Outer Casing . .	115

Radiation Interchange Between Flame-Tube Walls	116
Convection at the Inner Surface of the Flame-Tube Wall . .	117
Internal Convection with Film Cooling	118
Internal Convection with Transpiration Cooling	120
Convection at the Outer Surface of the Flame-Tube Wall . .	121
Gas Properties	121
Longitudinal Conduction Along Flame-Tube Wall	122
Solution of the Heat-Balance Equation	123
Structure of the Subprogram	124
LIMITATIONS OF THE COMPUTER PROGRAM	126
General	126
Diffuser Subprogram	127
Air-Flow Subprogram	127
Heat-Transfer Subprogram	128
Conclusion	129
TEST CASES	130
Diffuser Test Cases	130
Air-Flow Test Cases	137
Heat-Transfer Test Cases	141
Overall Test Cases	145
CONCLUSIONS	152
REFERENCES	154
TABLES	160
FIGURES	166
NOMENCLATURE	215

APPENDICES 221

I: IDEAL PRESSURE-RECOVERY COEFFICIENT IN A
DIFFUSER WITH NONUNIFORM INLET VELOCITY PROFILE . . 222

II: BOUNDARY-LAYER MOMENTUM THICKNESS 225

III: NEW ESTIMATE OF BOUNDARY-LAYER DISPLACEMENT
THICKNESS 227

IV: ESTIMATES OF BOUNDARY-LAYER SHAPE FACTORS 230

V: DEVELOPMENT OF MIXING EQUATION FOR INCOMPRESSIBLE
FLOW 232

VI: PRESSURE DROP ACROSS THE DOME 234

VII: INTEGRATION OF INTEGRAL PRESSURE TERM 236

LIST OF TABLES

Table I:	Values of Constants in Gas-Property Equation	161
Table II:	Combustor Geometry and Inlet Flow Conditions used for Overall Test Cases	162
Table III:	Program Options for Overall Test Cases	164
Table IV:	Flow Splits and Primary-Zone Temperatures for Overall Test Cases	165

LIST OF FIGURES

Figure 1:	Overall Flow Chart for Entire Program	167
Figure 2:	Overall Flow Chart for Diffuser Subprogram	168
Figure 3:	Overall Flow Chart for Air-Flow Subprogram	169
Figure 4:	Overall Flow Chart for Heat-Transfer Subprogram	170
Figure 5:	Effect of Inlet Mach Number on Diffuser Effectiveness . . .	171
Figure 6:	Two-Dimensional-Diffuser Data at 1.5 Per Cent Inlet Blockage	172
Figure 7:	Annular-Diffuser Data at 2 Per Cent Inlet Blockage	173
Figure 8:	Correlation for Predicting the Variation of Diffuser Effectiveness with inlet Blockage - Comparison with Experiment	174
Figure 9:	Comparison of the Experimental Results of Reneau, Johnston, and Kline for Two-Dimensional Diffusers with the Streamtube Method	175
Figure 10:	Swirler Data for 16 Combustor Designs	176
Figure 11:	Specific Heat for a Mixture of Combustion Products	177
Figure 12:	Dissociation Correction to Effective Fuel Calorific Value	178
Figure 13:	Pressure Loss in a Sudden Expansion in Compressible Flow	179
Figure 14:	Typical Center-Line Trajectories of Penetration Jets	180
Figure 15:	Decay of Center-Line Velocity in Penetration Jet	181
Figure 16:	Lateral Distribution of Velocity in Penetration Jet	182
Figure 17:	Correlation for Cross-Sectional Area of Penetration Jets	183
Figure 18:	Typical Velocity Profiles in a Wall Jet	184
Figure 19:	Effect of Pressure and Fuel Composition on Emissivity of Luminous Flames	185

Figure 20:	A New Correlation for the Emissivity of Luminous Flames	186
Figure 21:	Effect of Pressure and Gas Thickness on Radiation Transmittance	187
Figure 22:	Correlations of Film-Cooling Data	188
Figure 23:	Comparison of the Experimental Results of Sovran and Klomp for Annular Diffusers with the Streamtube Method	189
Figure 24:	Comparison of Experimental and Theoretical Effectiveness for Two-Dimensional Diffusers	190
Figure 25:	Position of First Stall for Two-Dimensional Diffusers . . .	191
Figure 26:	Comparison of Experimental and Theoretical Effectiveness for Annular Diffusers	192
Figure 27:	Comparison of Experimental and Theoretical Development of a Shear Flow in a Two-Dimensional Diffuser	194
Figure 28:	Comparison of Experimental and Theoretical Development of a Shear Flow in a Two-Dimensional Nozzle	195
Figure 29:	Variation of Pressure-Loss Factor with Reference Mach Number	196
Figure 30:	Variation of Pressure-Loss Factor with Total Hole Area . .	197
Figure 31:	Effect of Heat Release on Combustor Pressure-Loss Factor	198
Figure 32:	Comparison of Calculated Air-Flow Distributions	199
Figure 33:	Wall Temperatures, Convective Cooling Only	200
Figure 34:	Wall Temperatures, Film Cooling Only	201
Figure 35:	Wall Temperatures, Film and Convective Cooling	202
Figure 36:	Total-Pressure Loss in Diffuser as a Function of Flow Split for Overall Test Cases 1 Through 5	203
Figure 37:	NASA Test Case No. 1 -- Accumulated Fraction of Inlet Air in Flame Tube and Residual Air in Jets as Functions of Axial Position in Combustor	204

Figure 38:	NASA Test Case No. 1 -- Flame Temperature, Flame-Tube Wall Temperatures, and Fraction of Fuel Burned as Functions of Axial Position in Combustor	205
Figure 39:	NASA Test Case No. 2 -- Accumulated Fraction of Inlet Air in Flame Tube and Residual Air in Jets as Functions of Axial Position in Combustor	206
Figure 40:	NASA Test Case No. 2 -- Flame Temperature, Flame-Tube Wall Temperatures, and Fraction of Fuel Burned as Functions of Axial Position in Combustor	207
Figure 41:	NASA Test Case No. 3 -- Accumulated Fraction of Inlet Air in Flame Tube and Residual Air in Jets as Functions of Axial Position in Combustor	208
Figure 42:	NASA Test Case No. 3 -- Flame Temperature, Flame-Tube Wall Temperatures, and Fraction of Fuel Burned as Functions of Axial Position in Combustor	209
Figure 43:	NASA Test Case No. 4 -- Accumulated Fraction of Inlet Air in Flame Tube and Residual Air in Jets as Functions of Axial Position in Combustor	210
Figure 44:	NASA Test Case No. 4 -- Flame Temperature, Flame-Tube Wall Temperatures, and Fraction of Fuel Burned as Functions of Axial Position in Combustor	211
Figure 45:	NASA Test Case No. 5 -- Accumulated Fraction of Inlet Air in Flame Tube and Residual Air in Jets as Functions of Axial Position in Combustor	212
Figure 46:	NASA Test Case No. 5 -- Flame Temperature, Flame-Tube Wall Temperatures, and Fraction of Fuel Burned as Functions of Axial Position in Combustor	213
Figure 47:	NASA Test Case No. 3 -- Total and Static Pressures as Functions of Axial Position in the Combustor	214

SUMMARY

This is the first of two volumes devoted to a computer program for predicting the performance of an annular combustor. In this volume the correlations and calculation methods used in the program are presented, and the assumptions involved in applying them are discussed. The results of a number of test cases are also described.

The analysis falls naturally into three parts:

1. Performance of the diffuser.
2. Air-flow, pressure, and temperature distributions in the flame tube and annuli, including calculation of the combustor total-pressure loss.
3. Heat transfer and the calculation of the flame-tube-wall temperature distribution.

Each of these parts is discussed in detail in Volume I of this report.

Volume II gives a complete description of the computer program, forming a self-contained operating manual that permits the program to be operated without reference to Volume I.

INTRODUCTION

The cut-and-try methods generally used to design combustion chambers have been giving way in recent years to a more systematic approach based on analysis and correlation of experimental data. This approach is potentially capable of substantially reducing development time and expense while improving combustor performance. While the analytical methods and correlations presently available are crude in many respects, they are nonetheless sufficiently complex that computers can effectively be used in their solution.

The aim of the work described in this report has been to develop a computer program for the analysis of fluid flow, combustion, and heat transfer in annular combustors with diffusers, making use of currently available analytical methods and correlations. It is expected that the resulting program, used carefully in conjunction with experimental data, will prove to be a useful tool for the design of high-performance annular combustors.

The program has been extended to include analysis of rectangular test combustors. An approximate analysis of tubular geometries may be obtained from the program for rectangular combustors.

Background

A number of attempts have previously been made to calculate the air flow and heat transfer in gas-turbine combustors. Graves (Ref 1) and Grobman (Ref 2) analyzed the pressure loss and air-flow distribution in tubular combustors with uniformly tapered (or constant cross-section) flame tubes. This work included the effects of momentum transfer between the

gas streams in annulus and flame tube, annulus wall friction, heat release, hole discharge coefficients, and compressibility. Flow in the diffuser was not considered, and instantaneous mixing between cold-air jets and the gas in the flame tube was assumed. No heat-transfer analysis was undertaken. The results of these calculations exhibited many of the effects observable in practical combustors.

Samuel (Ref 3) used the same general approach as Grobman, with instantaneous mixing between cold-air jets and the main gas stream. A simple diffuser analysis was included, and both tubular and annular geometries could be treated. In the case of annular combustors, the calculation followed the three parallel streams in the inner and outer annuli and through the flame tube, and iterated on the initial mass-flow split between these streams until boundary conditions at the end of the combustor were satisfied. A similar approach is used in the present work. The output of Samuel's program was used as input for a heat-transfer program.

The most comprehensive heat-transfer analysis of aircraft-type combustors that has been published to date is that of Lefebvre and Herbert (Ref 4). This involved the solution of a heat-balance equation for each element of the wall, taking into account radiation from flame to wall and wall to casing, and forced convection on the inside and outside of the wall. Net heat transfer in the longitudinal direction was assumed to be negligible compared with radial heat transfer. Reasonable agreement with limited experiment was obtained.

Another heat-transfer analysis was carried out by Tipler (Ref 5), whose work dealt with an industrial combustor and included the effects of radiation transfer in a longitudinal direction.

Over the last few years, a number of new correlations and

techniques have been produced which provide the basis for a more sophisticated approach to the analysis of flow and heat transfer in combustors.

Sovran and Klomp (Ref 6) have provided a way of generalizing straight-walled two-dimensional and annular diffuser performance. An almost identical approach was used by Reneau, Johnston, and Kline (Ref 7), who extended the work to cover different inlet boundary-layer thicknesses; this aspect is particularly important for gas-turbine combustor diffusers. For the first time, therefore, there now exists a set of maps which enables the performance of straight-walled diffusers to be predicted with fair certainty for any length and area ratio and inlet boundary-layer thickness, at least within the range of interest.

Although many sets of data on the behavior and mixing of jets have been accumulated over the last 20 years, it is only recently that such data have been brought together, correlated, and presented in a generalized fashion. For example, a review of 16 experiments on jets penetrating a gas stream at an angle has recently been prepared by Northern Research. Spalding (Ref 8) refers to 18 experiments on wall jets in developing a new theory for this type of flow.

In the field of heat transfer, Spalding (Ref 9) has correlated the results of 9 experimenters to produce a new correlation for film-cooling heat transfer, and Sturgess (Ref 10) has shown that this correlation works moderately well for the practical film-cooling slots used in actual combustors. Schirmer and Quigg (Ref 11) have produced the most useful work yet published on the effect of pressure on radiation from luminous flames. Finally, Gruber (Ref 12) and Sparrow (Ref 13) have shown how view-factor data can be used to make a more comprehensive analysis of

radiative heat transfer in combustors than has hitherto been possible.

The works mentioned above, and others, provide useful new tools for combustor analysis, and open the way to removing some restrictions that have previously limited the utility and validity of such analyses.

Overall Objectives of Present Program

A computer program was therefore envisaged to achieve the following objectives:

1. Analyze the air mass-flow and pressure distributions in a combustor whose geometry is given, for specified inlet conditions.
2. Compute the temperature distribution on the flame-tube wall.
3. Predict whether separation occurs in the diffuser.

The rest of this report discusses these objectives further, and shows how they are achieved.

Arrangement of Report

The section following this introduction contains a summary of the overall approach used in this work, including the major assumptions. In the three subsequent sections are described the calculation methods and organization of the diffuser, air-flow, and heat-transfer analyses. Program limitations are considered in the next section.

The computer program has been applied to a number of sample cases designed to test individual subprograms as well as the overall program. The results of these cases are discussed in the next section. A final section contains conclusions derived from this work.

Detailed derivations, where not germane to the main discussion, are relegated to appendices.

OVERALL APPROACH

Introduction

This section is a general introduction to the computer program and the methods and assumptions upon which it is based. It is meant to provide the reader with a framework for the detailed discussions that follow in succeeding sections. Topics covered are:

1. Major assumptions.
2. Combustor geometry and nomenclature.
3. Input to the computer program.
4. Calculation options.
5. Functions of major subprograms: control, diffuser, air-flow, and heat-transfer.
6. Interaction between major subprograms; major interactive procedures.
7. Output of the computer program.

Major Assumptions

Assumptions affecting the program as a whole are listed below. Assumptions affecting individual parts of the program are introduced in the applicable detailed sections.

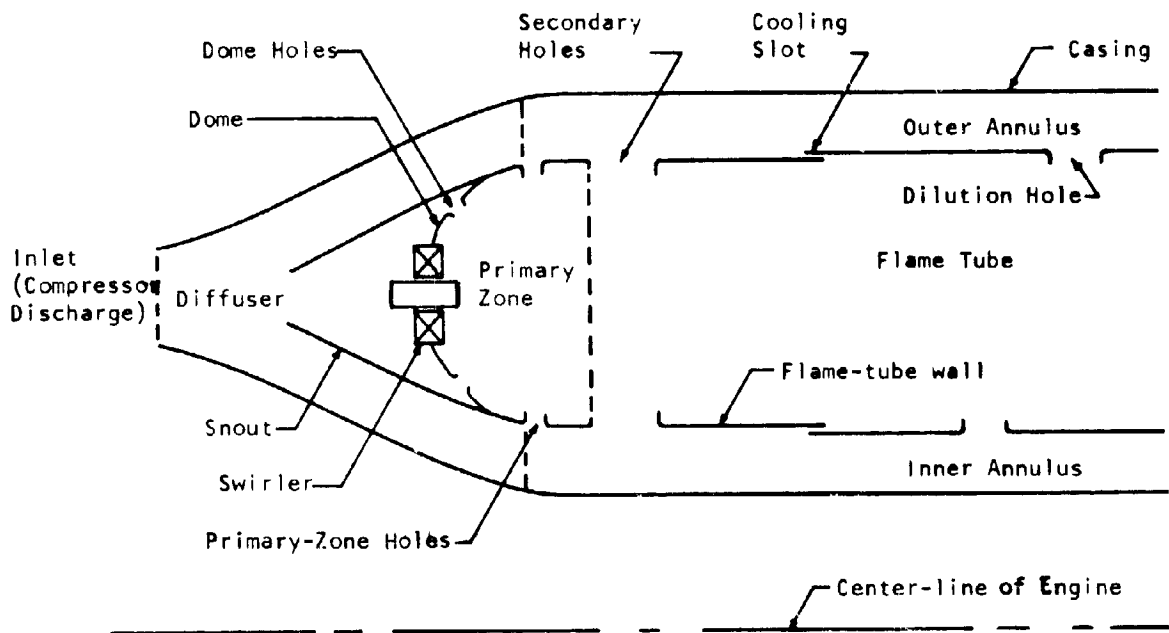
1. Conditions are steady: no quantity varies with time. This assumption is reasonable but it precludes the treatment of transient phenomena such as combustion oscillation.
2. Combustors are of annular or rectangular cross section. This precludes the direct simulation of tubo-annular (cannular) and tubular combustors. While flow conditions for these types may be approximated by appropriate selection of

dimensions, other parts of the simulation (for example, radiation heat transfer) will be of reduced accuracy.

3. Conditions are uniform around the circumference of the combustor; i.e. there is no circumferential variation in any quantity. This assumption is a major simplification; in practice, cyclic variations around the circumference occur, corresponding to the fuel-injection points. The results of this analysis will be useful, however, in indicating output parameters averaged around the circumference. In the case of combustors of rectangular cross section, this assumption implies that end effects due to the finite width of the combustor are ignored. This does limit the extent to which calculated results can be expected to agree with experiment.
4. The flow can be treated as quasi-one-dimensional. To represent the complex flow pattern existing in a real combustor is beyond the power of present analytical methods. Instead, the problem is broken down into two parts: flow in the main gas streams (one-dimensional) and flow and mixing of jets (predicted from correlated experimental data).
5. Radial-flow or reverse-flow combustors cannot be analyzed.
6. Flow conditions in the combustor are within the range of validity of the correlations used. The correlations are based on experimental data presently available. Outside their range of established validity, their accuracy is likely to be reduced.

Combustor Geometry and Nomenclature

The geometry of an annular combustor and the major terms used in describing it are shown in the sketch below:



Air from the compressor enters the diffuser, where it is split by the snout into three streams, which flow into the snout and the outer and inner annuli of the diffuser. After diffusing, the three streams enter the flame tube: the snout air through the swirler and the holes in the dome, the inner- and outer-annulus air through holes and cooling slots in the flame-tube walls.

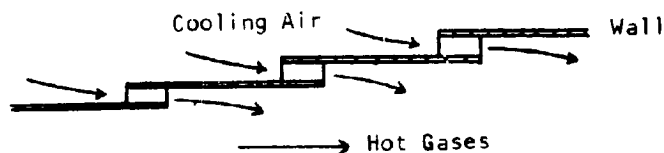
Swirler

A swirler is essentially a bladed passage, similar to a fan stator, which imparts swirl to the air flowing through it. Individual fuel injectors (of which there are many in an annular combustor) are often surrounded by swirlers to promote rapid mixing of air with the fuel spray.

The computer program includes a rather crude method for selecting swirler dimensions. A method for calculating swirler pressure drop is also included.

Holes and Slots

Apertures in the walls of the flame tube and in the dome are classified as penetration holes or cooling slots, according to their function. Penetration holes direct the entry of air jets into the flame tube for mixing and dilution of the hot combustion gases. Cooling slots introduce films of cool air just inside the flame-tube walls to act as thermal barriers. The cooling slots are assumed to be of the circumferentially continuous, dynamic-head type shown in the sketch below:



Correlations for the flow and mixing of penetration and wall jets are part of the computer program, as are film-cooling correlations.

Secondary Holes and Primary Zone

In this report the holes whose upstream edge marks the downstream boundary of the primary zone of the flame tube are defined as secondary holes. (Holes farther downstream are referred to as dilution holes.) Part of the air from the secondary holes recirculates upstream into the primary zone; the remainder passes downstream and is treated as ordinary penetration-jet air. It should be noted that recirculation is considered to occur only at the secondary holes, and that all secondary holes have their center-lines at one axial location in the combustor. The

secondary holes need not to be the first holes in the flame-tube wall.

Input to the Computer Program

Input quantities required by the computer program are of three kinds:

1. Library data.
2. Combustor geometry.
3. Case data (inlet flow conditions, calculation options, and so forth).

These quantities will now be described in general terms. A detailed description of the input format, units, and so forth, is given in Volume II.

Library Data

The library data are tables of quantities available for use by the program:

1. Discharge coefficients and jet angles for 100 hole types.
2. Performance data for straight-walled two dimensional diffusers and straight-walled annular diffusers.
3. Flame-emissivity data (none initially supplied).

The library data may be altered or supplemented by the user; appropriate instructions for so doing are given in Volume II.

Combustor Geometry

The following information must be supplied by the user to specify the combustor geometry.

1. Selection of annular or rectangular type.
2. Dimensions of walls of diffuser, snout, dome, flame tube, and casing.

3. Hole and cooling-slot data:
 - a. Hole type (selected from library data).
 - b. Number of holes in row.
 - c. Axial location; inner or outer wall.
 - d. Area (or cooling-slot height).
4. Identification of secondary-hole row (marks end of primary zone) and first hole row or slot in the flame-tube wall, as distinct from the dome (marks end of diffuser and start of combustor annulus).
5. Specification of swirler (optional):
 - a. No swirler.
 - b. Swirler designed within program.
 - c. Swirler dimensions supplied by user.

Case Data

The following information must be supplied for each case considered by the computer:

1. Flow conditions at inlet (compressor exit):
 - a. Total temperature.
 - b. Total pressure (weight-mean average).
 - c. Air mass flow rate.
 - d. Boundary-layer blockage and shape factors.
 - e. Velocity profile.
2. Other flow conditions:
 - a. Initial estimate of flow split among the snout and the inner and outer diffusing passages. (Optional. If not specified, program uses internal estimate.)

- b. Initial estimate of downstream blockage in diffuser.
 - c. Fraction of secondary-hole air recirculating upstream into primary zone. (Optional. If not specified, program calculates flow recirculation.)
 - d. Bleed air flowing from combustor annuli (optional):
 - i. Location (up to three locations).
 - ii. Fraction of inlet-air mass flow bled.
3. Information on combustor walls:
- a. Emissivity and absorptivity of flame-tube walls.
 - b. Thermal conductivity and thickness of flame-tube walls.
 - c. Emissivity of casing walls.
 - d. Temperature distribution of casing walls (optional; if not specified, assumed equal to compressor-discharge temperature).
4. Fuel characteristics and distribution:
- a. Overall fuel-air ratio.
 - b. Lower calorific value.
 - c. Hydrogen-to-carbon ratio.
 - d. Distribution of fuel burning rate, specified as an upper limit to the fraction of fuel burned up to each hole row.
5. Choice of optional calculation methods to be used within the program, and specification of data peculiar to the correlations employed in these methods. These options are discussed below, in connection with the major subprograms in which they appear.

6. Miscellaneous data:
 - a. Iteration limits.
 - b. Calculation-step sizes.

Overall Structure of Computer Program

The computer program comprises 35 subroutines; these are conveniently grouped by function into four major subprograms:

1. Control subprogram.
2. Diffuser subprogram.
3. Air-flow subprogram.
4. Heat-transfer subprogram.

The general functions of these subprograms and the flow of information among them are summarized in flow-chart form in Figure 1. Their operation is discussed in the following four subsections.

Control Subprogram

The control subprogram performs the preliminary operations necessary to prepare the computer for the main calculations. Its functions may be described as follows:

1. Read in and print out the case data and the combustor geometry.
2. Read in the library data; assemble and print out a short list of data (such as hole dimensions) actually needed for the cases being considered.
3. Calculate the combustor reference area (the maximum cross-sectional area bounded by the inner and outer casings).
4. Set up the system of geometrical indexing used in the diffuser, air-flow, and heat-transfer subprograms.

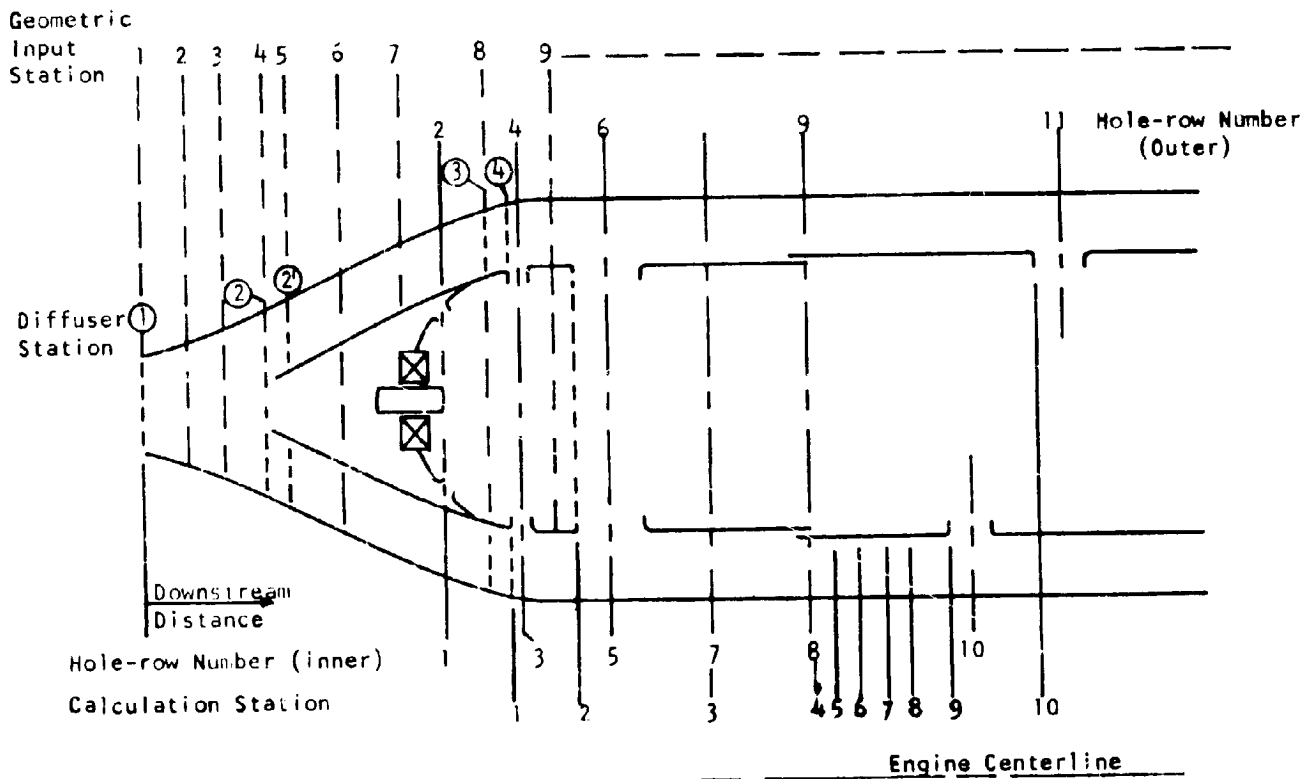
As familiarity with the geometrical indexing systems is basic to understanding the details of the various calculation methods, this subject is discussed in detail below.

Geometrical Indexing System

Four interrelated geometrical indexing systems are used within the program:

1. Input stations.
2. Hole rows.
3. Diffuser stations.
4. Flame-tube calculation stations.

These are illustrated by the sample numbering system on the sketch below:



Input Stations

The shapes of the walls of the diffuser, snout, dome, flame tube, and casing are described by their axial and radial dimensions at geometric input stations. Axial dimensions are measured from the diffuser inlet (compressor exit); radial dimensions from the engine center-line. For rectangular combustors widths are measured from an arbitrary datum point. Station numbers begin with Station 1 at the compressor exit.

Hole Rows

Holes are indexed in groups referred to as hole rows. A hole row comprises holes of identical size and shape, centered at the same axial location, and spaced at equal intervals around a single wall of the flame tube or dome. Up to six hole rows may be specified at a given axial location: hole rows may be interspersed on the same wall or paired on opposite walls of the flame tube. Indexing starts with the first hole row downstream of the compressor exit.

The indexing system for slots is similar to that for holes, except that slots are circumferentially continuous (as mentioned above) and hence only one slot may be placed on a given wall at any axial location. Noncontinuous slots may be approximated by continuous slots of equal area. Slots and holes are indexed together.

Dummy hole rows (holes of zero diameter) may be specified as input, for purposes of arranging the location of calculation stations (see the subsequent section on calculation stations).

Diffuser Stations

The calculations in the diffuser make use of the input-station indexing system. In addition, the diffuser is divided into major regions by a separate indexing system, labeled as follows in the above sketch:

- 1 Entrance to the diffuser (compressor exit).
- 2 Last geometric input station upstream of the start of the snout.
- 2' First geometric input station on the snout.
- 3 Last geometric station where diffusion takes place.
- 4 Entrance to the annulus (diffuser exit). This station coincides with the upstream edge of the first hole row in the flame tube, as distinct from the dome.

Flame-Tube Calculation Stations

The primary zone of the flame tube is bounded by the dome and swirler, the flame-tube walls, and (at its downstream end) by a plane passing through the upstream edges of the secondary holes. This zone is treated as a homogeneous stirred reactor; no calculation stations are used.

Calculations in the annulus and in the flame tube downstream of the primary zone are related to a system of calculation stations located as follows.

1. At the upstream edge of each hole row that is centered at a distinct axial location. Thus, for hole rows paired on opposite flame-tube walls only one calculation station is assigned.
2. At each dummy hole row.
3. At the axial location of each cooling slot having a distinct axial location.
4. At up to five axial locations spaced at a specified interval downstream of each cooling-slot location.
5. One station at the very end of the combustor.

Indexing of calculation stations starts with the first hole row in the

flame tube (as distinct from the dome) downstream of the compressor exit. The first calculation station thus coincides with the end of the diffuser annuli (Diffuser Station 4) and the start of the combustor annuli.

Diffuser Subprogram

The diffuser subprogram receives from the control subprogram inputs of geometry, inlet flow conditions, and certain quantities peculiar to the calculation option being used; it also receives a first estimate of the mass-flow split among the snout and the two annuli from the control subprogram, and subsequent estimates (during iterations on the flow split) from the air-flow subprogram.

Using these inputs and the calculation options chosen by the user, the diffuser subprogram performs the following functions:

1. Determines diffuser performance parameters:
 - a. Ideal pressure-recovery coefficient.
 - b. Actual pressure-recovery coefficient.
 - c. Effectiveness.
2. Evaluates flow mis-match at the snout.
3. Determines whether or not flow separation occurs and, if so, its location.
4. Calculates flow conditions on the dome and at the ends of the diffuser annuli:
 - a. Static pressure.
 - b. Static temperature.

These conditions are supplied as input to the air-flow subprogram.

For convenience in performing calculations the diffuser is divided into three diffusing regions (between Stations 1-2, and 2'-3 in the two

annuli, as shown in the sketch on page 14), and two mixing regions (between Stations 3 and 4). Within the diffusing regions the three diffuser calculation options (empirical-data method, streamtube method, and mixing-equation method) may be used in any of the following combinations:

Inlet Region (1 to 2)	Annular Regions (2' to 3)
Streamtube	Streamtube
Streamtube	Empirical Data
Streamtube	Mixing Equation
Empirical Data	Empirical Data
Empirical Data	Mixing Equation

For diffusers without snouts, diffusion in the annular regions 2 to 3 is treated by assuming that the flow expands isentropically from the dome stagnation pressure.

The mixing-equation method is always used in the mixing regions (Stations 3 to 4). In addition, area mismatch at the snout (Stations 2 to 2') is accounted for in all methods by calculating the total-pressure loss due to sudden expansion or contraction.

The three calculation options will now be briefly described.

Empirical-Data Method

This method is based on the direct evaluation of the effectiveness of a particular diffusing passage. There are two ways this can be done, at the user's option:

1. Diffuser effectiveness may be supplied directly as a program input.
2. Diffuser effectiveness may be calculated by the program from

correlations of experimentally measured effectiveness versus diffuser geometry that are contained in the library data. The results are corrected for deviation of the inlet boundary-layer blockage from that present in the experiments on which the correlations are based.

The remaining diffuser-performance parameters (ideal and actual pressure-recovery coefficients) and the outlet conditions are calculated directly from the effectiveness, the geometry, and the assumption that the total pressure is constant.

Streamtube Method

In this method the flow passage is divided into N streamtubes within which flow is assumed to be uniform and isentropic. In setting up the streamtubes, the distribution of boundary-layer displacement thickness supplied as a program input is used to adjust the flow area. The development of the flow (static pressure and velocity) is computed for each streamtube at each station along the diffusing passage. Boundary-layer calculations are performed to obtain a revised estimate of boundary-layer displacement thickness, which is then used in a revised streamtube analysis. This process is continued to convergence of the displacement thickness. The result of this method is the velocity distribution, static pressure, and blockage at the outlet from the diffusing passage.

Mixing-Equation Method

This is a rather crude method that can only be used between Stations 2 and 4. It takes into account the following effects occurring in these passages:

1. Pressure loss due to sudden expansion or contraction at the snout (Stations 2 to 2').
2. Mixing in the diffusing passage from Station 2' to 4.
3. Pressure loss due to curvature of the flow passage from 2' to 4.

A flow diagram of the diffuser subprogram is given in Figure 2.

Air-Flow Subprogram

The air-flow subprogram receives the following inputs from the control subprogram or program input:

1. Geometry of walls, holes, and swirler (if specified), at appropriate indexing stations.
2. Fuel data.
3. Jet-mixing model and entrainment constant.
4. Initial estimate of mass-flow split among snout and annuli.

From the diffuser subprogram it receives the static pressures and static temperatures on the dome and at the ends of the diffuser annuli.

Using these inputs, the air-flow subprogram performs the following functions:

1. Calculates the flow conditions in the primary zone (static pressure and temperature, mass-flow rate) and at calculation stations in the flame tube and annuli (static and total pressure and temperature, mass-flow rate, and velocity).
2. Calculates the combustor total-pressure loss.
3. Directs the iterative process by which the diffuser and air-flow subprograms together arrive at the correct flow split among the snout and the two annuli.

Options

The following options are available in the air-flow subprogram and must be specified by the user:

1. Jet-mixing models. The air-flow subprogram contains four models to represent the mixing of penetration and wall jets into the main gas stream. The user must choose a model, which is then used for both types of jet. Associated with each model is a constant that determines the actual rate of jet mixing. An individual value of this constant must be specified for each jet type.
2. Heat transfer from the flame-tube walls to the annulus air may be calculated or ignored at the user's option. If this quantity is calculated, an iteration in the overall calculation is required, because of the influence of heat input on the flow conditions in the annulus.

Calculation Procedure

The main steps in the calculation procedure within the air-flow subprogram are as follows:

1. Calculate the primary-zone pressure from the pressure on the dome, the snout air-flow rate, and the relations between pressure drop and flow rate for the swirler and the dome holes.
2. Calculate the air-flow rate into the primary zone through holes up to and including the secondary holes (recirculating part).
3. Calculate the primary-zone exit static pressure and temperature from the total flow rate, inlet conditions, and fuel

burned (up to stoichiometric). The primary zone is treated as a stirred reactor.

4. Proceed from calculation point to calculation point down the annuli and flame tube, calculating the mass-flow rates, velocities, and static and total pressures and temperatures.

At the end of this calculation procedure the flows at the ends of the annuli are inspected. If these flows are not correct (equal to zero, or the correct bleed flow, if any), the mass-flow split within the diffuser is altered according to the following scheme:

1. If the flows in the two annuli are of opposite sign, the annulus flows are adjusted, while the dome flow is held fixed.
2. If the flows in the annuli are of the same sign, the dome flow is altered and proportionate changes in annulus flows are made.

The entire sequence of diffuser and air-flow calculations is then repeated. This process is continued until the residual air flows at the ends of the annuli approach zero within a specified tolerance, or until the specified iteration limit is reached.

A flow diagram for the air-flow subprogram is given in Figure 3.

Heat-Transfer Subprogram

The heat-transfer subprogram receives as input the geometry of the flame tube and casing from the control subprogram and the axial distributions of velocity and temperature of the flame-tube gases from the air-flow subprogram. Additional data that may be specified as input at the option of the user are:

1. Temperature distribution of the outer casing.
2. Choice of calculation options.
3. Data needed for the calculation option chosen:
 - a. A constant characterizing cooling-film effectiveness.
 - b. The permeability coefficient for porous walls.
 - c. Flame-emissivity data (optional).
 - d. Thermal conductivity and thickness of flame-tube walls.
4. Fuel hydrogen/carbon ratio.
5. Flame-tube and casing absorptivities and emissivities.

The primary objective of the heat-transfer subprogram is to establish the axial distribution of temperature along the flame-tube walls for various program options. Under one program option, a further objective is to provide the air-flow subprogram with the axial variation of the heat-transfer rate from the flame-tube wall to the annulus air.

In operation, the subprogram evaluates various heat-flux components at a point on the flame-tube wall in terms of the wall temperature; the heat-flux components which are considered may include several or all of the following, depending upon the program options specified:

1. Convection from the flame-tube gases.
2. Convection to the annulus air.
3. Radiation from the flame.
4. Radiation to the outer casing.
5. Radiation interchange between the flame-tube walls.
6. Longitudinal conduction along the flame-tube wall.
7. Heat transfer to transpiring air for porous walls.

The heat-balance equation is then solved to determine the unknown temperature. These operations are performed at calculation stations along the

flame tube; no provision is made, however, for the inclusion of the flame-tube dome in the heat-transfer analysis.

Program Options

Several of the program options concern the heat-transfer subprogram; these options are listed below.

1. The flame-tube wall may be cooled by:
 - a. Convection to the annulus air and radiation to the outer casing.
 - b. Combined effects of (a) and film cooling.
 - c. Combined effects of (a) and transpiration cooling.
2. The emissivity of the flame may be computed from:
 - a. One of two equations for nonluminous flames.
 - b. One of three equations for luminous flames.
 - c. Emissivity data supplied as special input by the user.
3. The radiation from the flame to the flame-tube wall may be calculated on the basis of one of two assumptions:
 - a. Radiation is purely radial (one-dimensional).
 - b. Radiation to an element of the wall occurs from all (radial and axial) parts of the flame (two-dimensional).
4. The heat-balance equation may:
 - a. Include a term for heat conduction along the flame-tube walls.
 - b. Include a term for radiation interchange between the two flame-tube walls.
 - c. Include the terms in both (a) and (b).
 - d. Neglect the terms in (a) and (b).
5. An option is available to exclude the heat-transfer subprogram

from the program routing for cases in which heat-transfer results are not required.

A flow diagram of the heat-transfer subprogram is given in Figure 4.

Output of the Computer Program

A general description of the information printed out by the computer program follows. A sample printout is given in Volume II, Appendix III.

Input and Geometrical Data

The following information is printed out by the control subprogram. Part of the data are taken directly from input; the remainder are generated by geometrical manipulation of the input data.

1. Combustor geometry at input stations.
2. Swirler design data.
3. Details of holes at each hole row, separately for penetration holes and cooling slots.
4. At each hole row, ratios of cross-sectional areas of flame tube and annuli to reference area.
5. Total hole area in flame-tube wall, for penetration holes and cooling slots.
6. Ratio of total hole area, including swirler, dome holes, penetration holes, and cooling slots, to reference area.
7. Identification of various key locations in the combustor:
 - a. Last input station before the snout (diffuser Station 2).
 - b. Last input station in diffusing part of diffuser (diffuser Station 3).

- c. First hole row in the flame tube, as distinct from the dome (upstream edge is diffuser Station 4 and the start of the combustor annulus).
- d. Secondary hole row (upstream edge is end of primary zone).
- 8. Fraction of secondary air recirculating into primary zone (if specified as input).
- 9. Fraction of inlet air bled, and location.
- 10. Fuel data:
 - a. Overall fuel-air ratio.
 - b. Lower calorific value.
 - c. Hydrogen-to-carbon ratio.
 - d. Axial distribution of fuel burning rate.
- 11. Heat-transfer input data:
 - a. Thickness, thermal conductivity, emissivity, and absorptivity of flame-tube walls.
 - b. Emissivity of outer casing.
- 12. Inlet flow conditions (at compressor exit):
 - a. Total temperature.
 - b. Total pressure.
 - c. Mass-flow rate.
 - d. Boundary-layer blockage and shape factors.
 - e. Velocity profile.
- 13. First estimate of downstream blockage in diffuser.
- 14. Overall fuel-air ratio.
- 15. Fuel burning rate at calculation points.
- 16. Casing temperature at calculation points.
- 17. Details of program options:

- a. Diffuser options for various diffusing passages.
- b. Jet-mixing model and entrainment constants for penetration and wall jets.
- c. Heat transfer to annulus air (considered, or not considered).
- d. Flame luminosity correlation.
- e. Heat-transfer models for radiation and wall cooling.

Output of Diffuser Subprogram

The following quantities are printed out by the diffuser subprogram:

1. Reference conditions:
 - a. Reference area.
 - b. Reference velocity.
 - c. Inlet Mach number.
 - d. Reference Mach number.
 - e. Reference dynamic pressure.
2. Diffuser parameters in the three diffusing passages, (1) compressor exit to lip of snout, (2) inner passage between snout and casing, and (3) outer passage between snout and casing:
 - a. Ideal pressure-recovery coefficient.
 - b. Actual pressure-recovery coefficient.
 - c. Diffuser effectiveness.
 - d. Fractional total-pressure loss.
 - e. Velocity profile at exit of the first (1) diffusing passage (diffuser Station 2).
 - f. Boundary-layer displacement thickness and shape factor at inlet to the passage.

- g. Input point at which separation occurs, if any.
- h. Mismatch area ratio at the snout.

Output of Air-Flow Subprogram

The following results of air-flow calculations are printed out for each calculation station in the flame tube and the inner and outer annuli:

1. Total temperature.
2. Total and static pressures.
3. Bulk velocities.
4. Mach numbers.
5. Accumulated pressure loss due to friction and heat addition (annuli only).
6. Accumulated pressure loss due to expansion (annuli only).
7. Rate of fuel burning (flame tube).
8. Friction factor (annuli only).

In addition, the following total-pressure-loss factors are printed out for each annulus:

1. Combustor total-pressure loss relative to reference dynamic pressure.
2. Combustor total-pressure loss relative to compressor delivery pressure.
3. Expansion total-pressure loss relative to compressor delivery pressure.
4. Total-pressure-loss factor due to friction and heat addition, relative to compressor delivery pressure.

Also, the overall total-pressure loss for the combined diffuser and combustor, relative to the compressor delivery pressure, is printed out.

The following flow quantities for holes, calculated in the air-flow program, are printed out for each hole-row station:

1. Pressure-loss factor.
2. Discharge coefficient.
3. Effective hole area (area x discharge coefficient).
4. Initial jet angle.
5. Initial jet velocity.
6. Fraction of current annulus air flowing through current hole row.
7. Accumulated fraction of inlet air flow in flame tube.

Finally, the air mass-flow split is printed out.

Output of Heat-Transfer Subprogram

The heat-transfer calculations are performed for each calculation point; heat-transfer quantities are, therefore, available as functions of axial distance along the flame tube. In addition to the flame-tube wall temperatures, which are the quantities of principal interest, the following intermediate quantities are printed out in the computer results:

1. Adiabatic-wall temperature.
2. Film-cooling effectiveness.
3. Flame intensity.
4. Flame emissivity.
5. Heat transferred to transpiration air in the wall, where applicable.
6. Radiation interchange between each wall, where applicable.
7. Heat-transfer rates to and from the flame-tube walls by

radiation and convection.

8. Reynolds, Prandtl, and Nusselt numbers of the flow in the flame-tube and in the annuli.

DIFFUSER SUBPROGRAM - ANALYTICAL METHODS AND PROGRAM DEVELOPMENT

Introduction

The portion of a combustor treated by the diffuser subprogram is indicated in the sketches on the following page, for the two configurations which can be treated by the subprogram. The objectives of the diffuser subprogram are:

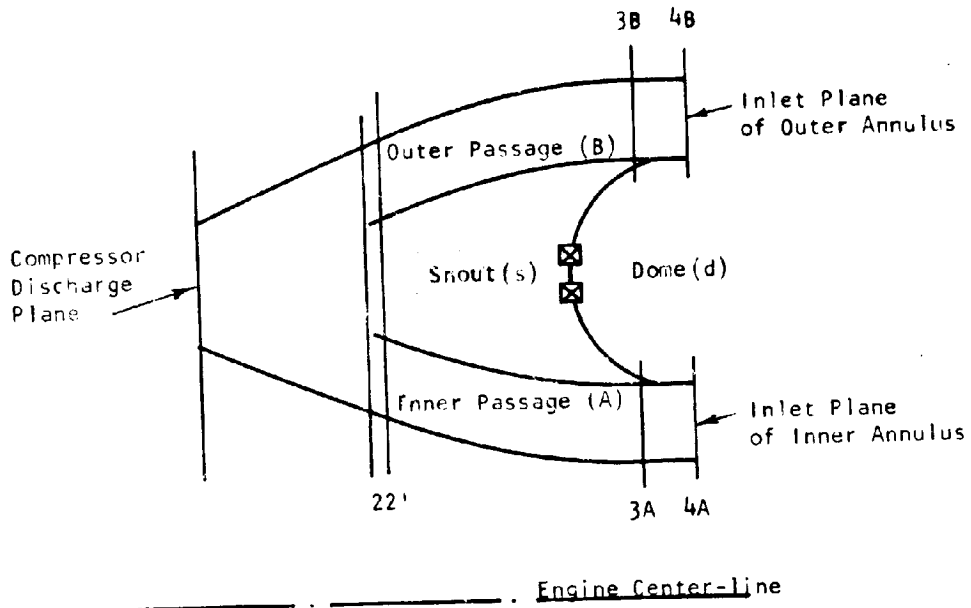
1. To provide the necessary inlet flow conditions to the annuli (Stations 4A and 4B); static pressure and temperature are the specific properties calculated, although all others can be derived from these two and the mass flow.
2. To determine the diffuser performance parameters of effectiveness, ideal pressure-recovery coefficient, and actual pressure-recovery coefficient for the sections 1-2, 2-3A, 2-3B, 2-4A, and 2-4B.
3. To determine whether separation occurs in the diffuser and, if so, at what points.
4. To evaluate the magnitude of the flow mismatch between Stations 2 and 2' (for diffusers with a snout).

The specific input quantities required by the diffuser subprogram and the output quantities provided have been previously listed in the OVERALL APPROACH sections, and will not be repeated here.

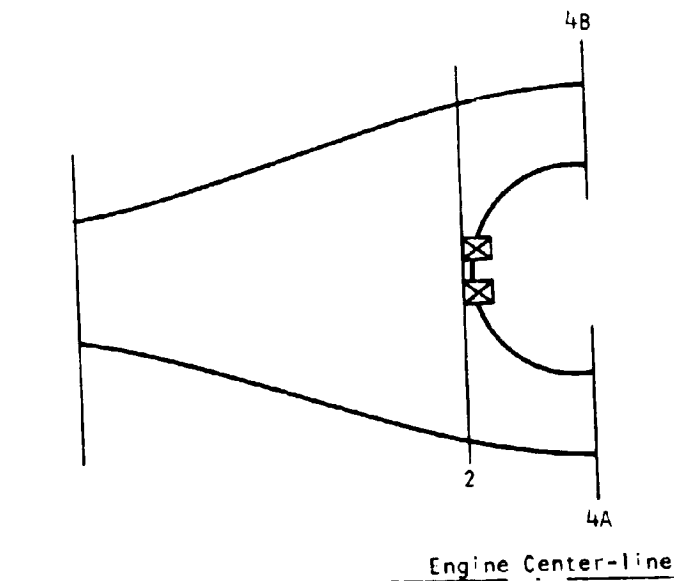
This chapter presents the options available in the subprogram to accomplish these objectives, and the assumptions made and equations used in the analyses.

Major Assumptions

The assumptions employed in the diffuser analysis which are



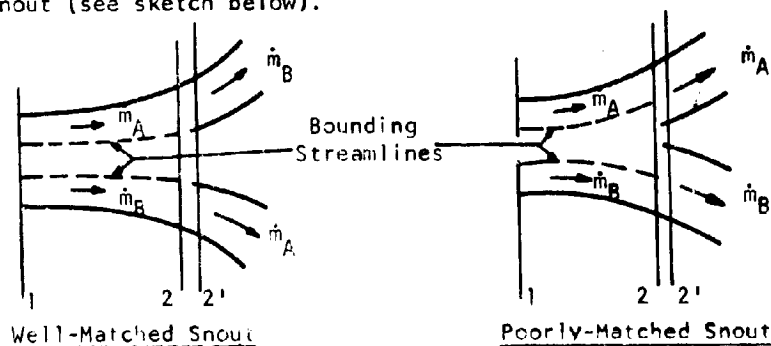
Diffuser With Snout



Diffuser Without Snout

common to all calculation options are:

1. The flow in the upstream part of the diffuser (1-2) is unaffected by the flow downstream of Station 2. An analysis based on any other assumption is beyond the present state of the art. This assumption is expected to be valid in well-designed diffusers (see 2 below).
2. If there is a snout, it is reasonably well matched to the flow; that is, the streamlines in the portion 1-2 which bound the flow required by the annular passages should have radial locations at Station 2 nearly equal to those of the snout (see sketch below).



If the flow is not well-matched, it is certain that the flow in the upstream part of the diffuser will be affected by flow in the downstream part, in which case the results of the diffuser subprogram are highly questionable.

3. If there is a snout, its performance as a diffusing passage is specified by an input value of the total-pressure-loss coefficient (i.e., ratio of total-pressure loss between Station 2s' and the dome to the dynamic head at 2s'). This is based on the presumption that the flow in the snout will

be dominated by either the colander (or orifice plate) or the downstream resistances supplied by the swirler and dome holes; in either case, it is not expected that the total-pressure loss due only to diffusion in the snout will be of sufficient magnitude to warrant a separate analysis.

4. If there is no snout, the performance of the passages 2-4A and 2-4B is specified by a single input value of total-pressure-loss coefficient between Stations 2 and 4 (i.e., ratio of total-pressure loss between Stations 2 and 4 to the dynamic head at Station 2). This is based on the presumption that in such cases the resemblance of these passages to a diffuser will be remote.
5. The static pressure across any diffusing passage is constant across any section normal to the passage center-line. This assumes that the flow will be subjected to mild curvatures, and it seems to yield reasonable results for well-designed diffusers.
6. The air in the diffuser may be treated as a perfect gas, with $\gamma = 1.4$ and $c_p = 0.24$ Btu per lbm-deg R.

Other assumptions which relate only to specific calculational options in the diffuser subprogram will be discussed subsequently.

Definition of Terms

To facilitate the subsequent discussion of analysis methods and calculational procedures employed in the diffuser subprogram, it is convenient to define some terms which will be frequently used. These terms fall

generally into two categories: flow parameters and diffuser-performance parameters.

Flow Parameters

The flow parameters which are most frequently used are the area-average velocity, the mass-average velocity, the ratio of equivalent free-flow area to total flow area, or blockage, and the dynamic head. All of these parameters refer to the flow at a given axial location, where the static pressure is assumed constant across any section normal to the passage center-line.

The area-average velocity, \bar{u}_a , is defined by

$$\bar{u}_a = \frac{1}{A} \int_0^A u dA \quad (1)$$

where u is the velocity component in the direction of the passage center-line (normal components are neglected) and A is the passage cross-sectional area normal to the passage center-line. For incompressible flow, \bar{u}_a is the velocity the flow would have if the profile were uniform across the entire passage.

The mass-average velocity, \bar{u}_m , is defined by

$$\bar{u}_m = \frac{\int_0^A u^2 dA}{\int_0^A u dA} \quad (2)$$

For incompressible flow, it is the velocity which when multiplied by the mass flow yields the total momentum flux.

The blockage is $1-E$, where E is defined by

$$E = \frac{\bar{u}_a}{\bar{u}_m} = \frac{1}{A} \frac{\left[\int_0^A u dA \right]^2}{\int_0^A u^2 dA} \quad (3)$$

For incompressible flow, E is the ratio of the area which would be occupied by a uniform flow, with a total pressure equal to the mass-averaged total pressure of the actual flow, to the actual area of the passage. A related term which is frequently used is the profile parameter, β , which is merely the reciprocal of E . A derivative of the general inlet blockage, $1-E$, is the inlet boundary-layer blockage, $1-E_{bl}$, where E_{bl} defined by

$$E_{bl} = \frac{A - A_{bl}}{A} \quad (4)$$

where A_{bl} is the area occupied by the boundary-layer displacement thickness. If the flow outside the boundary layer is uniform (i.e., $u = \text{constant}$ across the passage) then $E_{bl} = E$.

The dynamic head based on mass-average velocity, \bar{q} , is defined by

$$\bar{q} = \frac{1}{2} \bar{\rho} \bar{u}_m^2 = \frac{1}{2} \bar{\rho} \beta^2 \bar{u}_a^2 \quad (5)$$

where $\bar{\rho}$ is the average density across the passage

$$\bar{\rho} = \frac{\dot{m}}{\bar{u}_m EA} \quad (6)$$

For incompressible flow, \bar{q} is the actual mass-average dynamic pressure; for compressible flow, it is treated as a reference quantity.

Diffuser Performance Parameters

The diffuser performance parameters used herein are the ideal incompressible-flow pressure-recovery coefficient, the actual pressure-recovery coefficient, and the diffuser effectiveness.

The ideal pressure-recovery coefficient is defined by

$$C_{p,ideal} = \frac{\text{Maximum obtainable value of } (p_2 - p_1)}{\bar{q}_1} \quad (7)$$

where the subscripts 1 and 2 refer to inlet and exit, respectively. Two specific forms of this relation are used. First, the ideal incompressible-flow pressure-recovery coefficient, C_{pi} , defined by

$$C_{pi} = 1 - \frac{1}{AR^2} \quad (8)$$

where AR is the passage area ratio, A_2/A_1 . This expression in fact represents the maximum static-pressure rise which can be achieved in incompressible flow if the velocity profile at the diffuser inlet is uniform. If, however, the inlet velocity profile is non-uniform an additional increase in static pressure may be expected due to the mixing process. It is shown in Appendix I that the maximum achievable pressure rise is obtained by instantaneous mixing of the profile followed by diffusion, with the result that the ideal pressure-recovery coefficient in the presence of mixing can be expressed as

$$C_{pm} = \frac{1}{\beta_1^2} \left[2(\beta_1 - 1) + 1 - \frac{1}{AR^2} \right] \quad (9)$$

Although both Equations 8 and 9 are strictly meaningful physically only for incompressible flow, they are used here as reference quantities for compressible flow.

The actual pressure-recovery coefficient, C_p , is defined by

$$C_p = \frac{P_2 - P_1}{\bar{q}_1} \quad (10)$$

The diffuser effectiveness, ξ , is defined as the ratio of the actual pressure-recovery coefficient to the ideal pressure-recovery coefficient. Two definitions are used here, corresponding to the pressure-recovery coefficients defined by Equations 8 and 9:

$$\xi = \frac{C_p}{C_{pi}} \quad (11)$$

$$\xi_m = \frac{C_p}{C_{pm}} \quad (12)$$

Alternative Analysis Procedures Available in the Subprogram

For the purposes of analysis, the diffuser is considered as three separate diffusing passages: 1-2, 2-3A, and 2-3B; and two mixing passages: 3A-4A and 3B-4B (see sketch on page 32). The essential element of the diffuser analysis is then the evaluation of the performance of a single diffusing passage, including the determination of both the performance parameters and the outlet conditions. The diffuser subprogram contains the following three options for determining the performance of a single diffusing passage (the specific passages for which they can be used are indicated in parentheses):

Option 1: Empirical-Data Method (1-2, 2-3A, 2-3B)

Option 2: Streamtube Method (1-2, 2-3A, 2-3B)

Option 3: Mixing-Equation Method (2-4A, 2-4B)

Option 1 has two variations: the empirical performance data can be obtained from empirical tabulations included within the program or it may be specified directly as input. Option 3 is always used in mixing passages 3A-4A and 3B-4B, regardless of the option(s) used up to Stations 3A and 3B.

The following three sections present the analyses used in these options; subsequent sections deal with the overall calculational procedure used in the diffuser subprogram to integrate these individual analyses.

Empirical-Data Method

Assumptions

In addition to the general assumptions listed previously, the following assumptions are made in evaluating diffuser performance with

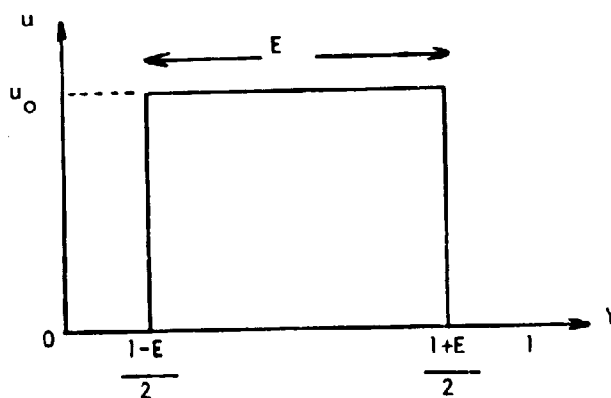
empirical data:

1. The velocity profile at any section can be characterized as a "top-hat" profile; specifically, for a particular value of blockage $(1-E)$, the profile is given by

$$u = 0 \text{ for } \frac{1-E}{2} > Y \text{ and } Y > \frac{1+E}{2} \quad (13)$$

$$u = u_m \text{ for } \frac{1-E}{2} \leq Y \leq \frac{1+E}{2} \quad (14)$$

where Y is the nondimensional annulus height. A "top-hat" profile is shown in the sketch below.



2. The total pressure is conserved in the flow. This results in the diffuser effectiveness being reflected solely by a change in blockage from inlet to outlet; the total-pressure loss is assumed to be associated with the so-called "mixing out" of the profile.
3. The effect of the inlet Mach number on diffuser effectiveness is negligible. This assumption is supported by the work of Henry, Wood, and Wilbur (Ref 14), Van Dewoestine and Fox (Ref 15), and Young and Green (Ref 16). Typical results from Reference 16 are shown in Figure 5; it is evident that Mach-number effects are not appreciable for $M \lesssim 0.6$.

Input Information Required

The input information required to assess the performance of a diffusing passage is as follows:

1. The inlet conditions defined by \dot{m} , p_1 , \bar{q}_1 , and E_1 (the subscript 1 refers to the inlet of the particular diffusing passage and is not necessarily coincident with diffuser Station 1).
2. The nondimensional diffuser geometry defined by the ratio of the length along the passage center-line to the passage height at inlet ($L/\Delta r_1$ for annular diffusers, L/W for two-dimensional diffusers), and the area ratio (A_2/A_1).
3. If the option to specify directly the diffuser effectiveness is used, then this value is of course required in place of the nondimensional length.

Empirical Correlations Used for Diffuser Performance

Two empirical correlations are included in the subprogram, in the form of tables, which yield values of the diffuser effectiveness, ξ , as a function of area ratio and nondimensional length, for a fixed value of inlet blockage ($1-E_1$). One correlation is based on data obtained for straight-walled, two-dimensional diffusers by Reneau, Johnston, and Kline (Ref 7). The data on which the tabulation is based are shown graphically in Figure 6. The second correlation is reproduced from work on straight-walled annular diffusers by Sovran and Klomp (Ref 6); this is shown graphically in Figure 7. The latter work was performed with diffusers having a hub-shroud ratio in the range of 0.55-0.7, and should only be used for diffusers in this range.

For the specified geometry, the effectiveness of the passage is found from the tabular forms of the data represented by Figures 6 and

7, depending upon whether a two-dimensional or an annular configuration is specified. The resulting uncorrected value of effectiveness is applicable only to the inlet blockages for which the data apply $[(1-E_1) = 0.015$ for two-dimensional diffusers and $(1-E_1) = 0.02$ for annular diffusers].

To account for different inlet blockages, the following empirical correlation has been developed:

$$\xi - \bar{\xi} = \frac{2}{1-E_1} \left[(1-E_1) - (1-\bar{E}_1) \right]^2 \cos \left[(\bar{\xi} - 0.5)\pi \right] \quad (15)$$

where $\bar{\xi}$ = value of ξ for $E_1 = \bar{E}_1 = 0.85$

This correlation applies in the range $1 > E_1 > 0.7$ and $0.5 < \xi < 0.9$ but it is mathematically unique for all feasible values of E_1 and ξ .

This correlation is compared with some experimentally determined inlet blockage effects (from Refs 7 and 17) in Figure 8.

The value of diffuser effectiveness corrected for inlet blockage is then obtained by first substituting the uncorrected value of ξ and the inlet blockage E_1 for which the tabulation is valid into Equation 15 to determine $\bar{\xi}$, and then solving Equation 15 again for the corrected value of ξ with the known values of $\bar{\xi}$, \bar{E}_1 , and the actual inlet blockage, E_1 .

If the effectiveness of the diffusing passage is a specified input value, then of course the empirical correlations are not used.

Determination of Diffuser Performance Parameters and Outlet Conditions

The diffuser performance parameters, in addition to the effectiveness, which are determined when the empirical-data method is used are the ideal and actual pressure-recovery coefficients. The ideal pressure-recovery coefficient is determined from Equation 8 and the actual pressure-recovery

coefficient is determined from Equation 11.

The outlet conditions determined in this method are the static pressure, the mass-average velocity, and the outlet blockage, E_2 . The static pressure is determined from the actual pressure coefficient.

$$p_2 = p_1 + C_p \bar{q}_1 \quad (16)$$

The outlet blockage is computed on the basis that the flow is incompressible and that the stagnation pressure is constant; the definition of stagnation pressure then yields

$$E_2^2 = \frac{E_1^2}{E_1 + AR^2 (1 - E_1)} \quad (17)$$

The remaining properties $\bar{\rho}_2$, \bar{u}_{m2} , \bar{T}_2 at the diffuser exit are determined from a simultaneous solution of the relations:

$$\dot{m} = \bar{\rho}_2 \bar{u}_{m2} E_2 A_2 \quad (18)$$

$$T_{o2} = T_{o1} = \bar{T}_2 + \frac{\bar{u}_{m2}^2}{2g_o J c_p} \quad (19)$$

$$p_2 = \bar{\rho}_2 R \bar{T}_2 \quad (20)$$

Limitations of the Method

The major limitations of the empirical-data method are due to two factors:

1. The empirical data used.
2. The one-dimensional treatment of the flow.

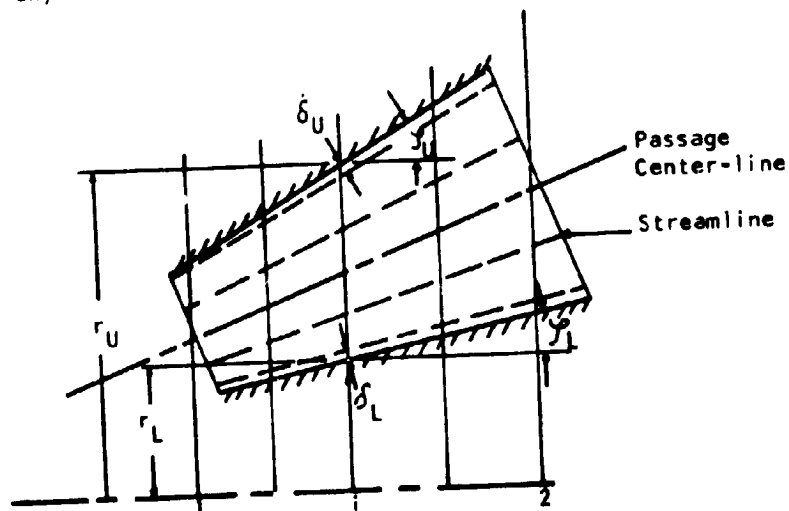
The empirical data incorporated within the program are valid only for straight-walled diffusers with uniform inlet velocity profiles and low inlet blockage. Although some data are available on curved-wall diffusers (Refs 18 to 21), they are either insufficient to produce a correlation, or they have been obtained for diffusers in which the exit profile has been

allowed to mix to substantially uniform conditions. No systematic data is available for diffuser configurations of the actual split-passage type found in combustors. Hence, the extrapolation of the present data to other conditions is at best uncertain.

The one-dimensional nature of the treatment precludes accurate analysis of diffusers with non-uniform inlet profiles; the effect of inlet nonuniformities is known to be quite important (in Reference 22 for example, a 1 per cent change in the annulus total pressure due to a change in diffuser velocity profile was calculated to produce an 18 per cent change in the mass flow through the dilution holes). Also, the velocity profile at the exit of the first portion of the diffuser (Station 2) has a large influence on the resulting mass-flow split in the annuli; this cannot be treated accurately in the present method.

Streamtube Method

This method involves a streamtube analysis to calculate the development of the velocity profile within the diffuser, as well as an analysis of the wall boundary layers to provide the location of separation points, if any. The model is indicated schematically below:



In the following subsections, the subscripts U and L will refer to the upper and lower walls of the passage, respectively.

Assumptions

The following assumptions specific to the streamtube method are made:

1. The flow can be represented by a number of streamtubes in each of which the flow is uniform and isentropic.
2. The boundary layer is identical to that on a flat plate with the same pressure gradient that exists in the diffuser, and its effect on the inviscid flow is to produce an effective displacement of the diffuser wall equal to the displacement thickness of the boundary layer.
3. The streamline slope varies linearly from one wall to the other at any axial station.
4. Separation of the boundary layer is assumed to occur when the shape factor H exceeds a critical value, H_{sep} . The latter value is an input to the program. For conical diffusers, Carmichael and Pustintev (Ref 23) show that a value of $H_{sep} = 3.0$ is typical. For airfoil sections, values of $H_{sep} = 1.8-2.2$ are more usual (Ref. 24). A value of $H_{sep} = 1.9$ has been assumed for this program. Figure 9 shows the results of the present calculational procedure, compared with the experimental results of Reference 7.
5. Subsequent to boundary-layer separation, no further static-pressure rise occurs in the section of the diffuser being considered.

Input Information Required

The input information required for a streamtube analysis is:

1. The geometry of the diffuser in the form of radial position of each wall as a function of axial distance.
2. The following inlet conditions:
 - a. Weight mean total pressure, P_1 .
 - b. Uniform stagnation temperature, T_{01} .
 - c. Mass flow rate, \dot{m} .
 - d. A velocity profile given by:

$$\frac{u}{U} = f(Y)$$

where U = an arbitrary normalization velocity

$f(Y)$ = a tabulated function of $\frac{u}{U}$ against Y

Y = nondimensional annulus height

- e. The boundary-layer displacement thickness, δ_1 .
 - f. The boundary-layer shape factor, H_1 .
3. The number of streamtubes into which the flow is to be divided, N .
4. An initial estimate of the boundary-layer displacement thickness on each wall at every axial location of a geometric input point.

Outline of Method of Solution

The method of solution proceeds in the following steps:

1. The determination of the static pressure at the inlet, and the mass flow, stagnation pressure, and velocity in each streamtube.
2. The calculation of the static pressure at each downstream location (specified by the location of the geometric input

points), and the resulting radial locations of, and velocities in, each streamtube. The first time this calculation is performed, the estimated values of boundary-layer blockage at all axial locations (supplied as input) are used; subsequent calculations are based on revised estimates of this blockage.

3. The determination of the boundary-layer displacement thickness on each wall, using the static pressures and wall-streamtube velocities obtained in Step 2.
4. Repeat Steps 2 and 3 until the displacement thicknesses determined in Step 3 are within a specified tolerance of those used in Step 2.

The details of these steps are presented in the following subsections where, for convenience, the geometrical relations are given only for annular configurations.

Inlet Conditions

The inlet conditions for each of N streamtubes are determined as follows (the subscript j refers to a particular streamtube):

1. Calculate the dimensionless coordinate Y_j of the midpoint of each (equal-area) streamtube from the relations

$$Y_j = \frac{\frac{R_j + R_{j+1}}{2} - R_1}{R_{N+1} - R_1} \quad (21)$$

$$R_{j+1} = \sqrt{\frac{A_j}{\pi} + R_j^2} \quad (22)$$

$$A_j = \frac{\pi}{N} (R_{N+1}^2 - R_1^2) \cos \left(\frac{\gamma_U + \gamma_L}{2} \right)$$

$$R_1 = r_L + \delta_L / \cos \left(\frac{\gamma_L + \gamma_U}{2} \right)$$

$$R_{N+1} = r_U - \delta_U / \cos \left(\frac{\gamma_L + \gamma_U}{2} \right)$$

At the compressor exit (Diffuser Station 1) it is assumed that

$$\cos\left(\frac{\gamma_U + \gamma_L}{2}\right) = 1$$

2. Find u_j/U for each streamtube by interpolation from the velocity profile (tabulated as a function of Y) provided as input.
3. Calculate ρ_{ch} , a characteristic density to provide a first guess for ρ_j from

$$\rho_{ch} = \frac{P_1}{RT_{o1}}$$

where P_1 = weight mean total pressure at inlet.

4. If the static pressure p_1 at inlet is not given, make a first guess at this pressure from

$$P_1 = P_1 - \frac{\rho_{ch}}{2g_o} \left[\frac{\dot{m}}{\rho_{ch} \cdot A_1} \right]^2 \quad (23)$$

where $A_1 = \sum A_j$

5. Calculate the first guess at U from

$$U = \frac{\dot{m}}{\sum_j \frac{u_j}{U} \rho_{ch} A_j} \quad (24)$$

6. Using this value of U , calculate u_j from the results of step 2 and the temperature, T_j , from

$$T_j = T_{o1} - \frac{u_j^2}{2C_p g_o J} \quad (25)$$

7. Calculate the density, ρ_j , from

$$\rho_j = \frac{P_j}{RT_j} \quad (26)$$

8. Calculate U from

$$U = \frac{\dot{m}}{\sum_j \frac{u_j \cdot \rho_j \cdot A_j}{U}} \quad (27)$$

9. If this value of U is significantly different from the previous value of U return to 6. If not continue.
10. Calculate the total pressure P_j in each streamtube from

$$\frac{P_1}{P_j} = \left[\frac{T_j}{T_{01}} \right]^{\frac{\gamma}{\gamma-1}}$$

where γ = ratio of specific heats (1.4).

11. Compute the mass flow in each streamtube from

$$\dot{m}_j = \rho_j u_j A_j$$

and the critical area of each streamtube A_j^* from the usual compressible-flow relations (p/P is sufficient to determine A/A^*).

12. If the static pressure at inlet is calculated in Step 4, calculate the new value of weight mean total pressure from

$$(P_1)_{\text{new}} = \frac{1}{\dot{m}} \sum_j \dot{m}_j \cdot P_j$$

where \dot{m}_j = mass flow in the j th streamtube

13. If this new value of total pressure is significantly different from the given value of total pressure, calculate a new value of p_1 from

$$(p_1)_{\text{new}} = P_1 \frac{P_1}{(P_1)_{\text{new}}} \quad (28)$$

and return to Step 7.

Hence, the quantities $\dot{m}_j, \rho_j, u_j, A_j^*, P_j$ are known at the inlet to each streamtube. The inlet dynamic head is calculated from

$$\bar{q}_1 = \left[\sum_j \left(\frac{\dot{m}_j}{\dot{m}} \rho_j \right) \right] \left[\sum_j \left(\frac{\dot{m}_j}{\dot{m}} \right) u_j^2 \right] / 2g_0 \quad (29)$$

Determination of Streamtube Properties
at Downstream Axial Locations

The conditions in each streamtube at each downstream axial location are determined in an iterative manner by estimating the static pressure at the axial location, computing the resulting total area of the streamtubes, and repeating the procedure until the computed total flow area equals the actual flow area normal to the passage center-line. The actual flow area is determined from the effective wall geometry obtained from the actual wall position and the estimate of boundary-layer displacement thicknesses.

The details of the procedure are as follows (where the subscript j refers to a streamtube and the subscript i refers to an axial location of a geometric input point):

1. As a first estimate, assume that the relative mid-streamtube streamline slope at $i+1$ is equal to that at i :

$$(\mathcal{Y}_{rj})_{i+1} = (\mathcal{Y}_{rj})_i \quad (30)$$

where
$$\mathcal{Y}_{rj} = \mathcal{Y}_j - \frac{\mathcal{Y}_L + \mathcal{Y}_U}{2}$$

$$\mathcal{Y}_j = \text{mid-streamtube streamline slope}$$

For the first axial location downstream of the inlet, assume

$$(\mathcal{Y}_{rj})_{i+1} = \left[\mathcal{Y}_{rL} + \frac{1}{N} (\mathcal{Y}_{rU} - \mathcal{Y}_{rL}) \right]_{i+1}$$

(since the relative streamline slope at the inlet is always assumed to be zero).

2. Estimate the pressure at the next axial location (i+1)

from

$$TA_{i+1} = \sum_{j=1}^N \left[\frac{\dot{m}_j^2 / 2 \rho_j g_o}{\dot{m}_j^2 / 2 \rho_j g_o A_j^2 - \Delta p} \right]^{1/2} (\cos \gamma_{rj})_i$$

and $p_{i+1} = p_i + \Delta p$ (31)

where TA_i = effective total area at axial Station i

$$= \pi \left\{ \left[\left(r_U - \delta_U \frac{\cos \gamma_{rU}}{\cos \frac{\gamma_U + \gamma_L}{2}} \right)^2 - \left(r_L + \delta_L \frac{\cos \gamma_{rL}}{\cos \frac{\gamma_L + \gamma_U}{2}} \right)^2 \right] \cos \frac{\gamma_U + \gamma_L}{2} \right\}_i$$

3. Calculate the static-to-total pressure ratio for each streamtube, p_{i+1}/p_i , and determine T_j/T_{01} , u_j , and A_j at i+1 from the usual compressible flow relations.
4. Compute total flow area based on initial estimate of streamline slope from

$$(TA)_{i+1} = \left(\sum_{j=1}^N A_j \cos \gamma_{rj} \right)_{i+1} \quad (32)$$

5. Reestimate the relative slope of each mid-streamtube streamline from

$$(\gamma_{rj})_{i+1} = \left[\gamma_{rL} + \gamma_j (\gamma_{rU} - \gamma_{rL}) \right]_{i+1} \quad (33)$$

where
$$\gamma_j = \frac{\sum_{k=1}^j (A_k \cos \gamma_{rk}) - \frac{A_j}{2} \cos \gamma_{rj}}{\sum_{k=1}^N (A_k \cos \gamma_{rk})}$$

and k is a dummy index.

6. Compute revised total flow area based on new estimate of streamline slope from Equation 33. Repeat Step 5 until two consecutive values of $(TA)_{i+1}$ are equal.

7. If $(TA)_{i+1}'$ does not equal TA_{i+1} obtained from Equation 31, then repeat entire process from Step 2 with $p_i, \rho_{ji}, A_{ji}, \mathcal{Y}_{ji}$ in Equation 30 being replaced by the current values of $p_{i+1}, \rho_{j,i+1}, A_{j,i+1}, \mathcal{Y}_{j,i+1}$.
8. Continue the preceding process until $p_2, \rho_{j2}, A_{j2}, \mathcal{Y}_{j2}, u_{j2}$ are obtained at the exit station of the diffuser.

Determination of Boundary-Layer Displacement Thickness

With the velocity, u_i , and density, ρ_i , in the bounding stream-tubes ($j=1$ and $j=N$) known, a new estimate of the boundary-layer displacement thickness along each wall is made in the following way:

1. The momentum thickness at each axial station i is computed from the following relation, derived in Appendix II from

the momentum integral equation for boundary layers:

$$\theta_{j,i+1} = \left[\theta_{j,i} \left(\frac{u_{j,i}}{u_{j,i+1}} \right)^{25/6} \left(\frac{\rho_{j,i}}{\rho_{j,i+1}} \right)^{7/6} + \frac{0.0076 \nu^{1/6}}{u_{j,i+1}^{25/6} \rho_{j,i}^{7/6}} \int_{x_i}^{x_{i+1}} \rho_j^{7/6} u_j^4 dx' \right]^{6/7} \quad (34)$$

where $j=1$ or N (referring to L and U walls, respectively)

and

$$x_{i+1}' - x_i' = (x_{i+1} - x_i) \frac{1}{\cos \left[\left(\frac{\mathcal{Y}_U + \mathcal{Y}_L}{4} \right)_i + \left(\frac{\mathcal{Y}_U + \mathcal{Y}_L}{4} \right)_{i+1} \right]} \quad (35)$$

2. The shape factor, H , of the boundary layer along each wall is computed from the empirical relationship of Dussord (Ref 25):

$$H_{j,i+1} = H_{j,i} + 70(H_{j,i} - 1.05) \frac{d\theta_j}{dx} \quad (36)$$

H_j is never permitted to be less than 1.1, since this relationship is not valid for highly accelerating flows, and since

the characteristics of the boundary layer when subjected to highly favorable gradients are of little interest in the present application. H_j is also never permitted to exceed 3.5; this value exceeds any reasonable separation value.

3. For all axial locations at which H does not exceed H_{sep} on either wall, calculate the resulting displacement thickness along each wall from

$$\delta'_{j,i} = H_{j,i} \theta_{j,i}$$

For axial locations where $H > H_{sep}$ on either wall, proceed to Step 5.

4. Since this value of displacement thickness tends to interact substantially with the bounding streamtube velocity, a new estimate of the displacement thickness is determined from the following relation:

$$\delta_{j,i} = \delta_{oj} + 0.2 \frac{\delta''_{1,i} - \delta_{o1,i}}{|\delta''_{j,i} - \delta_{oj}|} \quad (37)$$

where the subscript o refers to the initial estimates supplied as input to the boundary-layer calculation. $\delta''_{1,i}$ and $\delta''_{N,i}$ are determined from the solution to the following equations (derived in Appendix III):

$$(\psi_{1,i} + 1) \delta''_{1,i} + \psi_{1,i} \delta''_{N,i} = \delta'_{1,i} [1 - \psi_{1,i}] + \psi_{1,i} (\delta_{o1,i} + \delta_{oN,i})$$

$$\psi_{N,i} \delta''_{1,i} + (\psi_{N,i} + 1) \delta''_{N,i} = \delta'_{N,i} [1 - \psi_{N,i}] + \psi_{N,i} (\delta_{o1,i} + \delta_{oN,i})$$

where

$$\psi_{j,i} = \frac{\delta'_{1,i}}{r_B - r_A} \left[240 \frac{H_{o1,i}^{-1.05}}{H_{j,i}} \cdot \frac{\theta_{1,i}}{x_i - x_{i-1}} + \frac{24}{7} \right]$$

$$\varphi_{j,i} = 70 \frac{H_{oj,i} - 1.05}{H_{j,i}} \cdot \frac{\Delta\theta_{j,i-1}}{x_i - x_{i-1}}$$

$$\Delta\theta_{j,i-1} = -3.3 \theta_{j,i-1} \frac{\delta_{l,i-1}'' + \delta_{N,i-1}'' - \delta_{ol,i-1} - \delta_{oN,i-1}}{r_{U,i-1} - r_{L,i-1}}$$

If no separation occurs along either wall at any axial location, proceed to Step 7.

5. If $H > H_{sep}$ on either wall at an axial location, set $H = 3.5$ on the separated wall for reference purposes, and calculate the displacement thickness along the separation wall from, for example:

$$(r_L \cos \mathcal{J}_{cl} + \delta_l \cos \mathcal{J}_{rL})_i = \sqrt{(r_U \cos \mathcal{J}_{cl} - \delta_N \cos \mathcal{J}_{rU})_i^2 - \frac{(TA)_{sep} \cos \mathcal{J}_{cl,i}}{\pi}}$$

where $(TA)_{sep}$ = effective flow area at the separation point

$$= \pi \left\{ \frac{(r_U \cos \mathcal{J}_{cl} - \delta_N \cos \mathcal{J}_{rU})^2 - (r_L \cos \mathcal{J}_{cl} + \delta_l \cos \mathcal{J}_{rL})^2}{\cos \mathcal{J}_{cl} \cos \left(\frac{\mathcal{J}_{rL} + \mathcal{J}_{rU}}{4} \right)} \right\}_{sep}$$

and $\mathcal{J}_{cl} = \frac{\mathcal{J}_U + \mathcal{J}_L}{2}$

This assumes that the static pressure and hence the flow area remains constant after separation.

6. In the separated flow region, estimate the new values of displacement thickness from

$$\delta_{j,i} = \frac{1}{2} (\delta_{oj,i} + \delta'_{j,i})$$

7. If the newly estimated values of $\delta_{j,i}$ are not equal to the originally estimated ones, $\delta_{oj,i}$, return to the streamtube calculation with the newly estimated values. Repeat both

streamtube and boundary-layer calculations until agreement is obtained.

Determination of Diffuser Performance Parameters
and Outlet Conditions

The diffuser performance parameters of ideal pressure-recovery coefficient, actual pressure-recovery coefficient, and effectiveness are calculated in the following way:

$$C_{pi} = 1 - \left(\frac{A_1}{A_2}\right)^2 \quad (38)$$

$$C_p = \frac{p_2 - p_1}{\bar{q}_1} \quad (39)$$

$$\xi = \frac{C_p}{C_{pi}} \quad (40)$$

where \bar{q}_1 is the inlet dynamic head obtained from Equation 29.

The outlet conditions of p_2 , $\rho_2(r)$, $u_2(r)$ are directly available from the procedure, as well as ρ_j , u_j , \dot{m}_j , A_j for each streamtube. The blockage due to displacement thickness is also computed from

$$E_{bl} = 1 - \frac{\left(r_{U2} - \delta_{U2} \cdot \frac{\cos \mathcal{J}_{rU2}}{\cos \mathcal{J}_{c12}} \right)^2 - \left(r_{L2} + \delta_{L2} \cdot \frac{\cos \mathcal{J}_{rL2}}{\cos \mathcal{J}_{c12}} \right)^2}{r_{U2}^2 - r_{L2}^2} \quad (41)$$

In the computer program, only $u_2(r)$, p_2 , $p(x_i)$, $\delta(x_i)$, and $H(x_i)$ are printed as output information; the remainder of the quantities are used internally in transferring from one diffusing passage to another.

Limitations of the Method

The major limitations of the method are as follows:

1. Diffusers which are highly curved or in which streamline curvature effects are otherwise important (such as in mildly stalled diffusers) cannot be treated. In these cases, the

- static-pressure gradients across the passage are significant.
2. The results of the method tend to be quite sensitive to the inlet boundary-layer properties; an accurate estimate of these properties at the diffuser inlet is difficult in practical situations. (A method for estimating the inlet shape factor is outlined in Appendix IV.)
 3. The determination of the location of separation is subject to error. This is an age-old fluid-mechanics problem which remains beyond the reach of the present technological era.

The method does, however, represent a substantial improvement over the empirical-data method, and should be capable of treating a large number of diffusers accurately, particularly as experience with the use of the method increases.

Mixing-Equation Method

The mixing-equation method can only be applied to the diffusing passages 2-4A and 2-4B, and represents a very crude model of the flow in these diffusing passages.

Assumptions

The assumptions employed in the method are:

1. The losses in the diffusing process can be represented as the sum of mixing losses, losses due to curvature of the passage, and expansion or contraction losses at the snout lip.
2. The mixing losses can be evaluated from the determination of the pressure-recovery coefficient for incompressible flow, wherein the variation of the profile parameter, β ,

with passage area is of the form

$$\frac{A}{\beta - K} = \text{constant}$$

where $K > \beta_1$. This is merely a qualitative indication that the mixing process is delayed by diffusion.

Input Information Required

The information required by this method is:

1. The geometry of the passage, in terms of inlet area, exit area, the total angle difference between the slope of the passage center-line at inlet and that at exit, and the mean radius of curvature of the passage center-line.
2. The inlet conditions defined by \dot{m} , p_1 , \bar{q}_1 , and β_1 ; the subscript 1 here refers to conditions determined at diffuser Station 2.
3. The ratio of the area at diffuser Station 2 occupied by the mass flow in the annulus under consideration to the annulus area normal to the engine center-line at diffuser Station 2',

$A_{th}/A_{2'}$. That is, for example,

$$(A_{th})_{2A} = \pi [(r_{th})_{2A}^2 - (r_{2A})^2] \quad (42)$$

where $(r_{th})_{2A}$ is determined from

$$\dot{m}_A = \int_{r_{2A}}^{(r_{th})_{2A}} 2\pi r \rho u dr \quad (43)$$

where \dot{m}_A = mass flow in inner annulus

r_{2A} = radius of inner casing at Station 2A

ρ, u = properties from diffuser solution (Station 2)

A similar calculation may be performed for the outer annulus.

PAGES 57 AND 58
ARE MISSING FROM
ORIGINAL DOCUMENT

2. Calculate the diffuser performance between Stations 1 and 2, and the outlet conditions at 2, by either the empirical-data or streamtube method.
3. Determine inlet conditions for the second stage of diffusion in a form suitable for the diffuser analysis method to be used between Stations 2-3A and 2-3B, and the inlet conditions to the snout (if any).
4. Determine the stagnation pressure on the dome.
5. If the diffuser has no snout, determine the inlet conditions to the annuli by assuming an isentropic expansion around the dome.
6. If the diffuser has a snout, calculate the diffuser performance between Stations 2-4A and 2-4B and the outlet conditions at 4A and 4B, by using the empirical-data method or the streamtube method between Stations 2-3A and 2-3B and a mixing analysis between Stations 3A-4A and 3B-4B, or by using the mixing equation method between Stations 2-4A and 2-4B.

The following sections indicate the significant details of these steps, for the various combinations of analysis methods which can be used. These are five such combinations for diffusers with snouts:

Stations 1-2	Stations 2-4
Streamtube	Streamtube
Streamtube	Empirical data
Streamtube	Mixing equation
Empirical data	Empirical data
Empirical data	Mixing equation

It is pointed out that when the streamtube or empirical-data methods are used between Stations 2-4, it is always implied that the methods are used between Stations 2-3 followed by a mixing analysis between Stations 3 and 4.

For diffusers without snouts, the analysis of the flow between Stations 2-4 is independent of the option employed between Stations 1-2; this is indicated subsequently.

Determination of Inlet Conditions, Station 1

The inlet conditions to the diffuser which are available from the program input are:

1. Mass flow, \dot{m} .
2. Weight-mean total pressure, \bar{P}_1 .
3. Total temperature, T_{01} .
4. A nondimensional velocity profile, u/U .
5. The shape factor of the boundary layer, H_1 .
6. The inlet blockage, $1-E_1$, if the empirical-data method is to be used, or the fractional area occupied by the boundary-layer displacement thickness, $1-E_{b1}$, if the streamtube method is to be used.
7. The fraction of $1-E_{b1}$ which is on the inner wall.

If the streamtube method is used between Stations 1 and 2, this information is in the proper form to enter the method directly.

If the empirical-data method is used between Stations 1 and 2, it is necessary to determine the static pressure and the inlet dynamic head from the above information. The static pressure is determined by an

iterative solution of the following relations:

$$T_{01} = T_1 + \frac{\bar{u}_m^2}{2g_0 J c_p}$$

$$p_1 = \bar{\rho}_1 R T_1$$

$$\dot{m} = \bar{\rho}_1 \bar{u}_m E_1 A_1$$

$$\frac{p_1}{p_0} = \left(\frac{T_1}{T_{01}} \right)^{\frac{\gamma}{\gamma-1}}$$

which also yields \bar{u}_m , $\bar{\rho}_1$, and hence \bar{q}_1 .

Diffuser Performance Between Stations 1 and 2

This is accomplished by either the empirical-data method or the streamtube method, as previously described. A summary of the input and calculated quantities is given below:

Streamtube Method		Empirical-Data Method	
Input	Calculated	Input	Calculated
\dot{m}	$p_2^* \rho(x_1)^*$	\dot{m}	p_2
\bar{p}_1	$\rho_2(r)$	p_1	E_2
T_{01}	$u_2(r)^*$	\bar{q}_1	$\bar{\rho}_2$
$u_1(r)/U$		E_1	\bar{u}_m^*
E_{b11}			\bar{T}_2
H_1	$E_{b12}, \delta(x_1)^*, H(x_1)^*$		c_{pi}^*
	c_{pi}^*		c_p^*
	c_p^*		ξ_1^*
	ξ_1^*		

The asterisks in the above table denote quantities which are printed as output data by the program. The subscript i refers to axial locations of geometric input points.

Inlet Flow Conditions for Second
Stage of Diffusion

For diffusers without snouts, the only additional information required is the mass flow split, \dot{m}_A , \dot{m}_B , \dot{m}_S . This is supplied as input from the air-flow subprogram.

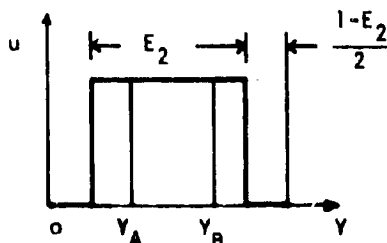
For diffusers with snouts, the information required in addition to the mass flow split, consists of the flow properties A_{th} , \bar{u}_a , β (or E) to be associated with the flows into the inner annulus, the outer annulus, and the snout. These are obtained somewhat differently, depending upon whether the empirical-data method or the streamtube method is used between Stations 1 and 2.

If the empirical-data method is used between Stations 1 and 2, these quantities are determined as follows:

1. The nondimensional annulus heights at Station 2 which bound the flow into the two annuli are calculated from (see sketch):

$$Y_A = \frac{1-E_2}{2} + \frac{\dot{m}_A}{\dot{m}} E_2 \quad (51)$$

$$Y_B = 1 - \left(\frac{1-E_2}{2} + \frac{\dot{m}_B}{\dot{m}} E_2 \right) \quad (52)$$



2. The areas of the passage at Station 2 which are occupied by the mass flows \dot{m}_A , \dot{m}_B , and \dot{m}_S are calculated from:

$$A_{th,2A} = A_2 Y_A \quad (53)$$

$$A_{th,2B} = A_2 (1 - Y_B) \quad (54)$$

$$A_{th,2s} = A_2 - A_{th,2A} - A_{th,2B} \quad (55)$$

3. The inlet blockages associated with the flows into the two annuli are calculated from:

$$E_{2A} = \frac{\dot{m}_A}{\dot{m}} \frac{E_2}{Y_A} \quad (56)$$

$$E_{2B} = \frac{\dot{m}_B}{\dot{m}} \frac{E_2}{1 - Y_B} \quad (57)$$

and hence

$$\beta_{2A,2B} = E_{2A,2B}^{-1} \quad (58)$$

It is assumed that $\beta_{2s} = E_{2s} = 1$.

4. The area-average velocities are determined from:

$$\bar{u}_{a,2A} = E_{2A} \bar{u}_{m2} \quad (59)$$

$$\bar{u}_{a,2B} = E_{2B} \bar{u}_{m2} \quad (60)$$

$$\bar{u}_{a,2s} = \bar{u}_{m2} \quad (61)$$

If the streamtube method is used between Stations 1 and 2, these same quantities are determined as follows:

1. The area of the passage at Station 2, $A_{th,2A}$ and $A_{th,2B}$, which are occupied by the mass flows \dot{m}_A and \dot{m}_B are determined from Equations 42 and 43 applied to both mass flows. Then $A_{th,2s}$ is determined from Equation 55.
2. The inlet area average velocities are determined from

$$\bar{u}_{a,2A} = \frac{1}{A_{th,2A}} \int_0^{A_{th,2A}} u dA \quad (62)$$

and a similar equation for $\bar{u}_{a,2B}$.

3. The inlet velocity profile parameters are calculated from

$$\beta_{2A} = \frac{\int_0^{A_{th,2A}} u^2 dA}{A_{th,2A} u_{a,2A}^2} \quad (63)$$

and a similar equation for β_{2B} . Again, it is assumed that $\beta_{2s} = 1$.

4. If the empirical-data method is to be used between Stations 2 and 3, the inlet blockages associated with the flows in the two annuli are calculated from:

$$E_{2A} = \frac{\delta_{2A}}{\delta_{2A} + \delta_{2B}} E_{b1,2} \quad (64)$$

$$E_{2B} = \frac{\delta_{2B}}{\delta_{2A} + \delta_{2B}} E_{b1,2} \quad (65)$$

For the purposes of the diffuser analysis between Stations 2 and 3, the areas of the diffusing passages at Station 2' are assumed to be

$$A_{th,2A'} = A_{th,2A} \cos \mathcal{J}_{C,A} \quad (66)$$

and

$$A_{th,2B'} = A_{th,2B} \cos \mathcal{J}_{C,B} \quad (67)$$

where \mathcal{J}_C is the angle of the slope of the passage center-line relative to the axis of the combustor. This assumes in effect that the inlet areas to the annular diffusing passages are the areas occupied by the respective flows at Station 2, projected normal to the passage center-line. It is obvious that this assumption is not valid when the areas $A_{th,2A'}$ and $A_{th,2B'}$ differ substantially from the actual geometrical areas of the diffusing passages at Station 2' ($A'_2 \cos \mathcal{J}_C$). The output of the computer program includes the ratios $A_{th,2B'}/A_{2B'}$ and $A_{th,2A'}/A_{2A'}$ (denoted as "area mismatch at the snout" in the program).

The inlet dynamic heads at the diffusing passages are calculated

from:

$$\bar{q}_{2A} = \frac{1}{2g_0} \frac{\dot{m}_A \beta_{2A}^2 \bar{u}_{a,2A}}{A_{th,2A}} \quad (68)$$

and a similar equation for \bar{q}_{2B} . The inlet dynamic head at the snout is determined from:

$$\bar{q}_{2s} = \frac{1}{2g_0} \frac{\dot{m}_s \bar{u}_{m2}^2}{A_{th,2s}} \quad (69)$$

Conditions on the Dome

If the diffuser has no snout, the stagnation pressure on the dome is assumed to be constant and is determined by

$$P_d = P_2 + (1 - K_d) \bar{q}_2 \quad (70)$$

where

$$\bar{q}_2 = \frac{1}{2g_0} \bar{f}_2 \frac{\bar{u}_m^2}{m^2} \quad (71)$$

The coefficient K_d is an input quantity representing the number of dynamic heads lost in the mixing and flow processes occurring around the dome.

The magnitude of K_d will depend upon the shape of the dome and the effectiveness of the diffuser between Stations 1 and 2, and is difficult to determine a priori. It is expected that its value would be in the range 0.2 - 0.5.

For diffusers with snouts, the static pressure just inside the snout, P_{2s} , is determined by assuming a sudden contraction or expansion process between the areas $A_{th,2s}$ and A_{2s} (the actual geometric area of the snout entrance); this is accomplished by the application of Equation 44 or 45. The dynamic head just inside the snout is calculated from

$$\bar{q}_{2s'} = \left(\frac{A_{th,2s}}{A_{2s}} \right)^2 \bar{q}_{2s}$$

The total pressure on the dome is then calculated from

$$P_d = P_{2s} + (1 - K_d) \bar{q}_{2s} \quad (72)$$

where K_d is an input quantity representing the number of dynamic heads lost in the flow through the snout.

Diffuser Exit Conditions If No Snout is Present

If no snout is present, the diffuser exit conditions at Stations 4A and 4B (the entrances to the annuli) are calculated by assuming that the flow expands isentropically from the dome stagnation pressure determined by Equation 70. For either annulus, the conditions at Station 4 are completely determined by \dot{m}_A (or \dot{m}_B), T_0 , P_d , and A_{4A} (or A_{4B}).

Diffuser Performance Between Stations 2 and 4 for Diffusers with Snouts

The procedure for determining the performance of the diffusing passages between Stations 2 and 4 depends upon the diffuser-analysis method employed. The procedures are indicated below.

Mixing-Equation Method

In this case, the procedure is identical to that described previously. The inputs required for the analysis are \dot{m}_A , P_2 , \bar{q}_{2A} , β_{2A} , $A_{th,2A}$ and a similar set for the outer annulus; these are determined in the manner indicated in the previous paragraphs. The calculated quantities are C_{pmA} , C_{pA} , ξ_{mA} , P_{4A} , T_{4A} , P_{4A} and a similar set for the outer annulus. All of these quantities are printed out by the computer program.

Streamtube Method

In this method, three steps are involved since the basic streamtube analysis is only applicable between Stations 2 and 3, and does not

consider any losses due to expansion or contraction of the flow at the snout lip. The steps are as follows:

1. A basic streamtube analysis, as previously described, is performed between Stations 2A-3A and 2B-3B. The inputs required for this analysis are \dot{m}_A , $A_{th,2A}$, p_2 , $u_2(r)$, δ_{2A} , H_{2A} and a similar set for the outer annulus; in addition it is assumed that the boundary-layer properties on the snout lip are $\delta = 0$ and $H = 1.4$. The only calculated quantities which are used subsequently are the static pressures, p_{3A} and p_{3B} , and the profile parameters, β_{3A} and β_{3B} , which are computed from Equation 63 applied to Stations 3A and 3B. The diffuser performance parameters C_p , C_{pi} , and ξ_1 as obtained from this analysis are printed as program output, however.
2. It is assumed that the profile mixes to a uniform one between Stations 3 and 4. The static pressure at Station 4 in the absence of area mismatch at the snout lip is accordingly obtained from Equation 5-7 in Appendix V:

$$\frac{p'_{4A} - p_{3A}}{\bar{q}_{3A}} = \frac{1}{\beta_{3A}^2} \left(1 + \frac{A_{3A}}{A_{4A}} \right) \left(\beta_{3A} - \frac{A_{3A}}{A_{4A}} \right) \quad (73)$$

3. The effects of any area mismatch at the snout are rather crudely approximated by assuming that the total-pressure loss between Stations 2 and 4 due to this process is given by the sudden expansion or contraction relations (Equations 46 and 47), and that this loss may be applied directly at

Station 4; that is, in the inner annulus for example:

$$\frac{P_{4A} - P'_{4A}}{\bar{q}_{2A}} = \frac{1}{2} \left(1 - \frac{A_{2A'}}{A_{th,2A'}} \right) \left(\frac{A_{th,2A'}}{A_{2A'}} \right)^2 \quad (74)$$

if $A_{2A'}/A_{th,2A'} < 1$. P'_{4A} is the total pressure corresponding to P'_{4A} , T_0 , \dot{m}_A , and A_{4A} .

The calculated quantities are the diffuser performance parameters C_{pm} , C_p , and ξ_m between Stations 2A-4A and 2B-4B, and the flow conditions P_{4A} , P'_{4A} , T_{4A} , P_{4B} , P'_{4B} , and T_{4B} . All of these quantities are part of the printed output of the computer program.

Empirical-Data Method

As in the streamtube method, three steps are involved in the procedure:

1. The basic empirical-data method, as previously described, is performed between Stations 2A-3A and 2B-3B. The inputs required for this calculation are \dot{m}_A , $A_{th,2A'}$, P_2 , \bar{q}_{2A} , E_{2A} , and a similar set for the outer annulus. The only calculated quantities which are used subsequently are the static pressures P_{3A} and P_{4A} , and the profile parameters β_{3A} ($= E_{3A}^{-1}$) and β_{4A} ($= E_{4A}^{-1}$). The diffuser performance parameters C_p , C_{pi} , and ξ as obtained from the basic method are printed as program output.
2. A mixing analysis is applied to the flow between Stations 3A-4A and 3B-4B. This is identical to the procedure used for the streamtube method.
3. The effects of any area mismatch at the snout are included in the manner used for the streamtube method.

The calculated quantities and the program output are identical

to those of the streamtube method.

Structure of the Subprogram

The diffuser subprogram consists of:

1. A subroutine which sets up starting conditions and directs the diffuser calculation through the other subroutines in the appropriate sequence.
2. A group of subroutines which perform the streamtube analysis.
3. A group of subroutines which perform the empirical-data analysis.
4. A group of library subroutines which provide gas properties and interpolation procedures.

Detailed flow charts and the program listings for the diffuser subprogram are presented in Volume II.

AIR-FLOW SUBPROGRAM - ANALYTICAL METHODS AND PROGRAM DEVELOPMENT

Introduction

The main objectives of the air-flow subprogram are:

1. To calculate the air mass flow and pressure distribution in the flame tube and annuli and, hence, the overall pressure loss.
2. To provide a starting point for the heat-transfer calculation by working out the temperature and velocity distributions of the gases in the flame tube and annuli.

To facilitate analysis, flow in the combustor is broken down into distinct but interacting streams:

1. The annulus air (inner and outer annuli).
2. The air flowing into the flame tube through:
 - a. Swirler.
 - b. Dome holes.
 - c. Penetration holes in the flame tube.
 - d. Wall-cooling slots in the flame tube.
 - e. Porous flame-tube walls.
3. The mixture of fuel, air, and combustion products flowing through the primary zone (the flame tube upstream of the secondary holes).
4. Parallel streams flowing through the flame tube downstream of the primary zone:
 - a. The hot stream, a mixture of combustion products, unburned fuel, and air.
 - b. The cold streams, those portions of the penetration jets and wall-cooling films, originating upstream, that remain unmixed at a given axial position.

This section of the report is devoted to a detailed description of the calculation methods and general organization of the air-flow subprogram.

Assumptions

The air-flow calculation rests on the following main assumptions, in addition to those discussed under OVERALL APPROACH:

1. The primary zone can be treated as a stirred reactor:
 - a. Static pressure, temperature, and fuel-air ratio are uniform throughout the zone.
 - b. Mixing and burning occur instantaneously.

This is one of the major simplifications in this work, and it precludes the possibility of calculating, for example, pressure distributions in this zone. It will be particularly invalid at low pressures, when burning in the primary zone is reaction-rate limited, unless an accurate estimate of the fuel-burning-rate distribution (see assumption 3) has been made.

2. The flow can be considered to be one-dimensional. This represents a considerable simplification, particularly in the case of the gases in the flame tube. However, reasonably simple methods are not available at the present time for treating flow and heat transfer in a gas stream having non-uniform temperature and velocity profiles.
3. The rate of fuel burning as a function of axial length can be specified as input. This assumption makes the calculations easier but a realistic estimate of the fuel-

burning rate will be difficult to make, particularly (as mentioned above) at low pressures. If the fuel-air ratio at any axial position, which will not be known in advance, exceeds the stoichiometric value, the excess fuel is assumed to be available for burning at the next downstream position.

Calculation Procedure - Outline

In calculating the flow conditions throughout the combustor, the air-flow subprogram goes through the following routine for each iteration on the mass-flow split:

1. The mass-flow rate through the dome is obtained from the flow split, and the total pressure on the dome is obtained from the diffuser calculation.
2. The pressure drop across the dome to the primary zone is found by equating the combined swirler and dome-hole flows (functions of pressure drop) to the total dome flow.
3. With the primary-zone static pressure established, flow conditions in the annulus and flow through flame-tube holes into the primary zone are computed for calculation stations up to the secondary holes (the end of the primary zone).
4. The portion of the secondary-hole flow that recirculates into the primary zone is calculated, either directly by the program or from a fraction specified as input.

All of the contributions to primary-zone air flow (through the swirler, dome holes, and flame-tube holes up to the secondary holes) are now known. In addition, the fuel flow into the primary zone is known from input.

5. The temperature rise due to combustion is calculated for the primary zone treated as a stirred reactor. (Excess fuel above stoichiometric is carried downstream.) Flow conditions at the end of the primary zone are then found.

For the remainder of the calculation the combustor is divided into axial control volumes bounded by adjacent calculation stations k and $k + 1$. Calculations proceed downstream from station to station. In general, the flow conditions at the upstream station, k , are known from the results of the previous calculation step. Conditions at the downstream station are found as follows:

6. From the annulus-to-flame-tube pressure drop at station k the mass flow rate through the holes just downstream of k is found. The mass flow remaining in the annulus is then known.
7. For the annulus, the equations of momentum, energy, continuity, and state are solved for the pressure, temperature, velocity, and density at station $k + 1$.
8. Correlations for flow and mixing of wall and penetration jets are used to compute the fluxes of mass, axial momentum, and enthalpy contained in the jets entering the control volume (through holes at station k and in the form of residual jets originating upstream of k) and leaving the control volume (residual jets at $k + 1$). The net transfer of mass, momentum, and enthalpy from the jets into the main gas stream in the flame tube may thus be found.
9. The equations of momentum, energy, continuity, and state are

written for the hot stream in the flame tube (excluding residual jets) between stations k and $k + 1$. Heat addition is included for fuel burned, up to stoichiometric; any excess fuel is carried downstream. The solution of these equations yields the temperature, pressure, density, and mass flow at station $k + 1$.

The sections that follow describe the detailed calculations that are performed in each of the above steps.

Flow Through Holes and Swirler; Swirler Design; Recirculation Flow Through Holes

The mass flow rates through the holes in the dome and in the flame-tube walls are calculated from the discharge equation:

$$\dot{m}_h = C_d A_h (2g_o \rho_{an} (P_{an} - p_{ft}))^{\frac{1}{2}} \quad (75)$$

where P_{an} = total pressure in annulus

$$= p_{an} + q_{an}$$

$$q_{an} = \rho_{an} u_{an}^2 / 2g_o$$

C_d = discharge coefficient

Discharge Coefficients

For dome holes a value of 0.6 is used for the discharge coefficient.

For flame-tube holes a table of experimentally measured discharge coefficients for 100 hole types is supplied as library data. An index to these hole types is given in Table I of Volume II. (Data for other hole types may be added to the library as required.) The tabulated data are drawn from experiments reported by Venneman (Refs 28 and 29), Marshall (Ref 30), Kaddah (Ref 31), and Dittrich and Graves (Ref 32 and 33).

The discharge coefficient is plotted against the hole pressure-loss factor:

$$\frac{P_{an} - P_{ft}}{q_{an}} = 1 + \frac{\Delta P_h}{q_{an}} \quad (76)$$

where $\Delta P_h = P_{an} - P_{ft}$

P_{ft} = Static pressure in flame tube

Pressure-Ratio Correction

It has been shown by Dittrich and Graves (Ref 32) that the effect of flame-tube velocity on discharge coefficient can be predicted by:

$$C_d = C_d^1 (0.75 + 0.25 p_{an}/p_{ft}) \quad (77)$$

where C_d = the actual discharge coefficient (which is a function of pressure ratio)

C_d^1 = the "corrected" discharge coefficient (which is independent of pressure ratio)

The values given on the library tape are corrected discharge coefficients.

In Equation 77, p_{an} is replaced by P_{an} if the hole is a scoop or other total-head device.

Swirler Flow

The equation used in the program for the flow through a swirler was taken from Reference 3¹¹:

$$\frac{\Delta P_{sw}}{q_{ref}} = K_{sw} \left[\frac{A_{ref}^2}{A_{sw}^2} \sec^2 \beta_{sw} - \frac{A_{ref}^2}{A_{ft}^2} \right] \frac{\dot{m}_{sw}^2}{\dot{m}_{ref}^2} \quad (78)$$

where A = area, ft^2

\dot{m} = mass flow, lbm per sec

q = dynamic head, lbf per ft^2

β = swirler angle

ΔP_d = total-to-static pressure drop, lbf per ft²

sw = swirler

ref = reference condition

ft = flame tube

In the program the constant K_{sw} has been given a value of 1.3, which is suitable for straight-bladed swirlers. For curved-wall swirlers, the value of K_{sw} could be changed to 1.15.

Swirler Design

A comprehensive literature search brought to light virtually no work on which such a sound theoretical swirler design method could be based. The method used is therefore based on an examination of swirler designs that have previously been used on 16 combustors, mainly of the tubular type. The results are shown in Figure 10. Although the range of D_{ft} does not cover the values normally encountered in annular combustors, the following may be used until more information on swirlers is available:

$$\text{Swirler O.D.} = 0.225 D_{ft} + 0.75 \text{ in}$$

$$\text{Swirler I.D.} = 0.10 D_{ft} + 0.25 \text{ in}$$

$$\text{No. of Blades} = 8$$

$$\text{Blade angle} = 50 \text{ degrees}$$

Recirculation

In an actual combustor a complex pattern of recirculating flow exists, particularly in the primary zone. Representation of recirculation is introduced in the computer program by a provision for partial recirculation of secondary-hole flow upstream into the primary zone. Only the flow through the secondary holes is treated in this way.

The fraction of secondary-hole air flowing into the primary zone, $\dot{m}_{sy,p}/\dot{m}_{sy}$, may be specified as input to the computer program. This must be set to zero if recirculation is not to be considered. If the recirculation fraction is not specified as input, it is generated within the program from the following formula:

$$\frac{\dot{m}_{sy,p}}{\dot{m}_{sy}} = 0.5 \sin \varphi \left[\frac{T_{an}}{T_{ft}} \right]^{1/2} \quad (79)$$

This is an empirical expression based chiefly on measurements obtained by Rosenthal (Ref 35) in a tubular combustor.

The air entering the primary zone by recirculation from the secondary holes is treated in exactly the same way as air entering through swirler, dome, and wall holes. Air going downstream is treated as ordinary penetration-jet air.

Primary Zone of Flame Tube

Pressure

The pressure in the primary zone, p_1 , is found from the pressure in the diffuser upstream of the dome, P_d , obtained by the diffuser sub-program, and the pressure drop across the dome, which is a function of the flow through the dome and the characteristics of the swirler and the dome holes:

$$P_d - p_1 = \frac{\dot{m}_d^2}{2 g_o \rho_{ref} \left[A_{dh} C_{dh} + \frac{1}{\sqrt{K_{sw} \left[\frac{\sec^2 \beta_{sw}}{A_{sw}^2} - \frac{1}{A_{ft}^2} \right]}} \right]^2} \quad (80)$$

where \dot{m}_d = total flow through dome

$$= \dot{m}_{sw} + \dot{m}_{dh}$$

\dot{m}_{dh} = flow through dome holes

C_{dh} = discharge coefficient of dome holes

K_{sw} = coefficient in swirler pressure-drop equation

β_{sw} = blade angle of swirler

A_{ft} = cross-sectional area of primary zone

This equation is derived in Appendix VI.

Temperature Rise

The energy equation for combustion in the primary zone takes the following form:

$$\dot{m}_1 h_{air, T_1} + \dot{q} = (\dot{m}_1 + \dot{m}_{fb}) h_{prod, T_2} \quad (81)$$

where \dot{m}_1 = air mass-flow rate

\dot{m}_{fb} = fuel burning rate

\dot{q} = heat release rate

h_{air} = enthalpy of air

h_{prod} = enthalpy of combustion products

and subscripts 1 and 2 refer to conditions before and after combustion, respectively. Velocity terms have been neglected because mean velocities in the primary zone are usually quite small.

The enthalpies of air and combustion products are calculated from the expression:

$$h = \int c_p \cdot dT \quad (82)$$

where the specific heat of air as a function of temperature is correlated by:

$$c_p = 0.2419 - 0.8181 \times 10^{-5} T + 17.91 \times 10^{-9} T^2 - 2.743 \times 10^{-12} T^3 \quad (83)$$

The data of Fielding and Topps (Ref 36), shown here in Figure 11, have been used to modify Equation 83 for calculating the specific heat of combustion products:

$$c_p = 0.2419 + 0.103f - (0.8181 - 22.6f) 10^{-5}T + (17.91 - 29.6f) 10^{-9}T^2 - (2.743 - 0.35f) 10^{-12}T^3 \quad (84)$$

where f = local fuel-air ratio.

This equation is suitable up to stoichiometric values of the fuel-air ratio:

$$f_{\text{stoich}} = 0.0867 \cdot \left(\frac{1 + H/C}{1 + 3H/C} \right) \quad (85)$$

where H/C = fuel hydrogen/carbon ratio by mass.

Dissociation

There are two factors in the heat balance for the primary zone (or between stations in the flame tube):

1. Burning of fuel.
2. Dissociation of products of combustion.

The equations for c_p given above neglect dissociation effects; Hodge (Ref 37) suggests that dissociation may be represented by defining an effective calorific value of the fuel:

$$h_{\text{eff},p} = h_p - \Delta h_{\text{eff},p}$$

where h_p = fuel lower calorific value, per unit mass of fuel

$\Delta h_{\text{eff},p}$ = energy supplied to cause dissociation of combustion products

In Figure 12, curves of $\Delta h_{\text{eff},p}$ are plotted as a function of temperature, pressure, and fuel-air ratio, for combustion of a fuel in air. The effect of pressure is ignored in the present work and the curves

are approximated by:

$$\Delta h_{\text{eff,p}} = \frac{3 \times 10^{-26} T_2^{7.5}}{f}$$

where f = local fuel-air ratio

T_2 = temperature of products of combustion

If the energy of dissociation is related to the enthalpy of the products, then the enthalpy of the products, including the effects of dissociation, h'_{prod} , is given by:

$$h'_{\text{prod}}(T_2) = h_{\text{prod}}(T_2) + \frac{3 \times 10^{-26} T_2^{7.5} f_g}{f}$$

where f_g = fuel-gas ratio

$$= \frac{f}{1+f}$$

T_b = base temperature for enthalpy

$$= 459.7 \text{ deg R}$$

Thus dissociation has the effect of lowering the temperature of the combustion products.

Hence for the combustion of fuel in a vitiated gas, when the enthalpies do not include the effects of dissociation, the heat release rate, \dot{q} , is adjusted to account for dissociation and recombination. In general, for combustion between conditions 1 and 2:

$$\dot{q} = \dot{m}_{fb} h_p + 3 \times 10^{-26} \left[\frac{\dot{m}_1 T_1^{7.5}}{1+f_1} - \frac{\dot{m}_2 T_2^{7.5}}{1+f_2} \right] \quad (86)$$

where \dot{m}_{fb} = rate of burning of fuel

For combustion in the primary zone the temperature rise is very large and the $T_1^{7.5}$ term in Equation (86) may be ignored. Equation (81) is now solved for T_2 , the primary-zone temperature.

The empirical method described above is widely used and gives satisfactory results in practical cycle-performance calculations.

Density and Velocity

The density is found from the equation of state:

$$\rho_2 = \frac{P_2}{R T_2}$$

and the velocity from the continuity equation:

$$u_2 = \frac{\dot{m}_2}{\rho_2 A_2}$$

where $\dot{m}_2 = \dot{m}_1$

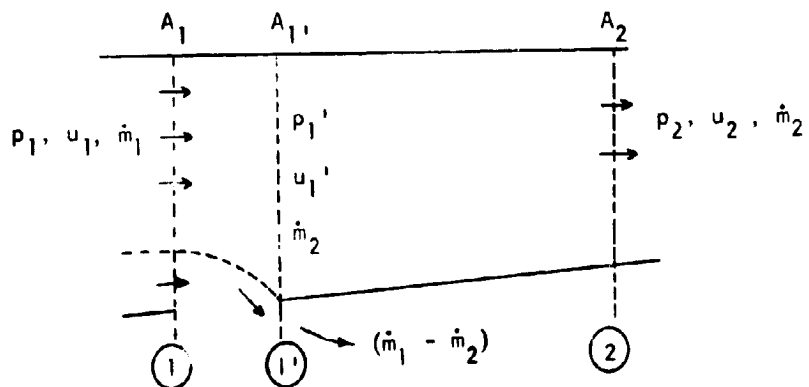
Hot Loss

The "hot loss" of total pressure, which is the change in total pressure due to heat addition, is given by

$$\begin{aligned} \Delta P_{\text{hot}} &= P_1 - P_2 & (87) \\ &= \frac{\rho_2 V_2^2}{2g_0} \left(1 - \frac{\rho_2}{\rho_1}\right) \end{aligned}$$

Flow in the Annulus

The equations of momentum, energy, continuity, and state are now set up for a section of one annulus between adjacent calculation stations, labeled 1 and 2 in the sketch below.



The resulting equations are then used to calculate conditions at Station 2 from the known conditions at Station 1.

Momentum Equation

Derivation of the equation for conservation of momentum between Stations 1 and 2 is complicated by the fact that, in the general case, the annulus wall between these stations contains a hole through which some momentum flows. To deal with this complication the calculation is carried out in three steps.

First, the flow through the hole, \dot{m}_h , is found from the hole type and size, the pressure drop across the hole, and discharge-coefficient data. (An expanded discussion of this topic will be found later in this section.)

Second, it is assumed that the air remaining in the annulus at Station 1', immediately downstream of the hole, undergoes a sudden expansion. The resulting total-pressure loss is given by the following empirical expression, from which $P_{an,1'}$, the total pressure at Station 1', may be calculated:

$$P_{an,1} - P_{an,1'} = 1.85 \frac{P_{an,1} u_{an,1}^2}{2g_0} \left[\frac{\dot{m}_h}{1.36\dot{m}_{an,1}} \right]^{1/(.5+.242M_{an,1}^{2.21})} \quad (88)$$

(This expression has been obtained by fitting the curves of Figure 13, which is taken from a review of empirical data on total-pressure losses due to sudden expansion in compressible flow, Reference 38.) With the total pressure at Station 1' known, the other flow conditions at Station 1' may be found from the equations for the isentropic flow of a perfect gas between Stations 1 and 1'. The most convenient approach is first to calculate the Mach number at Station 1', $M_{an,1'}$, from the following equation:

$$\frac{\dot{m}_{an,1'}}{A_{an,1'}} \left[= \frac{\dot{m}_{an,2}}{A_{an,1}} \right] = \left[\frac{\gamma}{R} \right]^{\frac{1}{2}} \frac{P_{an,1'}}{T_o^{\frac{1}{2}}} \frac{M_{an,1'}}{\left[1 + \frac{\gamma-1}{2} M_{an,1'}^2 \right]^{\frac{\gamma+1}{2(\gamma-1)}}} \quad (89)$$

where T_o = stagnation temperature, assumed to be constant across the expansion

$$= T_{an,1} + \frac{u_{an,1}^2}{2C_p g_o J}$$

The static temperature and static pressure are then determined from:

$$\frac{T_{an,1'}}{T_o} = \left[1 + \frac{\gamma-1}{2} M_{an,1'}^2 \right]^{-1}$$

$$\frac{P_{an,1'}}{P_{an,1'}} = \left[\frac{T_{an,1'}}{T_o} \right]^{\frac{\gamma}{\gamma-1}}$$

Then from the equation of state the density at 1' is:

$$\rho_{an,1'} = \frac{P_{an,1'}}{RT_{an,1'}}$$

From continuity, the velocity is:

$$u_{an,1'} = \frac{\dot{m}_{an,1'}}{\rho_{an,1'} A_{an,1}}$$

Thus, the assumption of a sudden expansion at Station 1' permits all of the necessary flow quantities at that station to be computed.

The third step is to apply the momentum equation for flow between

Stations 1' and 2:

$$p_{an,1'} A_{an,1} + \dot{m}_{an,2} u_{an,1'}/g_o + \int_{x_{1'}}^{x_2} p_{an} \frac{dA}{dx} dx$$

$$- \int_{x_{1'}}^{x_2} F A_w p_{an} u_{an}^2 / 2g_o \cdot dx = p_{an,2} A_{an,2} + \dot{m}_{an,2} u_{an,2} / g_o \quad (90)$$

where F = friction factor (Fanning)

$$= 0.0035 + 0.264 Re_{an,1}^{-.42} \quad (\text{Ref 39})$$

A_w = wetted wall area per unit length

A number of simplifications are made in this equation. Since the pressure losses due to wall slope and friction are small terms in the equation, an iteration loop can be avoided without a significant loss in accuracy by writing:

$$\int_{x_{1'}}^{x_2} F A_w p_{an} u_{an}^2 / 2g_o \cdot dx = F (C_A + C_B) p_{an,1'} u_{an,1'}^2 (x_2 - x_{1'}) / 2g_o$$

where C_A and C_B are the inner and outer wall areas per unit length between 1' and 2.

The integral pressure term can be evaluated if it is assumed that flow between Stations 1' and 2 is incompressible and that the mixing rate will be delayed by diffusion. With these assumptions the integral pressure term may be integrated as shown in Appendix VII, yielding:

$$\int_{x_{1'}}^{x_2} p_{an} \cdot \frac{dA}{dx} \cdot dx = (p_{an,1'} - p_{an,2}) \cdot \frac{2A_{an,1}A_{an,2}}{A_{an,1} + A_{an,2}} + p_{an,2}A_{an,2} - p_{an,1'}A_{an,1}$$

The final momentum equation thus becomes:

$$\frac{2 A_{an,1} A_{an,2}}{A_{an,1} + A_{an,2}} (p_{an,1'} - p_{an,2}) - F (C_A + C_B) \frac{\rho_{an,1'} u_{an,1'}^2}{2g_o} (x_2 - x_{1'}) = \dot{m}_{an,2} (u_{an,2} - u_{an,1'})/g_o \quad (91)$$

Energy Equation

The energy equation for flow in the annulus between Stations 1' and 2 is:

$$\left[h(T_{an,1}) + u_{an,1}^2/2g_o J \right] \dot{m}_{an,2} + \int_{x_1}^{x_2} \dot{q}_w C_A \cdot dx = \left[h(T_{an,2}) + u_{an,2}^2/2g_o J \right] \dot{m}_{an,2}$$

where $h(T)$ = static enthalpy of annulus air at temperature T

\dot{q}_w = heat transfer rate from unit area of the flame tube wall to the annulus air

The casing temperature is normally assumed to be equal to the compressor delivery temperature. Even when a different casing temperature is specified, however, the heat-transfer rate between casing and annulus air is assumed to be negligibly small.

Since the variations in annulus air temperature are normally small, $h(T)$ may be assumed equal to $c_p(T - T_b)$, where c_p is a mean specific heat. If mean values are also assumed for \dot{q}_w and C_A , the simplified energy equation becomes:

$$\left(c_p T_{an,1} + u_{an,1}^2/2g_o J \right) \dot{m}_{an,2} + \dot{q}_w C_A (x_2 - x_1) = \left(c_p T_{an,2} + u_{an,2}^2/2g_o J \right) \dot{m}_{an,2} \quad (92)$$

Continuity Equation

The continuity equation for flow in the annulus between Stations 1 and 2 is written as follows:

$$\rho_{an,1} u_{an,1} A_{an,1} \dot{m}_{an,2} / \dot{m}_{an,1} = \rho_{an,2} u_{an,2} A_{an,2} \quad (93)$$

Equation of State

The equation of state for the annulus air is:

$$\frac{p_{an,1}}{\rho_{an,1} T_{an,1}} = \frac{p_{an,2}}{\rho_{an,2} T_{an,2}} = R \quad (94)$$

Method of Solution of Annulus Equations

Since the mass flow through the holes between Stations 1 and 2, \dot{m}_h , is known, the downstream flow in the annulus, $\dot{m}_{an,2}$, is simply:

$$\dot{m}_{an,2} = \dot{m}_{an,1} - \dot{m}_h$$

There remain four unknowns, $u_{an,2}$, $p_{an,2}$, $\rho_{an,2}$, and $T_{an,2}$, which can be found by solving Equations 91, 92, 93, and 94.

These equations are easily reduced to a quadratic in $u_{an,2}$:

$$B_2 u_{an,2}^2 + B_1 u_{an,2} - B_0 = 0 \quad (95)$$

where $B_2 = 1 - \frac{Jc_p}{R} \frac{A_{an,1} + A_{an,2}}{A_{an,1}}$

$$B_1 = \frac{2 g_o Jc_p}{R} \left[p_{an,1} \frac{A_{an,2}}{\dot{m}_{an,2}} + u_{an,1} \left(\frac{A_{an,1} + A_{an,2}}{2 g_o A_{an,1}} \right) \right]$$

$$\cdot \left(1 - \frac{f (C_A + C_B) (x_2 - x_1)}{2 A_{an,1}} \right)$$

$$B_0 = u_{an,1}^2 + 2g_0 J c_p \left[T_{an,1} + \frac{\dot{q}_w C_A (x_2 - x_1)}{c_p \dot{m}_{an,2}} \right]$$

The solution of Equation 95 is

$$u_{an,2} = \frac{-B_1 + \sqrt{B_1^2 + 4B_0 B_2}}{2B_2} \quad (96)$$

where physical reasoning dictates the choice of the positive root.

With $u_{an,2}$ known, Equations 91, 93, and 94 are solved for

$P_{an,2}$, $\rho_{an,2}$, and $T_{an,2}$:

$$P_{an,2} = P_{an,1} + \frac{\dot{m}_{an,2}}{A_{an,2}} \left(\frac{A_{an,1} + A_{an,2}}{2 g_0 A_{an,1}} \right) \left[u_{an,1} \left(1 - \frac{f (C_A + C_B) (x_2 - x_1)}{2 A_{an,1}} \right) - u_{an,2} \right]$$

$$\rho_{an,2} = \frac{\dot{m}_{an,2}}{A_{an,2} u_{an,2}}$$

$$T_{an,2} = \frac{P_{an,2}}{R \rho_{an,2}}$$

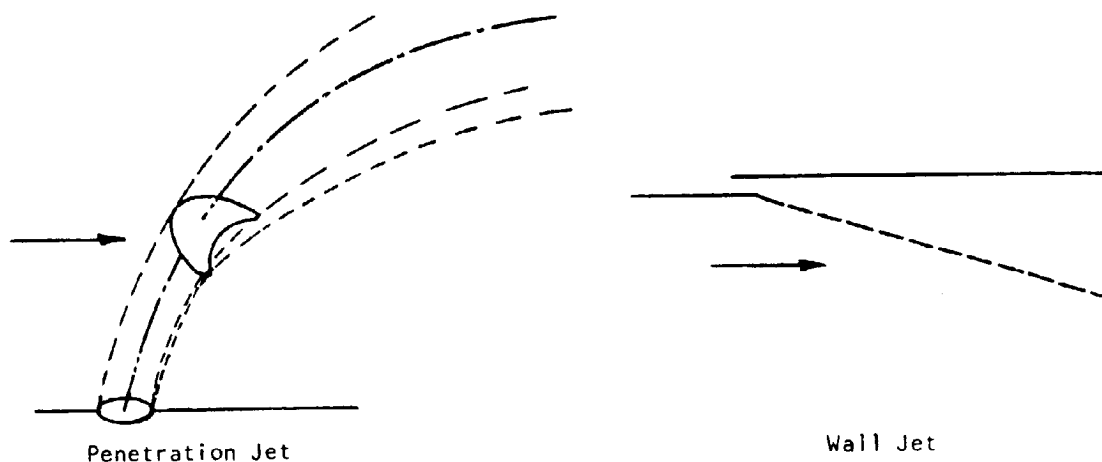
Introduction to Jet Flow and Mixing

The flow characteristics of jets entering the flame tube through holes and cooling slots is treated by the use of empirical correlations for:

1. The length of the jet (measured along its center line).
2. The cross-sectional area of the spreading jet as a function of jet length.
3. The jet center-line velocity and temperature as functions of jet length.

4. The development of the nondimensional velocity and temperature profiles across the jet with jet length.

Two sets of correlations are provided, one for wall jets (where the air enters the flame tube through a cooling slot in a direction parallel to the wall) and one for penetration jets. These two types of jet are illustrated in the sketch.



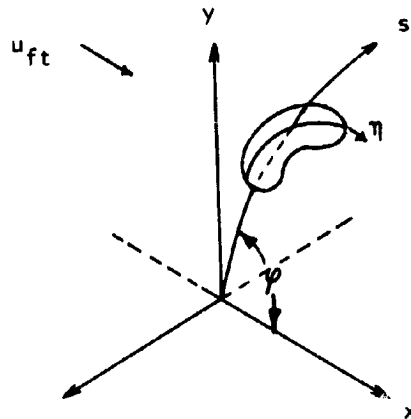
Once the jet properties have been estimated, the rate of mixing of the jet air into the main gas stream is estimated according to one of three optional mixing models. The same model, chosen by the user of the program, is used for both penetration and wall jets.

The characteristics of penetration and wall jets and of the three mixing models are given detailed discussion in subsequent sections.

Characteristics of Penetration Jets

The dimensions used in describing jet behavior are shown in

the sketch below, where x is the direction of flow of main-stream gas in the flame tube, y is jet penetration distance normal to the flame-tube wall, s is distance along the jet centerline, η is transverse width of the jet (measured normal to the jet center-line along lines of constant s), and φ is the angle between the initial jet trajectory and the flame-tube wall at the entry hole.



Initial-Jet-Angle Data

The jet-mixing correlations, and the momentum equations in the flame tube, make use of the initial jet angle φ . This is available as a function of pressure-loss factor for 47 of the hole types in the library data. Where the data do not exist, the following correlation is used:

$$\sin^2 \varphi = \frac{C_d}{C_{dn}} \quad (97)$$

where C_{dn} = the asymptotic value of C_d as $1 + \frac{\Delta p_h}{q_{an}}$ tends to infinity

This approximation gives reasonable results for round flush holes. For total-head devices its accuracy is unknown; in particular, the following

assumption must be made:

$$\varphi = 90 \text{ degrees when } C_d \geq C_{dn}$$

Penetration Distance

The penetration distance y , measured from the wall to the jet center-line, is calculated by an empirical correlation of experimental data obtained from 18 sources (Refs 40 through 57):

$$y = 0.87 d_h \left(\frac{\rho_{an}}{\rho_{ft}} \right)^{0.47} \left(\frac{u_{j,o}}{u_{ft}} \right)^{0.85} \left(\frac{x}{d_h} \right)^{0.32} \sin \varphi \quad (98)$$

where d_h = effective axial length of hole

$$= (C_d)^{\frac{1}{2}} \times \text{axial length}$$

$u_{j,o}$ = initial jet velocity

$$= \frac{\dot{m}_h}{\rho_{an} C_d \times \text{hole area}}$$

It is assumed that there is no change in density of the jet as the air passes through the hole. Equation 98 is plotted in Figure 14.

Jet Center-Line Velocity

An empirical equation for the jet center-line velocity has been obtained by fitting curves to the experimental data of Keffer and Baines (Ref 56, Fig 11), shown here on Figure 15:

$$\begin{aligned} \frac{s'}{d_j} < 3.45 & \quad u_{j,t} = u_{j,o} \\ 3.45 < \frac{s'}{d_j} < 5.2 & \quad u_{j,t} = u_{ft} + \left[1 - .229 \left(\frac{s'}{d_j} - 3.45 \right) \right] (u_{j,o} - u_{ft}) \\ 5.2 < \frac{s'}{d_j} & \quad u_{j,t} = u_{ft} + \left[3.6 e^{-.344 s'/d_j} \right] (u_{j,o} - u_{ft}) \end{aligned} \quad (99)$$

The effective distance along the jet center-line, s' , used in the above

equations, is calculated (Ref 56, page 492) from:

$$s' = s + (2.93 - 0.279 \frac{u_{j,0}}{u_{ft}}) d_j \quad (100)$$

$$\text{where } s = \int \left[1 + \left(\frac{dy}{dx} \right)^2 \right]^{\frac{1}{2}} dx \quad (101)$$

d_j = effective initial jet diameter

$$= (C_d \cdot \text{Hole Area} \cdot 4/\pi)^{\frac{1}{2}}$$

Transverse Velocity Profile

The correlating equations for the jet velocity profile, expressed in terms of the transverse coordinate η , are obtained from Figure 16 (Ref 56, Fig 9):

$$\begin{aligned} 0 < \eta < \eta_{\frac{1}{2}} \quad u_{j,\eta} &= u_{ft} + \left[0.5 \cos \left(\frac{\pi}{2} \frac{\eta}{\eta_{\frac{1}{2}}} \right) + 0.5 \right] (u_{j,0} - u_{ft}) \\ \eta > \eta_{\frac{1}{2}} \quad u_{j,\eta} &= u_{ft} + 1.74 e^{-1.25 \eta / \eta_{\frac{1}{2}}} (u_{j,0} - u_{ft}) \end{aligned} \quad (102)$$

where, from Figure 12 of Reference 56: $\eta_{\frac{1}{2}} = 0.215 s'$

Transverse Temperature Profile

The transverse temperature profile is assumed to be similar in form to the transverse velocity profile. The Prandtl number is proportional to the relative spreading rates of velocity and temperature profiles (Ref 58). Since the Prandtl number for air in the jets is about 0.7 for typical annulus-air temperatures, the dimensionless temperature profile is assumed to be roughly 1.4 times as wide as the velocity profile at a given position along the jet. For the same reason, the center-line temperature decreases more rapidly than the center-line velocity. The expressions relating temperature to velocity are then:

$$\frac{T_{j,\eta} - T_{ft}}{T_{j,\xi} - T_{ft}} = \frac{u_{j,\eta''} - u_{ft}}{u_{j,\xi} - u_{ft}} \quad (103)$$

$$\frac{T_{j,\xi,s'} - T_{ft}}{T_{j,o} - T_{ft}} = \frac{4.8}{6.5} \left(\frac{u_{j,\xi,s'} - u_{ft}}{u_{j,o} - u_{ft}} \right) \quad (104)$$

where $\eta'' = \eta/1.4$

The constants were taken from reviews of jet data by Forstall and Shapiro (Ref 58) and Squire (Ref 59).

Calculation of Jet Properties

Examination of the data of Jordinson (Ref 57), reproduced here in Figure 17, shows that the cross-sectional area of a jet in a plane normal to its center-line may be represented by:

$$A_{j,cs} = 0.12 \eta^{*1.8}$$

where η^* = the value of η at the assumed jet boundary.

The jet area normal to the combustor axis is then given by:

$$A_j = 0.12 \eta^{*1.8} / \cos \varphi_j \quad (105)$$

where φ_j = local jet angle
 $= \cos^{-1} \left[1 + \left(\frac{dy}{dx} \right)^2 \right]^{-1/2}$

Other jet properties needed for solution of the flame-tube equations may be calculated as follows:

$$\dot{m}_j = \int_0^{\eta^*} \rho_j u_{j,\eta} 0.12 \times 1.8 \eta^{0.8} d\eta \quad (106)$$

$$\dot{m}_j = \int_0^{\eta^*} \rho_j u_{j,\eta}^2 0.12 \times 1.8 \eta^{0.8} d\eta \cdot \cos \varphi_j \quad (107)$$

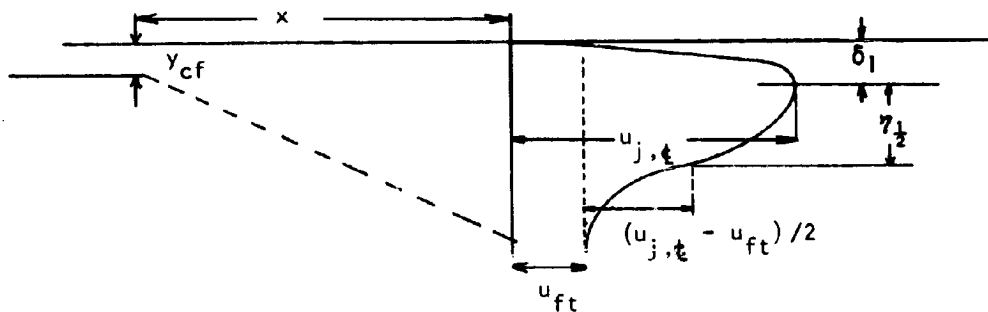
$$h_j = \int_0^{\eta^*} \rho_j u_{j,\eta} \left[c_p (T_{j,\eta} - T_b) + \frac{u_{j,\eta}^2}{2 g_o J} \right] 0.12 \times 1.8 \eta^{0.8} d\eta \quad (108)$$

The value of π^* depends on the mixing correlation employed; this topic is discussed after the wall-jet correlations have been presented.

Characteristics of Wall Jets

A large number of correlations for wall-jet characteristics are available in the literature; most give essentially identical results. The methods described have been chosen mainly on the grounds of simplicity.

The symbols used are defined by the sketch below.



Maximum Velocity

The maximum velocity in the wall jet is calculated from equations derived by Kruka and Eskinazi (Ref 60, Eqs 16, 17, and 18):

$$\begin{aligned}
 \underline{x = 0} \quad s' &= 0 \\
 u_{j,t} &= u_h \\
 \underline{x = x + dx} \quad s' &= s' + \left(1 - \frac{u_{ft}}{u_{j,t}}\right) dx \\
 u_{j,t} &= u_{ft} + \frac{0.0287 y_{cf}}{v(12s')^2} (u_h - u_{ft}) \quad (109)
 \end{aligned}$$

where u_h = initial jet velocity
 $= \frac{\dot{m}_h}{\rho_{an} C_d \times \text{slot area}}$

$$\alpha = \left[\frac{1.06}{1 - u_{ft}/u_h} - 0.5 \right]$$

The above equations apply for values of $u_{j,\xi}$ between u_h and u_{ft} . Otherwise, $u_{j,\xi}$ is set equal to u_h .

Velocity Profile

For purposes of analysis, the velocity profile is divided into two sections about its maximum. Near the wall ($\eta < \delta_1$) the equation of Kruka and Eskinazi (Ref 60) is used:

$$\frac{u_{j,\eta} - u_{ft}}{u_{j,\xi} - u_{ft}} = c \left(\frac{\eta}{\delta_1} \right)^{1/n}, \quad \eta \leq \delta_1 \quad (110)$$

where η = perpendicular distance from wall

$$c = 1.0$$

$$n = 10$$

$$\delta_1 = 0.0109s'$$

Since n is so large, it is sufficiently accurate to ignore the precise shape of the profile and to assume:

$$\int_0^{\delta_1} \frac{u_{j,\eta} - u_{ft}}{u_{j,\xi} - u_{ft}} d\eta = 0.95 \delta_1 \quad (111)$$

In the outer region ($\eta > \delta_1$) the equation of Harris (Ref 61, Eq 21 gives):

$$\frac{u_{j,\eta} - u_{ft}}{u_{j,\xi} - u_{ft}} = e^{-k\eta'^2} \quad (112)$$

where $k = 0.693$

$$\eta' = \frac{\eta - \delta_1}{\eta_{\frac{1}{2}} - \delta_1}$$

$$\eta_{\frac{1}{2}} = 0.065s' \text{ (Spalding, Ref 62 Table 1)}$$

Typical profiles are shown in Figure 18.

Temperature Profile

The same assumptions as before (Equations 103 and 104) are made about the relation between the velocity and temperature profiles.

Calculation of Jet Properties

The equations for the properties of wall jets are similar to those for penetration jets (Equations 105 to 108). The major difference is in the expression for elements of area.

$$A_j = c_A \eta^* \quad \text{on the inner wall} \quad (113)$$

$$\dot{m}_j = c_A \int_0^{\eta^*} \rho_j u_{j,\eta} \cdot d\eta \quad (114)$$

$$\dot{m}_j = c_A \int_0^{\eta^*} \rho_j u_{j,\eta}^2 \cdot d\eta \quad (115)$$

$$h_j = c_A \int_0^{\eta^*} \rho_j u_{j,\eta} \left[c_p (T_{j,\eta} - T_b) + \frac{1}{2g_0 J} u_{j,\eta}^2 \right] \cdot d\eta \quad (116)$$

Jet-Mixing Models

Three of the mixing models use the jet properties calculated above to predict the rate at which the penetration and wall jets mix into the gas stream. The quantities calculated are the mass flow, axial-momentum flux, and enthalpy flux remaining in the jet as functions of distance downstream from its point of origin. The fourth model assumes instantaneous mixing.

For each model the rate of mixing is governed by an entrainment constant, C , which is selected by the user, along with the mixing model to be used, as input to the computer program. The exact function of the

entrainment constant varies from model to model, as is explained below.

Mass-Loss Model

This is a simple model in which a specified fraction of the initial mass flow in the jet is assumed to mix with the main stream for each unit of distance along the jet. (In this model the above more sophisticated calculations of jet properties other than length are ignored.)

The mass flow remaining in the jet, \dot{m}_j , is then given by:

$$\dot{m}_j = \dot{m}_h (1 - C s'/d_j) \quad (117)$$

The entrainment constant, C , may be assigned any value between zero (no mixing) and one (instantaneous mixing).

The other jet-flow quantities are calculated directly from the residual mass flow, with the jet velocity, density, and temperature assumed uniform:

$$A_j = \frac{\dot{m}_j}{\rho_{an} u_{j,o} \cos \varphi_j} \quad (118)$$

$$\mathcal{M}_j = \dot{m}_j u_{j,o} \cos \varphi_j \quad (119)$$

$$h_j = \dot{m}_j \left[c_p (T_{an} - T_b) + \frac{1}{2g_{0j}} u_{j,o}^2 \right] \quad (120)$$

Equivalent-Entrainment Model

This model starts with the actual mass flow in the jet, $\dot{m}_{j,act}$, as estimated from Equation 106 for penetration jets or 114 for wall jets.

In these equations the integration of mass flow is carried across the jet to a value of the jet width, η^* , large enough that virtually all of the jet is included. The excess of this mass flow over the initial flow through the hole, $\dot{m}_{j,act} - \dot{m}_h$, is the mass flow of gases that have

been entrained into the jet from the main stream. It is then assumed that a fraction C of this entrained mass flow represents the jet mass flow that has been mixed into the main stream. The residual mass flow in the jet is then given by:

$$\dot{m}_j = \dot{m}_h - C (\dot{m}_{j,act} - \dot{m}_h) \quad (121)$$

An entrainment constant of zero again specifies no mixing; one specifies complete mixing when the computed flow of the actual jet reaches twice the initial jet flow; infinity (or a large number) implies instantaneous mixing.

Jet velocity, temperature, and density are again assumed uniform and the area, momentum, and enthalpy flux are calculated from equations 118, 119, and 120.

Profile-Substitution Model

In this model use is made of the jet temperature profile calculated by the methods discussed above. The boundary of the jet is defined to be that point η^* on the transverse temperature profile where the difference between the jet temperature and the temperature of the gases in the main stream has fallen to a specified fraction C of its initial value.

$$\frac{T_{j,\eta^*} - T_{ft}}{T_{j,0} - T_{ft}} = C \quad (122)$$

Air outside the boundary at η^* is assumed to have mixed with the main stream. The value of η^* defined by Equation 122 is then used to obtain \dot{m}_j , A_j , ρ_j , and h_j for penetration or wall jets from Equations 105, 106, 107 and 108 or from Equations 113, 114, 115, and 116, respectively.

An entrainment constant, C , of one implies instantaneous mixing; zero implies no mixing.

Aerodynamic Treatment of Porous Walls

When transpiration cooling is specified, the entire flame-tube wall is assumed to be made from material of uniform porosity. The usual number of holes for the admission of penetration air are permitted, but there should be no film-cooling slots.

The coolant flow through the wall is governed by the Darcy Equation (Ref 63):

$$\frac{P_{an}^2 - P_{ft}^2}{t_w} = \frac{2RT_w \mu_{an} G}{\kappa M_w g_o} \quad (123)$$

where t_w = wall thickness
 T_w = wall temperature
 μ = dynamic viscosity
 G = mass flow rate per unit area through the wall
 M_w = molecular weight of coolant

The porosity of the wall is characterized by the permeability coefficient κ which is defined by Equation 123 and has the units of ft^2 .

Calculation Procedure

When transpiration cooling is specified, the only additional input required is the permeability coefficient. The calculation proceeds in the following steps:

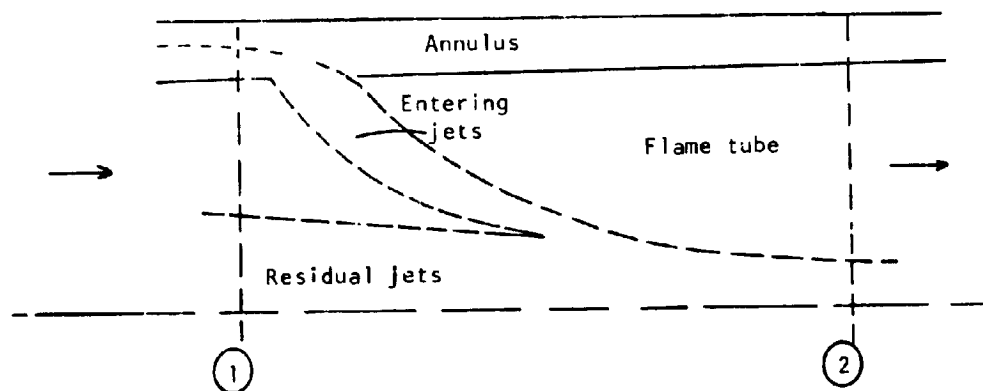
1. The air-flow subprogram is run, using an assumed wall temperature in Equation 123 to find the transpiration cooling flow rate.
2. This air-flow rate is used in the heat-transfer subprogram to obtain a first estimate of wall temperature.

3. This wall temperature distribution is used in the air-flow subprogram to obtain a new estimate of the transpiration flow rate.
4. The heat-transfer subprogram is entered once more to obtain a new wall-temperature distribution.

It is not possible, without major alterations in the program, to continue this iteration until any desired accuracy is achieved. Results show, however, that the above procedure gives adequate predictions.

Flow and Heat Addition in the Flame Tube

The equations of momentum, energy, continuity, and state will now be set up and solved for a section of the flame tube between adjacent calculation Stations 1 and 2. Contributions to the flow can be visualized from the sketch below.



Momentum Equation

The flame-tube equations include terms for the entering and residual jets. Since the gas velocity in the flame tube is typically one half, or less, of the velocity in the annulus, the friction

loss has been ignored.

The equation expressing the conservation of momentum within a control volume bounded by the flame-tube walls and by transverse planes at Station 1 and 2 is then

$$P_{ft,1} A_{ft,1} + \dot{m}_{ft,1} u_{ft,1}/g_0 + \sum_{\text{entering jets}} \dot{m}_{j,0} + \sum_{\text{residual jets}} \dot{m}_{j,1} + \int_{x_1}^{x_2} P_{ft} \frac{dA}{dx} dx$$

$$= P_{ft,2} A_{ft,2} + \dot{m}_{ft,2} u_{ft,2}/g_0 + \sum_{\text{all jets}} \dot{m}_{j,2}$$

where \dot{m}_j = axial component of jet momentum

$$= \dot{m}_j u_j \cos \varphi_j$$

φ_j = local angle between jet axis and flame-tube center line

\dot{m}_{ft} = mass flow of hot gases in flame tube. (This excludes unmixed air in the residual jets but includes the mass of fuel burned between stations 1 and 2.)

The integral pressure term is approximated by:

$$\int_{x_1}^{x_2} P_{ft} \frac{dA}{dx} \cdot dx = \frac{1}{2} (A_{ft,2} - A_{ft,1}) (P_{ft,1} + P_{ft,2})$$

The final form of the flame-tube momentum equation is then:

$$P_{ft,1} A_{ft,1} + \dot{m}_{ft,1} u_{ft,1}/g_0 + (A_{ft,2} - A_{ft,1}) (P_{ft,1} + P_{ft,2})/2 +$$

$$\sum_{\text{entering jets}} \dot{m}_{j,0} + \sum_{\text{residual jets}} \dot{m}_{j,1} = P_{ft,2} A_{ft,2} + \dot{m}_{ft,2} u_{ft,2}/g_0 + \sum_{\text{all jets}} \dot{m}_{j,2} \quad (124)$$

Energy Equation

The equation expressing conservation of energy between adjacent

calculation stations in the flame tube is written as follows:

$$\begin{aligned} & \left[h(T_{ft,1}) + u_{ft,1}^2/2g_oJ \right] \dot{m}_{ft,1} + \sum_{\text{entering jets}} h_{j,0} \dot{m}_{j,0} + \sum_{\text{residual jets}} h_{j,1} \dot{m}_{j,1} \\ & + \int_{x_1}^{x_2} \dot{q} \cdot dx = \left[h(T_{ft,2}) + u_{ft,2}^2/2g_oJ \right] \dot{m}_{ft,2} + \sum_{\text{all jets}} h_{j,2} \dot{m}_{j,2} \end{aligned} \quad (125)$$

where the enthalpy of hot gases is defined by:

$$h(T_{ft}) = \int_{T_b}^{T_{ft}} c_p(T) dT$$

The specific heat c_p is correlated as a function of temperature by Equation 84; the enthalpy of the jets, h_j , is obtained from the jet-mixing calculation, Equation 108, 116, or 120; and the heat-release rate, \dot{q} , from Equation 86.

Heat loss from the hot gases to the flame-tube walls has been ignored in Equation 125. Strictly speaking, this is quite unjustified since the heat loss reduces the effective value of \dot{q} , typically be about 5 per cent in the primary zone. Inclusion of this effect would, however, considerably complicate the calculation procedure.

Continuity Equation

The equation expressing the conservation of mass in the flame tube is:

$$\begin{aligned} & \rho_{ft,1} u_{ft,1} \left[A_{ft,1} - \sum_{\text{residual jets}} A_{j,1} \right] + \sum_{\text{residual jets}} \dot{m}_{j,1} + \sum_{\text{entering jets}} \dot{m}_h + \dot{m}_{fb} \\ & = \rho_{ft,2} u_{ft,2} \left[A_{ft,2} - \sum_{\text{all jets}} A_{j,2} \right] + \sum_{\text{all jets}} \dot{m}_{j,2} \end{aligned} \quad (126)$$

where \dot{m}_{fb} = fuel burning rate

The jet areas and mass-flow rates are obtained from the results of jet-mixing calculations, Equations 105, 106, 113, 114, 117, 118, and 121.

Equation of State

The equation of state may be written as follows:

$$\frac{P_{ft,1}}{\rho_{ft,1} T_{ft,1}} = \frac{P_{ft,2}}{\rho_{ft,2} T_{ft,2}} = R \quad (127)$$

where R = gas constant for air

It has been assumed in Equation 127 that R is independent of temperature. This is true to within 0.5 per cent for all conditions encountered in practice. It has been further assumed that the gas constant for a mixture of combustion products is equal to that for air and independent of the fuel-air ratio. The actual gas constant for a mixture having initial conditions of 60 deg F and 4 atmospheres varies only 0.2 per cent as the fuel-air ratio varies from zero to the stoichiometric value.

Method of Solution

The mass flow at Station 2 is known from jet-mixing results:

$$\dot{m}_{ft,2} = \dot{m}_{ft,1} + \sum \dot{m}_{j,o} + \sum \dot{m}_{j,1} - \sum \dot{m}_{j,2} \quad (128)$$

Since Equation 125 cannot be solved explicitly for $T_{ft,2}$, an iterative technique is used to arrive at a solution. In this equation the velocity terms make a small contribution to the total enthalpy. For the first stage in the iterative process, therefore, $u_{ft,2}$ is set equal to $u_{ft,1}$. In addition, the specific heat, c_p , and heat-release rate, \dot{q} , are computed for $T_{ft,2} = T_{ft,1}$. With these simplifications Equation 125 can be solved explicitly for a first estimate of $T_{ft,2}$. New values of c_p and \dot{q} are then computed for the new $T_{ft,2}$ and Equation 125 is solved again.

This process is repeated until $T_{ft,2}$ converges to an acceptable accuracy.

Using the value of $T_{ft,2}$ so obtained, Equations 124, 126, and 127 are solved to obtain a quadratic equation in $\rho_{ft,2}$:

$$\rho_{ft,2}^2 R T_{ft,2} (A_{ft,2} + A_{ft,1})/2 - \rho_{ft,2} K_1 + \dot{m}_{ft,2}^2/g_0 (A_{ft,2} - \sum A_{j,2}) = 0 \quad (129)$$

where
$$K_1 = \frac{1}{2} \rho_{ft,1} (A_{ft,2} + A_{ft,1}) + \dot{m}_{ft,1} u_{ft,1}/g_0$$

$$+ \sum m_{j,c} + \sum m_{j,1} - \sum m_{j,2}$$

The resulting value of $\rho_{ft,2}$ is substituted in the following version of Equation 126 to obtain $u_{ft,2}$:

$$u_{ft,2} = \dot{m}_{ft,2}/\rho_{ft,2} (A_{ft,2} - \sum A_{j,2})$$

This value of $u_{ft,2}$ is inserted in Equation 125 and a new value of $T_{ft,2}$ is found. This process is repeated until both $T_{ft,2}$ and $u_{ft,2}$ have converged to within specified tolerances.

Structure of the Subprogram

The air-flow subprogram consists of:

1. A subroutine which sets up starting conditions and directs the air-flow calculation through the other subroutines in the appropriate sequence.
2. Subroutines for solving the equations for flow in the annulus and flame tube.
3. Subroutines for calculating the heat addition due to fuel burning and the temperature in the primary zone.
4. A subroutine for calculating the rate of mixing of the entering jets.

Detailed flow charts and program listings for the air-flow subroutines are given in Volume II.

HEAT-TRANSFER SUBPROGRAM -
ANALYTICAL METHODS AND PROGRAM DEVELOPMENT

Introduction

The principal operations in the heat-transfer subprogram comprise the formation of the various heat flux components at the flame-tube wall in terms of the wall temperature, the solution of the heat-balance equation to determine the wall temperature, and the evaluation of the wall heat fluxes. This section of the report presents the assumptions and relations employed in the subprogram. Program options which relate to the heat-transfer subprogram are also discussed.

Heat Balance in Flame Tube

The heat-flux balance is performed on an elemental length of the flame-tube wall; conditions in the circumferential direction are assumed to be uniform. The heat-flux components considered in the balance are:

1. Radiation from the flame to the flame-tube wall, R_1 .
2. Convection in the flame-tube gases at the wall, C_1 .
3. Radiation from the flame-tube wall to the outer casing, R_2 .
4. Convection in the annulus air at the outside surface of the flame-tube wall, C_2 .
5. Longitudinal conduction in the flame-tube wall, ΔK .
6. Radiation interchange between the flame-tube walls, R_3 .
7. Heat transfer between porous wall and transpiring gases, Q_{tr} , when transpiration cooling is specified.

Equating the heat gained by the element of wall to the heat

lost, the following equation results:

$$R_1 + C_1 + \Delta K = R_2 + C_2 + R_3 + Q_{tr} \quad (130)$$

Each of the components of heat flux depends upon the flame-tube wall temperature in the manner shown in the following sections. Substitution of the various heat-flux expressions into equation 130 yields a polynomial in the wall temperature which is solved numerically. The methods used for solving this equation are described in a later section after the various heat-flux expressions have been derived.

Calculation Options and Assumptions

Several of the assumptions associated with the heat-transfer subroutine apply only under certain program options. The remainder of the assumptions are more general and apply in all cases; these latter assumptions will be considered first.

General Assumptions

The following is a list of the general assumptions which apply under all program options:

1. For the purpose of heat-transfer calculations, the combustor can be considered as two-dimensional, that is, conditions are assumed to be constant in the circumferential direction for the annular geometry and in the lateral direction, with negligible edge effects, for the rectangular geometry.
2. Steady-state conditions prevail.
3. The quantities supplied by the air-flow subprogram, for example, temperature and velocity distributions in the flame

- tube and annuli, are reasonable approximations to real conditions. This assumption is potentially one of the largest sources of error in the heat-transfer calculations.
4. The flame and walls are gray radiators, that is, spectral effects can be ignored. In the case of the wall, spectral effects are unlikely to be very significant; flame emission is discussed again in a later assumption.
 5. Wall emissivities and absorptivities are constant. In fact, they are functions of temperature, but the range of variation in emissivity is small.
 6. The effect of the wall-to-bulk temperature ratio can be neglected; fluid properties used in the heat-transfer relations are evaluated at the bulk fluid temperature. With this assumption the rate of heat transfer to the annulus air may be overestimated by as much as 10 per cent for Reynolds Numbers greater than 10,000.

Calculation Options and Additional Assumptions

A list of the program options which are concerned with the heat-transfer subprogram was presented in an earlier section of the report. Here the various options are reconsidered in the light of the additional assumptions associated with them.

1. The options to specify film or transpiration cooling of the flame-tube walls introduce all the assumptions associated with the methods employed for treating these cases, namely the method of Spalding (Ref 9) for film cooling and the

method of Wheeler (Ref 64) for transpiration cooling.

2. The use of empirical correlations to estimate the emissivity of the flame introduces large uncertainties. One of the major assumptions here is that the effect of the fuel type on the flame luminosity factor may be characterized by the hydrogen/carbon ratio of the fuel.
3. The one-dimensional radiation option assumes that the temperature gradients in the flame-tube are small, a situation which is unlikely to be realized in practice. In the case of the two-dimensional radiation option, it is assumed that there are no sudden temperature changes at the ends of the combustor.
4. The exclusion of longitudinal conduction and radiation interchange between the flame-tube walls from the heat-balance equation assumes that temperature gradients along the walls are small and that the two walls are at approximately the same temperature. These assumptions are, in general, quite valid; however, the option does exist to include either or both of these effects if they are thought to be significant in a particular case.
5. Unless the outer-casing temperature distribution is specified in the program input, it is assumed that the casing temperature is close to the compressor-discharge temperature. This is not a serious assumption since the radiation from the flame tube to the casing is generally small compared with the convection to the annulus air.

Radiation From the Flame to the Flame-Tube Wall - One-Dimensional Model

The one-dimensional-radiation model describes the case where each element of wall receives radiation only from elements of flame at the same axial position. This model is accurate when axial temperature gradients and end effects are small and the length-to-diameter ratio of the flame tube is large.

The usual expression for radiant heat transfer between a gray flame at temperature T_{ft} and a black container at temperature T_w is:

$$R_1 = \sigma (\epsilon_{ft} T_{ft}^4 - \alpha_{ft} T_w^4)$$

where σ = Stefan-Boltzmann constant

ϵ_{ft} = emissivity of flame at temperature T_{ft}

α_{ft} = absorptivity of flame to radiation of temperature T_w

Since the wall is not black, but has an absorptivity α_w which will normally be between 0.8 and 1.0, a correction should be made for absorption, reflection, re-absorption and so on. McAdams (Ref 26, p. 91) suggests a factor $(1 + \alpha_w)/2$ to allow for this effect.

A further simplification is introduced by the use of an empirical formula suggested by Lefebvre and Herbert (Ref 4):

$$\frac{\alpha_{ft}}{\epsilon_{ft}} = \left[\frac{T_{ft}}{T_w} \right]^{1.5}$$

$$\text{Then } R_1 = \frac{1}{2} \sigma (1 + \alpha_w) \epsilon_{ft} T_{ft}^{1.5} (T_{ft}^{2.5} - T_w^{2.5}) \quad (131)$$

The emissivity of the flame, ϵ_{ft} , is either calculated from one of several alternative empirical equations presented below or supplied as special input as a function of pressure and temperature. Another way of obtaining

flame-emissivity data would be to use tables of empirical information compiled by Hottel (Ref 26) and others. Although these data are the most accurate that are available within their range of applicability, the alternative approach of supplying data in functional form has been adopted here. This is equally valid, because:

1. The functions used fit the empirical data to within one or two per cent.
2. Most of the empirical data apply only at pressures near 1 atmosphere; the excessive extrapolation required to obtain emissivities at normal gas-turbine operating conditions renders the data less useful.
3. The only comprehensive data are for nonluminous flames; it is anticipated that luminous-flame correlations will prove more useful.

Nonluminous Flame - Distillate Fuel

This correlation was produced by Reeves (Ref 65).

$$\epsilon_{ft} = 1 - \exp \left[- 18.5 p_2 (l_b f_x)^{0.5} T_{ft}^{-1.5} \right] \quad (132)$$

where

- f_x = local fuel-air ratio
- l_b = mean beam path length
= $3.6 \times \text{Volume/Surface area}$

Nonluminous Flame - Residual Fuel

This correlation (Ref 65) is similar:

$$\epsilon_{ft} = 1 - \exp \left[-154 p_2^{0.75} (1_{bfx})^{0.5} T_{ft}^{-1.5} \right] \quad (133)$$

Lefebvre Correlation

Lefebvre, in Reference 4, used Reeves's distillate-fuel correlation with a "luminosity factor", Λ :

$$\epsilon_{ft} = 1 - \exp \left[-18.5 p_2 \Lambda (1_{bfx})^{0.5} T_{ft}^{-1.5} \right] \quad (134)$$

A correlation for Λ was based on data from two sources.

$$\Lambda = 7.53 (C/H - 5.5)^{0.84} \quad (135)$$

where C/H = carbon to hydrogen ratio of the fuel, by mass

This expression is invalid below carbon-hydrogen ratios of about 5.7.

NREC 1964 Correlation

By 1964, further data on the effect of C/H on Λ were available.

An examination of these sources showed that a better correlation for Λ in Equation 134 is:

$$\Lambda = \exp \left(\frac{C/H - 4.4}{2.3} \right) \quad (136)$$

NREC 1966 Correlation

Schirmer and Quigg, in a recent paper (Ref 11), examined the effect of pressure on flame radiation in a 2-inch diameter tubular combustor. Their data have been converted from radiation flux to emissivity at an assumed flame temperature of 3500 deg R and are plotted in Figure 19, together with the predictions of Equations 134 and 136; agreement is poor at C/H ratios above about 7. A new correlation, which fits the data reasonably well over the whole range, has therefore been produced. This is:

$$\epsilon_{ft} = 1 - \exp \left[-4.7 p_2^{1.3} \Lambda (l_b f_x)^{0.5} T_{ft}^{-1.5} \right] \quad (137)$$

$$\text{where } \Lambda = \left(\frac{C/H - 5}{0.16} \right)^{0.74} \quad (138)$$

This correlation is compared with the experimental results of Reference 11 in Figure 20.

Radiation From the Flame to the Flame-Tube Wall - Two-Dimensional Model

This section describes the option for calculating the heat received by a wall element from elements of flame at all axial locations. The radiative heat transfer to an element of the wall from an elemental volume of flame is equal to the product:

$$\begin{aligned} &\text{Volume of flame element} \times \text{Emission per unit volume} \\ &\times \text{Transmittance} \times \text{View factor} \end{aligned} \quad (139)$$

The quantities in this product will now be considered individually.

Volume of Flame Element

The elements of flame considered have elemental length in the axial direction of ΔX_{ft} and inner and outer (flame-tube-wall) radii of r_2 and r_1 respectively. Thus, the volume of each flame element is:

$$\Delta X_{ft} \cdot \pi (r_1^2 - r_2^2) \quad (140)$$

Emission Per Unit Volume

Following Hottel (Ref 26), the radiation emitted by unit volume of flame at temperature T_{ft} is:

$$4 \sigma T_{ft}^4 p_G \left(\frac{d\epsilon_{ft}}{dp_G} \right)_{p_G^1 = 0} \quad (141)$$

where p_G = partial pressure of radiating gas (i.e., water vapor and carbon dioxide), lbf per sq ft.

The quantity $\left(\frac{d\epsilon}{dp_{G'b}}\right)_{p_{G'L} = 0}$ is chiefly a function of temperature.

For a typical value of $p_{G'}/p_{ft} = 0.05$ and for a non-luminous flame it can be approximated by (Ref 26):

$$\left(\frac{d\epsilon}{dp_{G'b}}\right)_{p_{G'b} = 0} = \frac{3.6}{T_{ft}} \quad (142)$$

The form of the expressions for flame emissivity (Eqs 132 through 138) indicates that for luminous flames, the following equation is approximately true:

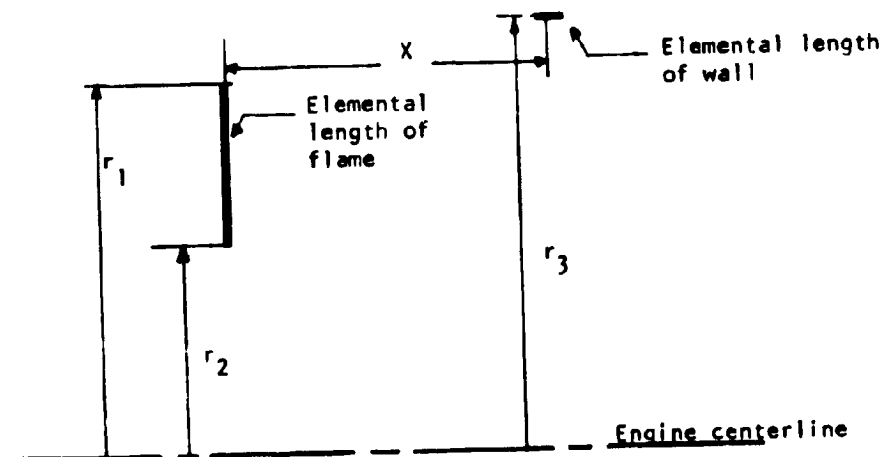
$$\left[\left(\frac{d\epsilon}{dp_{G'b}}\right)_{p_{G'b} = 0}\right]_{\text{luminous}} = \Lambda \times \left[\left(\frac{d\epsilon}{dp_{G'b}}\right)_{p_{G'b} = 0}\right]_{\text{non-luminous}}$$

Thus a more general form of Equation 142 is:

$$\left(\frac{d\epsilon}{dp_{G'b}}\right)_{p_{G'b} = 0} = \frac{3.6 \Lambda}{T_{ft}} \quad (143)$$

View Factor

The sketch below illustrates the nomenclature of the axially symmetric configuration considered.



Employing an equation derived by Hamilton and Morgan (Ref 66) and the principle of superposition, the following equation is obtained for the view factor of the flame element radiating to an element of length

$$F_{FW} = \frac{1}{4} \frac{\Delta x_w}{(r_3 - r_2)} \left[1 - \frac{x}{\sqrt{x^2 + (r_3 - r_2)^2}} \right] - \frac{1}{4} \frac{\Delta x_w}{(r_3 - r_1)} \left[1 - \frac{x}{\sqrt{x^2 + (r_3 - r_1)^2}} \right] \quad (144)$$

Δx_w in the outer wall:

Transmittance

The transmittance accounts for the radiative energy which is not absorbed by the intervening gas; it is a function of the distance the radiation travels through the gas, the gas composition and the gas temperature. Here a curve has been fitted to typical data prepared by Hottel (Ref 26) and shown in Figure 21. The expression developed is:

$$\tau = \frac{14.82}{p_G s + 14.82} \quad (145)$$

where s = distance from element at considered point on the wall to element of the flame, ft

Since s varies over different parts of the flame, an averaging procedure is used over the radial dimension of the flame to determine a single, mean value of the transmittance for each axial location of the flame element. The resulting expression for the transmittance to an outer wall element is:

$$\tau_{\text{mean}} = \frac{1}{20} \sum_{i=1}^{20} \frac{14.82}{14.82 + p_G \sqrt{x^2 + \left[r_3 - r_2 - \left(\frac{i}{20} - \frac{1}{40} \right) (r_1 - r_2) \right]^2}} \quad (146)$$

Partial Pressures

The partial pressures of carbon dioxide and water vapor that

are required for Equations 141 and 146 are obtained from stoichiometry

Then:

$$p_G = p_{ft} (x_{CO_2} + x_{H_2O}) \quad (147)$$

where x = mole fraction of constituent in product mixture. Local air-fuel ratios are calculated in the air-flow subprogram in such a way that the mixture can never be richer than stoichiometric.

Total Radiation

Introducing a wall temperature, T_w , and an effective wall absorptivity, $(1 + \alpha_w)/2$, the radiation absorbed by the wall element from the flame element is:

$$4\sigma \Gamma_{\text{mean}} \frac{(1 + \alpha_w)}{2} p_G \left(\frac{d\epsilon}{dp_G L} \right)_o \Delta x_{ft} \pi (r_1^2 - r_2^2) F_{FW} (T_{ft}^4 - T_w^4)$$

Hence, the total radiation per unit time at a point on the outer flame-tube wall receiving radiation from all positions of the flame, is:

$$4\pi\sigma \frac{(1 + \alpha_w)}{2} \sum_{\text{all flame positions}} \left[\Gamma_{\text{mean}} p_G \left(\frac{d\epsilon}{dp_G L} \right)_o \Delta x_{ft} (r_1^2 - r_2^2) F_{FW} (T_{ft}^4 - T_w^4) \right]$$

The radiative heat flux per unit time and area of flame tube is, therefore, given by:

$$R_1 = \frac{(1 + \alpha_w)\sigma}{\Delta x_w R_3} \sum_{\text{all flame positions}} \left[\Gamma_{\text{mean}} p_G \left(\frac{d\epsilon}{dp_G L} \right)_o \Delta x_{ft} (r_1^2 - r_2^2) F_{FW} (T_{ft}^4 - T_w^4) \right] \quad (148)$$

A similar expression applies for radiation to the inner flame-tube wall.

It should be noted that it is not necessary to specify the length of the wall element, Δx_w , since in Equation 148 Δx_w in the denominator cancels with Δx_w appearing in the expression for the view factor, F_{FW} .

Radiation from the Flame-Tube Wall to the Outer Casing

The radiant heat flux from the flame-tube wall to the outer casing is given by the equation:

$$R_2 = F_{wc} \sigma (T_w^4 - T_c^4) \quad (149)$$

where T_c = temperature of casing. This may be supplied as input as a function of axial length; if it is not, it is assumed equal to the compressor discharge temperature.

F_{wc} = overall interchange factor which accounts for the re-emission and absorption between surfaces.

For the case where only two surfaces are involved and where both surfaces have high emissivities, the overall interchange factor is approximately given by (Ref 26, p. 76):

$$F_{wc} = \left(\frac{1}{\epsilon_w} - 1 \right) + \frac{A_w}{A_c} \left(\frac{1}{\epsilon_c} - 1 \right) + \frac{1}{F_{wc}} \quad (150)$$

where \bar{F}_{wc} = black-surface overall interchange factor

ϵ_c = emissivity of casing (assumed equal to absorptivity)

A_w = surface area of flame-tube wall

A_c = surface area of casing

For radiation across an annular space, the black-surface interchange factor can be assumed to be equal to unity. With this simplification and some rearrangement, Equation 150 becomes:

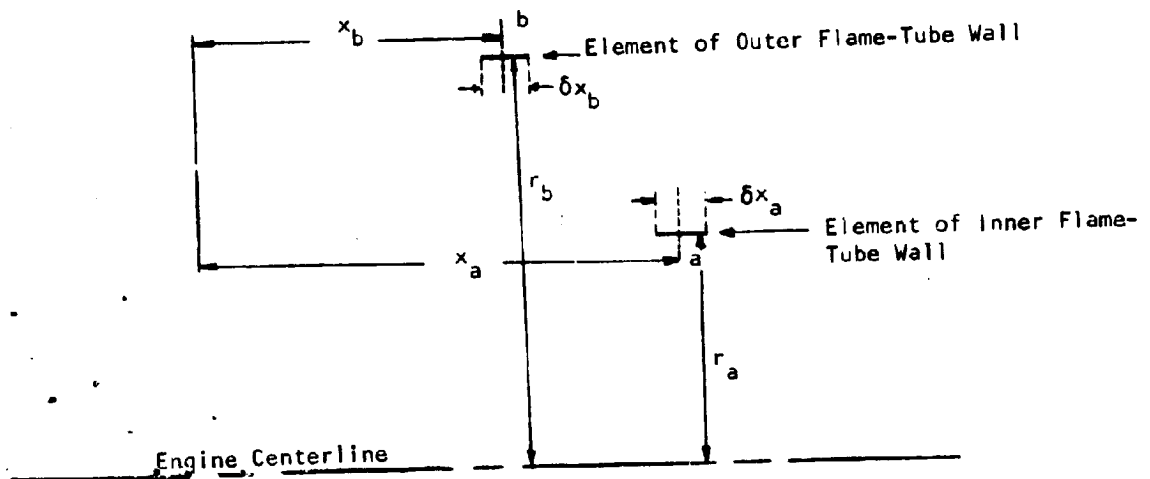
$$F_{wc} = \frac{\epsilon_w \epsilon_c}{\epsilon_c + \epsilon_w (1 - \epsilon_c)} \frac{A_w}{A_c} \quad (151)$$

Thus, from Equations 149 and 151 the radiant heat flux from the wall to the outer casing is:

$$R_2 = \sigma \left[\frac{\epsilon_w \epsilon_c}{\epsilon_c + \epsilon_w (1 - \epsilon_c)} \frac{A_w}{A_c} \right] (T_w^4 - T_c^4) \quad (152)$$

Radiation Interchange Between Flame-Tube Walls

Under some conditions, radiation interchange between the combustor walls can become important. The net rate of heat transfer to a section of the flame-tube wall from all other "visible" parts of the flame-tube wall is derived using the nomenclature shown in the sketch:



Radiation emitted by element δx_b , which is received by element δx_a (neglecting any reflections) is:

$$\epsilon \epsilon_w^2 2\pi r_b \delta x_b F_{ba} \Gamma (T_{wb}^4 - T_{wa}^4) \quad (153)$$

where F_{ba} = View factor for radiation from b to a

$$F_{ba} = \frac{\delta x_a (r_b - r_a)^2}{2 [(r_b - r_a)^2 + (x_a - x_b)^2]^{3/2}}$$

Γ = Transmittance between b and a

$$\Gamma = \frac{14.82}{p_G \sqrt{(x_a - x_b)^2 + (r_b - r_a)^2} + 14.82} \quad (154)$$

Radiation interchange per unit time and area of inner wall is given by:

$$\Delta R_3 = \frac{\sigma \epsilon_w^2 r_o \delta x_b (r_b - r_a)^2 \Gamma(T_{wb}^4 - T_{wa}^4)}{r_a^2 [(r_b - r_a)^2 + (x_a - x_b)^2]^{3/2}} \quad (155)$$

Thus the net rate of heat transfer per unit area to the point on the inner wall under consideration, from all parts of the outer wall is:

$$R_3 = \frac{\sigma \epsilon_w^2}{2} \sum_{\substack{\text{all b-wall} \\ \text{positions}}} \frac{r_b (r_b - r_a)^2 \Gamma(T_{wb}^4 - T_{wa}^4) \delta x_b}{r_a [(r_b - r_a)^2 + (x_a - x_b)^2]^{3/2}}$$

A similar expression applies for radiation from all parts of the inner wall to a point on the outer wall.

Convection at the Inner Surface of the Flame-Tube Wall

The correlation employed for the internal convective heat transfer at the flame-tube wall is one suggested by Humble, Lowdermilk and Desmon (Ref 67) for subsonic flow through smooth tubes at high surface and fluid temperatures:

$$C_1 = 0.023 \frac{k}{D_{ft}} Re^{0.8} Pr^{0.4} (T_{ft} - T_w) \quad (156)$$

where k = thermal conductivity of gas

D_{ft}^1 = hydraulic diameter of the flame tube, equal to twice the distance between the flame-tube walls for both annulus and rectangular geometries.

The effect of annulus diameter ratio is small and is ignored in this treatment. Reynolds and Prandtl numbers and thermal conductivity are based on properties of a gas mixture taking account of the amount of fuel present. The methods used to evaluate these properties are described in a later section.

Entry-Length Effect

When starting conditions on the wall are uniform, there is a developing boundary layer and the expression for the Nusselt number is usually multiplied by a factor for the entry-length effect. Typically (Ref 26), this is:

$$\left[1 + \left[\frac{L}{D_{ft}} \right]^{-0.7} \right]$$

Because of the intensely turbulent conditions in the combustor, the relationship for fully developed flow (Equation 156) gives a better representation and has been used in the program.

Internal Convection with Film Cooling

The contribution of internal convection to the wall heat balance is computed from Equation 156 only when film cooling and transpiration cooling are absent. For the case in which film cooling is employed, Equation 156 is modified by replacing the hot-gas temperature, T_{ft} , by an adiabatic wall temperature, T_{ad} , thus:

$$C_1 = 0.023 \frac{k}{D_{ft}'} Re^{0.8} Pr^{0.4} (T_{ad} - T_w) \quad (157)$$

The adiabatic wall temperature is a quantity measured experimentally and has been correlated by Spalding (Ref 9) to geometric and flow variables by means of a film-cooling effectiveness, τ , and a downstream-distance parameter, X :

$$\tau \equiv \frac{T_{ft} - T_{ad}}{T_{ft} - T_{cf}} \quad (158)$$

$$X = 0.91 \left(\frac{U_{ft}}{\bar{U}_{cf}} \cdot \frac{x}{y_{cf}} \right)^{0.8} (Re_{cf})^{-0.2} + 1.41 \left[\frac{x}{y_{cf}} \left| 1 - \frac{U_{ft}}{\bar{U}_{cf}} \right| \right]^{0.5} \quad (159)$$

where T_{cf} = inlet temperature of cooling film

y_{cf} = slot width

x = downstream distance of wall element from cooling slot.

Figure 22 shows an envelope enclosing 90 per cent of the data points employed by Spalding; these data may be represented by the three straight lines:

$$\tau = 1$$

$$\text{or } \tau = \left(\frac{X_0}{3.5x}\right)^{0.22} \quad (160)$$

$$\text{or } \tau = \frac{X_0}{x} \quad \text{whichever is the smallest}$$

$$\text{where } X_0 = 7.0$$

These relations correlate well the nine sets of experimental data on which they were based, but their validity for practical combustion systems, in which the slot may be obstructed by structural elements and imperfections left after fabrication, is uncertain. This uncertainty is supported by the data published by Sturgess (Ref 10) which are also plotted on Figure 22. These data for, so-called, "dirty" slots may be represented by the same equation (Eq 160) that was used to represent the data for "clean" slots; however, the value of X_0 is reduced from 7.0 to 3.5.

Equation 160 is employed in the computer program and X_0 is supplied as program input by the user; its value can be determined in one of two ways:

1. If experimental data are available, these are plotted in the form $\tau - x$, and a value of X_0 that fits the data best is chosen and supplied as input to the program.
2. If no experimental data are available, the recommended values

for X_0 are: 3.5 for "dirty" slots; 7.0 for "clean" slots.

The procedure employed by the program to determine the convective heat flux is as follows: For a particular wall element considered, a value for X is computed. This value, together with the value of X_0 supplied as input, are used to calculate the cooling effectiveness τ from Equation 160. Equation 158 is then employed to give the adiabatic wall temperature, T_{ad} , which is substituted into Equation 157 to give the convective heat flux.

Internal Convection with Transpiration Cooling

The transpiration-cooling flow rate is obtained from the air-flow subprogram. It is assumed that the coolant leaves the wall at the wall temperature.

The heat-transfer rate is calculated by a method suggested by Wheeler (Ref 64). With this method, the convective heat-transfer coefficient for the transpiration-cooled wall is given by:

$$Nu = 0.002 Re_{ft}$$

The Nusselt and Reynolds numbers are based on the bulk properties of the gas in the flame tube.

Hence, the convective heat flux from the hot gas to the wall is:

$$C_1 = 0.002 \frac{k}{D_{ft}} Re_{ft} (T_{ft} - T_w) \quad (16i)$$

It should be emphasized, however, that no independent assessment of the validity of this method for the present application has been made. It is expected that, if a serious study of transpiration cooling is to be undertaken with this program, more sophisticated and powerful methods such as that of Spalding (Ref 68), or actual test data from practical combustors, will be used.

Convection at the Outer Surface of the Flame-Tube Wall

External convection from the flame-tube walls to the annulus air is governed by an equation similar to Equation 156:

$$C_2 = 0.023 \frac{k}{D_{an}^1} Re_{an}^{0.8} Pr^{0.4} (T_w - T_{an}) \quad (162)$$

where D_{an}^1 is equal to twice the distance between the flame-tube and outer casing for both annular and rectangular geometries.

In the case of transpiration cooling, there is an additional component Q_{tr} representing heat transferred to the coolant as it passes through the wall:

$$Q_{tr} = G C_p (T_w - T_{an}) \quad (163)$$

Gas Properties

The gas properties used in the above relations are obtained from empirical correlations derived from a survey of all available literature. Values for air are used in the equations for heat transfer on the annulus side of the wall. In the case of gases in the flame tube, the molal gas composition is found from stoichiometry, and the properties of the constituents are combined according to formulæ recommended by Perry (Ref 69) to obtain the properties of the mixture.

The effect of pressure has been ignored.

The equations used for the specific heat, the dynamic viscosity and the thermal conductivity can all be expressed in the form:

$$Z = a + bT + cT^2 + dT^3 \quad (164)$$

where Z represents the gas property

The constants take different values for each property and for each gas considered as shown in Table I. Table I also shows the temperature range covered by the data employed to determine the values of the constants

for each gas; the percentage accuracy of the equations is also indicated.

Properties of Gas Mixtures

The specific heat of a mixture is obtained from:

$$C_p = \sum m_i C_{pi} \quad (165)$$

where m_i = mass fraction of i th component

C_{pi} = specific heat of i th component

The viscosity of a mixture is obtained from:

$$\mu = \frac{\sum x_i \mu_i (M_i)^{1/2}}{\sum x_i (M_i)^{1/2}} \quad (166)$$

where x_i = mole fraction of i th component

M_i = molecular weight of i th component

The thermal conductivity of a mixture is obtained from:

$$k = \frac{\sum x_i k_i (M_i)^{1/3}}{\sum x_i (M_i)^{1/3}} \quad (167)$$

Longitudinal Conduction Along Flame-Tube Wall

The longitudinal conduction effect can be estimated on the basis of average temperature gradients. For the inner flame-tube wall the rate of heat flow to the section of wall (n) under consideration from an adjacent one ($n + 1$) is given by:

$$q = \frac{k_w t_w C_A (T_{w,n+1} - T_{w,n})}{x_{n+1} - x_n} \quad (168)$$

where k_w = thermal conductivity of wall material

t_w = wall thickness

Per unit area, the heat gain is:

$$K = \frac{k_w t_w (T_{w,n+1} - T_{w,n})}{x_{n+1} - x_n} \frac{2}{x_{n+1} - x_{n-1}}$$

Combining this with a corresponding quantity for heat flow from the $n-1$ element, the net heat received becomes:

$$\Delta K = \frac{2k_w t_w}{x_{n+1} - x_{n-1}} \left[\frac{T_{w,n+1} - T_{w,n}}{x_{n+1} - x_n} - \frac{T_{w,n} - T_{w,n-1}}{x_n - x_{n-1}} \right] \quad (169)$$

Solution of the Heat-Balance Equation

When all of the heat-flux terms are considered, the heat-balance equation for an element of the flame-tube wall is:

$$R_1 + C_1 + \Delta K = R_2 + C_2 + R_3 + Q_{tr}$$

Both the longitudinal conduction term, ΔK , and the radiation interchange term, R_3 , are functions of the wall temperature distribution (rather than the local temperature of the wall element) and, therefore, an iterative method of solution of Equation 130 is required when these terms are considered. Often, however, the user will not wish to consider ΔK and R_3 , in which case a non-iterative solution of Equation 130 is possible.

Non-Iterative Solution

In this case Equation 130 becomes:

$$R_1 + C_1 = R_2 + C_2 + Q_{tr} \quad (170)$$

Q_{tr} is zero when there is no transpiration cooling.

Substituting for R_1 from Equation 131 or 140; for C_1 from Equation 156, 157, or 161; for R_2 from Equation 149; for C_2 from Equation 162; and for Q_{tr} from Equation 163; Equation 170 becomes:

$$D_1 T_w^4 + D_2 T_w^{2.5} + D_3 T_w = D_4 \quad (171)$$

where D_1 , D_2 , D_3 , and D_4 are known, their values depending upon the program option. Newton's approximation is used to solve Equation 171.

For use in Newton's approximation, a first estimate of T_w is obtained from one of the following equations:

$$D_1 T_w^4 = D_4$$

$$D_2 T_w^{2.5} = D_4$$

$$D_3 T_w = D_4$$

$$T_w = T_{ft}$$

The chosen T_w is that which leads to the smallest value of ϵ when Equation 171 is written in the form:

$$D_1 T_w^4 + D_2 T_w^{2.5} + D_3 T_w - D_4 = \epsilon \quad (172)$$

With this initial estimate of T_w , Newton's approximation is used to find a value of T_w that satisfies Equation 171.

Iterative Solution

The iterative heat-balance solution is only called for after a noniterative calculation; an approximate wall-temperature distribution will therefore always be available. The iterative heat balance is repeated until the maximum temperature change between any two iteration cycles is less than the specified tolerance.

End Effects

The boundary conditions assumed at the ends of the combustor can have an important effect on the overall wall temperature distribution. Since the highest temperature gradients frequently occur away from the ends, it has been assumed that the wall temperatures at the ends are as given by the noniterative calculation.

Structure of the Subprogram

The heat-transfer subprogram consists of:

1. A subroutine for solving the noniterative heat balance.
2. A subroutine for solving the iterative heat balance.
3. A group of library subroutines which provide gas properties, correlations for wall cooling and flame emissivity, and the solution of the fourth-power heat-balance equation.

Detailed flow charts and program listings for the heat-transfer subprogram are given in Volume II.

LIMITATIONS OF THE COMPUTER PROGRAM

The computer program represents a significant advance in the analysis of annular combustors, in that it draws together reasonable representations of the pertinent flow, burning, and heat-transfer phenomena into an integrated computing tool. Because of limitations in the models and in the experimental data available, and the need to keep the program to a manageable size, however, it has been necessary to make a number of assumptions and compromises that limit the accuracy of the results. Most of these have been discussed in connection with the analytical methods. To emphasize the importance of understanding these limitations in making intelligent use of the program, they are summarized here.

General

The analysis is one-dimensional: circumferential variation of flow quantities such as pressure and temperature is ignored throughout the program; radial variation of these quantities is considered in the streamtube method of diffuser analysis, but not elsewhere. It is well known that the flow in an actual combustor departs significantly from one-dimensionality, because of the presence of swirlers, fuel atomizers, holes, swirl at the compressor exit, and so forth. At present, however, neither the theoretical methods nor the experimental data are available upon which to base a more detailed model. This is, then, a limitation of the program as a whole. Its effect is difficult to assess. It should be kept in mind when using the program in connection with experimental data, however, that unusually large departure from one-dimensionality in the experiment may cause considerable disagreement between experiment and analysis.

Diffuser Subprogram

The analytical methods used in the diffuser program contain several important limitations:

1. Flow in the diffuser is assumed to be unaffected by downstream conditions. If the flow is well matched at the snout, this assumption is expected to be valid. Otherwise, serious errors will undoubtedly result. Snout design should, therefore, receive careful attention.
2. No provision is made for including splitter vanes in the diffuser analysis.
3. The program does not attempt to treat flow after separation.

Air-Flow Subprogram

The more important limitations of the air-flow subprogram are as follows:

1. The treatment of the primary zone as a stirred reactor limits the information obtained. For example, if the detailed burning rate and flame temperature were known, the flame-tube wall temperature could be calculated as a function of position. Present understanding of the flow, mixing, and combustion processes in the primary zone is inadequate to support a more detailed analysis.
2. The program does not calculate the fuel-burning rate directly, but receives it as input and only serves to keep it below stoichiometric at any location. The results are limited by the judgment of the user and by his access to experimental data. For a more accurate estimate of flow conditions, particularly at low pressures

where reaction rates decrease, it should be possible to devise a fuel-burning rate correlation.

3. The jet-mixing models suffer from a lack of experimental data upon which to base the choice of models and entrainment constants; in addition, the program does not relate the mixing rate of wall jets to the film-cooling analysis carried out in the heat-transfer section.
4. The swirler-design method contained in the program is crude. When more experimental data become available, a more refined method should be incorporated.
5. If the use of transpiration cooling is to be explored in detail, an assessment of calculation methods should be made.

Heat-Transfer Subprogram

There are several significant limitations to the heat-transfer program:

1. The film-cooling model is idealistic; there is a serious lack of experimental data upon which to base choice of the characteristic distance X_0 used in the correlation; in addition, as mentioned above, the film-cooling and wall-jet-mixing models are not related.
2. Data is lacking on the emissivity of luminous flames.
3. There is a lack of data on transpiration cooling, with which to judge the reliability of the theory used.
4. No heat balance is performed to calculate the temperatures of the inner and outer casing walls.

Conclusion

Before making extensive use of this program, it would be useful to make a more exhaustive survey of the influence of program options than has been possible within the limitations of time and budget in the present project. For example, jet-mixing rates, and consequently the flame-temperature distribution, are quite sensitive to the choice of entrainment function and constant. By experiment, a "most reasonable" choice may be found.

TEST CASES

In this section, the results of a number of test cases illustrating aspects of the program are presented.

Diffuser Test Cases

Introduction

The diffuser test cases are mainly concerned with checking the validity of the analytical "streamtube" method. The following cases were specified:

1. Comparison with experimental data on two-dimensional diffusers, compiled by Cochran and Kline in Reference 70.
2. Comparison with data on annular diffusers, compiled by Abramovich and Vasil'yev in Reference 71.

In addition, the results of a number of test cases used during program development are presented in this section.

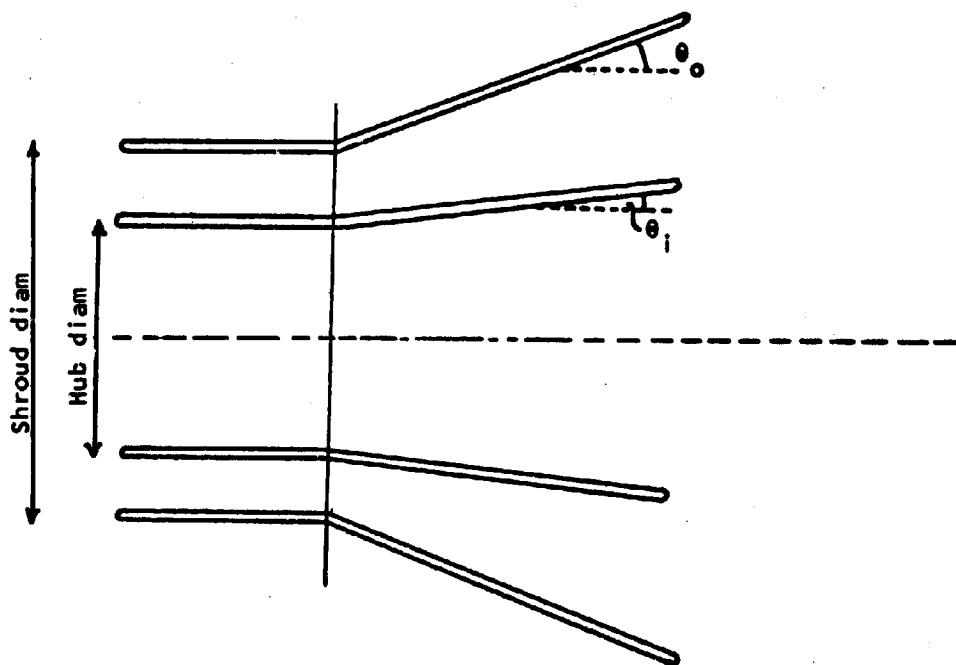
Choice of Separation Shape Factor

Before the test cases were run, it was necessary to select a value for H_{sep} , the value of the shape factor at which separation occurs. In conical diffusers, H_{sep} is typically 3.0, but for airfoils at moderate incidence, a value in the range of 1.8-2.2 is more usual.

The value of $H_{sep} = 1.9$ is used for comparison of the streamtube calculation method and the empirical-data method. The latter is based in the case of two-dimensional diffusers on the experimental results of Reneau, Johnston, and Kline (Ref 7). A comparison between streamtube and empirical-data methods is shown in Figure 9 for diffusers with area ratios in the range 1.2 to 5.0 and

nondimensional lengths of 1.0 to 20.0. The only assumption made in obtaining these results was that the shape factor at entry is 1.4.

For annular diffusers the empirical-data method is based on data of Sovran and Klomp (Ref 6). The experimental results are based on diffusers with inlet hub-to-shroud ratios of 0.55 and 0.70 and various values of θ_i and θ_o (see sketch below) and inlet blockage.



In Figure 23 the experimental results of Sovran and Klomp are compared with the predicted performance using the streamtube method. The following assumptions were made:

1. Shape factor at inlet = 1.4
2. Separation shape factor = 1.9
3. Blockage at inlet = 3 per cent

4. Hub-to-shroud ratio = 0.55

5. $\theta_1 = 0$ degrees

The inlet blockage assumed in the calculations was somewhat higher than the 2 per cent assumed in Reference 6 for the following reasons:

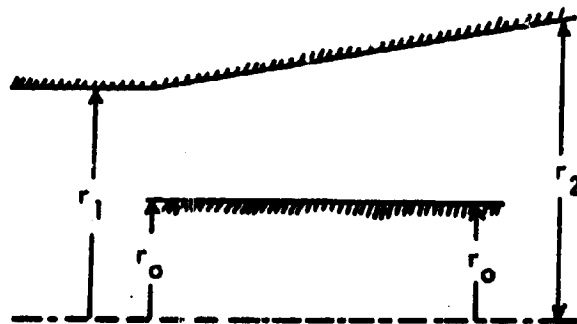
1. The flat-plate Reynolds number at entry appears from the geometry of the system to be of the order of 10^7 giving a blockage of 4 per cent.
2. The maximum diffuser effectiveness recorded was 85 per cent which indicates a high inlet blockage.

The difference between Figures 9 and 23 is not due only to the different values of inlet blockage, but is also due to differences in the variation of area ratio with length. For a two-dimensional diffuser:

$$A = A_1 + (A_2 - A_1) \cdot \frac{x}{L}$$

$$\frac{d \left(\frac{A}{A_1} - 1 \right)}{d \left(\frac{x}{L} \right)} = \frac{A_2 - A_1}{A_1} \quad (173)$$

For a simple annular diffuser:



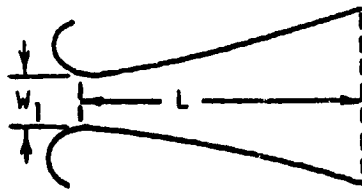
$$A = A_1 \frac{\left[r_1 + (r_2 - r_1) \cdot \frac{x}{L} \right]^2 - r_0^2}{r_1^2 - r_0^2}$$

$$\frac{d(A/A_1 - 1)}{d\left(\frac{x}{L}\right)} = \left[\frac{A_2}{A_1} - 1 \right] \left[\frac{2}{\frac{r_2}{r_1} + 1} + \frac{2x}{L} \frac{\frac{r_2}{r_1} - 1}{\frac{r_2}{r_1} + 1} \right] \quad (174)$$

Equations 173 and 174 reduce to the same form for $r_2 \approx r_1$, i.e. $A_2 \approx A_1$ or for large values of r_0 . Thus the performances of annular and two-dimensional diffusers show the most difference at large area ratios.

Two-Dimensional Diffuser Geometries

The test cases for two-dimensional diffusers are taken from Cochran and Kline (Ref 70) and the earlier work on similar apparatus by Moore and Kline (Ref 72). The geometry of the diffuser section is shown below:



This geometry is not entirely suitable to test the streamtube method for the following reasons:

1. The boundary layers at inlet are formed on highly curved surfaces, and not, as assumed, on a flat plate.
2. The static-pressure profile at inlet is distorted due to

the curvature of the flow. In the streamtube method the static pressure is assumed to be uniform across each cross-section.

These difficulties notwithstanding, it is felt that the results provide an adequate basis for assessment of the streamtube method. It is to be noted that these results are also included in the compilation and correlation of experimental data presented in Reference 7.

For the purposes of obtaining a concise comparison of the diffuser effectiveness obtained from the streamtube method with experimental results over an adequate range, a family of diffusers was selected from the data of Reference 70. These diffusers all have a nondimensional length of approximately 8, and cover a range of area ratios from 2 to 6.5. The geometric data are summarized below.

Included Angle degrees	Nondimensional length L/W_1	Area Ratio A_2/A_1
7.0	8.04	1.99
14.0	8.08	2.96
16.8	8.10	3.40
21.0	8.12	3.94
28.0	8.09	4.94
31.1	8.06	5.44
35.0	8.03	5.94
38.2	8.00	6.46

For these configurations, measured values of the shape factor at inlet were in the range 1.43 to 1.79 and measured values of the blockage were in the range 0.004 to 0.006. To circumvent the difficulty associated with obtaining the experimental velocity profile at the inlet to the diffuser, the streamtube method was used assuming a uniform inlet velocity profile; to account for the fact that the actual velocity at the wall was some 20 per cent greater than that

in midstream, the test cases were run with a blockage of 0.0075, and a corresponding shape factor of 1.47 (since the deceleration rate along the wall will be greater for the nonuniform velocity profile, a larger blockage should be used with a uniform velocity profile to simulate this effect).

For obtaining a comparison of the results of the streamtube method for the prediction of separation with experimental results, the data of Reference 72 were used. Again, the streamtube method was used with values of the inlet blockage and shape factor of 0.0075 and 1.47, respectively.

Comparison of Results for Diffuser Effectiveness

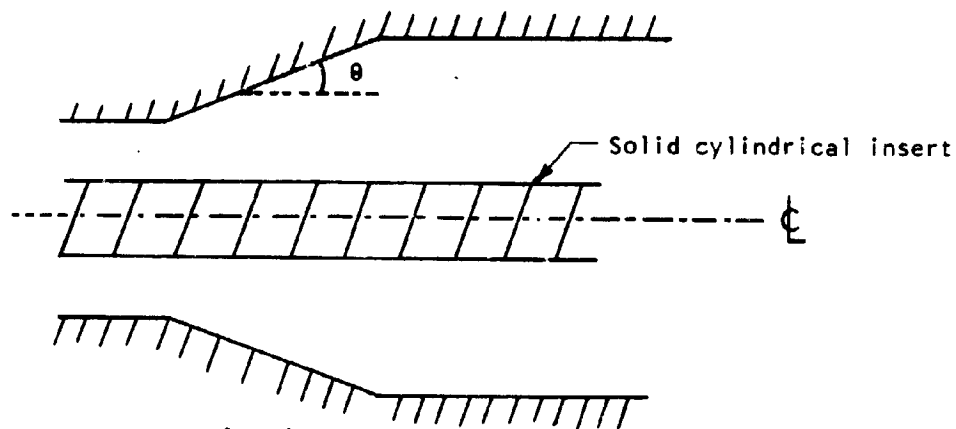
The effectiveness as computed by the streamtube method is shown with the experimental results in Figure 24. The agreement is reasonable, considering both the approximations made with regard to inlet conditions and the fact that the experimental accuracy was reported as ± 5 per cent.

Results - Line of First Stall

In Figure 25, lines are drawn dividing geometries in which separation occurs from those in which the flow does not separate. A comparison is made between the results of Moore and Kline (Ref 72), in which a flow visualization technique was used, and the results obtained using the streamtube method. Agreement is quite good.

Annular-Diffuser Geometries

The test cases for annular diffusers were taken from Abramovich and Vasil'yev (Ref 71). The geometry considered is shown below:



The two test cases analyzed were:

Area Ratio A_2/A_1	Range of θ degrees
2.0	5-40
3.8	5-40

The following assumptions were made:

1. Shape factor at inlet = 1.4
2. Shape factor at separation = 1.9

Annular-Diffuser Results

In Figure 26 a comparison is made of the results of the stream-tube method with the experimental results given by Abramovich and Vasil'yev (Ref 71). As the blockage is not quoted, theoretical curves are given for 1 per cent, 2 per cent, and 3 per cent blockage. A blockage of 1.5 per cent gives good agreement between the theoretical and experimental results. It is to be noted that the inlet blockage has a significant effect on the computed effectiveness, as is expected from the consideration that the effectiveness is determined by the displacement thickness at the exit (until separation occurs) and that this thickness is roughly proportional to the inlet displacement thickness.

Unfortunately, no data on the occurrence of separation in annular diffusers is available for comparison with analytical results.

Shear Flow in a Diffuser

The streamtube method provides a means of predicting the change in velocity profile through the diffuser. The main assumptions made in the method are that the profile at entry is in equilibrium, and that mixing effects can be neglected.

To test the method, the experimental results of Horlock and Lewis (Ref 73) are analyzed. In these experiments straight-walled diffusers and nozzles were used and velocity profiles at inlet and exit were measured. Two geometries were considered:

Type	Area Ratio	Total Included Angle, degrees
Nozzle	0.7	10
Diffuser	1.47	15

The results of these tests are shown in Figures 27 and 28; the agreement between the streamtube method and the experimental results is good.

Air-Flow Test Cases

Introduction

The air-flow test cases were designed to check the pressure-drop and air-flow-distribution calculations. For comparison, the experimental and theoretical work of Dittrich (Ref 74) and Graves and Grobman (Ref 1) was used.

The tests used for comparison were carried out on a straight-walled tubular combustor without a diffuser. Seven test cases were run, varying three main parameters:

1. Reference Mach number
2. Overall temperature ratio
3. Ratio of total hole area to reference area

Input Conditions

Since this program only deals with annular combustors and combustors of rectangular cross section, it was impossible to match the geometry used in the original tests. Instead, a hypothetical combustor of rectangular cross section was set up. This was 12 inches wide and had all cross-sectional areas equal to those in the NASA combustor. The dimensions of the hypothetical combustor are shown in the table below.

Geometry employed in Test Case		NASA Combustor (Tubular)	
Flame-tube height	2.37 in	Flame-tube diam	6.0 in
Casing height	3.95 in	Casing diam	7.75 in
Overall length	52.0 in	Overall length	52.0 in
No. of holes per row on each wall	3	No. of holes per row	6
Area per hole	1.48 sq in	Area per hole	1.48 sq in

Input quantities specified by NASA are listed below:

Compressor-discharge total temperature	80 deg F
Compressor-discharge total pressure	15 psia
Fraction of air entering secondary holes that recirculates upstream	0
Rate of jet mixing	instantaneous

The total pressure was assumed to be 15 psia at the beginning of each annulus.

Three hole arrangements were used, as indicated below:

Axial location, inches	6	10	14	18	22	26	30	34
Run I	✓	✓		✓	✓		✓	✓
Run II	✓	✓	✓	✓	✓	✓	✓	✓
Run III	✓				✓			✓

In Run I, input conditions were varied from case to case as follows:

	Overall Fuel-air Ratio	Air Mass Flow Rate lbm per sec
Case 1	0.0	2.46
Case 2	0.0	1.23
Case 3	0.0	4.92
Case 4	0.00724	2.46
Case 5	0.0152	2.46

The three fuel-air ratios correspond, according to Figures 21 and 23 of Reference 36, to temperature ratios (combustor outlet/inlet) of 1, 2, and 3. The three mass flows correspond to reference velocities of 50, 100, and 150 ft per sec.

Results

In Figure 29, the variation of pressure-loss factor with reference Mach number as calculated by the present method is compared with the results

of Reference 74. The agreement with the experimental data is very good, considering the difference in geometric configurations. However, the sharper increase in pressure drop at higher Mach numbers, apparent in the experimental data, is not so marked in the curve representing the present predictions.

Figure 30 shows the effect of changing the ratio of total hole area to reference area. Here the agreement with experimental results is exceptionally good, particularly at high values of the area ratio.

The effect of heat addition on the pressure-loss factor is shown in Figure 31; again the agreement with the experimental results is good.

Figure 32 is a plot of the fraction of total air flow in the flame tube against the ratio of cumulative open hole area in the flame-tube wall to total hole area. The results obtained here differ from those of Graves and Grobman (Ref 1) at high values of the ratio of total hole area to reference area, A_{HT}/A_{ref} . No experimental results are available to check the validity of the two methods.

Conclusion

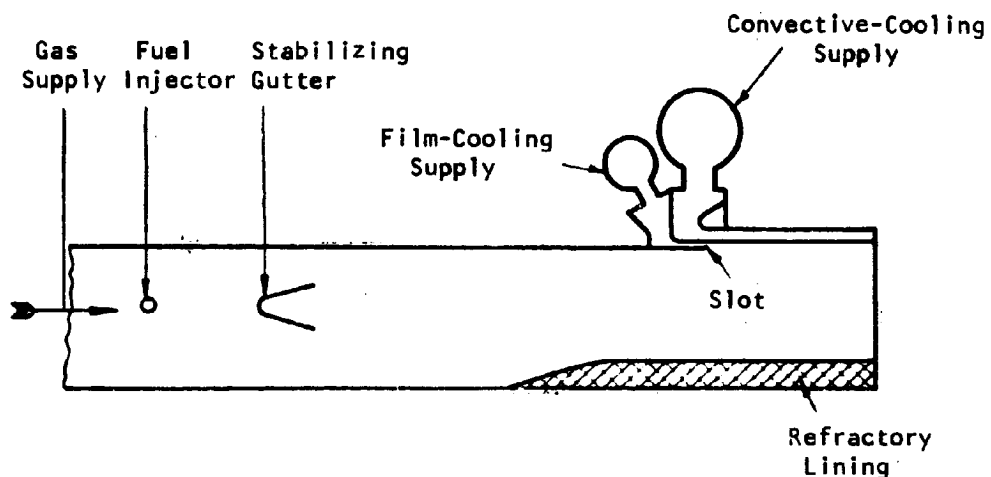
In view of the differences between the geometrical configuration of the experimental combustor in Reference 74 and the configuration employed for the present computations, the comparison between the calculated and the measured pressure losses is particularly good. The only effect which the computations apparently do not accurately predict is the effect of high Mach numbers on the pressure-loss factor. However, the Mach number at which the divergence becomes appreciable is outside the normal range of reference Mach numbers for gas-turbine combustion chambers.

Heat-Transfer Test Cases

The predictions of the heat-transfer subprogram were compared with experimental data presented by Milford and Spiers in Reference 75.

Experimental Conditions

The apparatus used is shown in the sketch.



Three sets of results were obtained:

1. Convective cooling (on annulus side) only
2. Film cooling only
3. Convective and film cooling

Some of the test conditions were as follows:

Hot-gas temperature 3510 deg R

Hot-gas Mach number 0.25

Convective Cooling (Cases 1, 2, 3, and 4)	{	Cooling-gas temperature 1440 deg R Cooling-gas Mach numbers 0, 0.11, 0.14 and 0.20
--	---	--

Film Cooling (Cases 5, 6, and 7)	}	Cooling-gas temperature 1440 deg R
		Slot-gas velocities 260, 570, and 800 ft per sec
Convective and Film Cooling (Cases 8, 9, 10, and 11)	}	Cooling-gas temperature 1530 deg R
		Convective-stream Mach number 0.15 Slot-gas velocities 0, 260, 580, and 825 ft per sec

Assumptions

The information provided in Reference 75 was insufficient to specify the problem. A thorough search of the literature revealed no other published experimental results in which heat-transfer measurements had been made with combined film and convective cooling. Thus, other than abandon the heat-transfer test case, the only course left open was to estimate or assume values for the information missing from Reference 75. The information required to complete the problem specifications and the assumed values are as follows:

Distance across flame tube	4.5 in
Annulus height	0.45 in
Slot height	0.036 in
Static pressure	Atmospheric
Fuel-air ratio	0.067
Fuel hydrogen-carbon ratio	0.12

The casing temperature was calculated assuming natural convection and radiation to a room-temperature background. (The actual heat-transfer coefficients were obtained from McAdams, Ref 26, Table 7-2.) Heat transfer from the casing to the annulus air was ignored. The casing temperature distributions thus obtained were as follows:

Case	Casing Temperature, deg R		
	Distance Downstream of Slot, in		
	2.0	4.0	5.5
1	1997	1872	1786
2	1808	1780	1750
3	1770	1752	1720
4	1720	1707	1698
5	1800	1762	1723
6	1610	1661	1662
7	1580	1639	1647
8	1762	1757	1720
9	1566	1617	1609
10	1461	1542	1550
11	1448	1518	1537

The flame-tube wall absorptivities and emissivities were taken as 0.85; the casing emissivity was taken as 0.8. The flame was assumed to be luminous (1966 NREC correlation, Equations 137 and 138), and a value of $X_o = 7.0$, the value for "clean" slots, was assumed in Spalding's film-cooling correlation (Equation 160).

Discussion of Results

The results are shown in Figures 33, 34, and 35. Figure 33 shows Cases 1 to 4 - those with convective cooling only. Agreement is reasonably good, the predicted results showing a somewhat greater effect of annulus convection than the experimental ones. The inconsistency may be due to:

1. Incorrect assumptions about the dimensions of the test combustor.

2. Incorrect assumptions about the heat loss from the casing.

The casing temperature does, in this case, exert an important influence on the flame-tube wall temperature, since radiation from the flame-tube wall to the casing becomes significant in the absence of film cooling.

The steep slope of the "radiation-only" curve was not well predicted. It is interesting to note that Milford and Spiers' own calculations also failed to predict this trend. This is clearly due to two-dimensional effects which become increasingly important as the convective-heat-transfer components are reduced. Two-dimensional effects were not included in this calculation.

Figure 34 shows cases 5 to 7 - those with film cooling only. At the lowest-slot gas velocity, the correlation predicts poorer cooling near the slot than was obtained in the experiment. At higher velocities, the effect of film cooling was found to be greater than in the experiment. Again this is probably due to incorrect assumptions about the dimensions of the slot.

Figure 35 shows the results for combined convective and film cooling. As expected, the predicted effect of film cooling at low slot-gas velocities is again lower than the experimental one.

Conclusion

The most striking differences between the calculated and the experimental curves are in their slopes. There appears to be a dominant two-dimensional heat-transfer mode that is causing the experimentally measured wall temperatures to fall off rapidly with distance downstream. This effect is most apparent in the radiation-only results (experimental curves A of Figures 33 and 34), but it must also be present in the other

experimental results. Since the experimental conditions of Reference 75 are poorly documented, it is not possible to simulate this two-dimensional effect in any meaningful way.

From the results of the present computer calculations it is concluded that the film- and convective-cooling models used are producing results that agree with the main trends of this experiment, ignoring undocumented two-dimensional effects.

Overall Test Cases

Operation of the complete computer program has been checked by running five overall test cases having identical geometry and inlet conditions (Table II). The program options specified by NASA for these test cases are given in Table III. The results of the test cases are discussed in the following paragraphs.

The pressure-loss characteristics of the diffuser are summarized on Figure 36. Subsequent figures are grouped in pairs by individual test case. For Test Case 1 the cumulative fraction of inlet air present in the flame tube and the fractions of inlet air contained in the residual jets, as functions of axial position, are shown on Figure 37, the axial distributions of the flame temperature, the flame-tube wall temperatures, and the cumulative fraction of fuel burned on Figure 38. Figures 39 through 46 are similarly ordered. On Figure 47 are shown the axial distributions of total and static pressures in the flame tube and the annuli for Test Case 3, as a typical example of pressure distributions.

The complete input and output data for Test Case 3 may be found in Appendices II and III of Volume II.

Diffuser Performance

Figure 36 portrays the pressure-loss characteristics of the diffuser as obtained from the five diffuser calculation options employed in the test cases. The range of flow splits obtained for each option is that which occurred during the air-flow iterations in the process of obtaining a solution (the narrow ranges shown for Cases 1 and 2 are a result of accurate initial estimates of the flow splits). The large difference between Case 1 and Cases 2 and 3, each of which employs the streamtube method in the diffuser section between the compressor discharge and the snout, is due to the fact that when the streamtube method is used in the annuli, the calculated blockage decreases considerably between Stations 2 and 3, and hence small mixing losses result. In Case 2, where separation occurs between Stations 1 and 2, the blockage at Station 3 is assumed to be equivalent to that at Station 2, and hence rather large mixing losses result. In Case 3, the mixing loss again includes the loss associated with the blockage at Station 2. The generally lower pressure losses in the inner annulus indicated by Cases 1, 2, and 3 as compared to Cases 4 and 5 are due to the distorted velocity profile at the compressor discharge which results in a higher local total pressure in the inner annulus; only when the streamtube method is used between Stations 1 and 2 is this distortion in total pressure reflected in the annulus calculations. In the present examples, which result in a badly mismatched flow at the snout, the use of the streamtube method between Stations 1 and 2, and the mixing method between Stations 2 and 4 (as in Case 3), is recommended.

The pressure losses in the diffusing passages influence the mass-flow split at the snout. Table IV summarizes the fractional flows through the snout and the inner and outer annuli for the two test cases. The

dependence of flow split on pressure drop may be seen by comparing entries in Table IV with corresponding points on Figure 36.

The flow split at the snout in turn influences the temperature level in the flame tube. As the amount of fuel available for burning in the primary zone does not vary from case to case, and as the total temperature of the entering air is substantially constant, the effect of a decrease in flow through the dome into the primary zone is to raise the temperature of the combustion products. This trend is evident in Table IV, where the primary-zone temperatures are listed. The primary-zone temperature influences the general level of temperature in the flame tube for some distance downstream.

The temperature and flow distributions for the individual test cases are discussed in subsequent sections. Reference should be made to Table III for the program options used in running these cases.

Test Case I

The choice of entrainment constants for this case has a pronounced effect on the results. As shown on Figure 37, the penetration jets dissipate before the first calculation point downstream of their origin; this is to be expected for the entrainment constant (1) used here. The wall jets, however, with an entrainment constant (0) that implies no mixing, remain unchanged from their origin to the end of the flame tube. The virtually instantaneous mixing of the penetration jets results in a sharply falling flame temperature immediately downstream of each hole row (Fig 38). As the wall jets do not mix at all, the amount of gas available in the flame tube is reduced by the contents of the wall jets and the resulting flame-temperature distribution is considerably higher

than it would have been, had the wall jets mixed with the main stream in the flame tube.

In the program option used for this test case, film cooling is ignored. (It should be recalled that there is no interconnection in the program between wall jets and film cooling.) Despite the lack of film cooling, the general level of the flame-tube wall temperature is relatively low. The explanation is, of course, the assumption of a nonluminous flame. The temperatures of the flame-tube walls follow the general variation of the flame temperature reasonably closely, as would be expected with a one-dimensional calculation of radiation from the flame to the walls, up to an axial position of about 24 inches. Downstream of this position the sharply dropping radiative heat transfer from the flame is roughly balanced by a drop in convective heat transfer in the annuli caused by sharply reduced air velocities in the annuli downstream of the dilution holes. Near the end of the combustor the air velocities in the annuli fall nearly to zero, forcing the wall temperatures to rise sharply.

Test Case 2

Although the change in the flow split at the snout for this case causes a drop of about 140 deg F in the flame temperature at the end of the primary zone, the most pronounced changes in the temperature distributions for this test case, when compared with those of Test Case 1, are attributable to the change in the entrainment constant for wall jets and the inclusion of film cooling.

As in Test Case 1, the penetration jets effectively mix instantaneously (Fig 39). The wall jets, however, dissipate within about $1\frac{1}{2}$ inches of their origins and their cool air is mixed into the

flame-tube gases. As a result, the flame temperature drops sharply downstream of the cooling slots. Because of the lower primary-zone temperature and the more rapid jet mixing, the flame-temperature profile and the peak temperature are much lower than in Test Case 1.

The inclusion of the film-cooling effect and the relatively low flame temperature combine to hold the flame-tube wall temperatures (Fig 40) at a general level about 400 deg F lower than in Test Case 1. The wall-temperature profile is quite jagged in this case: essentially step changes in temperature at the cooling-slot positions are followed by rapidly increasing temperature as the cooling film dissipates.

Test Case 3

The most significant change in program option in this case is from nonluminous to luminous flames. The radiation heat transfer for Case 3 is greater by about a factor of three than that for Case 1. In addition, the behavior of the jets is substantially altered by the change in jet-mixing model (Fig 41). The penetration jets now remain distinct from two to four inches downstream of their origins; for the model used here (equivalent entrainment) the entrainment constant (1) implies complete jet dissipation when the mass flow in the "actual" jet has grown to twice the mass flow at the hole of origin. The wall jets mix very slowly and are extant at the end of the flame tube.

Because of the relatively slow mixing of the jets, the flame temperature (Fig 42) is relatively high throughout the combustor, compared to that in Case 2, where mixing was rapid. The high flame temperature and luminosity combine to increase the flame-tube wall temperatures to a general level even higher than those for Case 1. The predominance of radiation as a heat-transfer mechanism is apparent from the manner in which the wall

temperatures decrease in step with the flame temperature in the downstream end of the combustor.

Test Case 4

The luminous-flame correlation used in this case gives luminosities considerably lower than were found in Case 3 (about 0.25 vs about 0.4). This accounts for the generally lower level of wall temperatures in this case (Fig 44), despite the exclusion of film cooling. The combination of no film cooling and two-dimensional radiation causes the wall temperature profile to be relatively flat, compared to the profiles of previous cases.

Cases 3 and 4 use the same mixing model, with changes in the entrainment constants for penetration and wall jets too small to affect jet behavior significantly (compare Figs 41 and 43). For this reason the flame-temperature profiles of these two cases are quite similar.

The calculated effect of radiation interchange between the flame-tube walls is negligibly small.

Test Case 5

With the entrainment constants and the mixing model used, the penetration jets mix in a distance too short for a residual jet to be observed at the next calculation station downstream of the jet origin. The wall jets survive for roughly the distance to the next penetration-hole row (Fig 45). As a result, the flame-temperature profile is relatively low, with periodic bumps attributable to the influence of lingering wall jets.

The luminosity correlation and relatively low flame temperatures result in low wall temperatures (Fig 46). The typically jagged profiles for wall cooling are tempered somewhat by two-dimensional radiation.

It should be noted that the effects of including radiation interchange between the flame-tube walls and conduction along them are small and cannot be distinguished on these plots because of the stronger effects of changes in luminosity and jet-mixing correlations.

Conclusions

The results of the test cases indicate the sensitivity of calculated conditions in the combustor to the models used. The diffuser options, mixing and flame-luminosity correlations, and the presence or absence of film cooling, can influence flow and temperature distributions dramatically. Choice of reasonable correlations is mostly a matter of judgment. A poor choice can result in ridiculous values. For example, a poor choice of entrainment constant in the profile-substitution model can result in wall jets that do not disappear, or worse yet, grow with downstream distance.

It has not been possible, within the scope of the present program, to investigate fully the influence of various arbitrary program inputs, such as entrainment constants, on program results. Such an investigation should be carried out by the user, preferably in conjunction with appropriate experimental data, to select reasonable values of these constants.

CONCLUSIONS

The main conclusions of this work are:

1. A computer program for analyzing the aerodynamic and heat-transfer characteristics of annular and rectangular gas-turbine combustors has been completed.
2. All computer-program options have been checked and are found to operate satisfactorily.
3. The diffuser, air-flow, and heat-transfer sections of the computer program have been tested individually by comparing their predictions of appropriate quantities with experimental data available in the open literature. The correlation between calculated and experimental values is judged to be reasonably good.
4. The complete computer program has been tested for satisfactory operation by running a series of five hypothetical overall test cases, using geometry, inlet conditions and program options specified by NASA. The main trends of the results, as inferred by comparing changes in pressures, flows, and temperature distributions from case to case, are reasonable. It is therefore concluded that the program as a whole is operating properly.
5. The wide range of program options available makes this program a useful tool for predicting the effect on combustor performance of changes in combustor geometry, inlet conditions, and fuel distribution.

6. The results of the streamtube diffuser calculation are surprisingly good in view of the gross assumptions made. If the equations are examined further and the potentialities and limitations of the method explored, this technique could provide a powerful new tool for more general application.

REFERENCES

1. Graves, C. C. and Grobman, J. S., Theoretical Analysis of Total-Pressure Loss and Airflow Distribution for Tubular Turbojet Combustors with Constant Annulus and Liner Cross-Sectional Areas (NACA Rep. 1373), National Advisory Committee for Aeronautics, 1958.
2. Grobman, J. S., Comparison of Calculated and Experimental Total-Pressure Loss and Airflow Distribution in Tubular Turbojet Combustors with Tapered Liners (NASA Memo 11-26-58E), National Aeronautics and Space Administration, 1959.
3. Samuel, B. P., A Jet Engine Combustor Design Analysis Suitable for Electronic Computers (ASME Preprint 61-WA-305), American Society of Mechanical Engineers, 1951.
4. Lefebvre, A. H. and Herbert, M. V., "Heat-Transfer Processes in Gas-Turbine Combustion Chambers", Proc. Inst. Mech. Engrs., England, vol. 174, 1960.
5. Tipler, W., "Combustion Chambers and Control of the Temperature at Which They Operate", Inst. Mech. E. - ASME Joint Conference on Combustion, Institution of Mechanical Engineers, England, 1955.
6. Sovran, G. and Klomp, E. D., Experimentally-Determined Optimum Geometries for Rectilinear Diffusers with Rectangular, Conical or Annular Cross-Section, presented at the Symposium "Fluid Mechanics of Internal Flow", General Motors Research Laboratories, Michigan, September, 1965.
7. Reneau, L. R., Johnston, J. P., and Kline, S. J., Performance and Design of Straight, Two-Dimensional Diffusers (ASME Prep. 66-FE-10), American Society of Mechanical Engineers, May, 1966.
8. Spalding, D. B., A Unified Theory of Friction, Heat Transfer and Mass Transfer in the Turbulent Boundary Layer and Wall Jet (ARC CP No. 829), Aeronautical Research Council, England, 1965.
9. Spalding, D. B., "Prediction of Adiabatic Wall Temperatures in Film-Cooling Systems", AIAA Journal, vol. 3, no. 5, May, 1965, pp 965-967.
10. Sturgess, G. T., Comment on "Prediction of Adiabatic Wall Temperatures in Film-Cooling Systems", AIAA Journal, vol. 4, no. 4, April, 1966.
11. Schirmer, R. M. and Quigg, H. T., Effect of JP Fuel Composition on Flame Radiation and Hot Corrosion (Res. Div. Rep. 4230-65R), Phillips Petroleum Company, Bartlesville, Okla., 1965.

12. Gruber, G., "A Method of Calculating Wall Temperatures in a Radiation-Cooled Rocket Nozzle", Pyrodynamics, vol.1, no.3, July, 1964.
13. Sparrow, E. M., "Radiation Heat Transfer Between Surfaces", Advances in Heat Transfer, vol.2, Academic Press, New York, 1965.
14. Henry, J. R., Wood, C. C., and Wilbur, S. W., Summary of Subsonic-Diffuser Data (NACA RM L56F05), National Advisory Committee for Aeronautics, 1956.
15. Van Dewoestine, R. V. and Fox, R. W., An Experimental Investigation into the Effects of Subsonic Inlet Mach Number on the Performance of Conical Diffusers (Tech. Rep. FMTR-66-1), Purdue University, Indiana, 1966.
16. Young, A. D. and Green, G. L., Tests of High-Speed Flow in Diffusers of Rectangular Cross Section (ARC R & M 2201), Aeronautical Research Council, England, 1944.
17. Corkrell, D. J. and Markland, E., "A Review of Incompressible Diffuser Data", Aircraft Eng'g, vol.35, October, 1963, pp 286-292.
18. Fox, R. W. and Kline, S. J., "Flow Regimes in Curved Subsonic Diffusers", J. Basic Eng., Trans. ASME, series D, vol.84, September, 1962.
19. Wood, C. C. and Higginbotham, J. T., Effects of Diffuser and Center-Body Length on Performance of Annular Diffusers with Constant-Diameter Outer Walls and with Vortex-Generator Flow Controls (NACA RM L54G21), National Advisory Committee for Aeronautics, 1954.
20. Wilbur, S. W. and Higginbotham, J. T., Investigation of Two Short Annular Diffuser Configurations Utilizing Suction and Injection as a Means of Boundary Layer Control (NACA RM L54K18), National Advisory Committee for Aeronautics, 1955.
21. Nelson, W. J. and Popp, E. G., Performance Characteristics of Two 6° and Two 12° Diffusers at High Flow Rates (NACA RM L9H09), National Advisory Committee for Aeronautics, 1949.
22. Clarke, J. S. and Jackson, S. R., General Considerations in the Design of Combustion Chambers for Aircraft and Industrial Gas Turbines (SAE Preprint 444A), Society of Automotive Engineers, 1962.
23. Carmichael, A. D. and Pustintsev, G. N., The Prediction of Turbulent Boundary Layer Development in Conical Diffusers (TWF/TN/15), Imperial College of Science and Technology, London, June, 1966.
24. Doenhoff, A. E. von and Tetervin, N., Determination of General Relations for the Behaviour of Tubulent Boundary Layers (NACA Rep 772), National Advisory Committee for Aeronautics, 1943.

25. Dussourd, J. L., et al., Aerodynamic Criteria for Optimum Design of Mixed-Flow Impellers - Experimental Results for Impellers I and IB (WADC TN 58-88), AIRResearch Manufacturing Company, June, 1960.
26. McAdams, W. H., Heat Transmission, Third Edition, McGraw-Hill Book Company, New York, 1954.
27. Livesey, J. L., Jones, P. K., Parker, E., and Shaw, J. P., "Aerodynamics of Tube-Type Gas-Turbine Combustion Chamber Entry Sections", J. Mech. Eng. Sc., vol.2, no.3, 1960, pp 202-26.
28. Venneman, W. F., Flow Coefficients and Jet Deflection Angles for Combustor-Liner Air-Entry Holes, Part I, General Electric Company, Schenectady, New York, 1959.
29. Venneman, W. F., Flow Coefficients and Jet Deflection Angles for Combustor-Liner Air-Entry Holes, Part II, General Electric Company, Schenectady, New York, 1960.
30. Marshall, L. A., Aerodynamic Characteristics of Combustor-Liner Air-Entry Passages (Rep. R58 AGT 558), Aircraft Gas Turbine Division, General Electric Company, Cincinnati, 1958.
31. Kaddah, K. Sh., Discharge Coefficient and Jet Deflection Studies for Combustor-Liner Air-Entry Holes, Thesis No. 17/10, College of Aeronautics, Cranfield, England, June, 1964.
32. Dittrich, R. T. and Graves, C. C., Discharge Coefficients for Combustor-Liner Air-Entry Holes, I - Circular Holes (NACA TN 3663), National Advisory Committee for Aeronautics, 1956.
33. Dittrich, R. T., Discharge Coefficients for Combustor-Liner Air-Entry Holes, II - Flush Rectangular Holes, Step Louvers, and Scoops (NACA TN 3924), National Advisory Committee for Aeronautics, 1958.
34. Knight, M. A. and Walker, R. B., "The Component Pressure Losses in Combustion Chambers", ARC R & M 2987, 1957.
35. Rosenthal, J., Exploratory Methods for the Determination of Gas Flow and Temperature Patterns in Gas Turbine Combustors (ARL ME Note 235), Aeronautical Research Laboratory, Department of Supply, Australia, 1959.
36. Fielding, D. and Topps, J. E. C., Thermodynamic Data for the Calculation of Gas Turbine Performance (ARC R and M 3099) Aeronautical Research Council, England, 1959.
37. Hodge, J., Cycles and Performance Estimation, Butterworths Scientific Publications, London, England, 1955.

38. Flow Through a Sudden Enlargement in a Pipe (Aerodynamics Data Sheet 00.03.29), Royal Aeronautical Society, London, January, 1964.
39. Wilson, R. E., McAdams, W. H., and Seltzer, M., "The Flow of Fluids through Commercial Pipe Lines", Ind. Eng. Chem., vol. 14, no. 2, 1922, pp 105-119.
40. Gandamihardja, O., Jet Deflection (Thesis 15/16/C), College of Aeronautics, Cranfield, England, 1962.
41. Haupt, T., "Control of Secondary Air Jets in Combustion Chambers of Gas Turbines", Energetyka, Poland, no. 7, 1962, (Translation FTD-TT-62-1786), Wright-Patterson Air Force Base, Ohio, 1962.
42. Abramovich, G. N., The Theory of Turbulent Jets, translated by Scripta Technica, Massachusetts Institute of Technology Press, 1963.
43. Hawthorne, W. R., Rogers, G. F. C., and Zaczek, B. Y., Mixing of Gas Streams - The Penetration of a Jet of Cold Air into a Hot Stream (RAE Tech. Note Eng. 271), Royal Aircraft Establishment, England, 1944.
44. Pfeiffer, A., Murati, G. T., and Engel, A. B. Mixing of Gas Streams (M.S. Thesis), Massachusetts Institute of Technology, 1945.
45. Callaghan, E. E. and Ruggeri, R. S., Investigation of the Penetration of an Air Jet Directed Perpendicularly to an Air Stream (NACA TN 1615), National Advisory Committee for Aeronautics, 1948.
46. Ruggeri, R. S., Callaghan, E. E., and Bowden, D. T., Penetration of Air Jets Issuing from Circular, Square, and Elliptical Orifices Directed Perpendicularly to an Air Stream (NACA TN 2019), National Advisory Committee for Aeronautics, 1950.
47. Callaghan, E. E. and Ruggeri, R. S., A General Correlation of Temperature Profiles Downstream of a Heated Air Jet Directed Perpendicularly to an Air Stream (NACA TN 2466), National Advisory Committee for Aeronautics, 1951.
48. Beauregard, J. P., The Mixing of Cold Air Jets with a Hot Gas Stream (M.E. Thesis), McGill University, Canada, 1952.
49. Chakko Chakko, P., The Mixing of Hot Subsonic Jets with Cold Air Streams (M.E. Thesis), McGill University, Canada, 1956.
50. Norster, E. R., First Report on Jet Penetration and Mixing Studies (Rep. PD/JP1), College of Aeronautics, Cranfield, England, 1962.
51. Norster, E. R., Second Report on Jet Penetration and Mixing Studies (Rep. PD/JP2), College of Aeronautics, Cranfield, England, 1964.

52. Ivanov, Yu. V., "Some Patterns of a Free Stream Developing in External Transverse Flow", Izvestiya Akademiya Nauk Otdelenie Tekhnicheskikh Nauk, USSR, vol. 2, no. 8, 1954.
53. Shandorov, G. S., "Flow from a Channel into Stationary and Moving Media", Zh. Tekhn. Fiz., USSR, vol. 37, no. 1, 1957.
54. Sullivan, L. J., On Mixing of Cold Air Jets with a Hot Gas Stream (M.E. Thesis), McGill University, Canada, 1953.
55. Ruggeri, R. S., General Correlation of Temperature Profiles of a Heated Air Jet Directed at Various Angles to an Air Stream (NACA TN 2855), National Advisory Committee for Aeronautics, 1952.
56. Keffer, J. F. and Baines, W. D., "The Round Turbulent Jet in a Cross Wind", J. Fluid Mech., vol. 15, April, 1963.
57. Jordinson, R., Flow in a Jet Directed Normal to the Wind (ARC R and M 3074), Aeronautical Research Council, England, 1958.
58. Forstall, W. and Shapiro, A. H., "Momentum and Mass Transfer in Coaxial Gas Jets", J. Appl. Mech., December, 1950, pp 399-408.
59. Squire, H. B., "Jet Flow and its Effects on Aircraft", Aircraft Eng., England, vol. 22, March, 1950.
60. Kruka, V. and Eskinazi, S., "The Wall-jet in a Moving Stream", J. Fluid Mech., vol. 20, part 4, 1964, pp 555-579.
61. Harris, G. L., The Turbulent Wall Jet in a Moving Stream, "Recent Developments in Boundary Layer Research" (AGARDograph 97), North Atlantic Treaty Organization, May, 1965, pp 125-158.
62. Spalding, D. B., A Unified Theory of Friction, Heat Transfer and Mass Transfer in the Turbulent Boundary Layer and Wall Jet (ARC CP No. 829), Aeronautical Research Council, England, 1965.
63. Green, L. and Duwez, P., "Fluid Flow Through Porous Metals", J. Appl. Mech., vol. 18, 1951, pp 39-45.
64. Wheeler, H. L., Resume of Sweat Cooling, Bendix Filter Division, Bendix Corporation, Michigan, March, 1959.
65. Reeves, D., Flame Radiation in an Industrial Gas Turbine Combustion Chamber (NGTE Memo M285), National Gas Turbine Establishment, England, 1956.
66. Hamilton, D. C. and Morgan, W. R., Radiation-Interchange Configuration Factors (NACA TN 2836), National Advisory Committee for Aeronautics, 1953.

67. Humble, L. V., Lowdermilk, W. H., and Desmon, L. E., Measurements of Average Heat Transfer Coefficients for Subsonic Flow of Air in Smooth Tubes at High Surface and Fluid Temperatures (NACA Rep. 1020), National Advisory Committee for Aeronautics, 1951.
68. Spalding, D. B., Auslander, D. M., and Sundaram, T. R., "The Calculation of Heat and Mass Transfer Through the Turbulent Boundary Layer on a Flat Plate at High Mach Numbers, With and Without Chemical Reaction", Supersonic Flow, Chemical Processes and Radiative Transfer, Pergamon Press, Oxford, 1964.
69. Perry, J. H., Chemical Engineers' Handbook, Fourth Edition, McGraw-Hill Book Company, New York, 1963.
70. Cochran, D. L. and Kline, S. J., Use of Short Flat Vanes for Producing Efficient Wide-Angle Two-Dimensional Subsonic Diffusers (NACA TN 4309), National Advisory Committee for Aeronautics, 1958.
71. Abramovich, S. F. and Vasil'yev, L. G., "Investigation of Annular Diffusers of Marine-Gas-Turbine Installations", Sudostroyeniye no. 3, 1963, pp 34-38, Translation FTD-TT-63-1039, Wright-Patterson Air Force Base, Ohio, 1963.
72. Moore, C. A. and Kline, S. J., Some Effects of Vanes and of Turbulence in Two-Dimensional Wide-Angle Diffusers, (NACA TN 4080), National Advisory Committee for Aeronautics, June, 1958.
73. Horlock, J. H. and Lewis, R. I., "Shear Flows in Straight-Sided Nozzles and Diffusers", Int. J. Mech. Sci., vol. 2, 1961, pp 251-266.
74. Dittrich, R. T., Comparison of Experimental with Theoretical Total-Pressure Loss in Parallel-Walled Turbojet Combustors (NACA RM E56117), National Advisory Committee for Aeronautics, 1957.
75. Milford, C. M. and Spiers, D. M., "An Investigation into Film Cooling by Slots", Part IV, Section A, Number 79, International Developments in Heat Transfer, American Society of Mechanical Engineers, 1961.
76. Schlichting, H., Boundary Layer Theory, McGraw-Hill Book Co., Inc., New York, 1960.
77. Kutateladze, S. S. and Leont'ev, A. I., Turbulent Boundary Layers in Compressible Gases, Translated by D. B. Spalding, Edward Arnold Ltd., London, 1964.
78. Hama, F. R., "Boundary Layer Characteristics for Smooth and Rough Surfaces", Trans. Soc. Naval Arch. Mar. Engrs., vol. 62, 1954, pp 333-358.

PRECEDING PAGE BLANK NOT FILMED. 160

TABLES

TABLE 1 - VALUES OF CONSTANTS IN GAS-PROPERTY EQUATION

The gas-property equation (Eq 164) is: $Z = a + bT + cT^2 + dT^3$ where Z is the gas property. Values of the four constants are given in the table for various gases for the gas properties indicated.

Specific Heat

Gas	a	b x 10 ⁴	c x 10 ⁸	d x 10 ¹¹	Range Deg R	Per Cent Accuracy
Air	0.2419	-0.08181	1.791	-0.2743	180-3600	1.9
Carbon Dioxide	0.1397	1.349	-2.646		400-2500	1.1
Nitrogen	0.2540	-0.2067	2.658	-0.4718	200-3600	1.9
Oxygen	0.2126	0.1564	0.9044	-0.2294	700-2700	1.1
Water Vapor	0.5632	-2.346	18.51	-3.351	700-2700	1.1

Viscosity

Air	-0.2853	3.268	-0.8253	1.239	200-1800	0.5
Carbon Dioxide	-1.180	1.582	0.7728		400-1100	0.5
Nitrogen	-0.01937	3.194	-0.7820	0.8990	200-2200	0.5
Oxygen	-0.4704	3.270	-0.5915		200-1100	0.5
Water Vapor	-2.316	2.280	0.1756		700-1500	0.5

Thermal Conductivity

Air	3.057	8.607	-2.279	2.908	700-3200	1.8
Carbon Dioxide	-1.203	7.786	-1.796	2.320	400-3000	0.5
Nitrogen	2.142	8.838	-2.766	4.295	400-3600	2.5
Oxygen	4.770	9.024	-1.994	2.368	400-3600	3.0
Water Vapor	6.200	2.442	1.926	-4.428	700-2700	1.6

**TABLE II - COMBUSTOR GEOMETRY AND INLET FLOW
CONDITIONS USED FOR OVERALL TEST CASES**

Configuration of Combustor Walls

Axial Position From Compressor Discharge Inches	Inner Casing	Inner Snout	Inner Dome or Flame Tube Wall	Outer Dome or Flame Tube Wall	Outer Snout	Outer Casing	Geometric Input Point Number
0.	32.500	-0.	-0.	-0.	-0.	35.700	1
0.500	32.300	-0.	-0.	-0.	-0.	35.900	2
1.000	32.000	-0.	-0.	-0.	-0.	36.200	3
1.500	31.800	-0.	-0.	-0.	-0.	36.400	4
2.000	31.500	-0.	-0.	-0.	-0.	36.700	5
2.500	31.300	-0.	-0.	-0.	-0.	36.900	6
2.800	31.100	33.100	-0.	-0.	35.100	37.100	7
3.000	31.000	33.000	-0.	-0.	35.200	37.200	8
4.000	30.500	32.500	-0.	-0.	35.700	37.700	9
5.000	30.100	32.100	-0.	-0.	36.100	38.100	10
6.000	29.600	31.600	-0.	-0.	36.600	38.600	11
7.000	29.100	31.100	34.100	34.100	37.100	39.100	12
8.000	28.600	30.600	31.100	37.100	37.600	39.600	13
8.800	28.200	30.200	30.200	38.000	38.000	40.000	14
9.000	28.200	30.200	30.200	38.000	38.000	40.000	15
9.100	28.200	29.900	29.900	38.300	38.300	40.000	16
14.000	28.200	29.900	29.900	38.300	38.300	40.000	17
15.000	28.200	29.900	29.900	38.300	38.300	40.000	18
15.100	28.200	29.600	29.600	38.600	38.600	40.000	19
20.000	28.200	29.600	29.600	38.600	38.600	40.000	20
21.000	28.200	29.600	29.600	38.600	38.600	40.000	21
21.100	28.200	29.300	29.300	38.900	38.900	40.000	22
26.000	28.200	29.300	29.300	38.900	38.900	40.000	23
27.000	28.200	29.300	29.300	38.900	38.900	40.000	24
27.100	28.200	29.000	29.000	39.200	39.200	40.000	25
29.000	28.200	29.000	29.000	39.200	39.200	40.000	26
30.000	28.200	29.000	29.000	38.200	38.200	40.000	27
31.000	28.200	29.000	29.000	37.200	37.200	40.000	28
32.800	28.200	29.000	29.000	37.200	37.200	40.000	29

Swirler Design (Specified as Input)

Number of Swirlers = 24
 Number of Blades = 8
 Blade Stagger Angle = 45.00 Degrees
 Inner Diameter = 1.00 Inches
 Outer Diameter = 1.50 Inches
 Area Per Swirler = 0.98 Square Inches (Ignoring Blockage Due to Vanes)

TABLE II, CONTINUED - COMBUSTOR GEOMETRY AND INLET FLOW
CONDITIONS USED FOR OVERALL TEST CASES

Details of Holes and Cooling Slots

Hole Row Number	Axial Position of Hole Center-Line Inches	Inner or Outer Wall	Number of Holes in Row	Description of Hole or Cooling Slot
1	9.000	Inner	1	Cooling slot: stepped louvre 0.095 in high, with wiggle strip
2	9.000	Outer	1	
3	12.000	Inner	50	Round holes 0.75 in diameter with scoop 0.75 in wide and 0.636 in high
4	12.000	Outer	50	
5	13.500		0	Dummy hole row (no holes)
6	15.000	Inner	1	Cooling slot: stepped louvre 0.095 in high, with wiggle strip
7	15.000	Outer	1	
8	16.500		0	Dummy hole row (no holes)
9	18.000	Inner	40	Flush holes 2.0 in long and 1.0 in wide
10	18.000	Outer	40	
11	19.500		0	Dummy hole row (no holes)
12	21.000	Inner	1	Cooling slot: stepped louvre 0.095 in high, with wiggle strip
13	21.000	Outer	1	
14	22.500		0	Dummy hole row (no holes)
15	24.000	Inner	75	Flush holes 2.0 in long and 1.0 in wide
16	24.000	Outer	75	
17	27.000	Inner	1	Cooling slot: stepped louvre 0.095 in high, with wiggle strip
18	27.000	Outer	1	
19	32.700		0	Dummy hole row (no holes)

Inlet Flow Conditions

Total Temperature at Compressor Discharge = 1150.000 Deg F
 Total Pressure at Compressor Discharge = 90.000 psia
 Air Flow Rate at Compressor Discharge = 96.000 lbm per sec
 Overall Fuel-Air Ratio = 0.018

TABLE III - PROGRAM OPTIONS FOR OVERALL TEST CASES

Program Option	Test Case Number																
	1	2	3	4	5												
Calculation method in first part of diffuser: a. Streamtube b. Empirical Data	a	a	a	b	b												
Calculation method in second part of diffuser: a. Streamtube and Mixing b. Empirical Data and Mixing c. Sudden Expansion and Mixing	a	b	c	b	c												
The following combinations of diffuser calculations are permitted: <table border="1" style="margin: 10px auto;"> <tr> <td>First Part</td> <td>a</td> <td>a</td> <td>a</td> <td>b</td> <td>b</td> </tr> <tr> <td>Second Part</td> <td>a</td> <td>b</td> <td>c</td> <td>b</td> <td>c</td> </tr> </table>	First Part	a	a	a	b	b	Second Part	a	b	c	b	c					
First Part	a	a	a	b	b												
Second Part	a	b	c	b	c												
Entrainment function for jet mixing: 1. Direct Mass Loss 2. Equivalent Entrainment 3. Profile Substitution	1	1	2	2	3												
Entrainment constant for penetration jets	1	1	1	0.75	0.5												
Entrainment constant for wall jets	0	0.1	0.2	0.3	0.4												
Luminosity correlations for flame emissivity: 1. Reeves Distillate Fuel (nonluminous) 2. Reeves Residual Fuel (nonluminous) 3. Lefebvre (luminous) 4. NREC 1964 (luminous) 5. NREC 1966 (luminous)	1	2	3	4	5												
One- or two-dimensional radiation?	1	1	1	2	2												
Radiation interchange between walls?	No	No	No	Yes	Yes												
Cooled walls?	No	Yes	Yes	No	Yes												
Longitudinal wall conduction?	No	No	No	No	Yes												
Heat transfer to annulus air?	No	Yes	No	No	Yes												

TABLE IV - FLOW SPLITS AND PRIMARY-ZONE TEMPERATURES FOR OVERALL TEST CASES

Test Case No.	1	2	3	4	5
Fraction of Inlet Air Entering Snout or Dome	.04847	.06174	.06230	.05759	.06313
Fraction of Inlet Air Entering Inner Annulus	.43117	.42020	.42994	.40121	.41369
Fraction of Inlet Air Entering Outer Annulus	.52036	.51806	.50775	.54120	.52317
Temperature of Gases in Primary Zone, deg F	3890.1	3730.1	3758.8	3800.0	3725.7

FIGURES

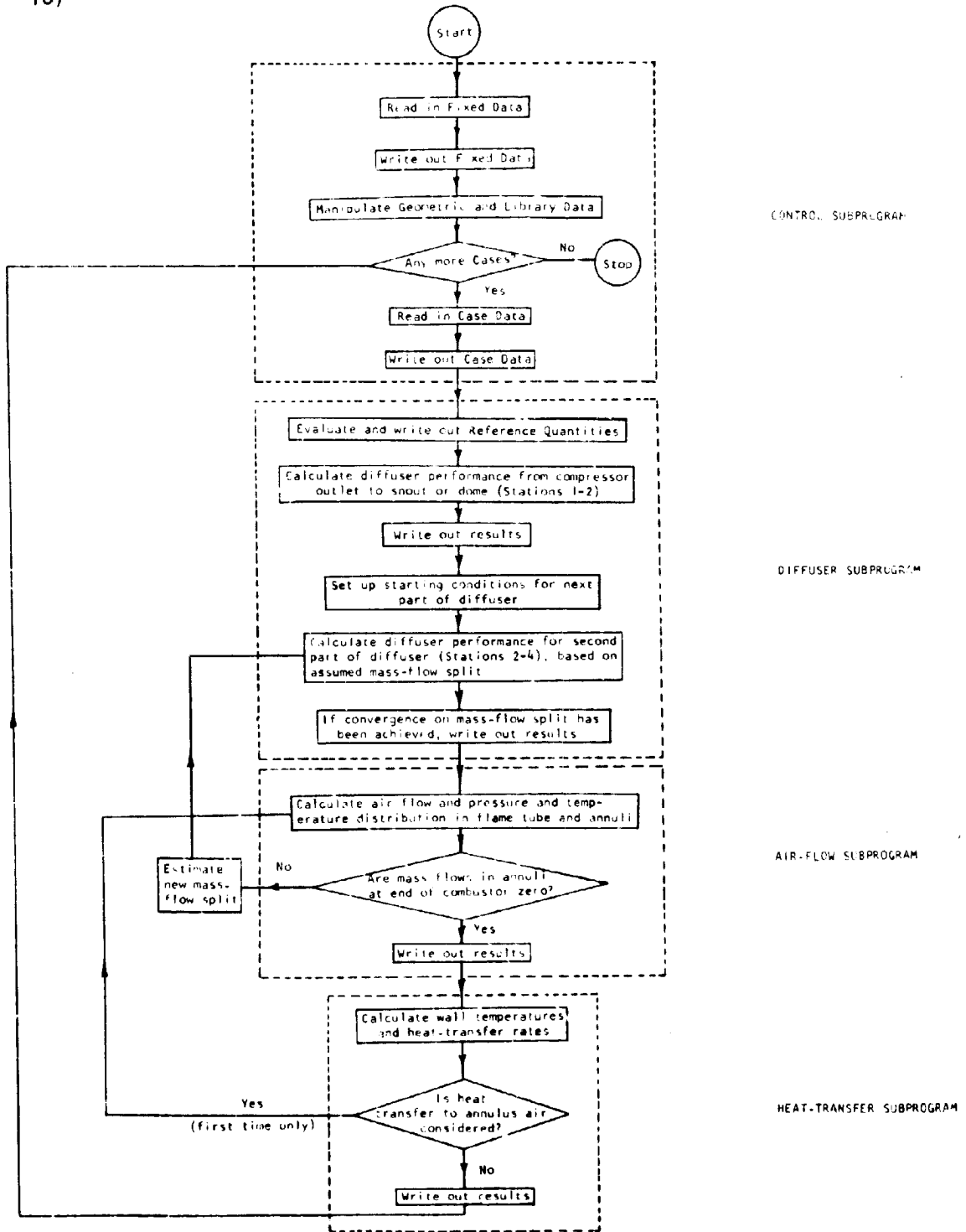
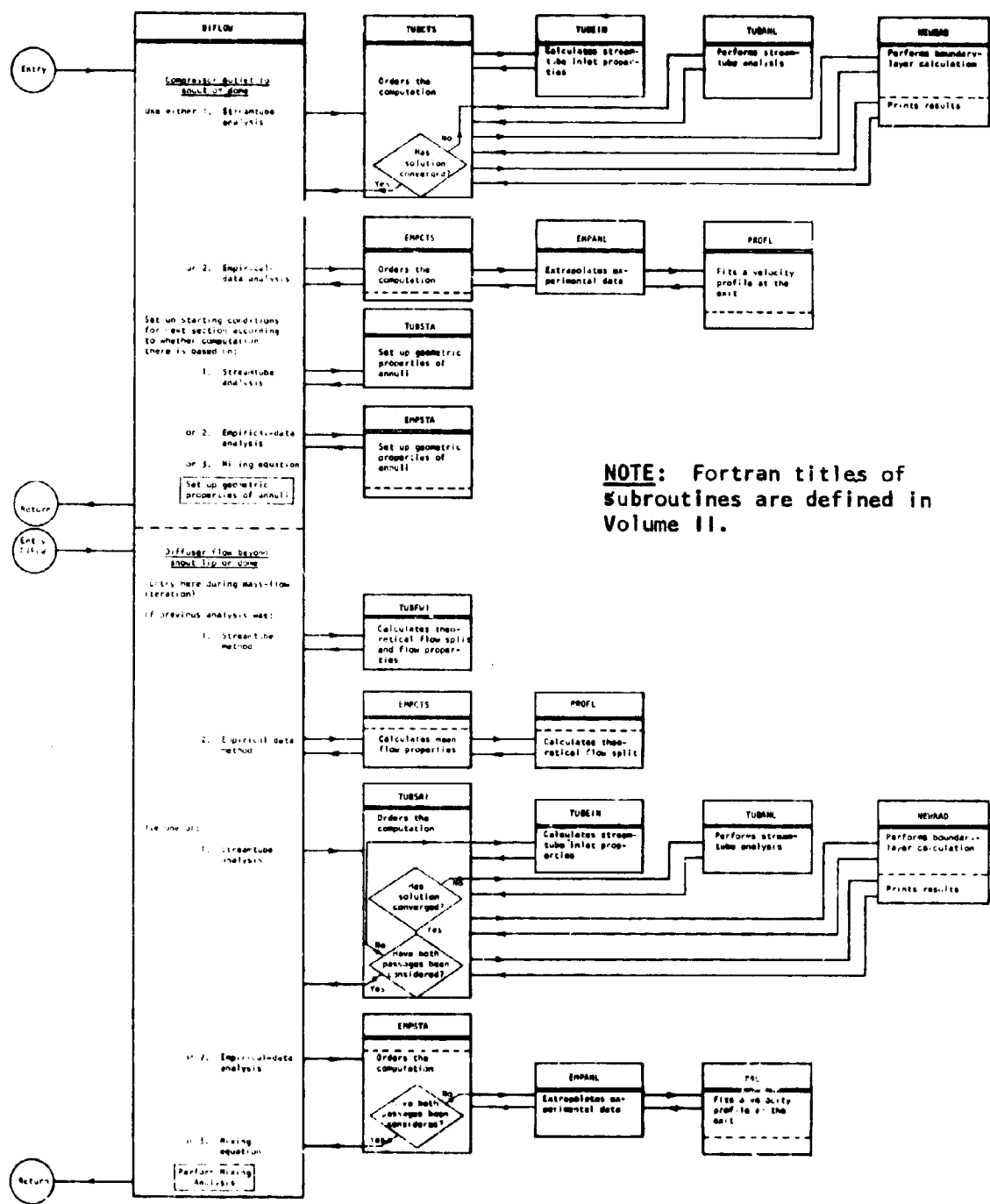
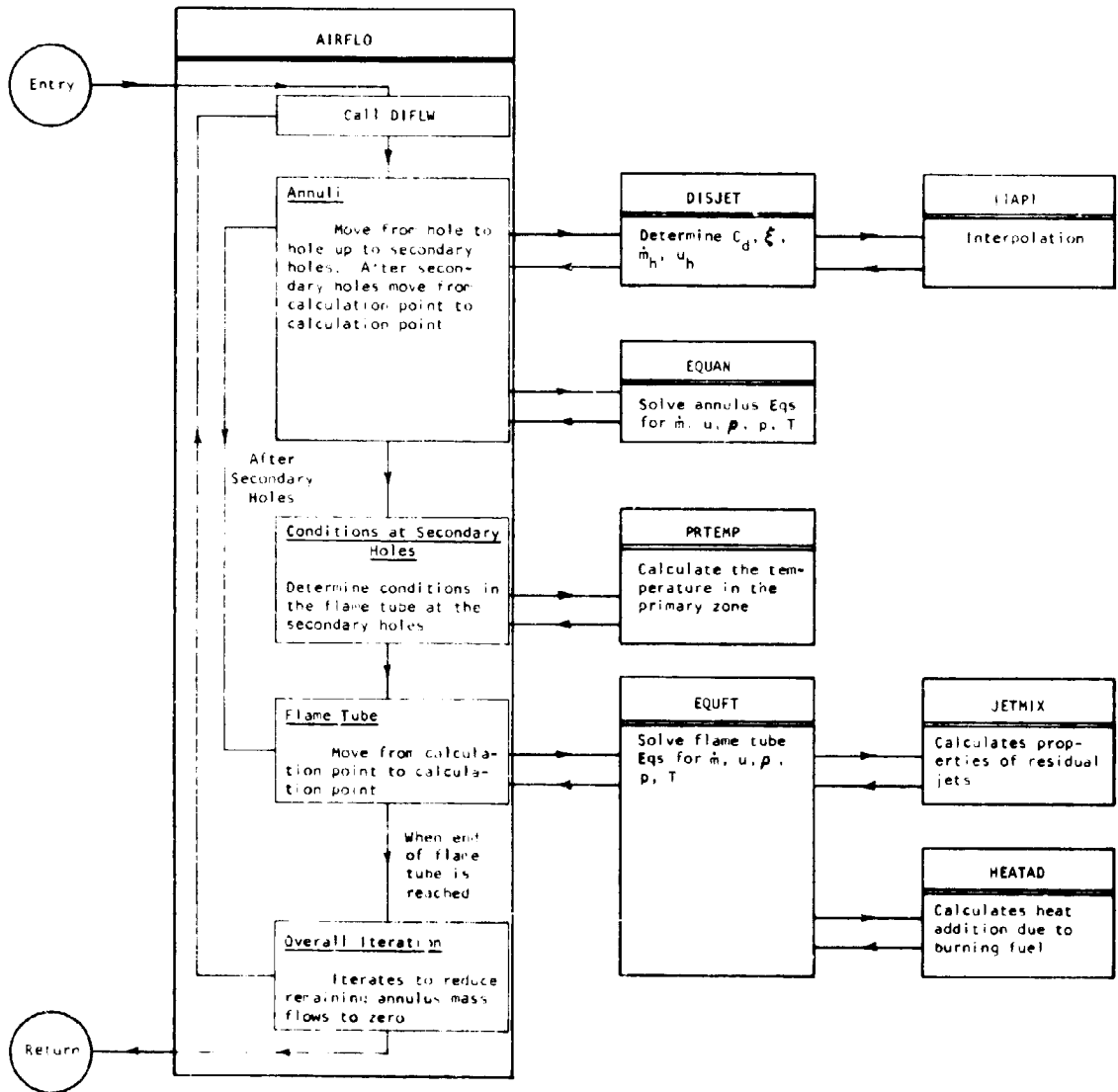


FIGURE 1 - OVERALL FLOW CHART FOR ENTIRE PROGRAM



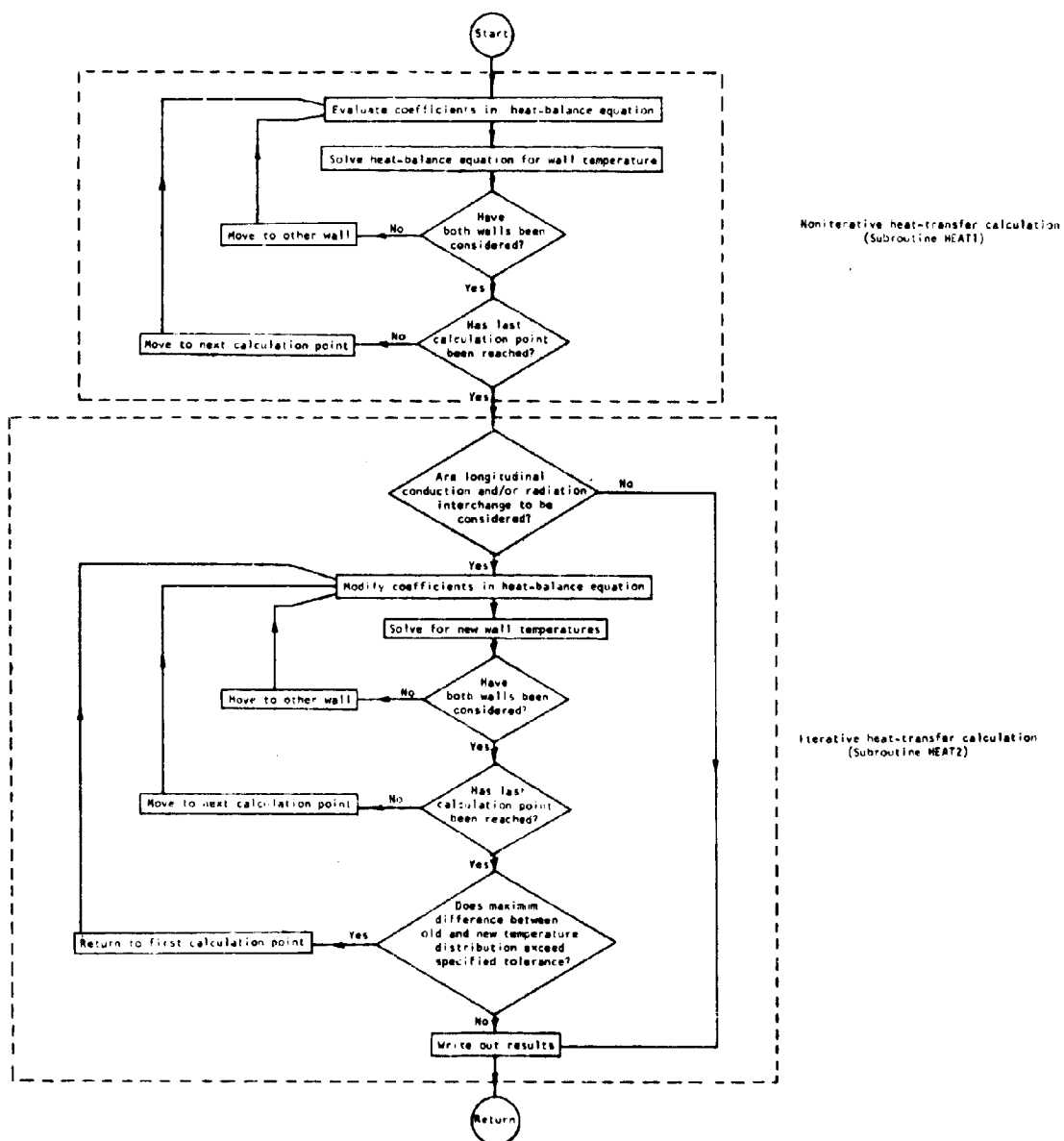
NOTE: Fortran titles of subroutines are defined in Volume II.

FIGURE 2 - OVERALL FLOW CHART FOR DIFFUSER SUBPROGRAM



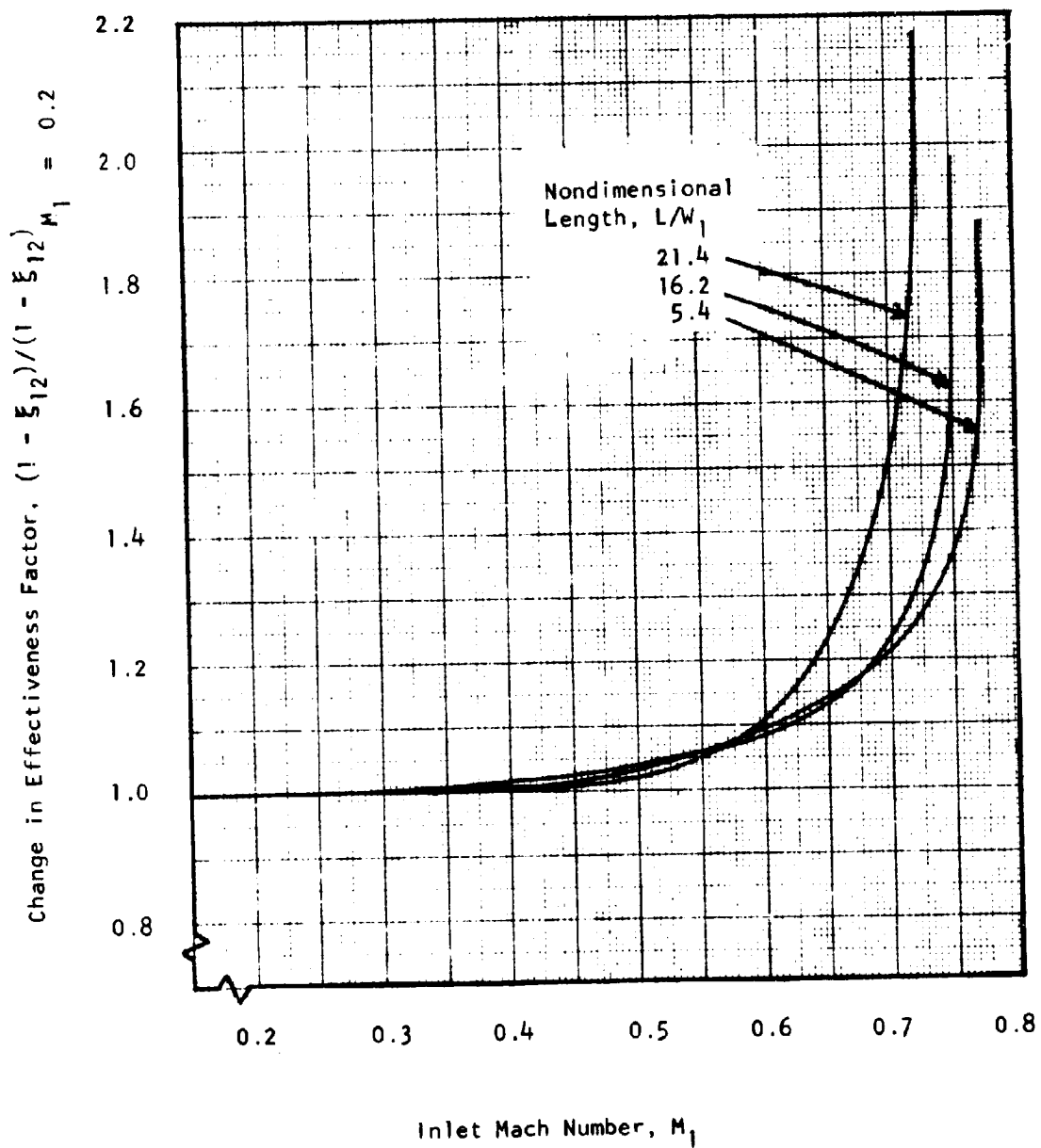
NOTE: Fortran titles of subroutines are defined in Volume II.

FIGURE 3 - OVERALL FLOW CHART FOR AIR-FLOW SUBPROGRAM



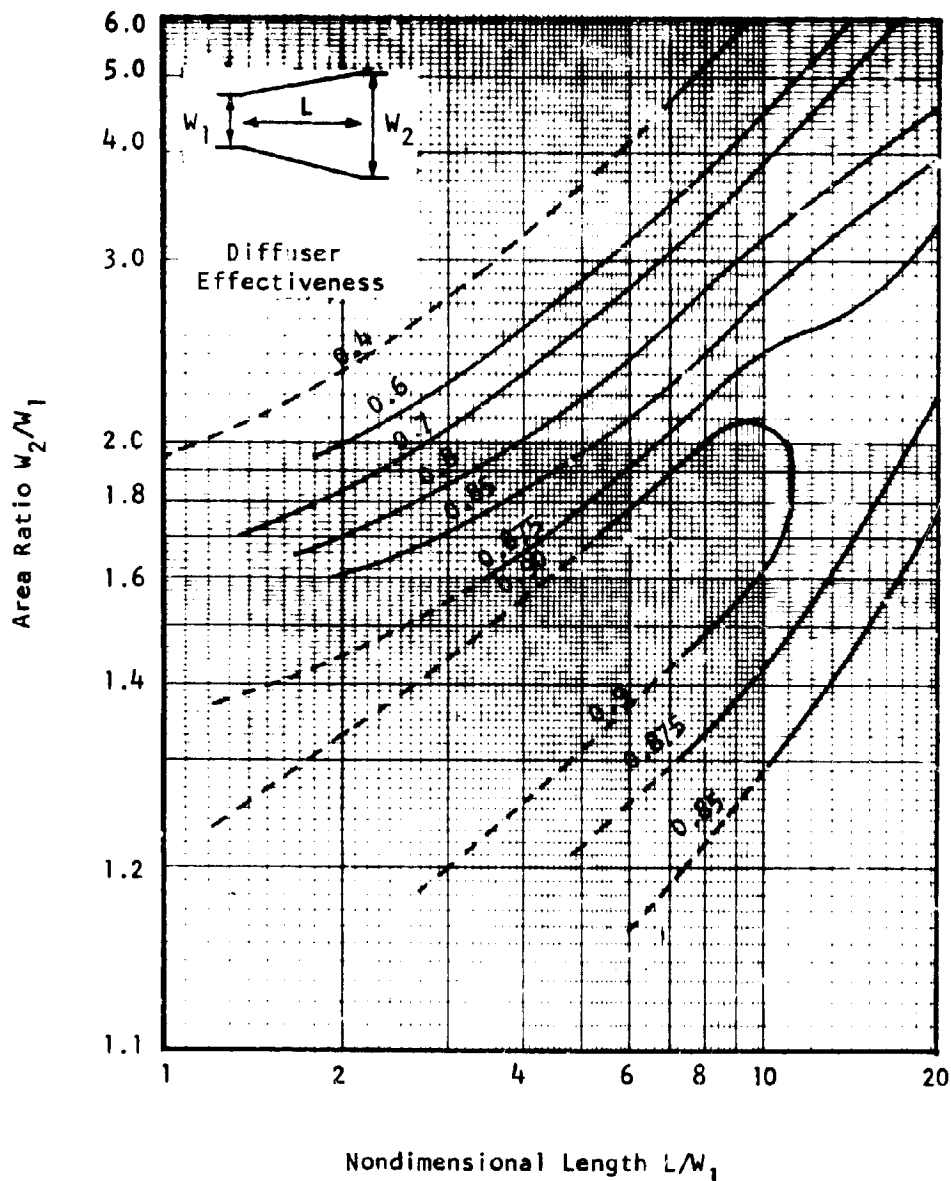
NOTE: Fortran titles of subroutines are defined in Volume II.

FIGURE 4 - OVERALL FLOW CHART FOR HEAT-TRANSFER SUBPROGRAM



From: Young and Green (Ref 16)

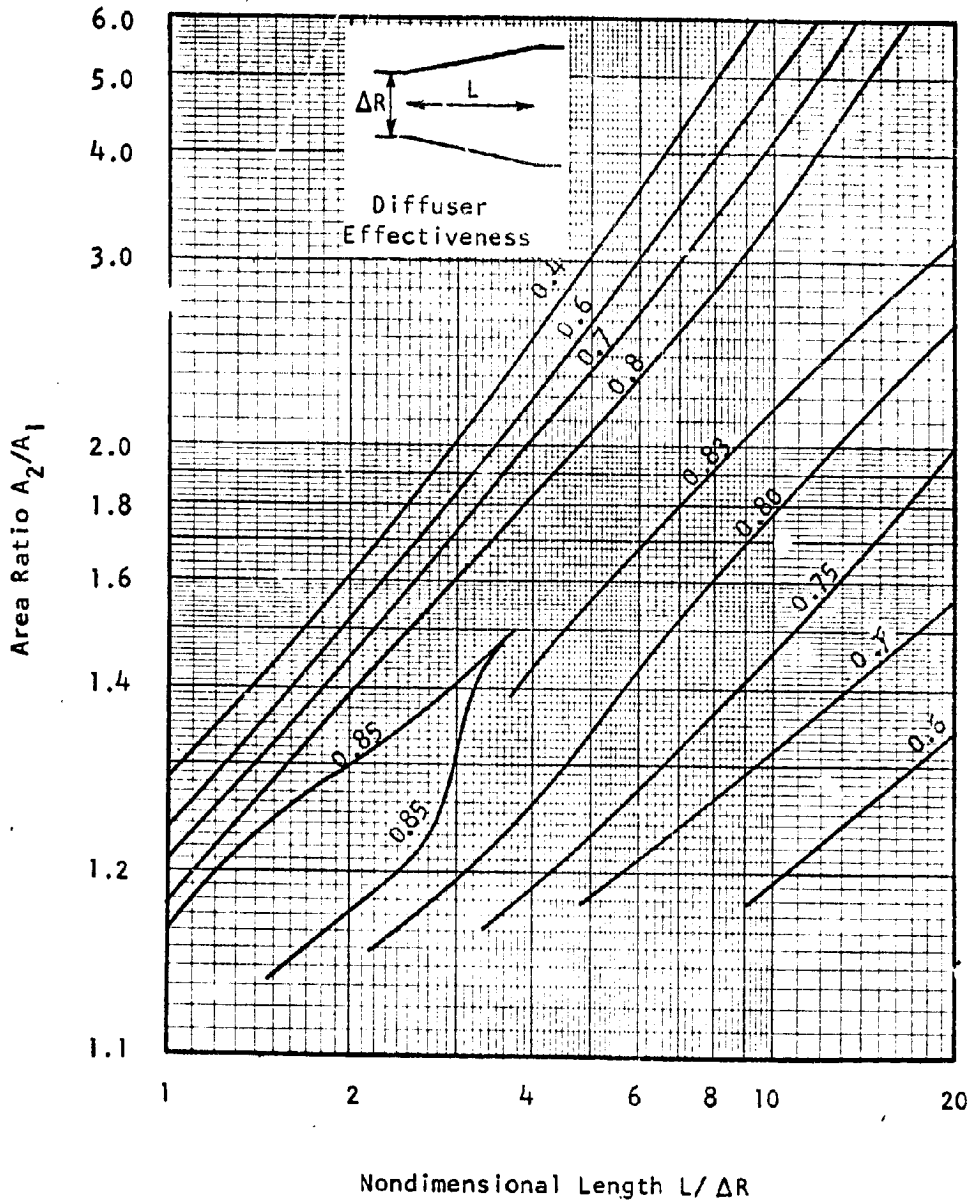
FIGURE 5 - EFFECT OF INLET MACH NUMBER ON DIFFUSER EFFECTIVENESS



Extrapolated data - - - - -

From Reneau, Johnston, and Kline (Ref 7)

**FIGURE 6 - TWO-DIMENSIONAL-DIFFUSER DATA AT
1.5 PER CENT INLET BLOCKAGE**



From Sovran and Klomp (Ref 6)

FIGURE 7 - ANNULAR-DIFFUSER DATA AT 2 PER CENT INLET BLOCKAGE

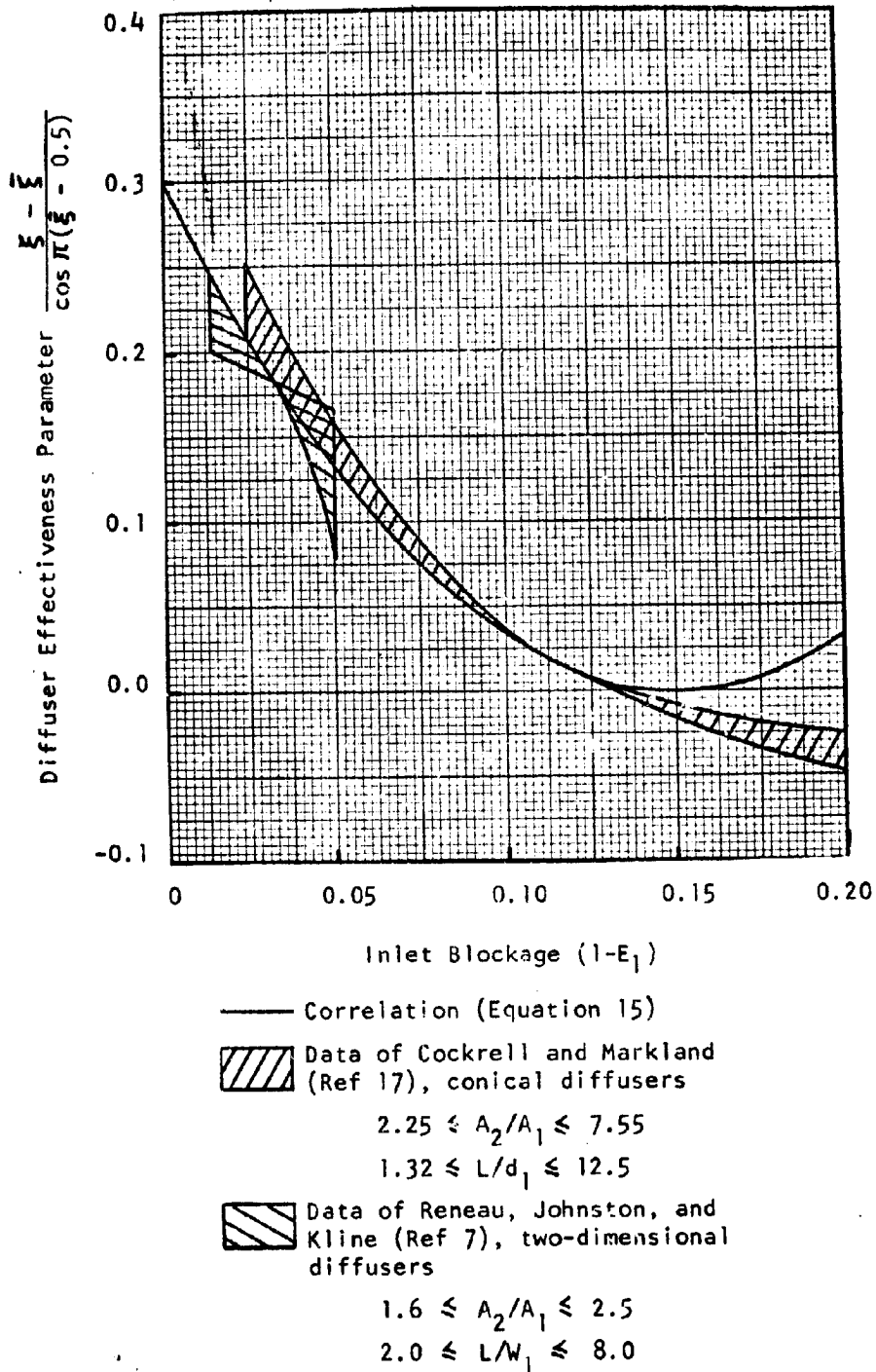
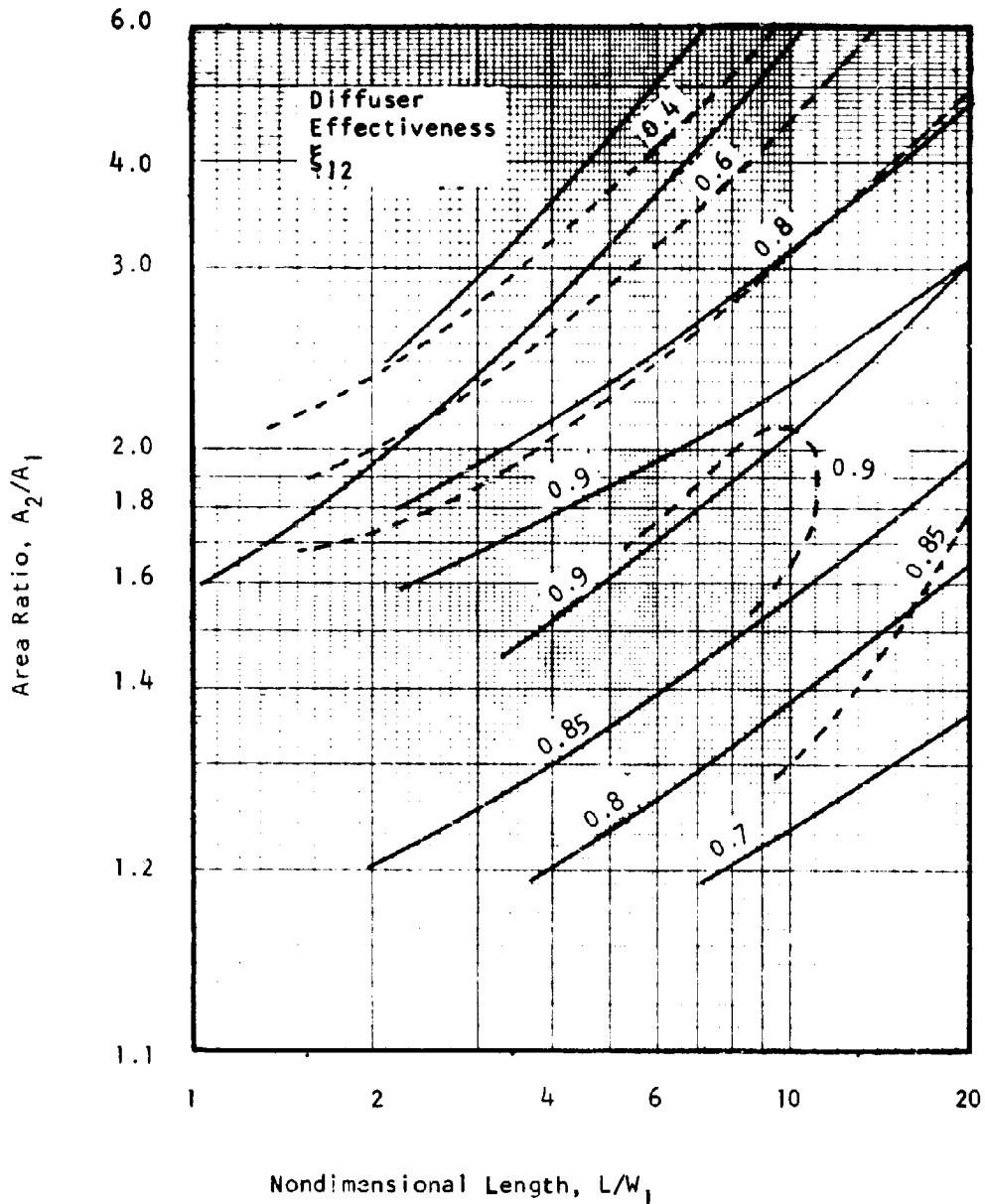


FIGURE 8 - CORRELATION FOR PREDICTING THE VARIATION OF DIFFUSER EFFECTIVENESS WITH INLET BLOCKAGE - COMPARISON WITH EXPERIMENT



- Experimental results of Reneau, Johnston, and Kline (Ref 7) for 0.015 inlet blockage
- Streamtube method with
 Initial shape factor = 1.4
 Shape factor at separation = 1.9
 Inlet blockage = 0.015

FIGURE 9 - COMPARISON OF THE EXPERIMENTAL RESULTS OF RENEAU, JOHNSTON, AND KLINE FOR TWO-DIMENSIONAL DIFFUSERS WITH THE STREAMTUBE METHOD

No. of blades	7	8	9	10	11	12
No. of designs	1	9	3	2	-	1

Blade angle degrees	40 - 50	50 - 60	60 - 70
No. of designs	9	6	1

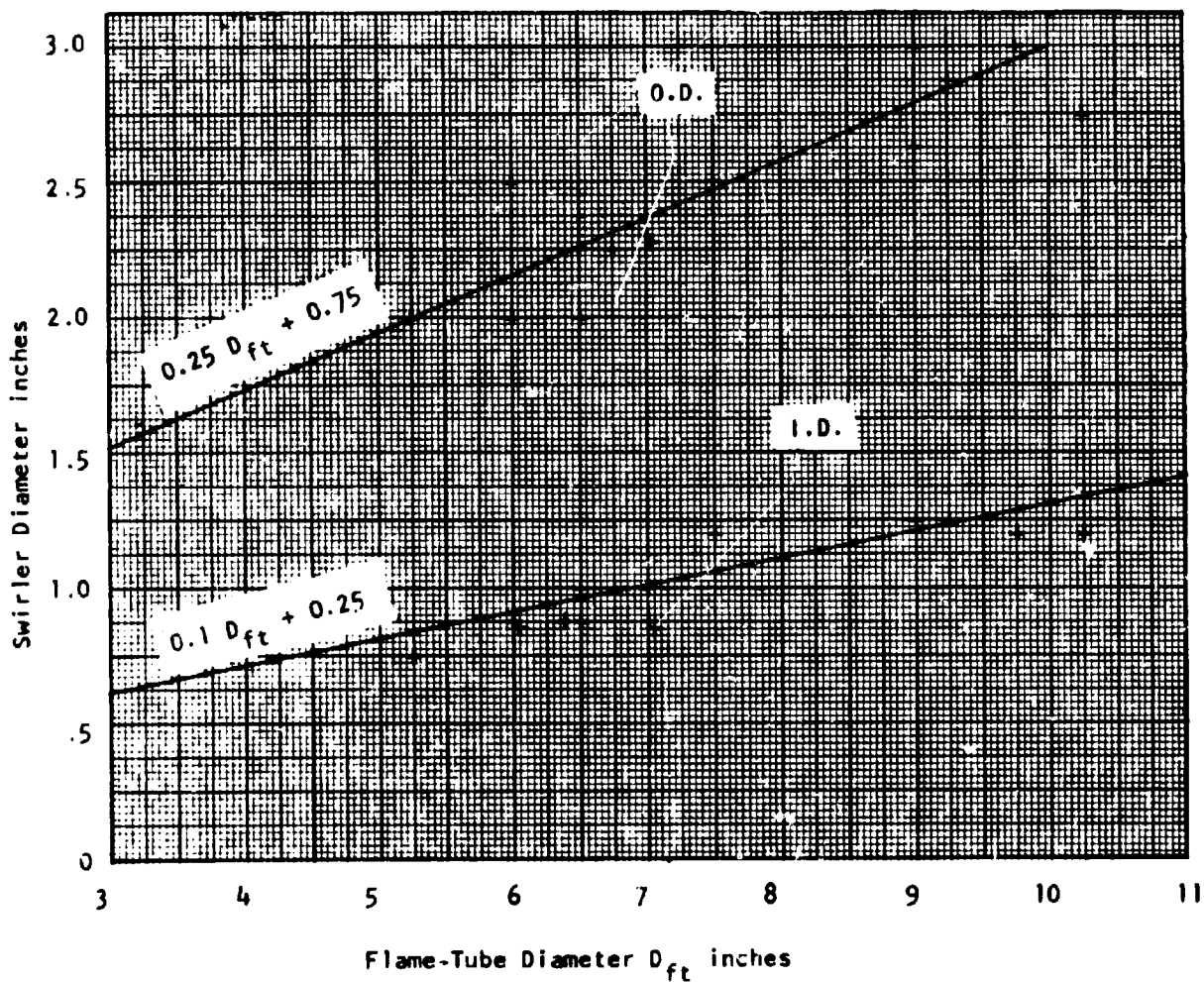


FIGURE 10 - SWIRLER DATA FOR 16 COMBUSTOR DESIGNS

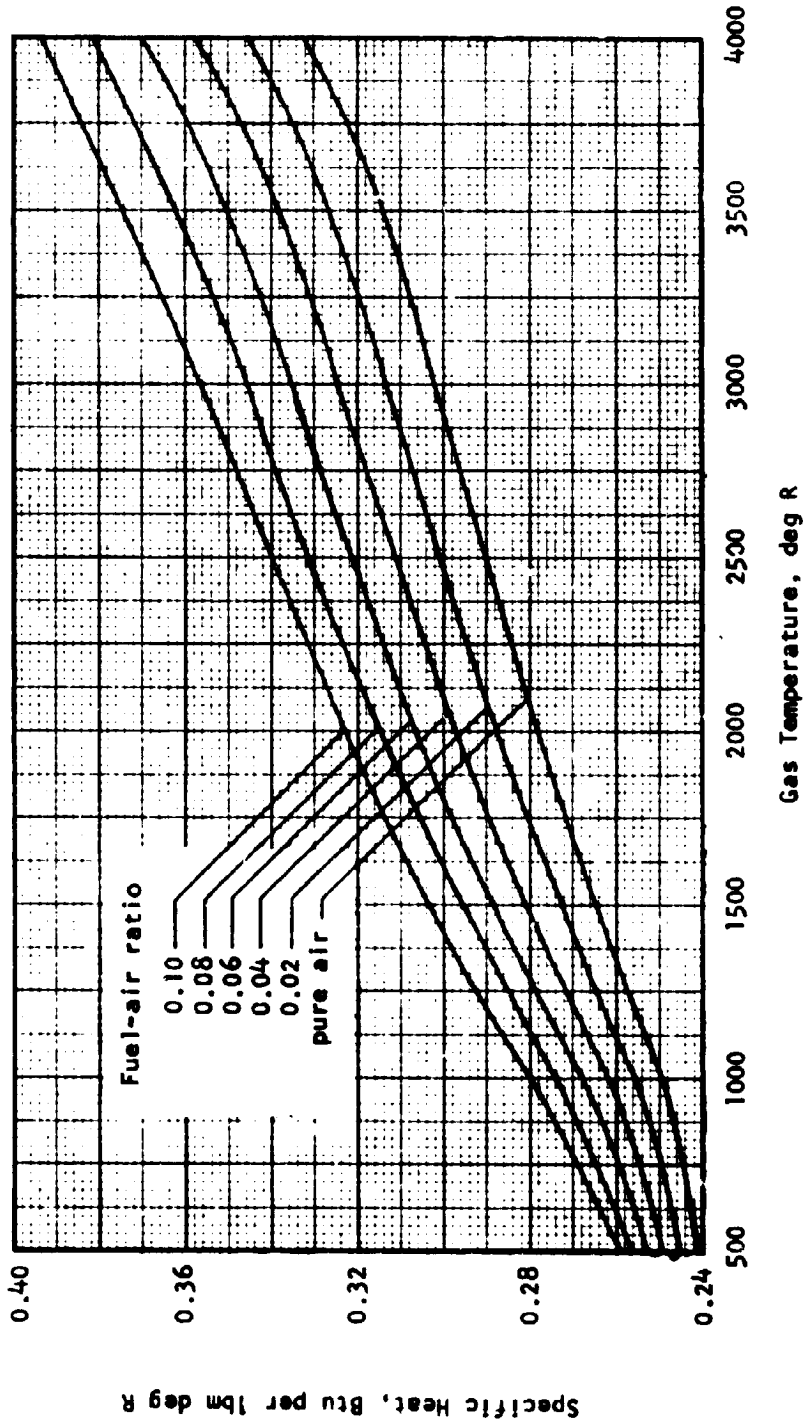
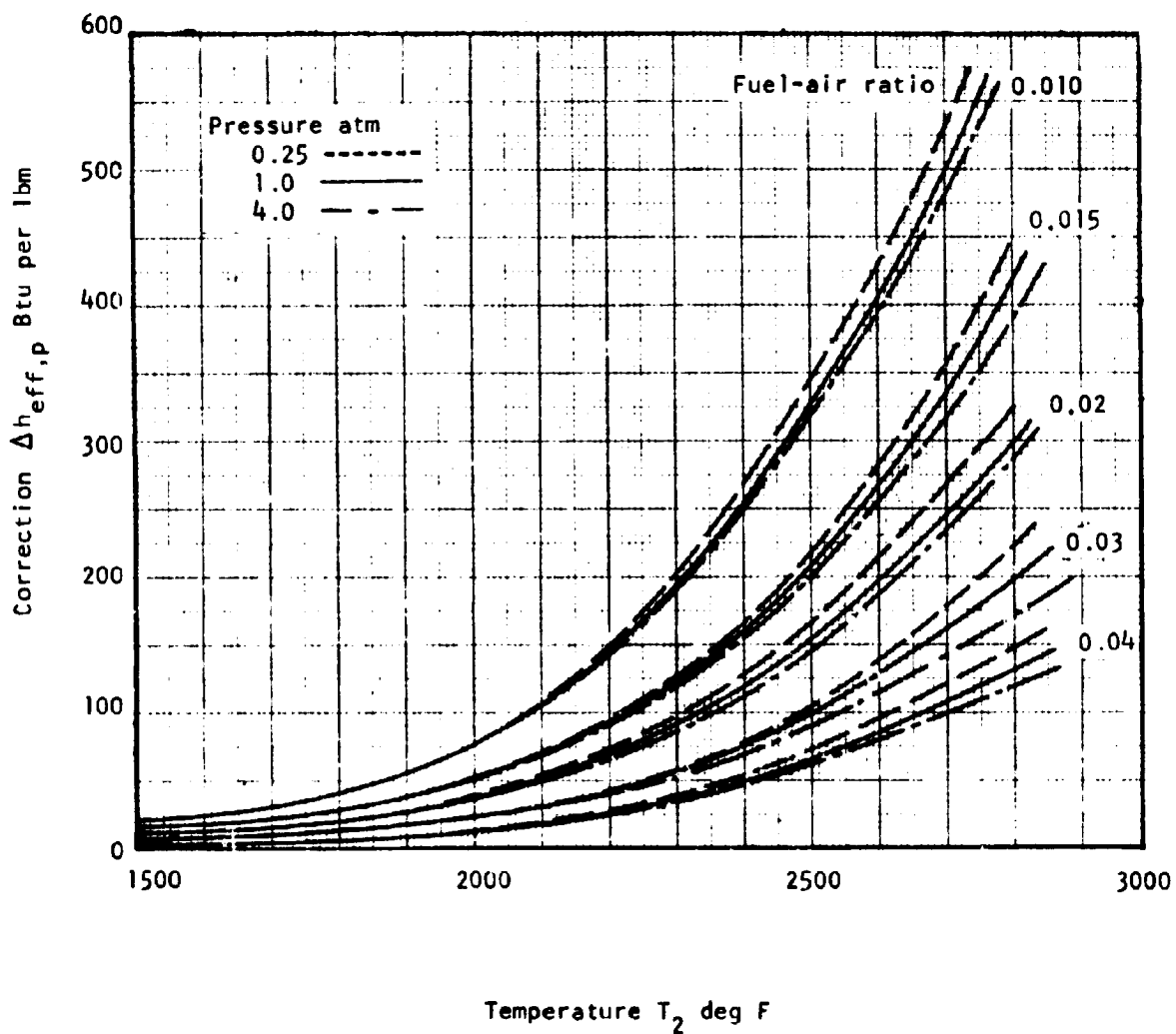
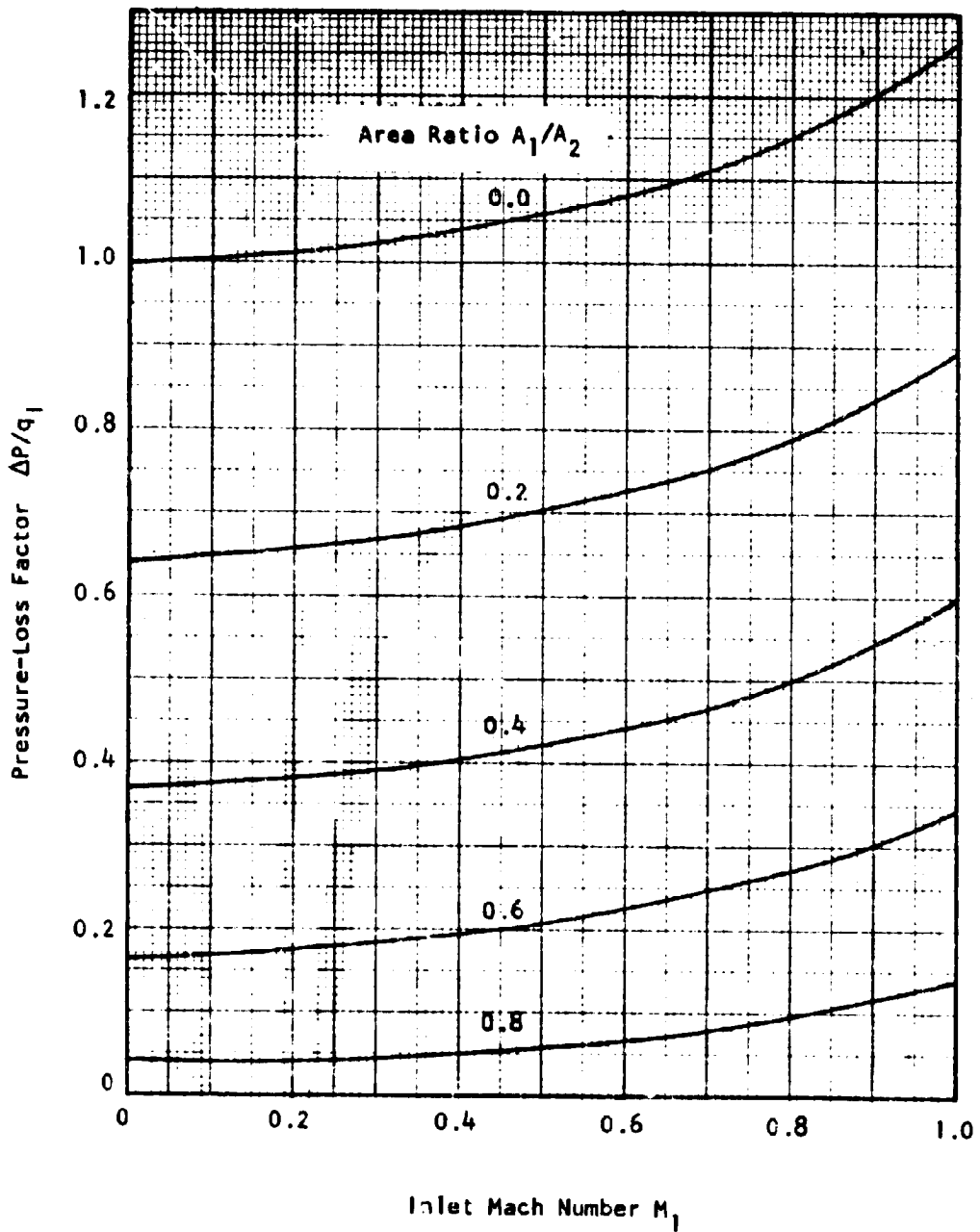


FIGURE 11 -- SPECIFIC HEAT FOR A MIXTURE OF COMBUSTION PRODUCTS
 From Fielding and Topps (Ref 36)



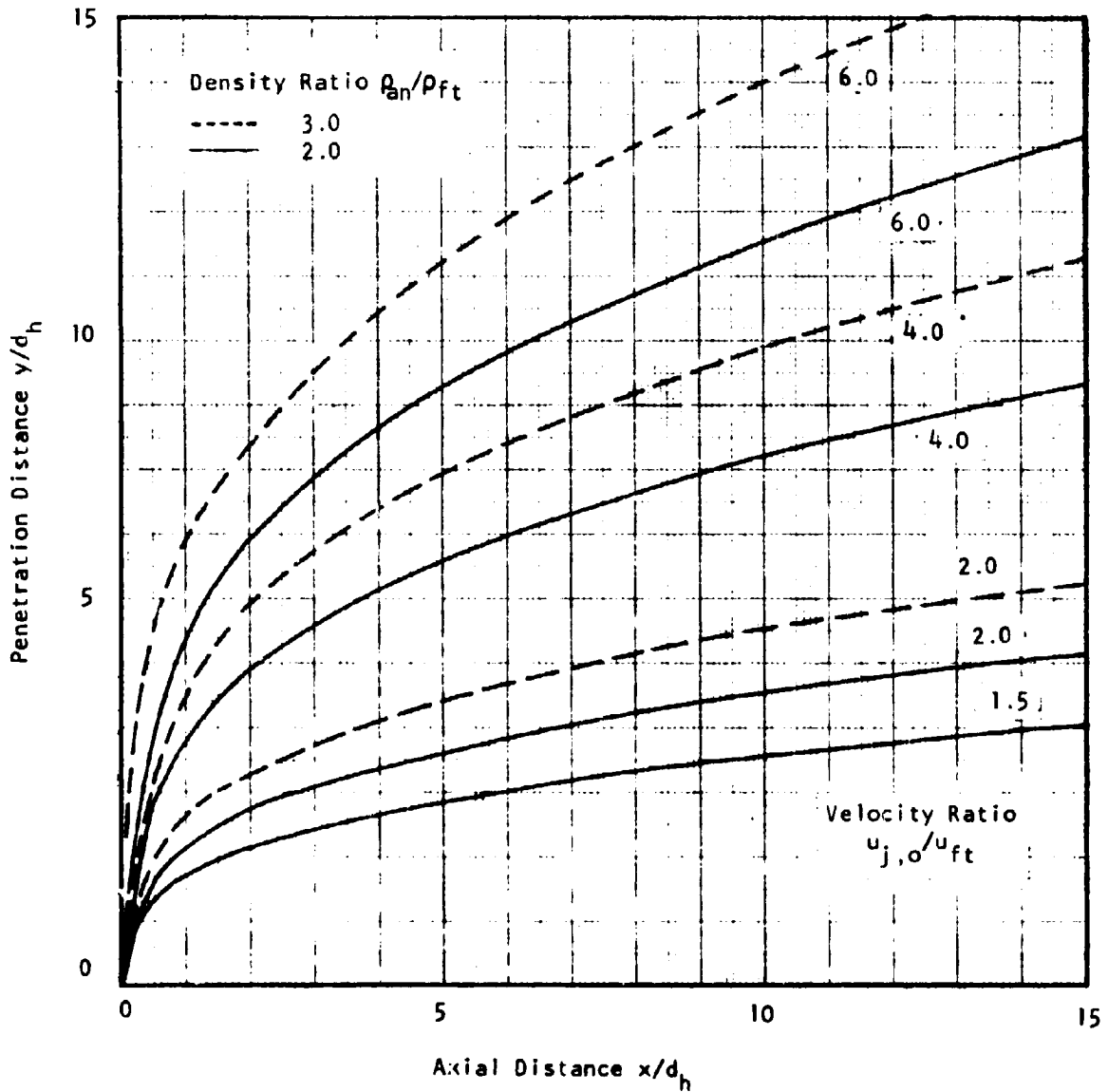
From Hodge (Ref 37)

FIGURE 12 - DISSOCIATION CORRECTION TO EFFECTIVE FUEL CALORIFIC VALUE



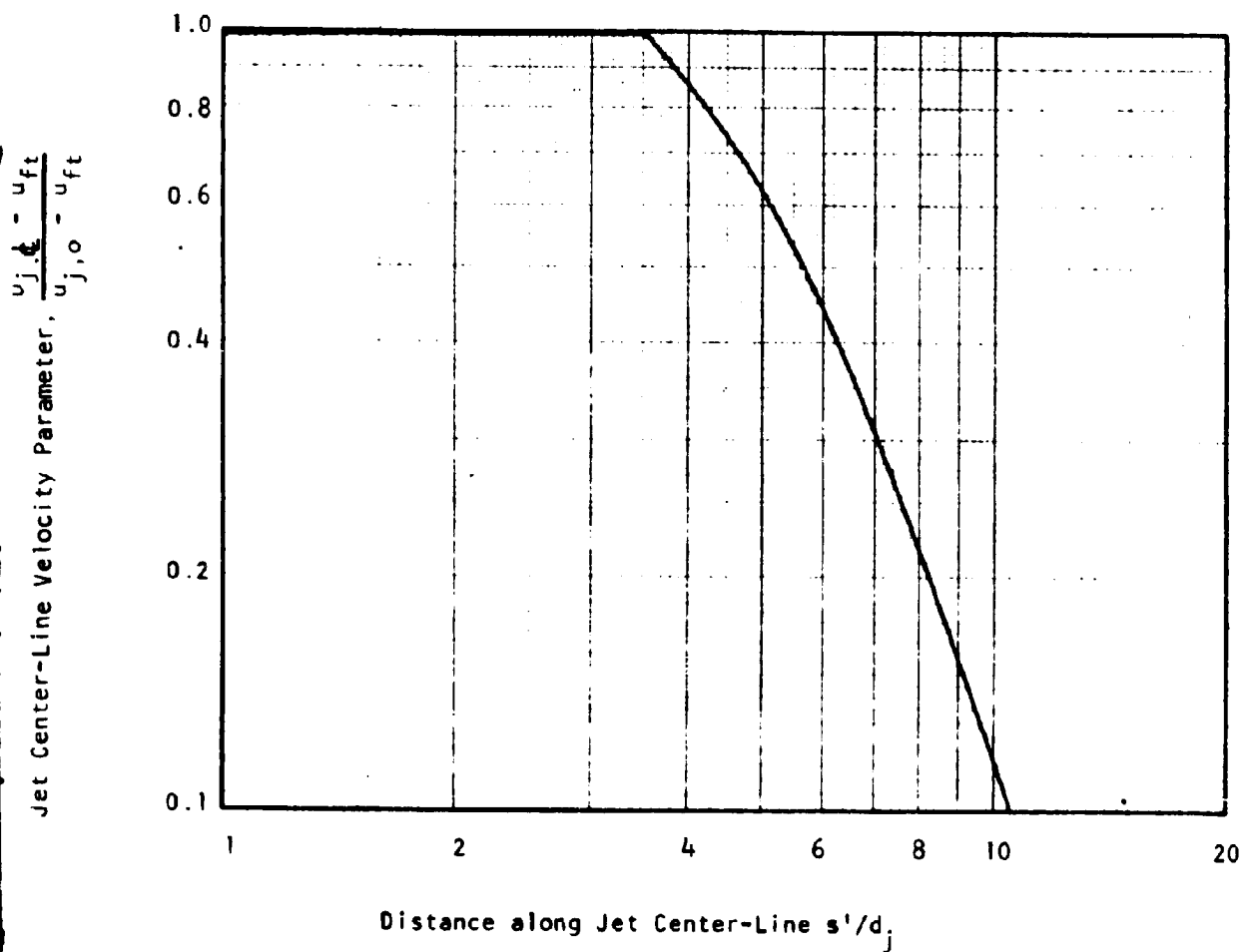
From Reference 38

FIGURE 13 - PRESSURE LOSS IN A SUDDEN EXPANSION IN COMPRESSIBLE FLOW



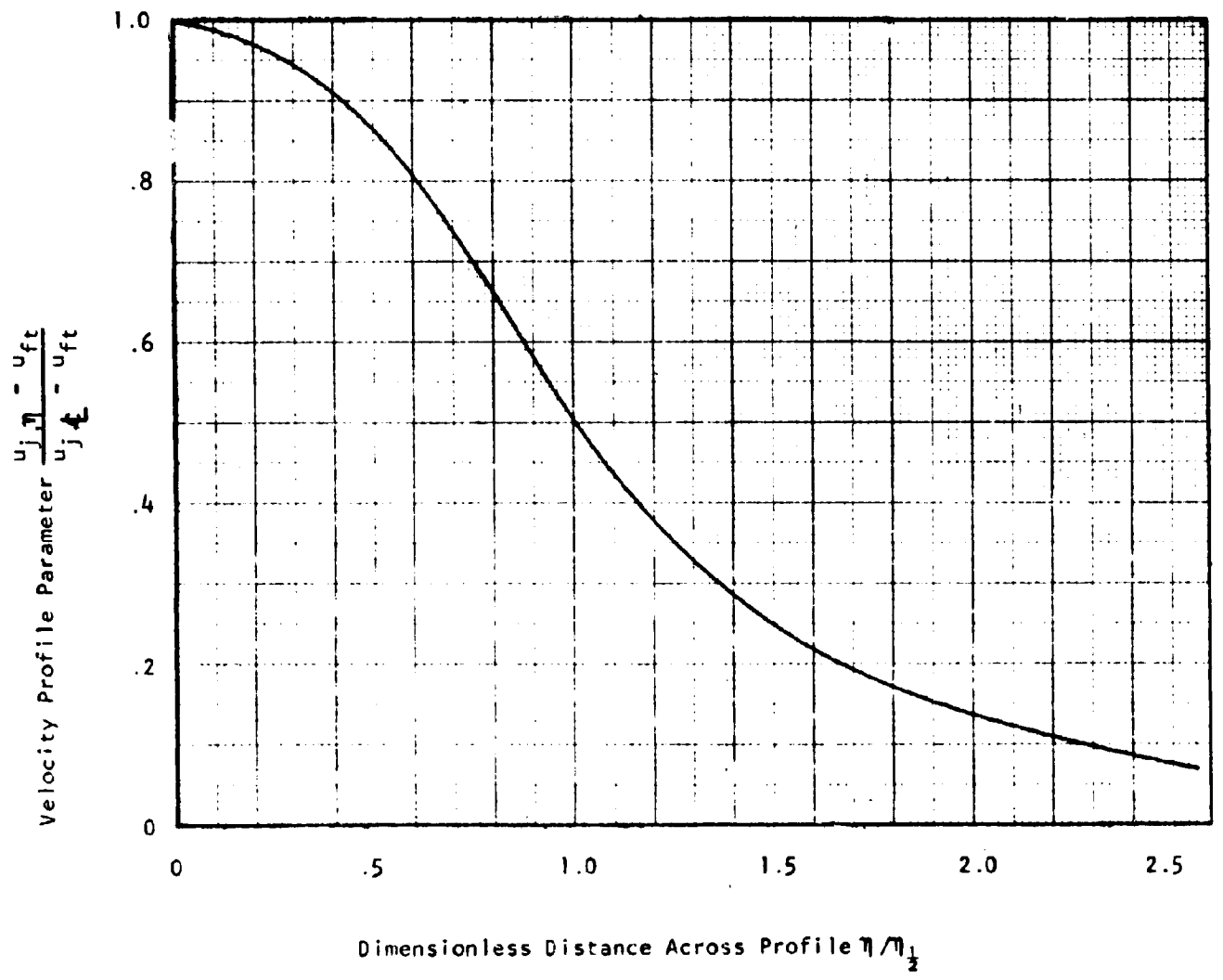
Initial Jet Angle = 90 degrees

FIGURE 14 - TYPICAL CENTER-LINE TRAJECTORIES OF PENETRATION JETS



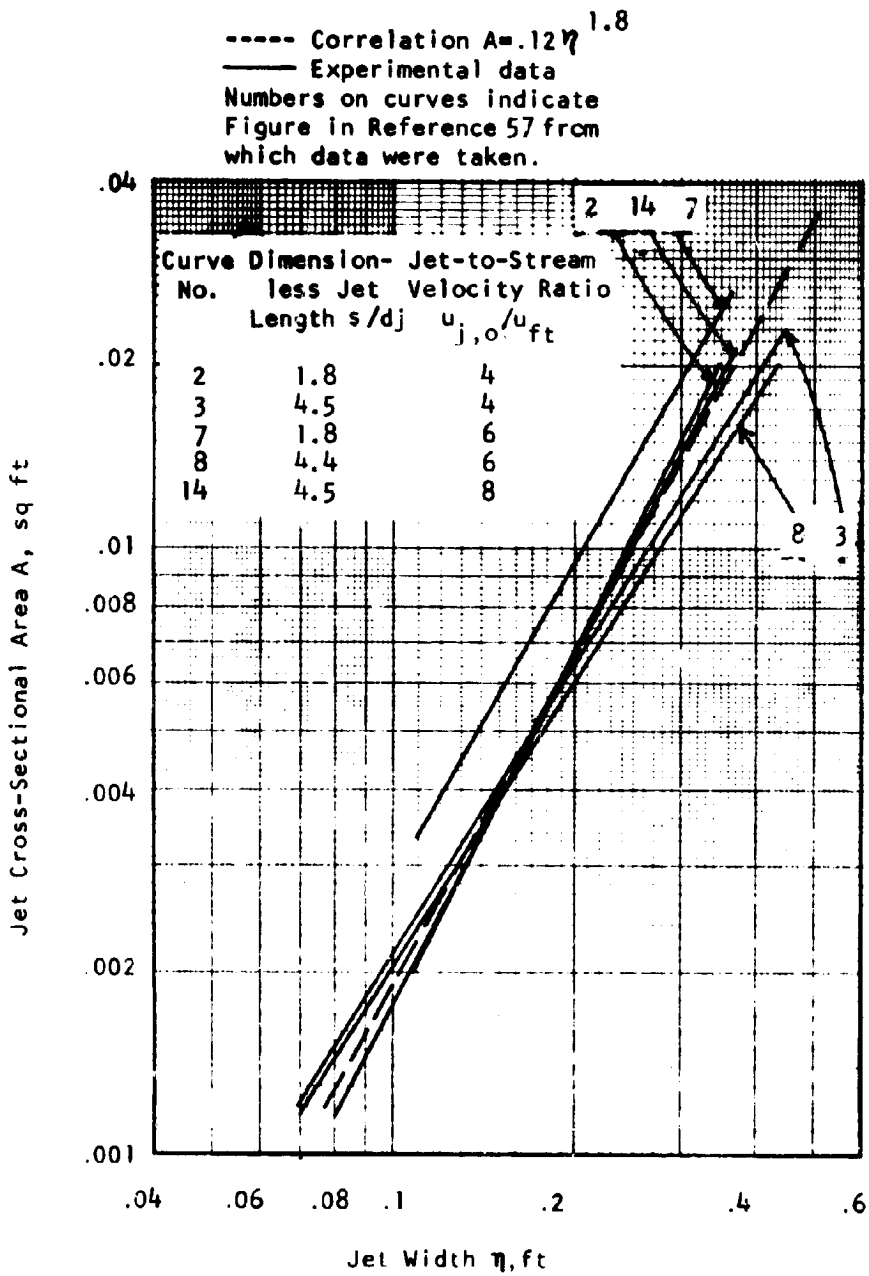
From Keffer and Baines (Ref 56)

FIGURE 15 - DECAY OF CENTER-LINE VELOCITY IN
PENETRATION JET



From Keffer and Baines (Ref 56)

FIGURE 16 - LATERAL DISTRIBUTION OF VELOCITY
IN PENETRATION JET



Data from Jordinson (Ref 57)

FIGURE 17 - CORRELATION FOR CROSS-SECTIONAL AREA OF PENETRATION JETS

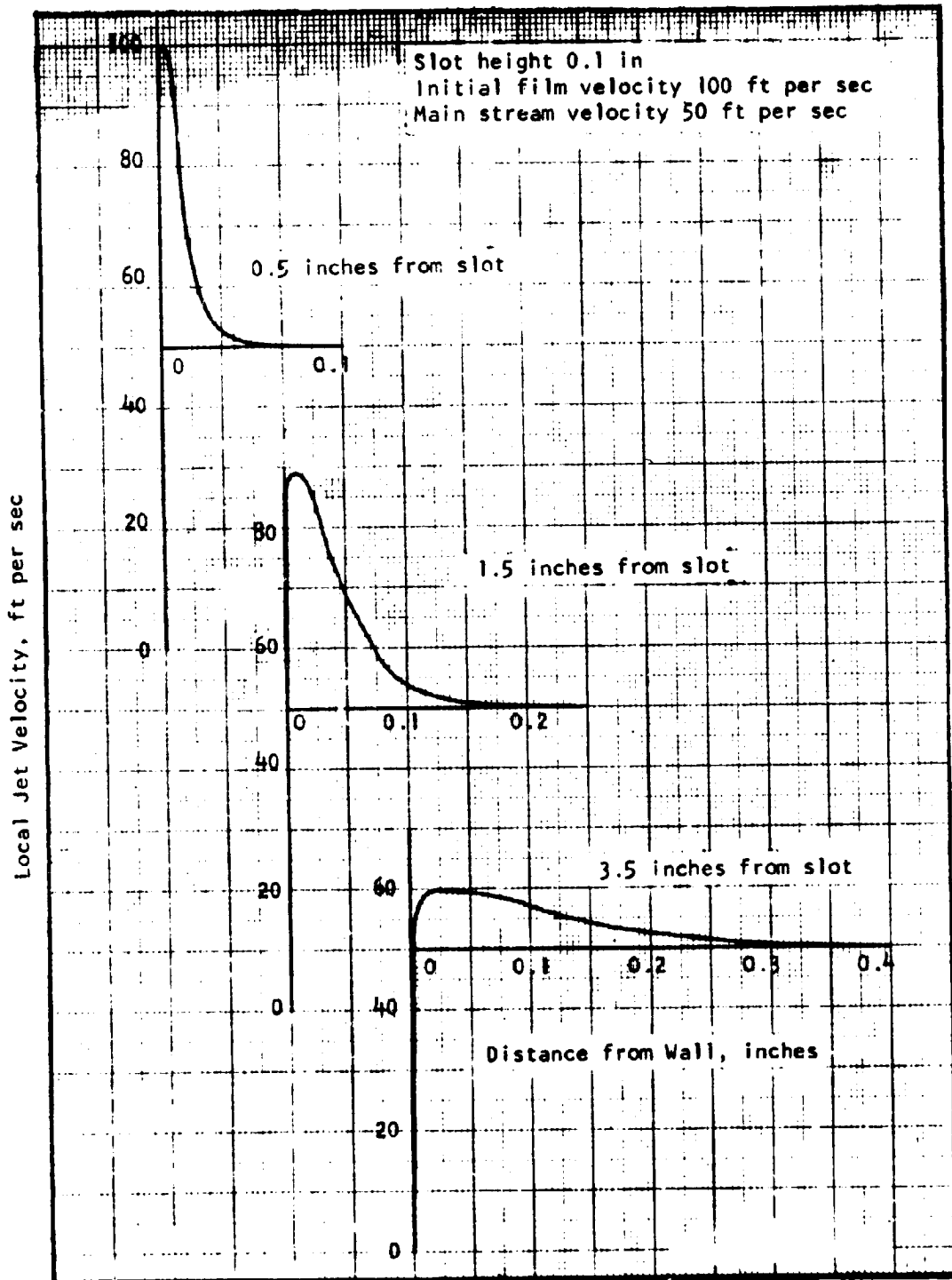
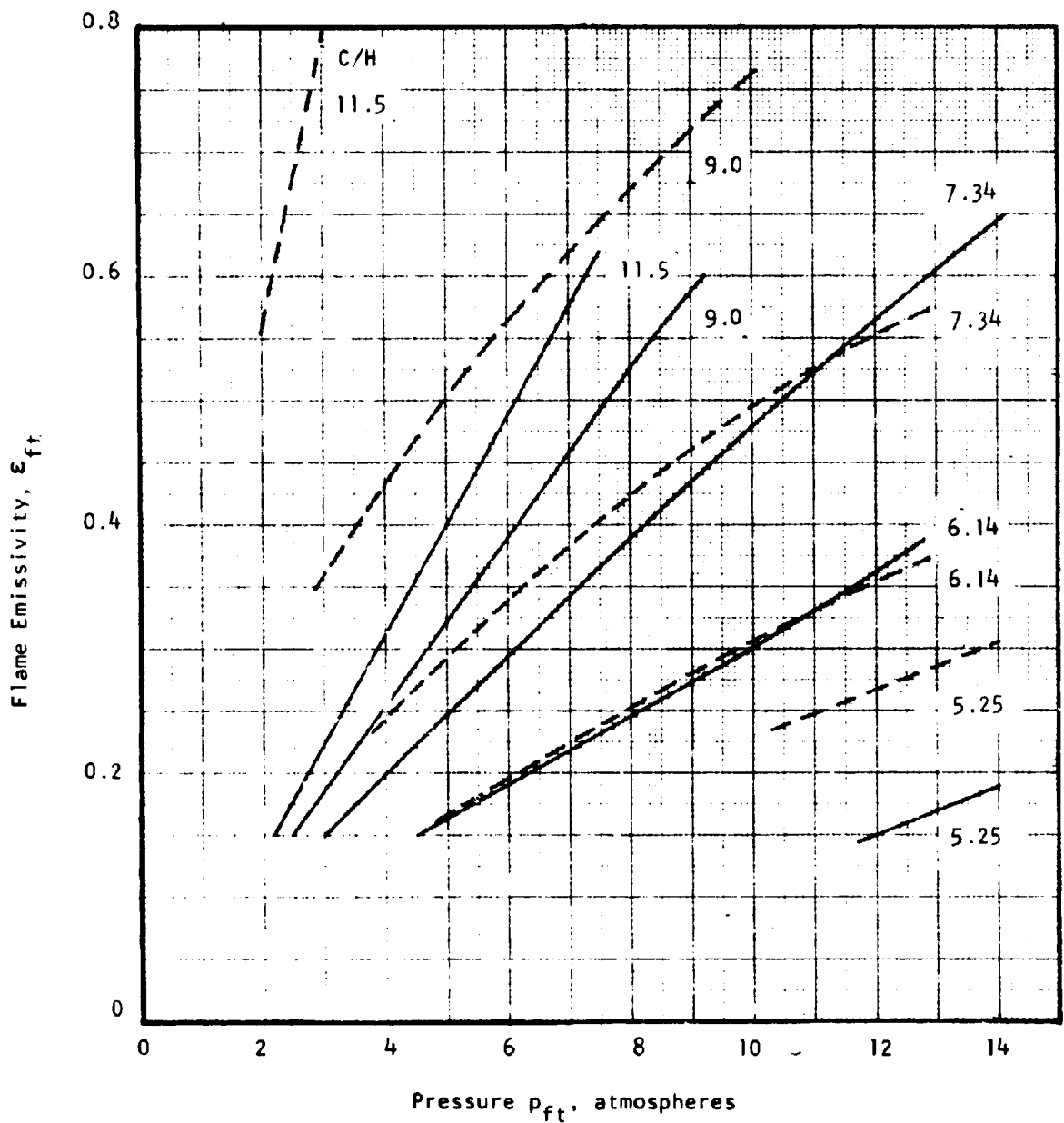


FIGURE 18 - TYPICAL VELOCITY PROFILES IN A WALL JET



- Data from Schirmer and Quigg (Ref 11) assuming $T_{ft} = 3500$ deg R
 - - - Values predicted from NREC 1964 correlation (Equations 134 and 136)

FIGURE 19 - EFFECT OF PRESSURE AND FUEL COMPOSITION ON EMISSIVITY OF LUMINOUS FLAMES

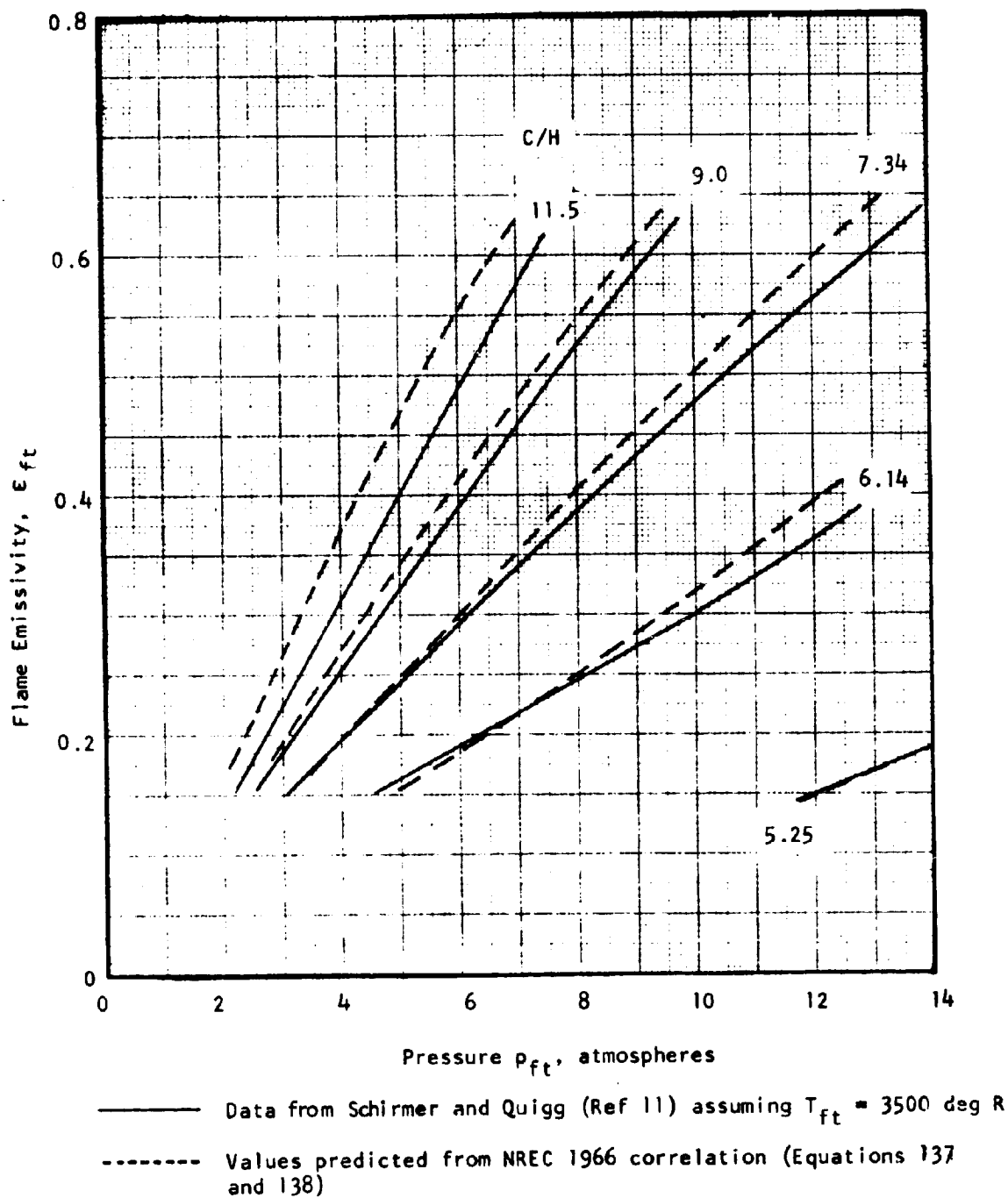


FIGURE 20 - A NEW CORRELATION FOR THE EMISSIVITY OF LUMINOUS FLAMES

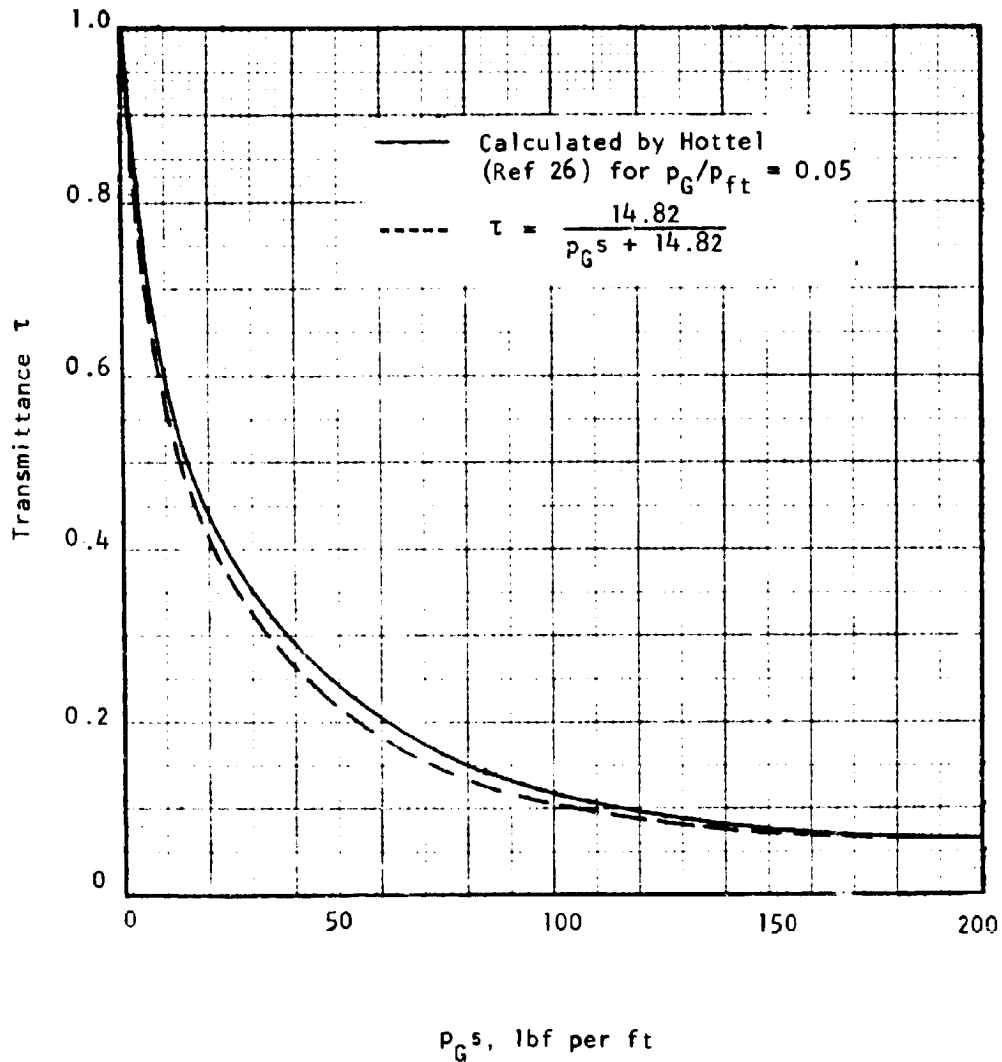


FIGURE 21 - EFFECT OF PRESSURE AND
GAS THICKNESS ON RADIATION TRANSMITTANCE

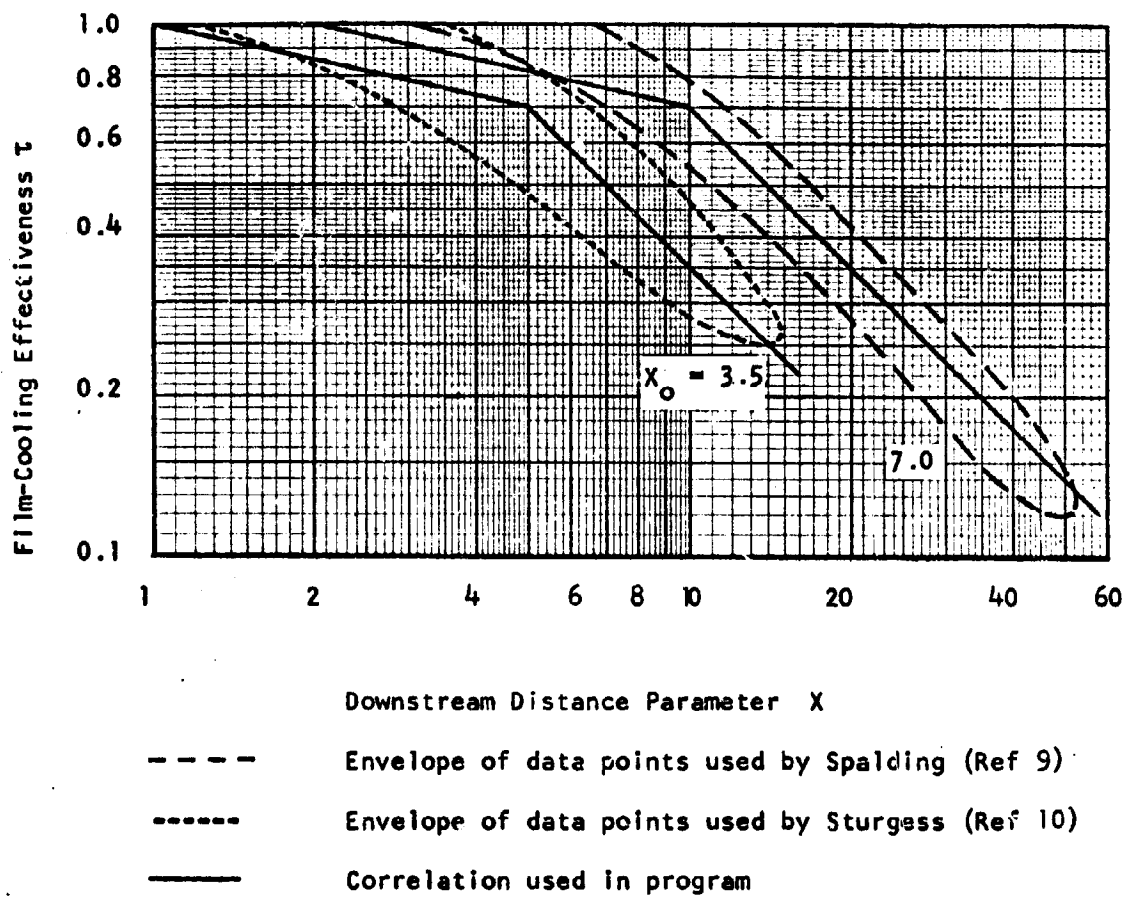
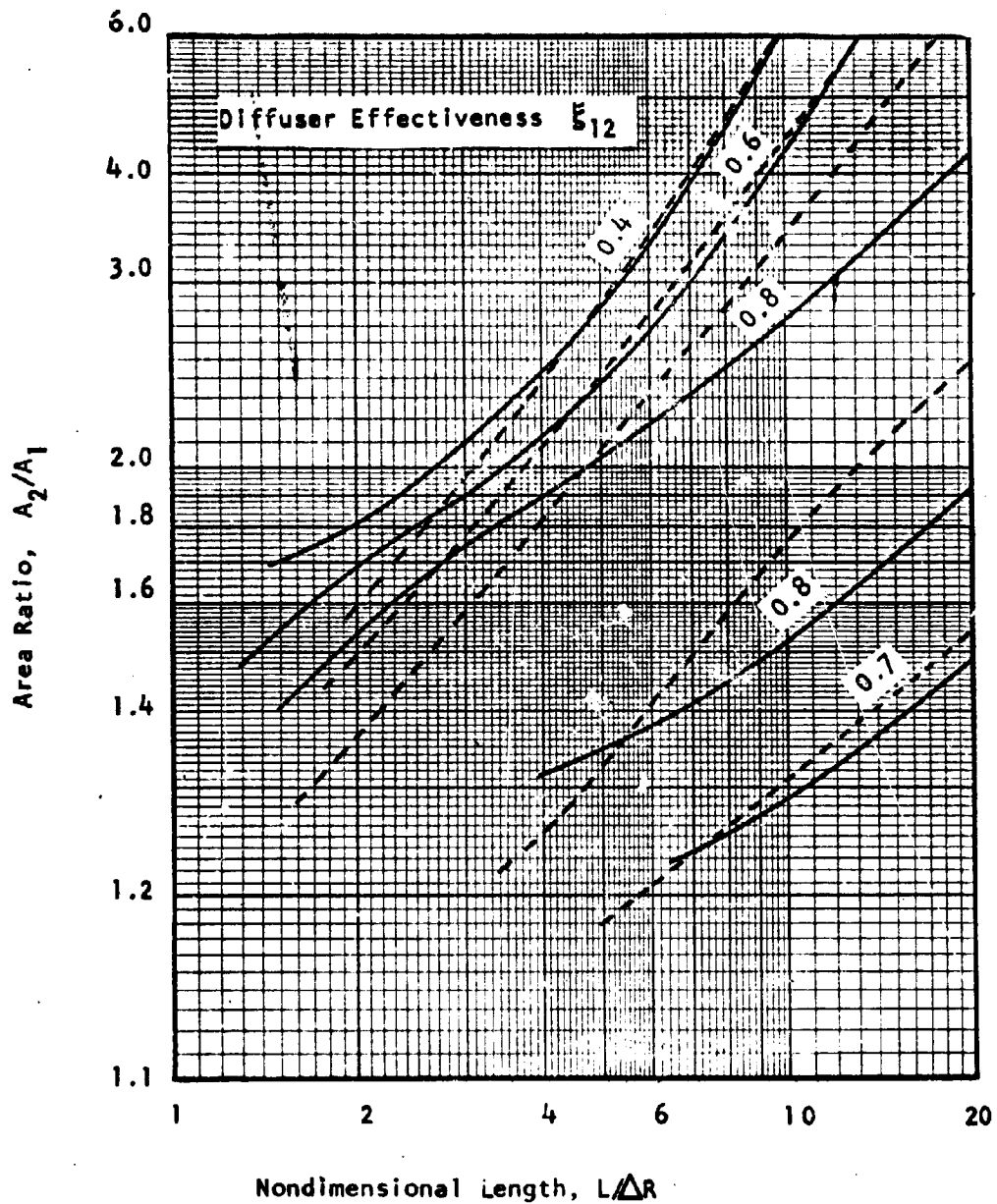


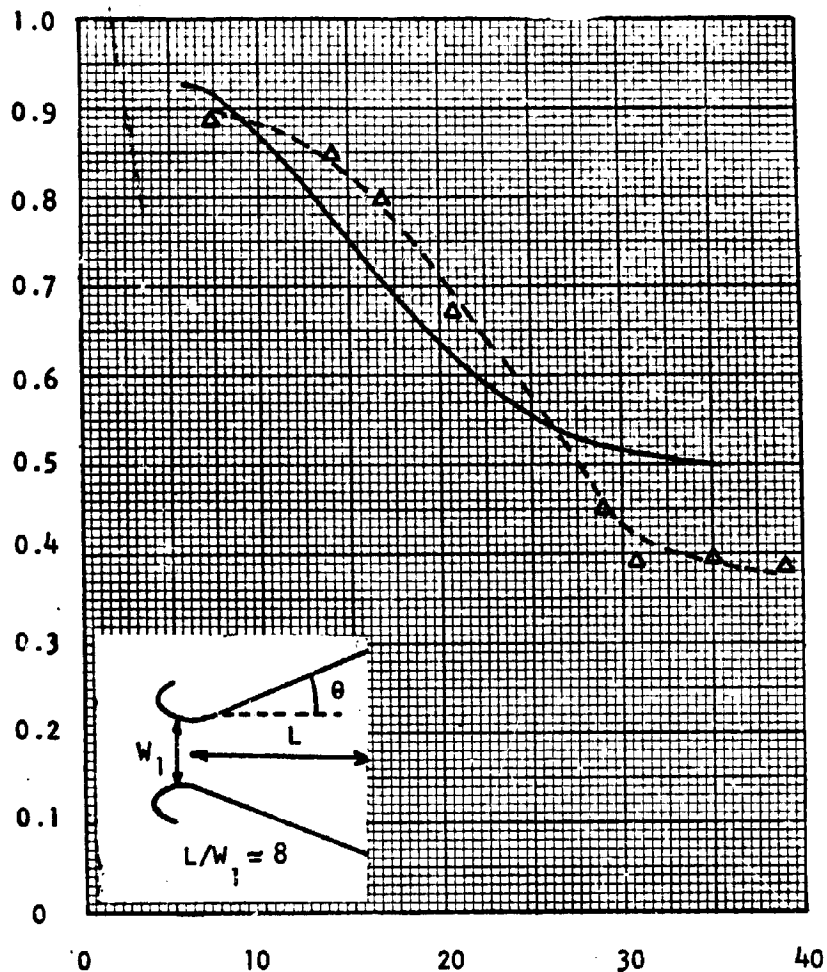
FIGURE 22 - CORRELATIONS OF FILM-COOLING DATA



- Experimental results of Sovran and Klomp (Ref 6)
- Streamtube method with:
- Hub/Shroud ratio at inlet = 0.55
 - Initial blockage = 0.03
 - Initial shape factor = 1.4
 - Shape factor at separation = 1.9

FIGURE 23- COMPARISON OF THE EXPERIMENTAL RESULTS OF SOVRAN AND KLOMP FOR ANNULAR DIFFUSERS WITH THE STREAMTUBE METHOD

Diffuser Effectiveness, ξ_{12}



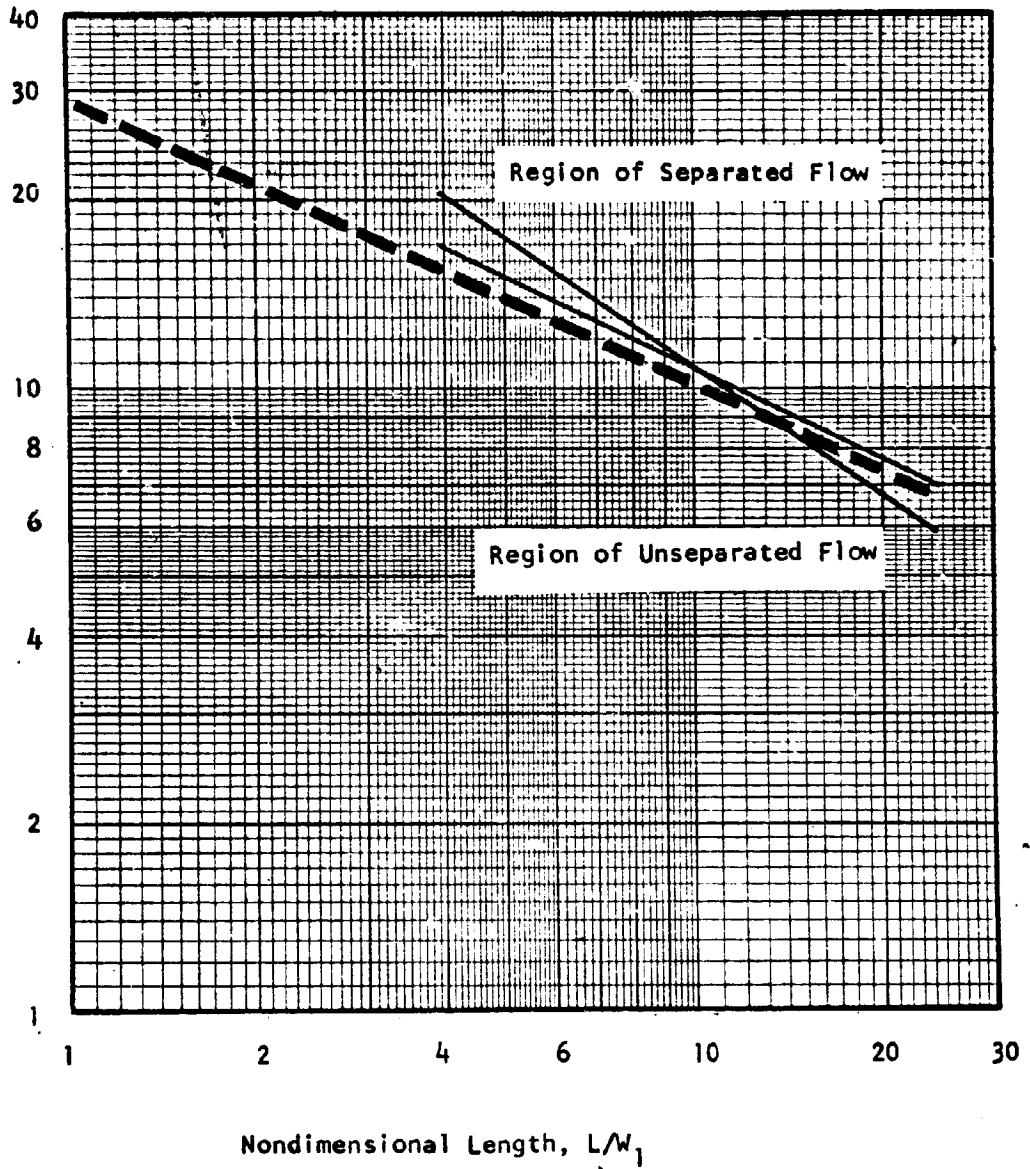
Total Included Angle, 2θ

Δ --- Δ Experimental results of Cochran and Kline (Ref 70)

— Streamtube method with:
 Inlet blockage = 0.0075
 Inlet shape factor = 1.47

FIGURE 24 - COMPARISON OF EXPERIMENTAL AND THEORETICAL EFFECTIVENESS FOR TWO-DIMENSIONAL DIFFUSERS

Total Included Angle, 2θ



==== Experimental results of Moore and Kline (Ref 72)

----- Streamtube method

**FIGURE 25 - POSITION OF FIRST STALL
FOR TWO-DIMENSIONAL DIFFUSERS**

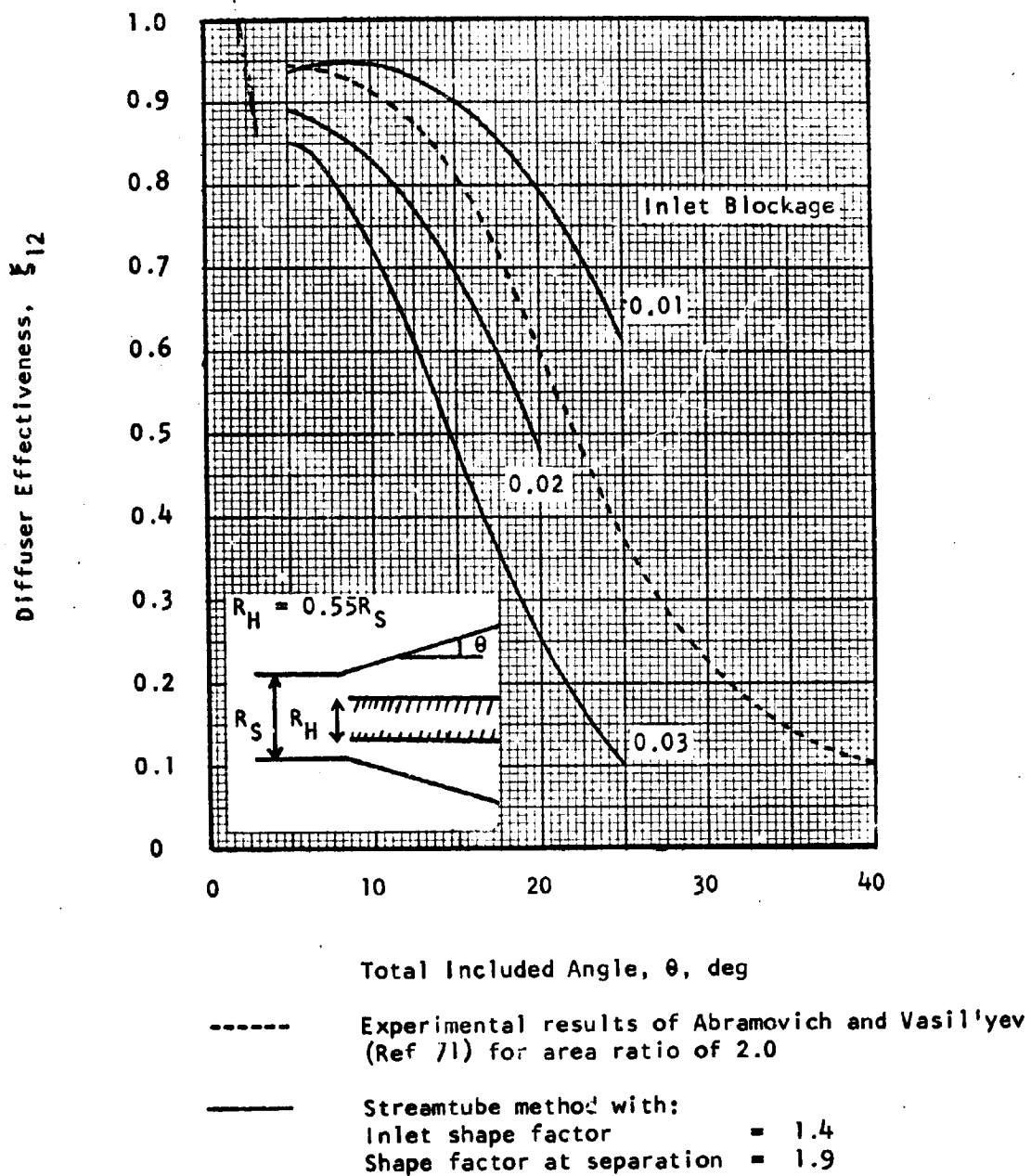
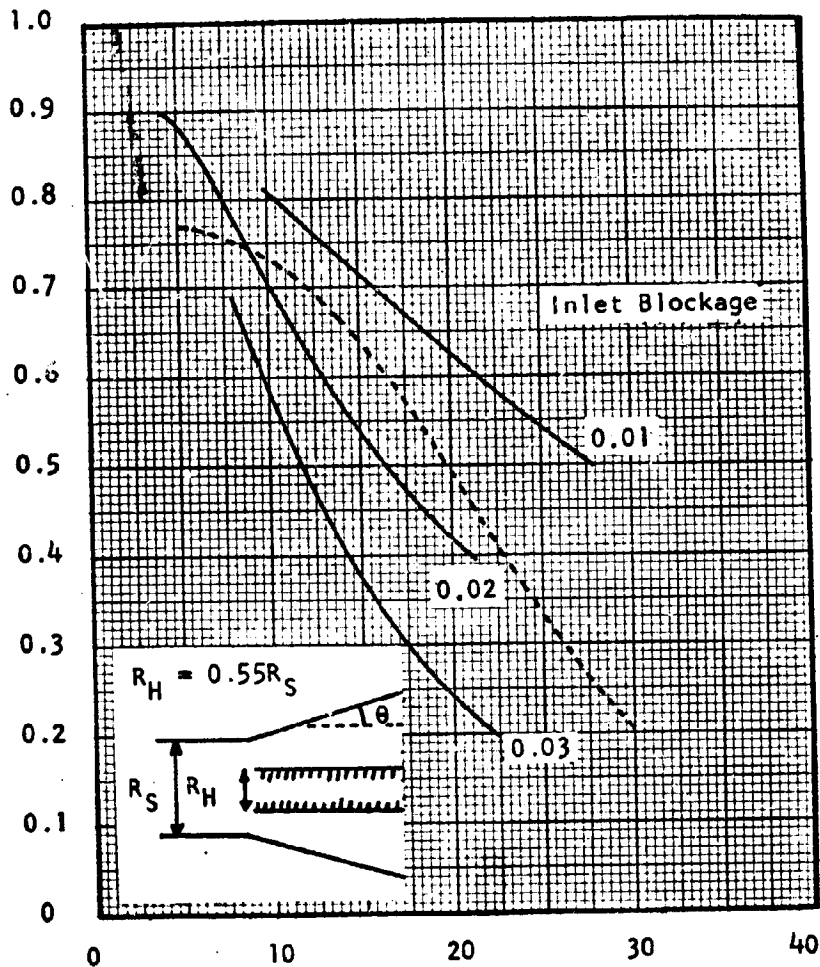


FIGURE 26 - COMPARISON OF EXPERIMENTAL AND THEORETICAL EFFECTIVENESS FOR ANNULAR DIFFUSERS

Diffuser Effectiveness, ξ_{12}

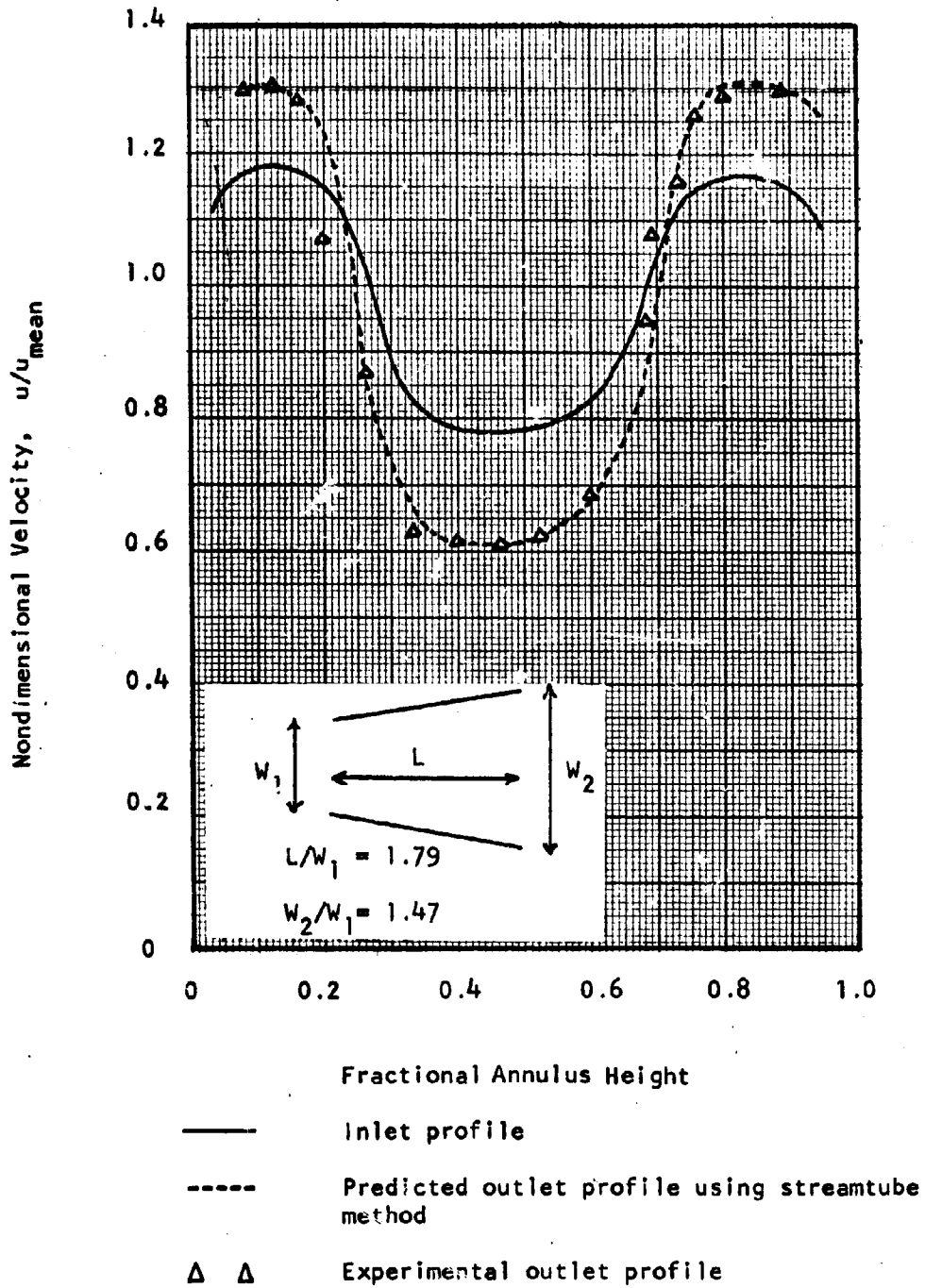


Total Included Angle, θ , deg

----- Experimental results of Abramovich and Vasil'yev (Ref 71) for area ratio of 3.8

———— Streamtube method with:
 Initial shape factor = 1.4
 Shape factor at separation = 1.9

FIGURE 26 CONTINUED - COMPARISON OF EXPERIMENTAL AND THEORETICAL EFFECTIVENESS FOR ANNULAR DIFFUSERS



From Horlock and Lewis (Ref 73)

FIGURE 27 - COMPARISON OF EXPERIMENTAL AND THEORETICAL DEVELOPMENT OF A SHEAR FLOW IN A TWO-DIMENSIONAL DIFFUSER

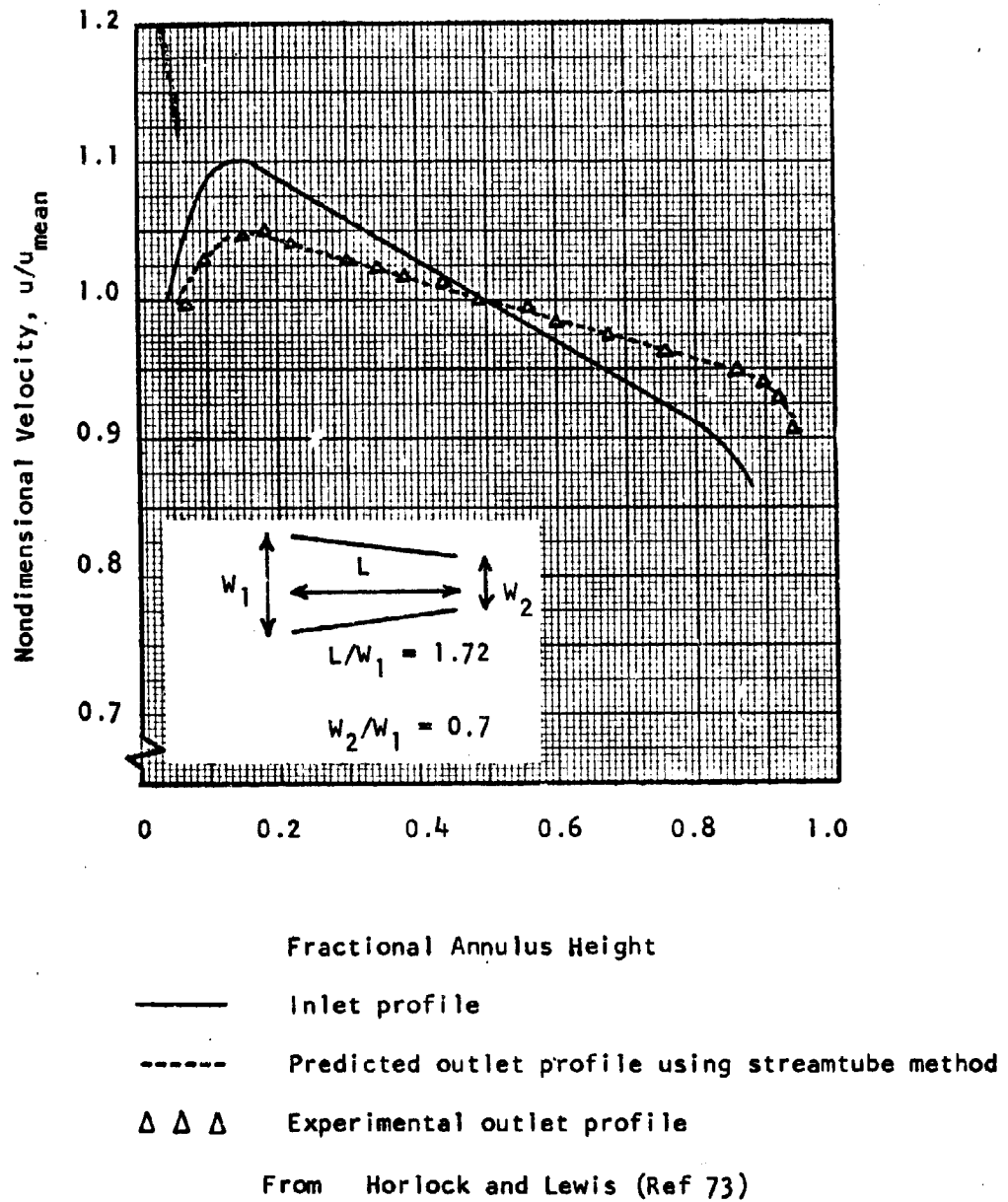
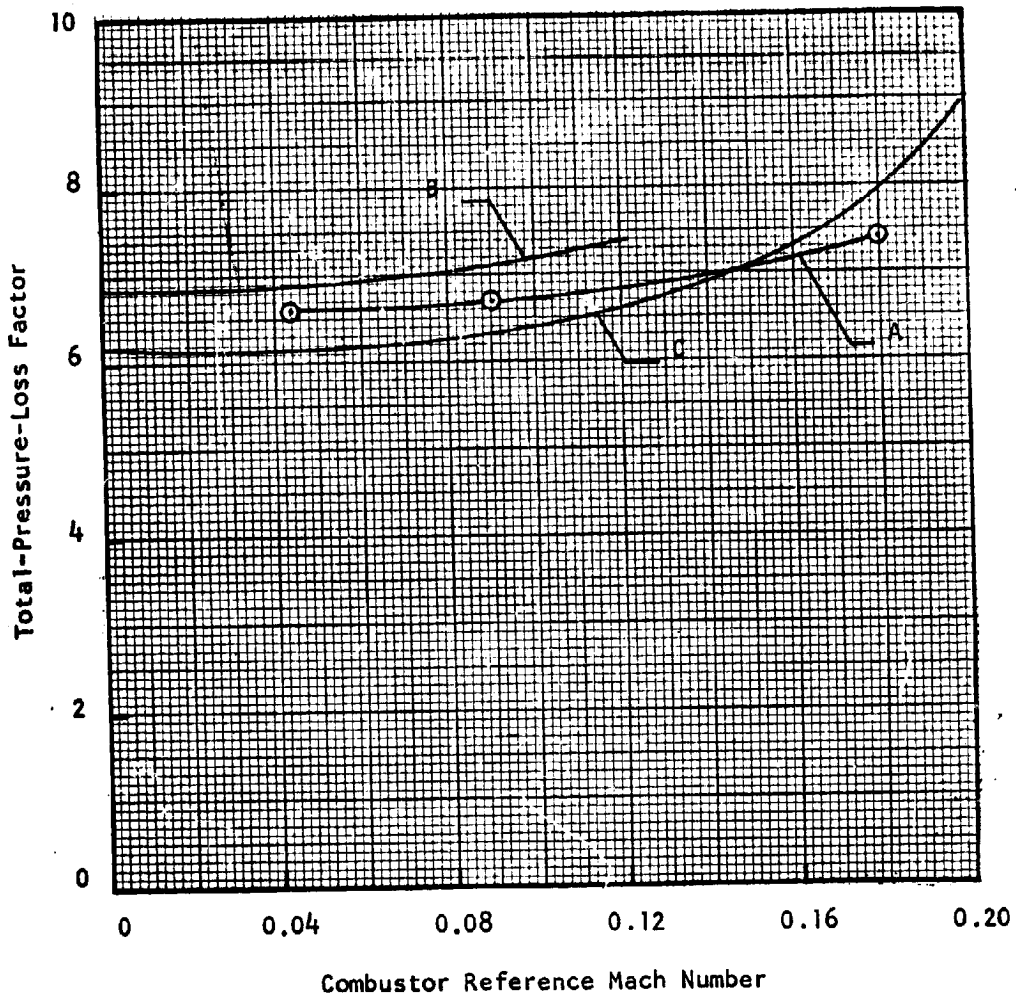


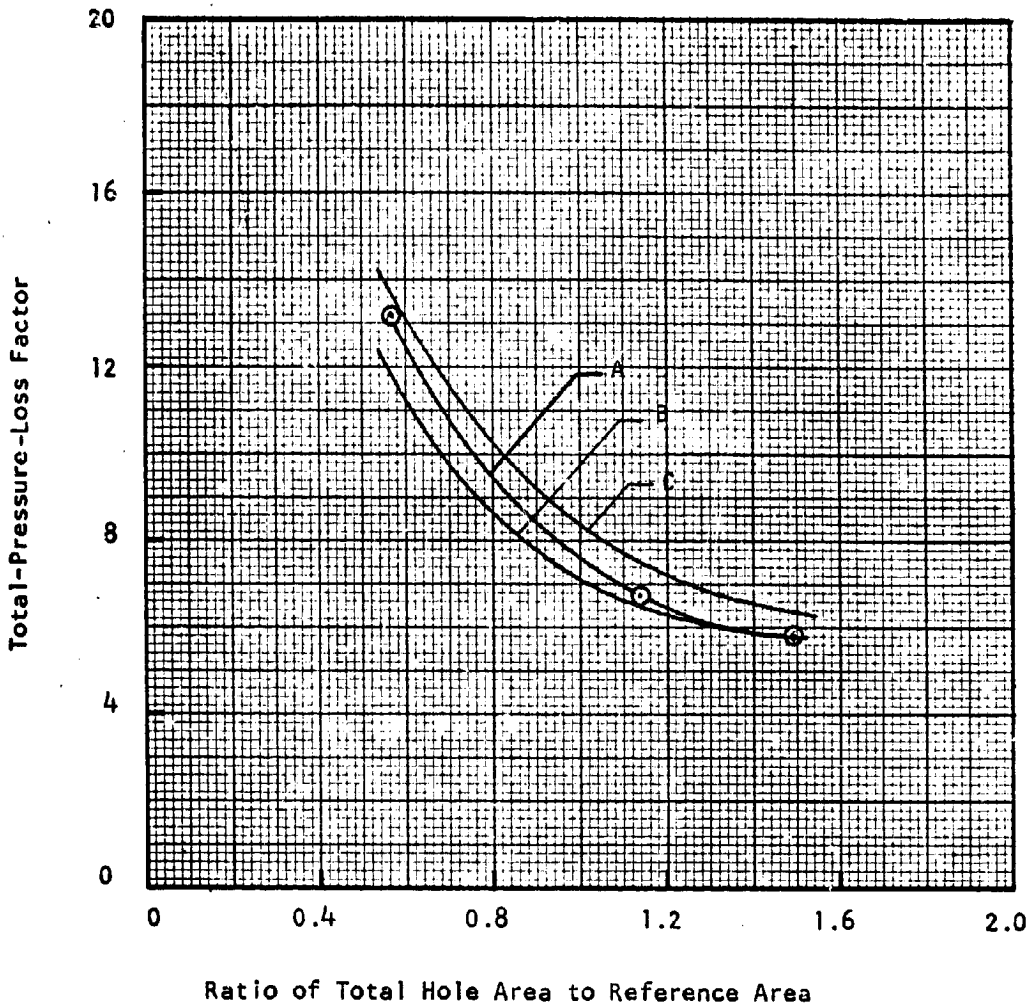
FIGURE 28 - COMPARISON OF EXPERIMENTAL AND THEORETICAL DEVELOPMENT OF A SHEAR FLOW IN A TWO-DIMENSIONAL NOZZLE



$A_{hT}/A_{ref} = 1.14$
 $A_{ft}/A_{ref} = 0.6$

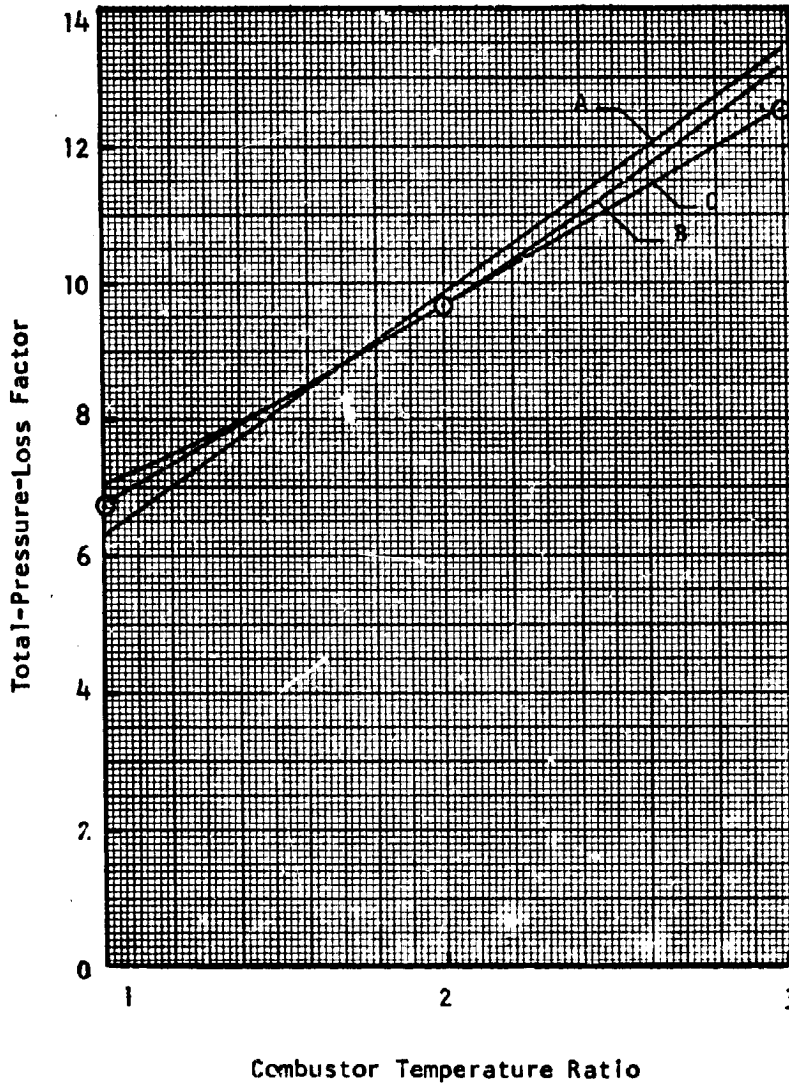
A Calculated - NREC, $A_{ref} = 47$ sq in
 B Calculated - NASA (Ref 74)
 C Experimental (Ref 74)

FIGURE 29 - VARIATION OF PRESSURE-LOSS FACTOR
 WITH REFERENCE MACH NUMBER



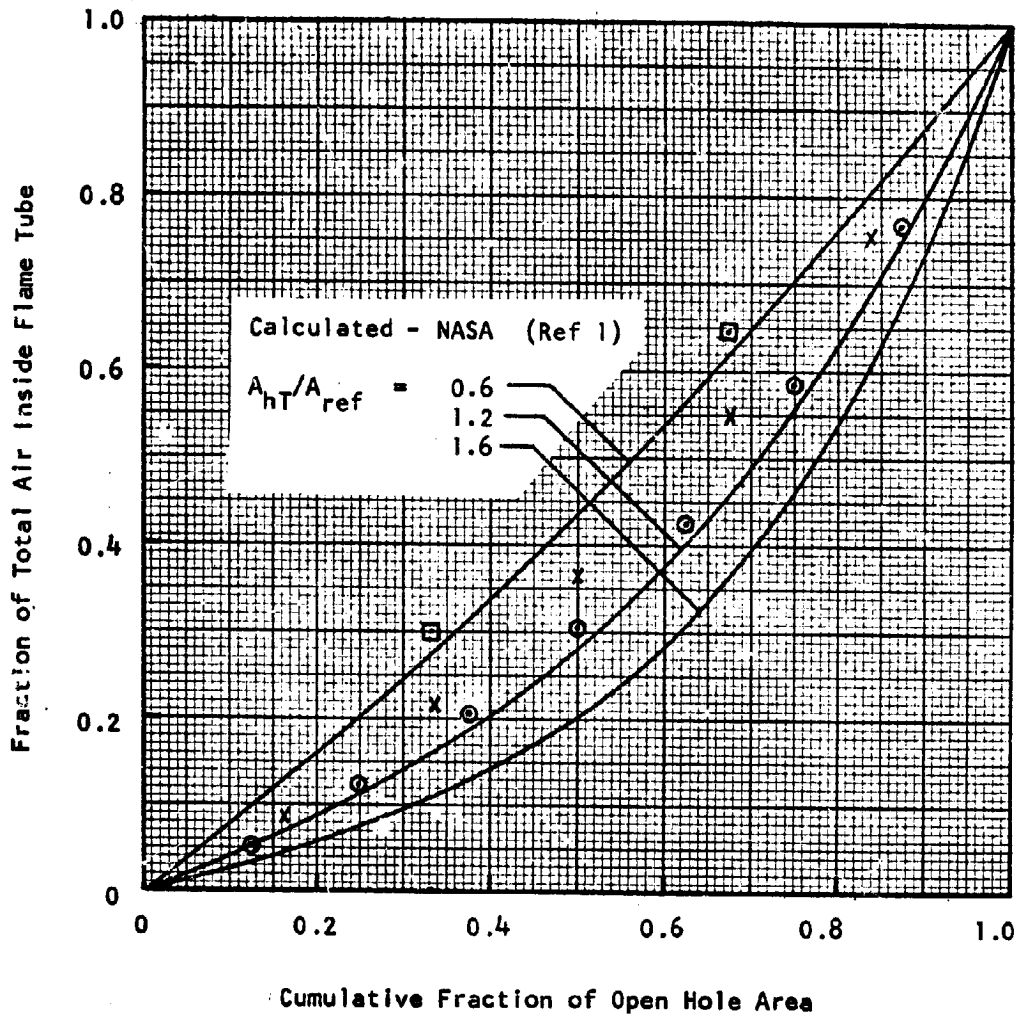
Reference Mach Number = 0.087 A Calculated - NREC, $A_{ref} = 47$ sq in
 B Experimental (Ref 74)
 $A_{ft}/A_{ref} = 0.6$ C Calculated - NASA (Ref 74)

FIGURE 30 - VARIATION OF PRESSURE-LOSS FACTOR WITH TOTAL HOLE AREA



$A_{hT}/A_{ref} = 1.14$	A Experimental (Ref 74)
$A_{ft}/A_{ref} = 0.6$	B Calculated - NASA (Ref 74)
$M_{ref} = 0.087$	C Calculated - NREC, $A_{ref} = 47$ sq in

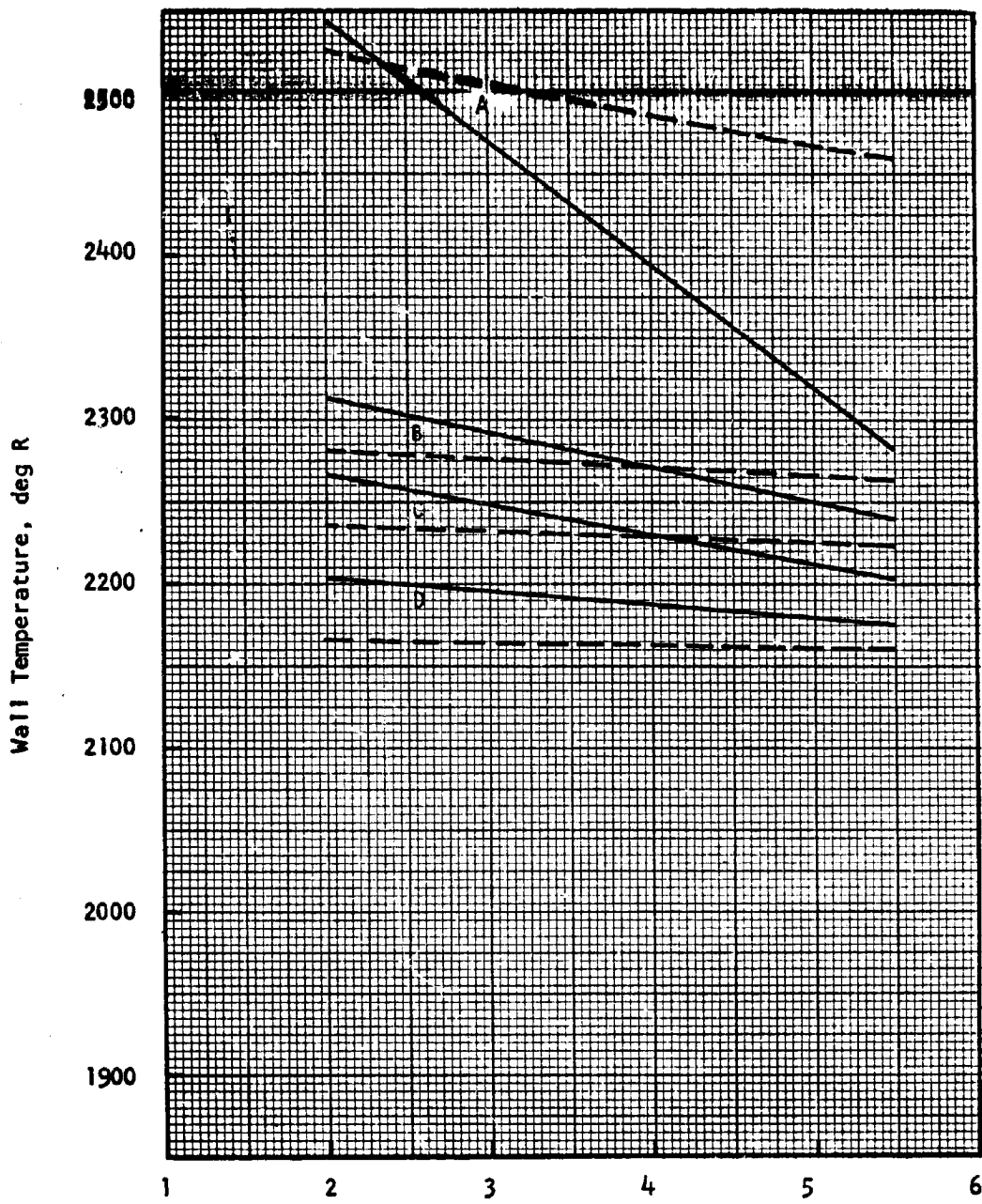
**FIGURE 31 - EFFECT OF HEAT RELEASE ON
 COMBUSTOR PRESSURE-LOSS FACTOR**



Calculated - NREC
 A_{hT}/A_{ref} = 0.57 □
 1.14 X
 1.51 ●

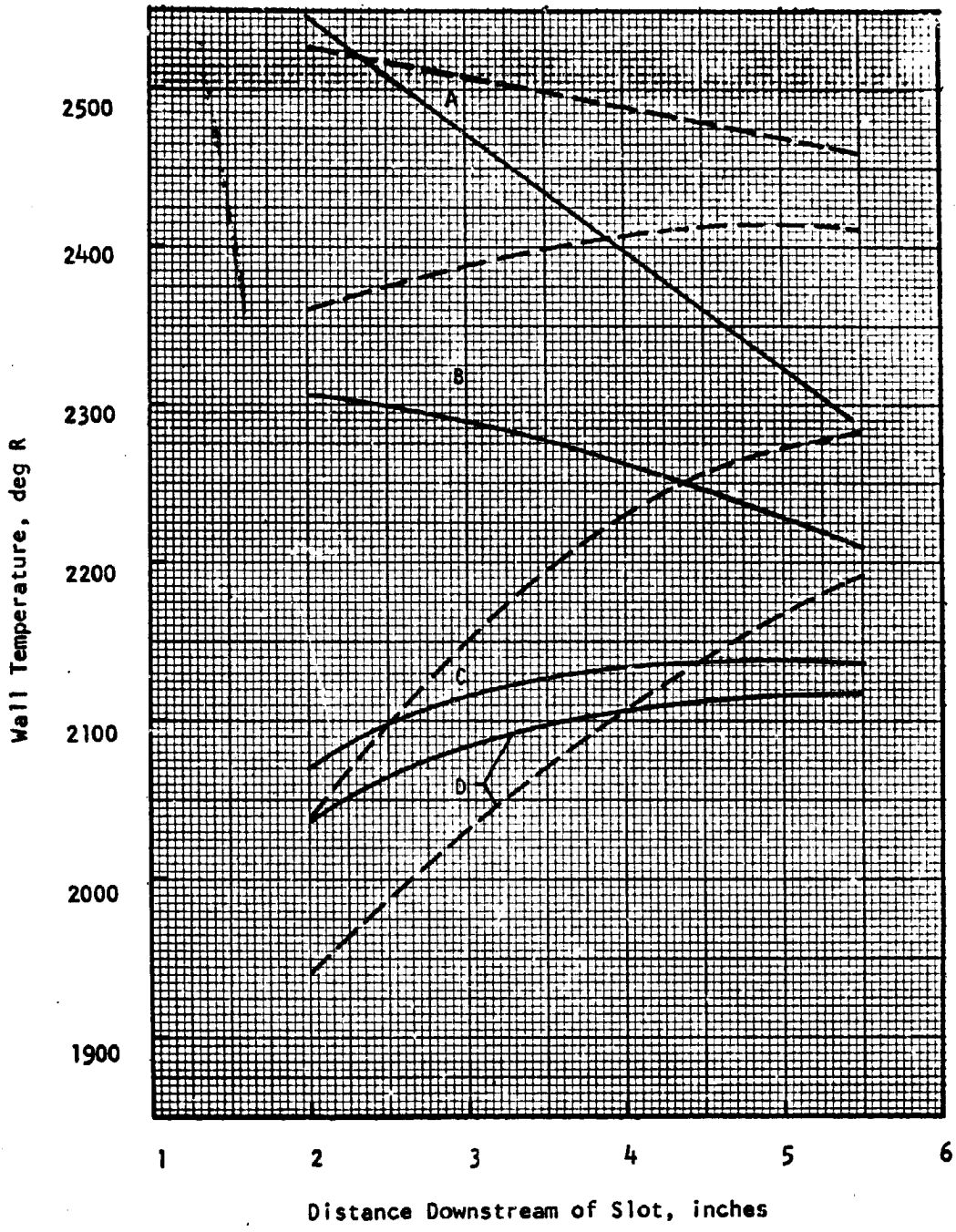
Results shown are for $A_{ref} = 47$ sq in

**FIGURE 32 - COMPARISON OF CALCULATED
 AIR-FLOW DISTRIBUTIONS**



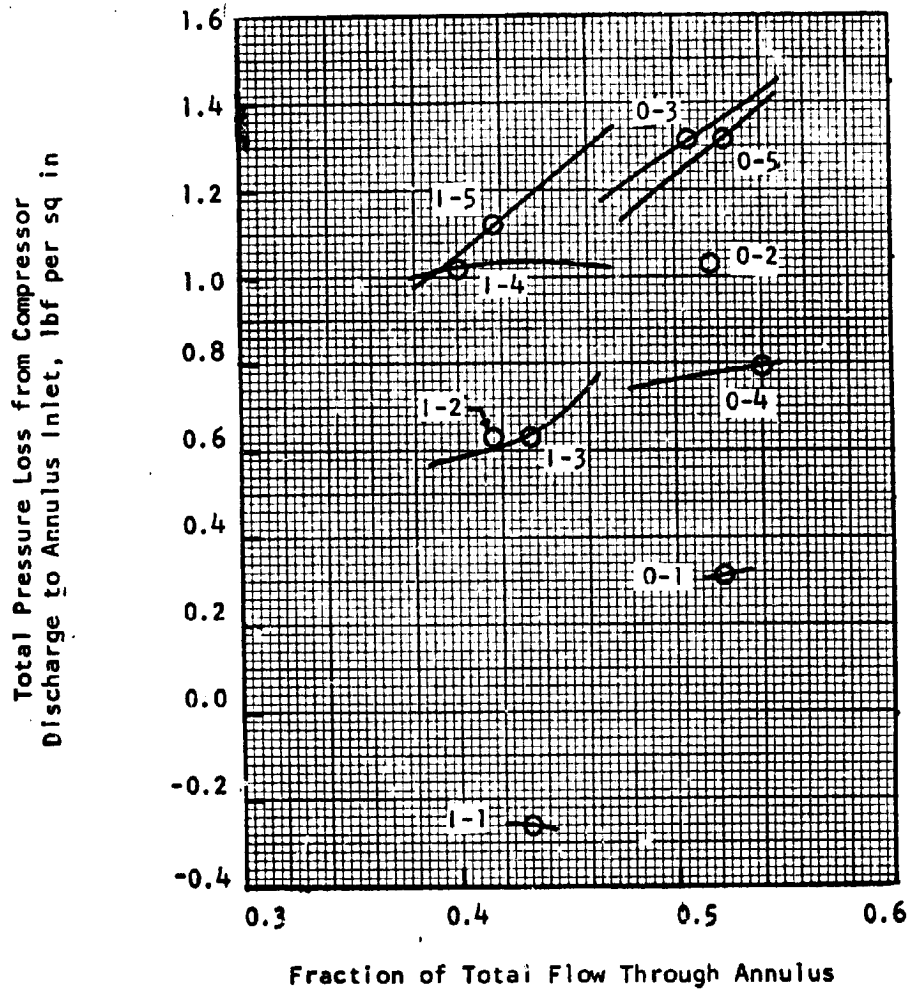
Cooling Stream Mach Number A 0 ——— Experimental (Ref 75)
 B 0.11 ——— Calculated
 C 0.14 ———
 D 0.2 ———

FIGURE 33 - WALL TEMPERATURES, CONVECTIVE COOLING ONLY



Slot-Gas Velocity, ft per sec	A 0	— Experimental (Ref 75)
	B 260	--- Calculated
	C 570	
	D 800	

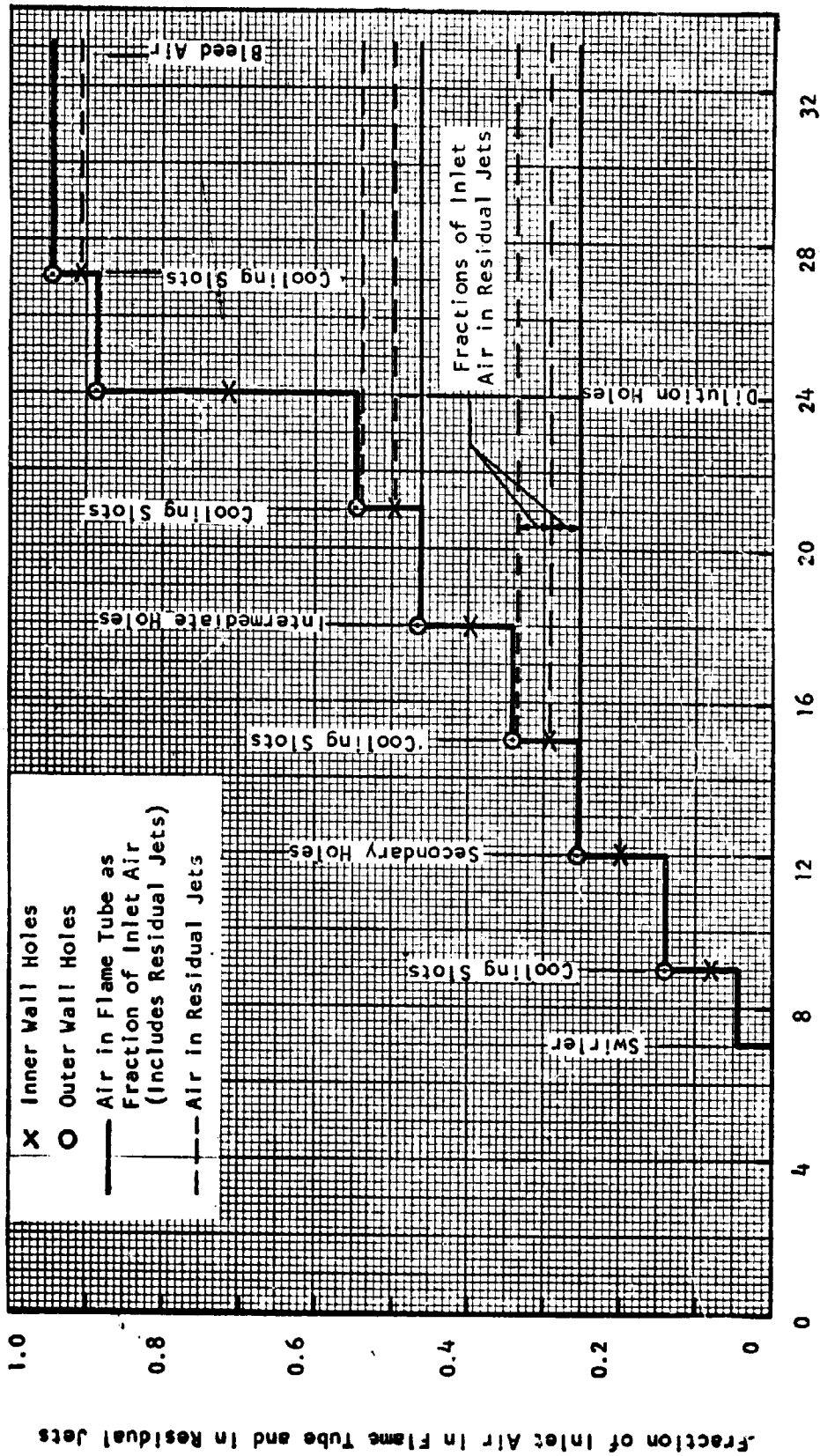
FIGURE 34 - WALL TEMPERATURES, FILM COOLING ONLY



Key

- 1,0 - Inner, Outer Annulus
- 1-5 - Overall Test Case Number
- - Indicates Position of Converged Air Mass-Flow Split

**FIGURE 36 - TOTAL-PRESSURE LOSS IN DIFFUSER
AS A FUNCTION OF FLOW SPLIT FOR OVERALL
TEST CASES 1 THROUGH 5**



Distance Downstream of Compressor Delivery, in

FIGURE 37 - NASA TEST CASE NO. 1 -- ACCUMULATED FRACTION OF INLET AIR IN FLAME TUBE AND RESIDUAL AIR IN JETS AS FUNCTIONS OF AXIAL POSITION IN COMBUSTOR.

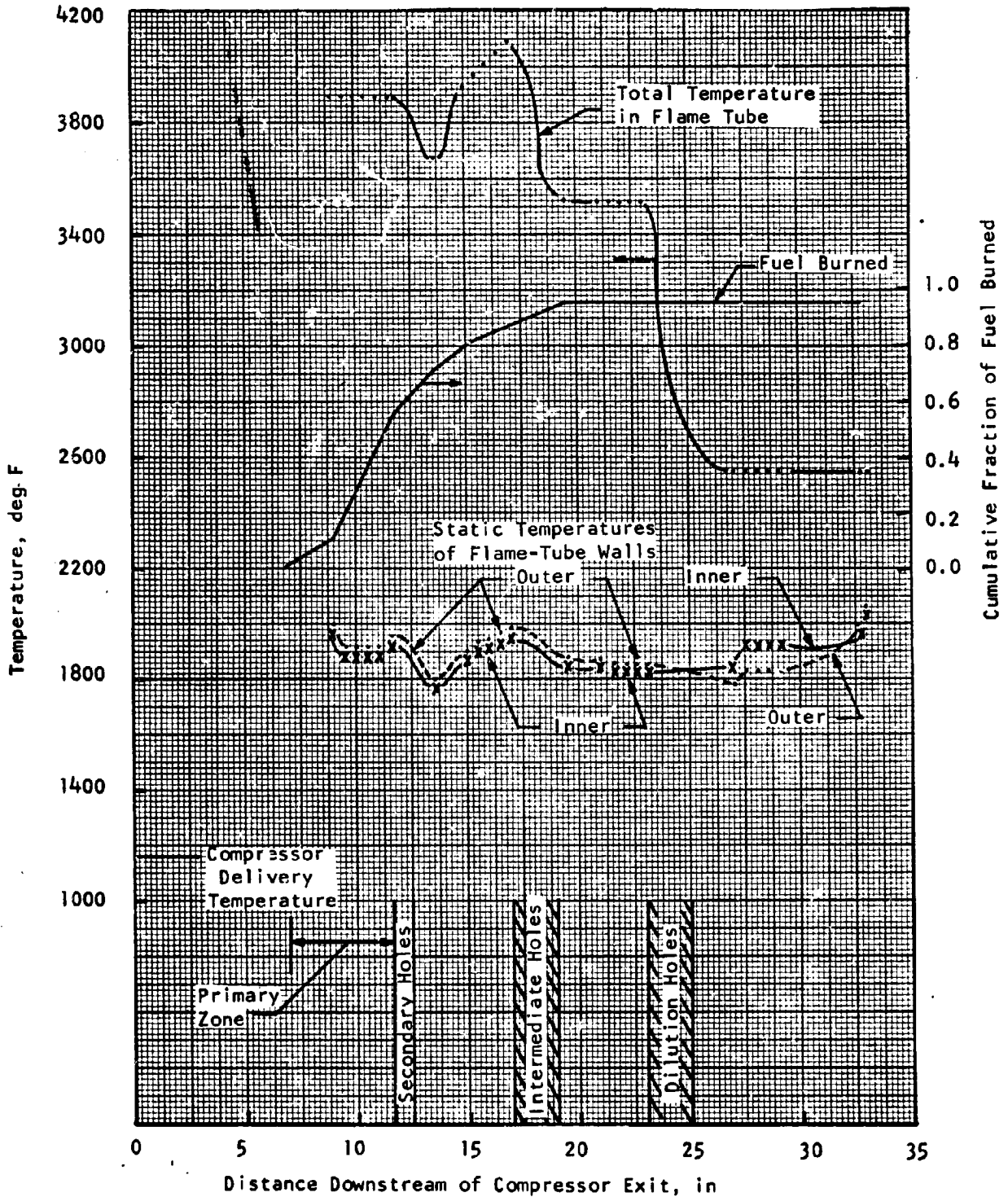


FIGURE 38 - NASA TEST CASE NO. 1 -- FLAME TEMPERATURE, FLAME-TUBE WALL TEMPERATURES, AND FRACTION OF FUEL BURNED AS FUNCTIONS OF AXIAL POSITION IN COMBUSTOR

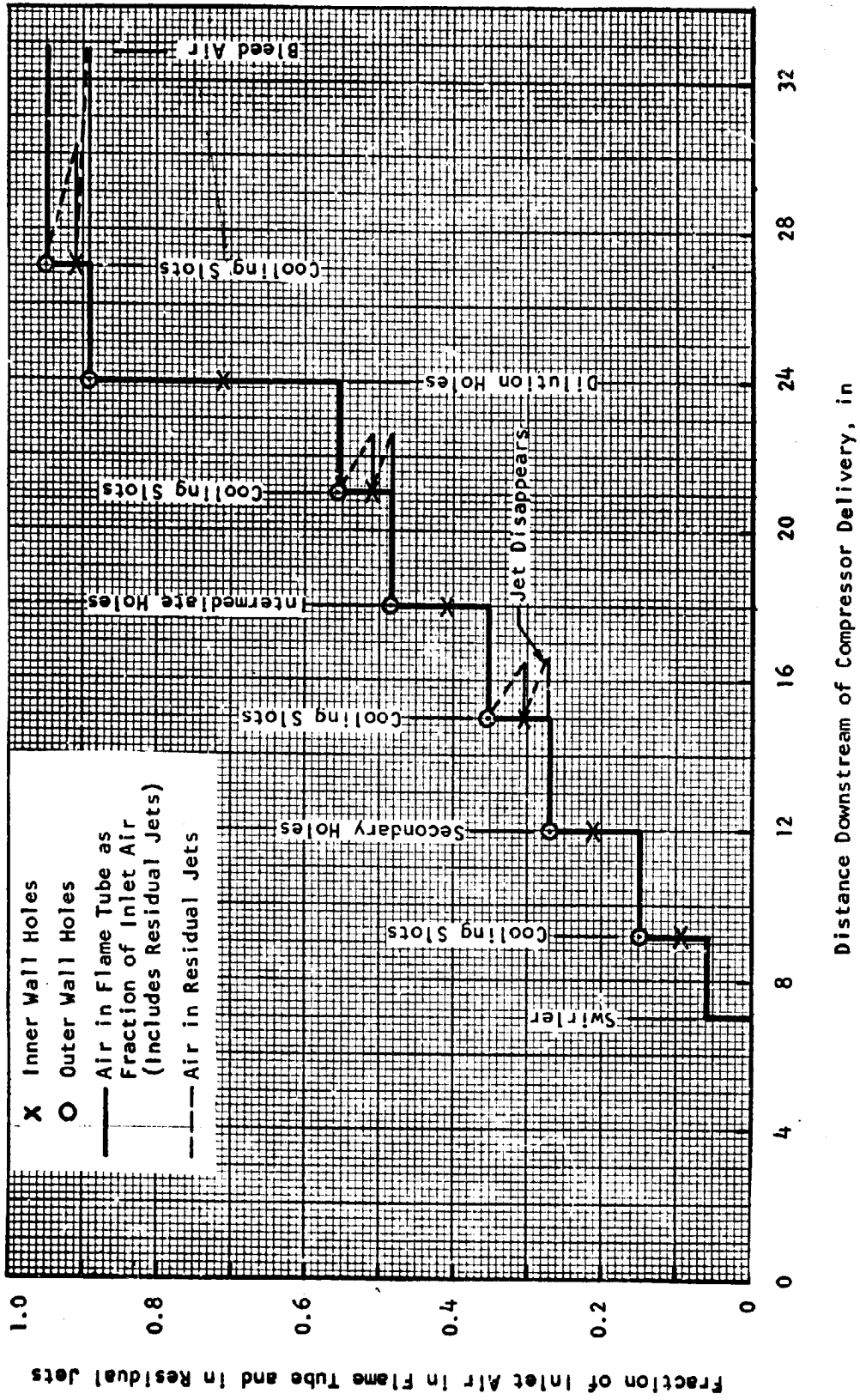


FIGURE 39 - NASA TEST CASE NO. 2 -- ACCUMULATED FRACTION OF INLET AIR IN FLAME TUBE AND RESIDUAL AIR IN JETS AS FUNCTIONS OF AXIAL POSITION IN COMBUSTOR

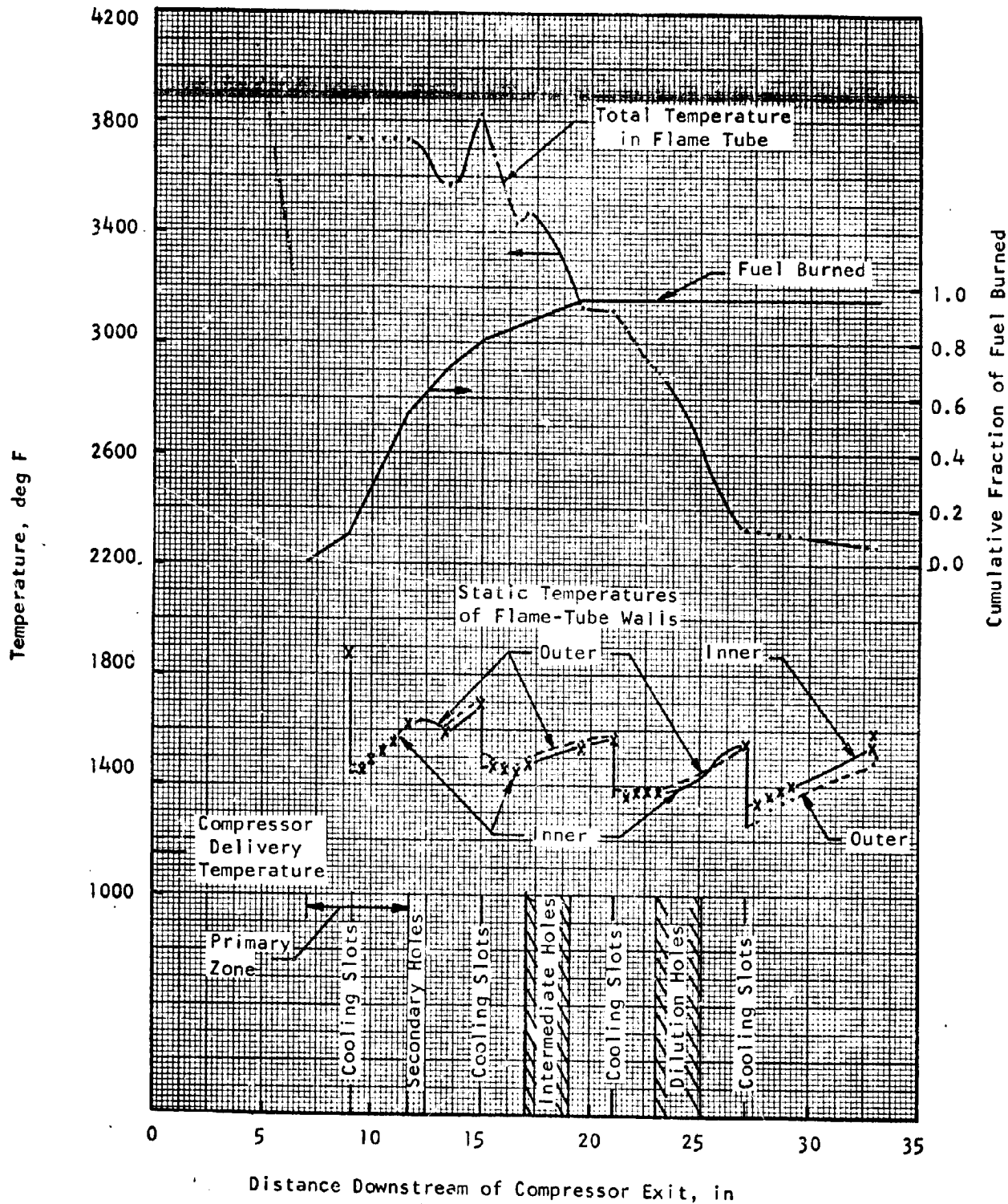


FIGURE 40 - NASA TEST CASE NO. 2 -- FLAME TEMPERATURE, FLAME-TUBE WALL TEMPERATURES, AND FRACTION OF FUEL BURNED AS FUNCTIONS OF AXIAL POSITION IN COMBUSTOR

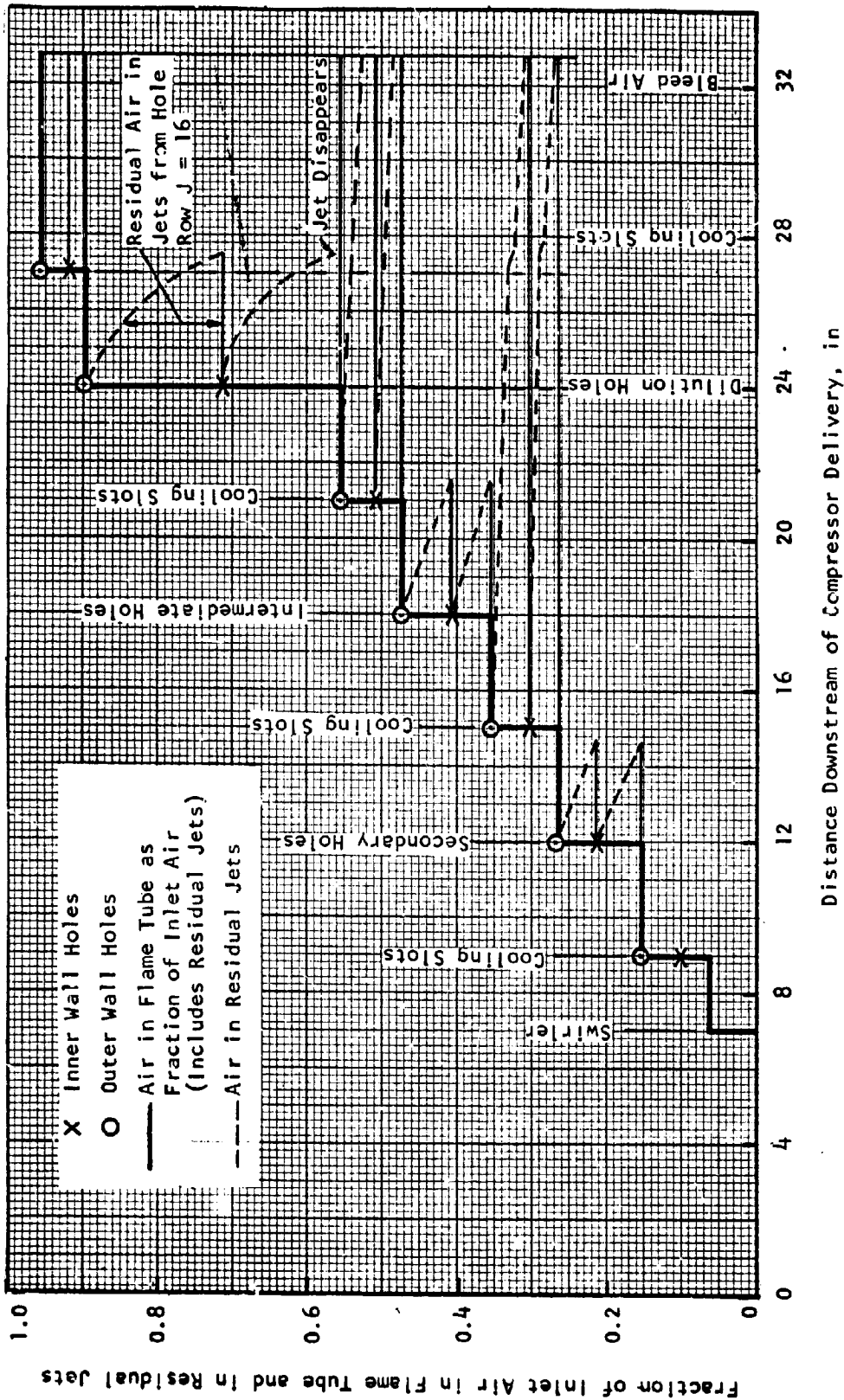


FIGURE 41 - NASA TEST CASE NO. 3 -- ACCUMULATED FRACTION OF INLET AIR IN FLAME TUBE AND RESIDUAL AIR IN JETS AS FUNCTIONS OF AXIAL POSITION IN COMBUSTOR

209

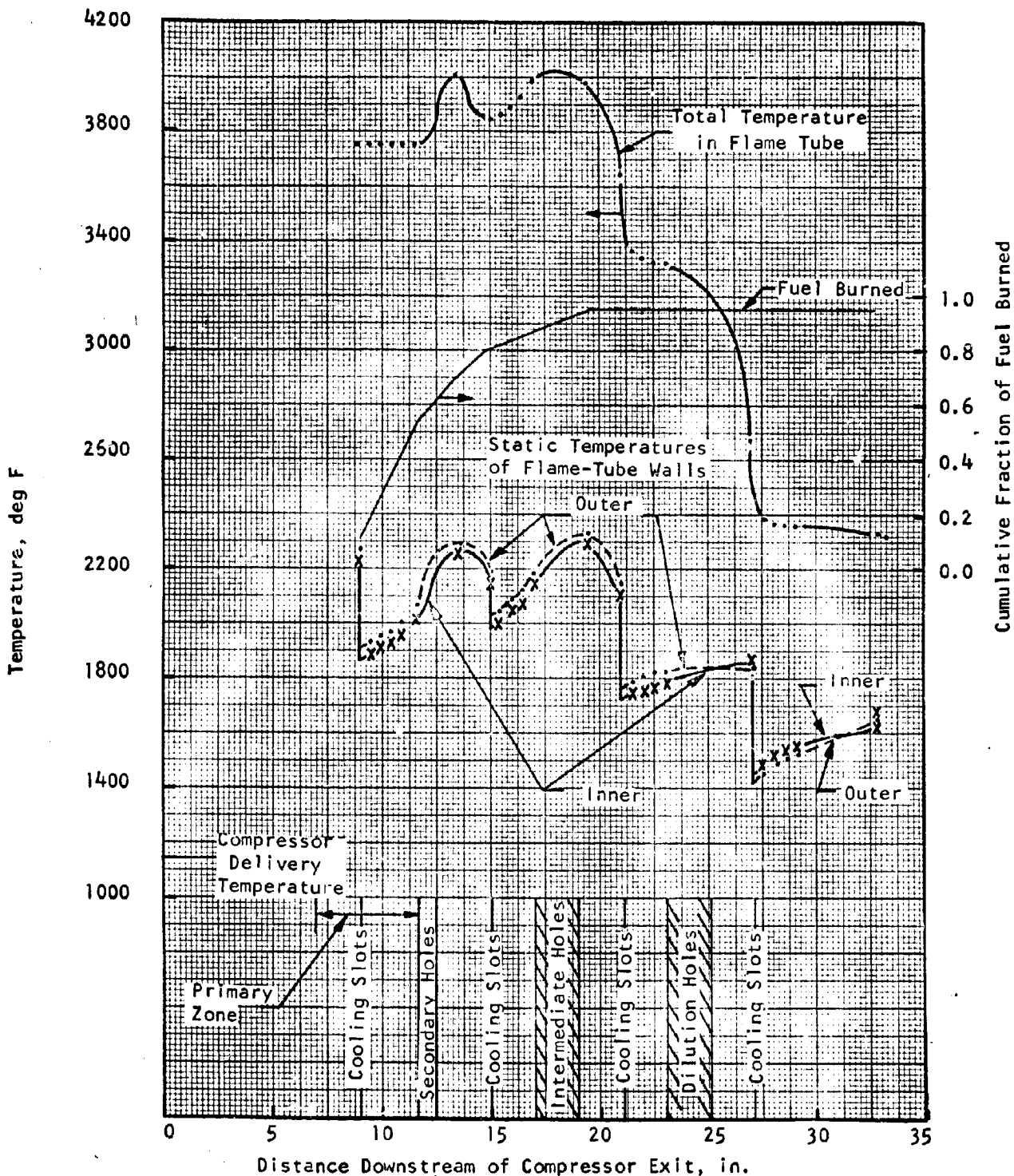


FIGURE 42 - NASA TEST CASE NO. 3 -- FLAME TEMPERATURE, FLAME-TUBE WALL TEMPERATURES, AND FRACTION OF FUEL BURNED AS FUNCTIONS OF AXIAL POSITION IN COMBUSTOR

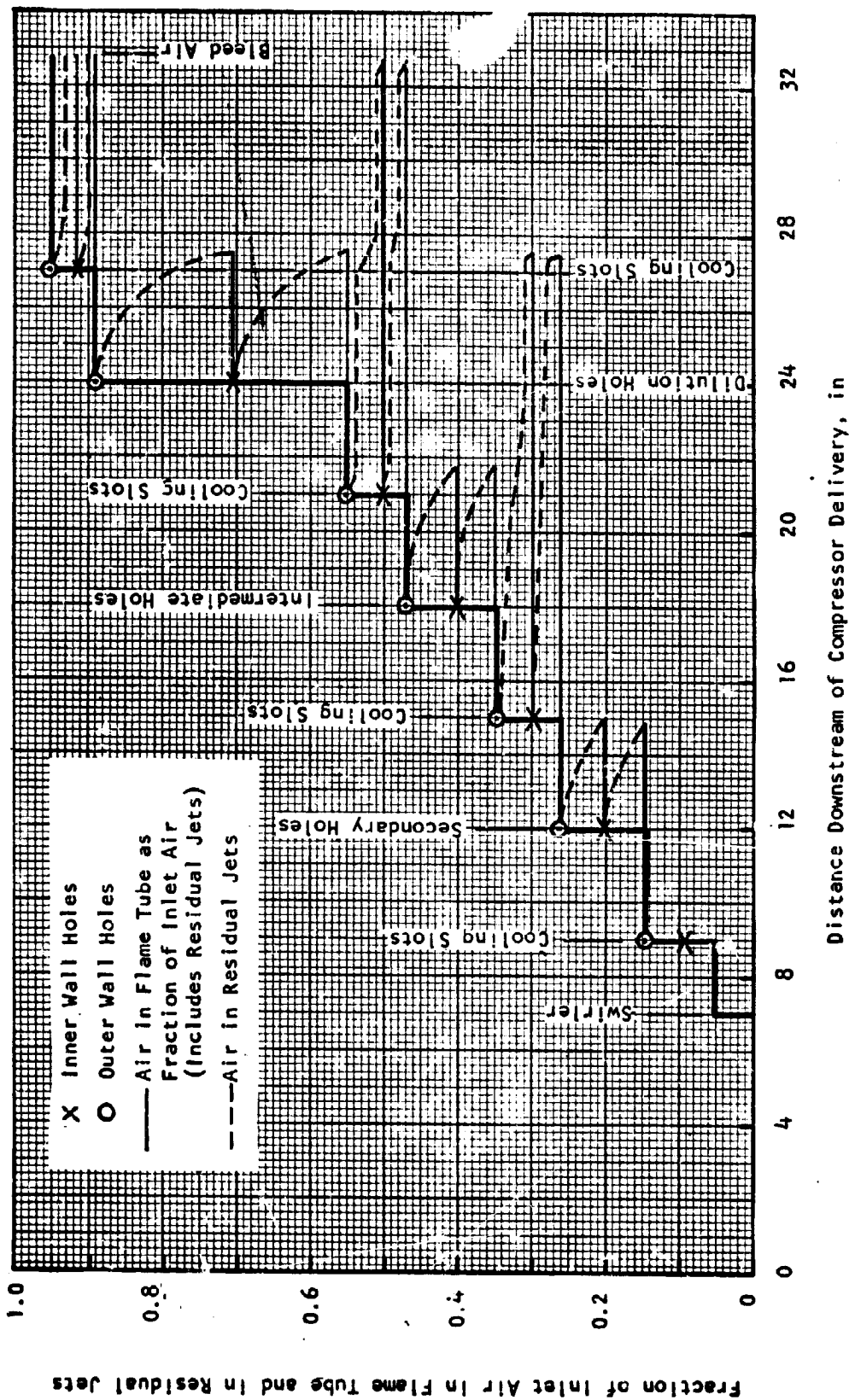


FIGURE 43 - NASA TEST CASE NO. 4 -- ACCUMULATED FRACTION OF INLET AIR IN FLAME TUBE AND RESIDUAL AIR IN JETS AS FUNCTIONS OF AXIAL POSITION IN COMBUSTOR

211

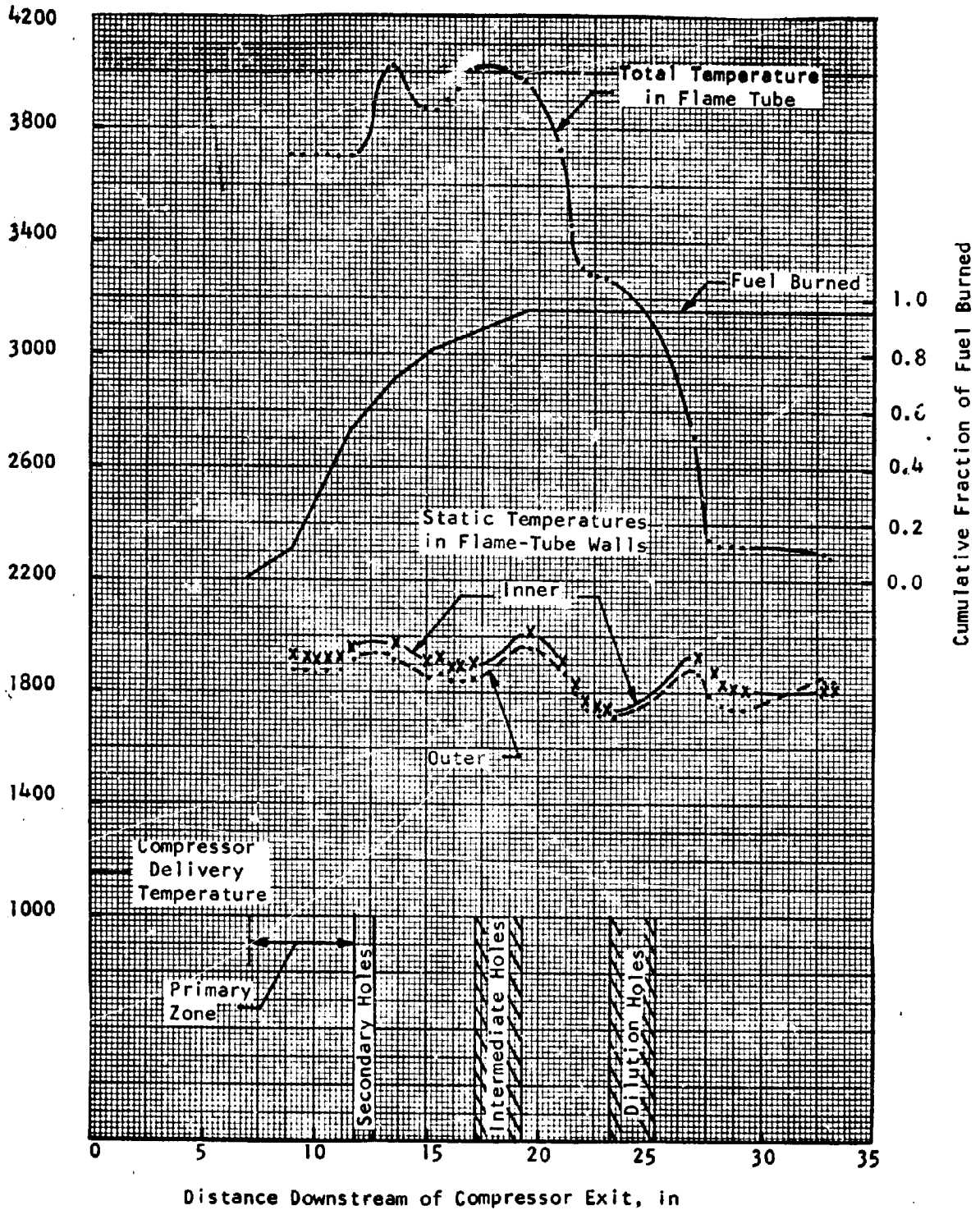


FIGURE 44 - NASA TEST CASE NO. 4 -- FLAME TEMPERATURE, FLAME-TUBE WALL TEMPERATURES, AND FRACTION OF FUEL BURNED AS FUNCTIONS OF AXIAL POSITION IN COMBUSTOR

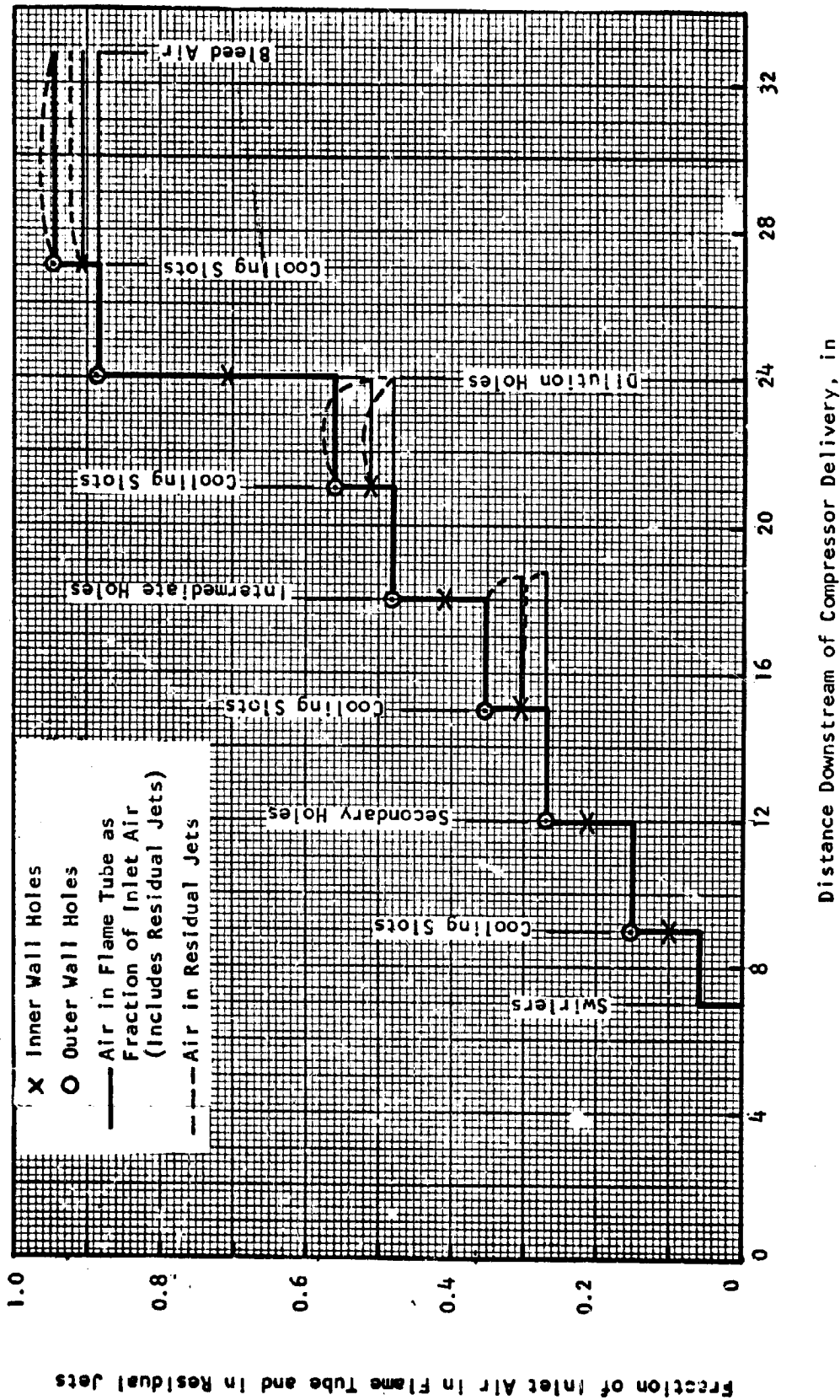


FIGURE 45 - NASA TEST CASE NO. 5 -- ACCUMULATED FRACTION OF INLET AIR IN FLAME TUBE AND RESIDUAL AIR IN JETS AS FUNCTIONS OF AXIAL POSITION IN COMBUSTOR

213

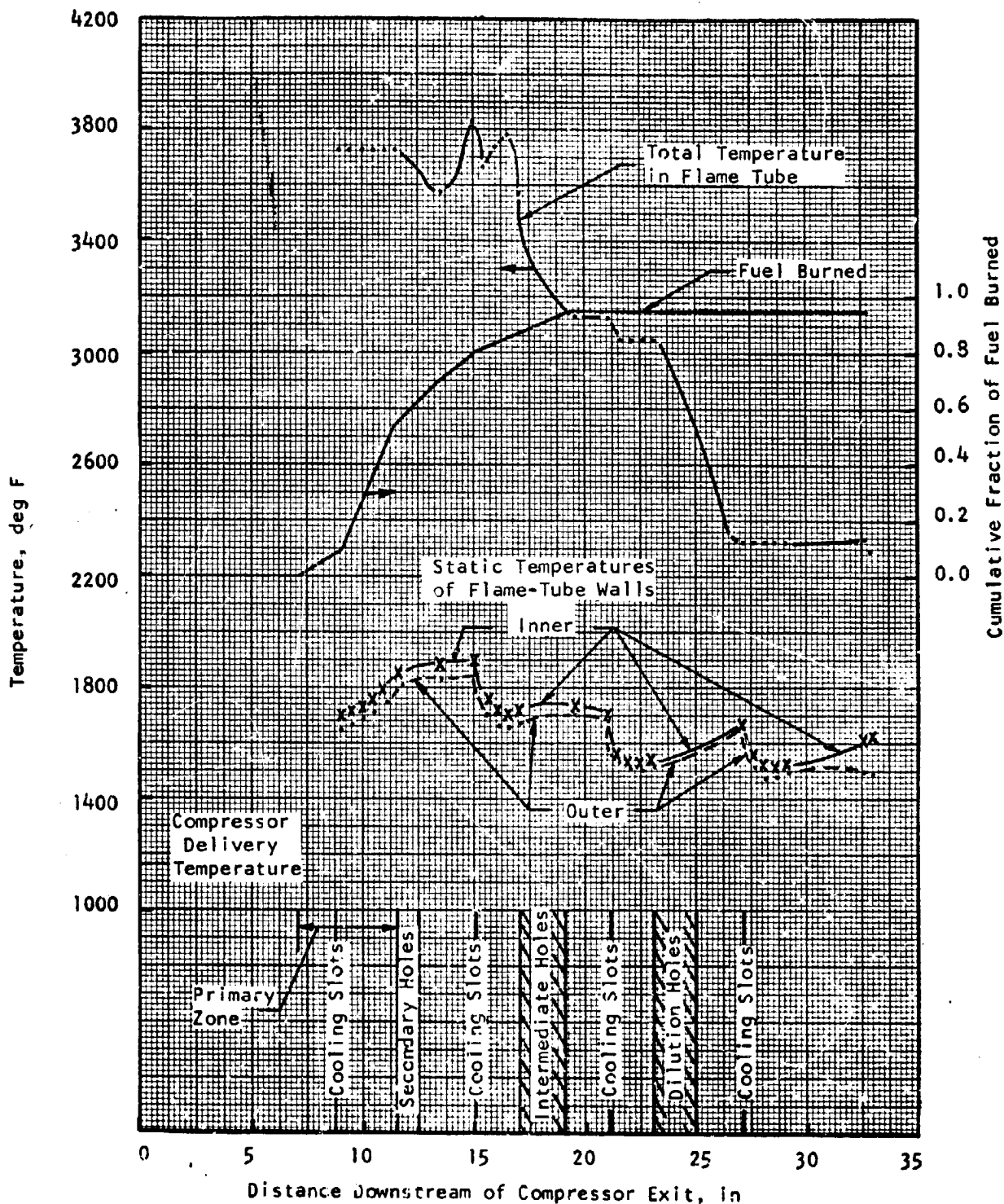


FIGURE 46 - NASA TEST CASE NO. 5 -- FLAME TEMPERATURE, FLAME TUBE WALL TEMPERATURES, AND FRACTION OF FUEL BURNED AS FUNCTIONS OF AXIAL POSITION IN COMBUSTOR

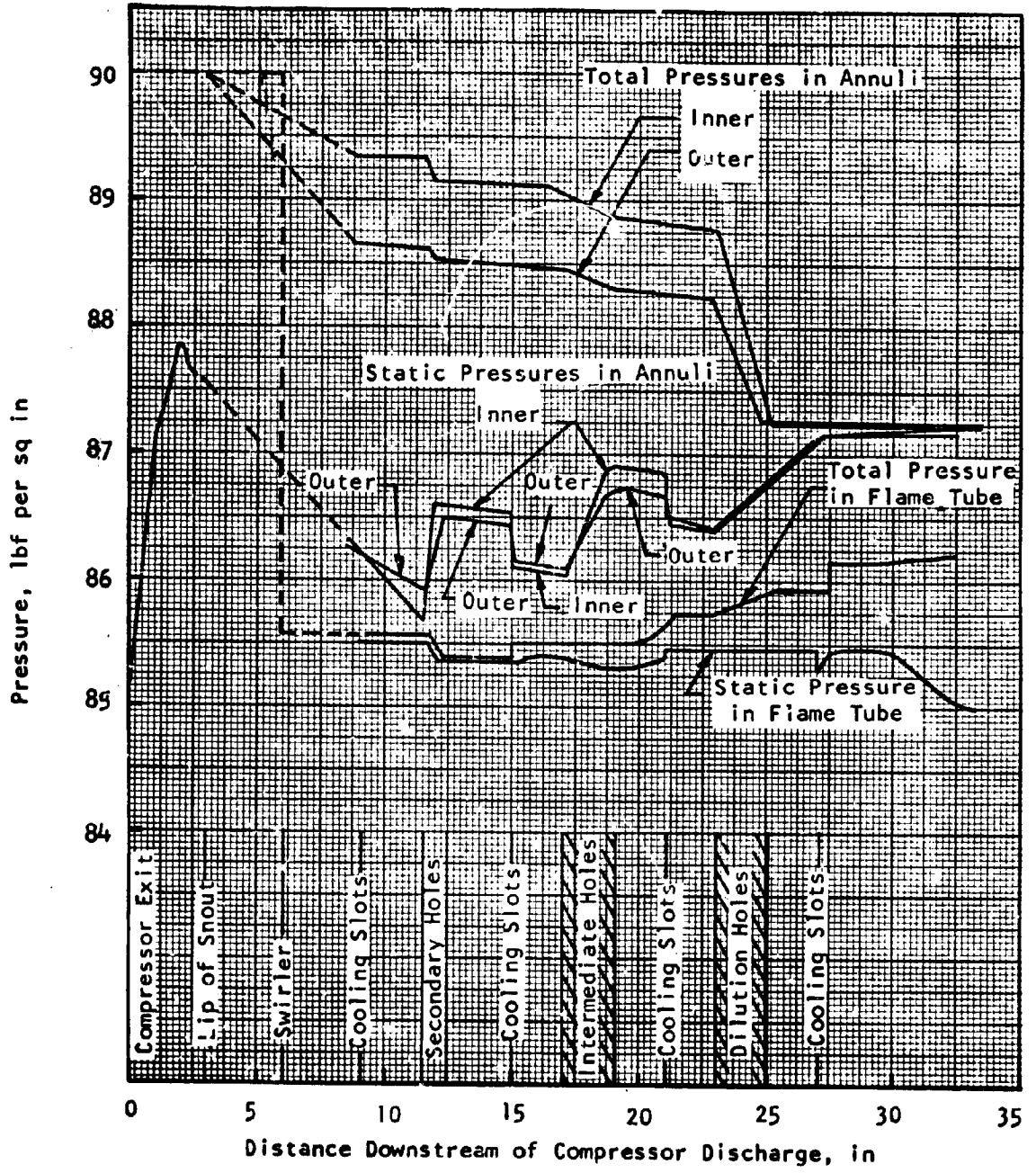


FIGURE 47 - NASA TEST CASE NO. 3 -- TOTAL AND STATIC PRESSURES AS FUNCTIONS OF AXIAL POSITION IN THE COMBUSTOR

NOMENCLATURE

<u>Symbol</u>	<u>Description</u>	<u>Units</u>
A	Area	sq ft
A_{bl}	Area occupied by boundary-layer displacement thickness	sq ft
A_h	Hole area	sq ft
A_{th}	Cross-sectional area occupied by a specified mass flow at diffuser station 2	sq ft
A_w	Wetted wall area per unit length	ft
A^*	Critical area, for which Mach number equals 1.0	sq ft
AR	Area Ratio A_2/A_1	-
C	Entrainment constant	-
C_1	Rate of heat transfer by convection from the hot gases (or the cooling film) to the flame-tube wall	Btu per sq ft sec
C_2	Rate of heat transfer by convection from the wall to the annulus air	Btu per sq ft sec
C_A	Inner wall area per unit length	ft
C_B	Outer wall area per unit length	ft
C_d	Discharge coefficient	-
C_d^I	"Corrected" discharge coefficient	-
c_p	Specific heat	Btu per lbm deg F
C_p	Pressure-recovery coefficient	-
C_{pi}	Ideal pressure-recovery coefficient	-
C_{pm}	Ideal pressure-recovery coefficient in the presence of mixing	-
D_{an}^I	Hydraulic diameter of annulus	ft

<u>Symbol</u>	<u>Description</u>	<u>Units</u>
D_{ft}	Wall-to-wall width of flame tube	ft
D_{ft}^1	Hydraulic diameter of flame tube (= $2D_{ft}$)	ft
D_{ref}	Combustor reference diameter	ft
d_h	Effective axial length of hole	ft
d_j	Effective initial jet diameter	ft
$I-E$	Diffuser blockage	-
$I-E_{bl}$	Diffuser boundary-layer blockage	-
F_{12}	View factor of receiving surface 2 from radiating object 1	-
F	Fanning friction factor	-
f	Fuel-air ratio	-
G	Mass flow rate per unit area	lbm per sq ft sec
G_0	Constant in Newton's law	ft lbm per lbf sec ²
h	Enthalpy	Btu per lbm
H	Boundary-layer shape factor	-
H_1	Shape factor at diffuser inlet	-
H_{sep}	Shape factor at which separation occurs	-
H/C	Fuel hydrogen-carbon ratio	-
$h_{eff,p}$	Effective fuel lower calorific value	Btu per lbm
h_p	Fuel lower calorific value	Btu per lbm
J	Mechanical equivalent of heat	ft lbf per Btu
K_d	Number of dynamic heads lost in flow from diffuser station 2 or 2' to dome	-
ΔK	Net rate of heat transfer by conduction into unit area of the flame-tube wall from adjacent wall elements	Btu per sq ft sec

<u>Symbol</u>	<u>Description</u>	<u>Units</u>
k	Gas thermal conductivity	Btu per ft sec deg F
k_w	Thermal conductivity of wall material	Btu per ft sec deg F
L	Length	ft
l_b	Mean beam path length	ft
M	Mach number	-
M_w	Molecular weight of coolant	-
\dot{m}_j	Axial component of jet momentum flux	ft lbm per sec ²
m	Mass fraction of component in mixture	-
\dot{m}	Mass flow rate	lbm per sec
\dot{m}_h	Mass flow rate through hole	lbm per sec
N	Number of streamtubes in diffuser analysis	-
Nu	Nusselt number	-
P	Total pressure	lbf per sq ft
ΔP_{hot}	Loss of total pressure due to combustion	lbf per sq ft
Pr	Prandtl number	-
p	Static pressure	lbf per sq ft
P_G	Partial pressure of radiating gas	lbf per sq ft
Q_{tr}	Heat transferred to transpiration coolant as it passes through the wall	Btu per sq ft sec
\bar{q}	Dynamic head, $\rho \bar{u}_m^2 / 2g_0$	lbf per sq ft
\dot{q}	Rate of heat addition due to fuel burning	Btu per sec
\dot{q}_w	Heat transfer rate from the flame-tube wall to the annulus air	Btu per sq ft sec
R	Gas constant	ft lbf per lbm deg R

<u>Symbol</u>	<u>Description</u>	<u>Units</u>
R_1	Rate of heat transfer by radiation from the hot gases to the flame-tube wall	Btu per sq ft sec
R_2	Rate of heat transfer by radiation from the wall to the casing	Btu per sq ft sec
R_3	Net rate of heat transfer by radiation from the flame-tube wall to all parts of the opposite wall	Btu per sq ft sec
Δr	Diffuser inlet width, for annular diffusers	ft
r	Radius	ft
Re	Reynolds number	-
Re_{cf}	Reynolds number of cooling film, based on slot height	-
Re_{ft}	Reynolds number of gas in flame tube, based on flame-tube hydraulic diameter	-
s	Distance along jet center-line	ft
s'	Distance along jet center-line from virtual origin	ft
T	Static temperature	deg R
T_0	Stagnation temperature	deg R
T_{ad}	Adiabatic-wall temperature	deg R
T_b	Base temperature for enthalpy	deg R
T_c	Casing temperature	deg R
T_{cf}	Temperature of cooling air	deg R
T_{ft}	Static temperature of hot gases	deg R
T_w	Wall temperature	deg R
TA	Total cross-sectional area of streamtubes	sq ft
t_w	Wall thickness	ft
U	Main-stream velocity	ft per sec
U_{ft}	Bulk velocity of gas in flame tube	ft per sec

<u>Symbol</u>	<u>Description</u>	<u>Units</u>
\bar{u}_{cf}	Mean initial velocity of cooling film	ft per sec
u	Velocity	ft per sec
\bar{u}_a	Area-average velocity	ft per sec
\bar{u}_m	Mass-averaged velocity	ft per sec
W	Diffuser width, for rectangular diffusers	ft
X	Nondimensional distance downstream of cooling slot	-
X_0	Parameter in film-cooling correlation	-
x	Mole fraction	-
x	Downstream distance	ft
x	Distance downstream of cooling slot	ft
Δx_{ft}	Thickness of slab of hot gas	ft
Δx_w	Axial length of strip of wall	ft
Y	Nondimensional distance across diffuser	-
y	Distance across diffuser or flame tube, measured from the wall	ft
Y_{cf}	Height of film-cooling slot	ft
φ	Streamline slope	radians
α_{ft}	Flame absorptivity	-
α_w	Wall absorptivity	-
K	Permeability coefficient	sq ft
β	Profile parameter	-
γ	Ratio of specific heats	-
δ	Boundary-layer displacement thickness	ft
ϵ_{ft}	Flame emissivity	-
η	Transverse jet coordinate	ft

<u>Symbol</u>	<u>Description</u>	<u>Units</u>
$\eta_{\frac{1}{2}}$	Value of η at which nondimensional velocity profile parameter equals 0.5	ft
η^*	Value of η at the assumed jet boundary	ft
θ	Boundary-layer momentum thickness	ft
Λ	Luminosity factor	-
λ_{diff}	Diffuser total-pressure-loss coefficient	-
μ	Dynamic viscosity	lbm per ft sec
ν	Kinematic viscosity	sq ft per sec
φ	Initial jet angle	radians
ξ_m	Diffuser effectiveness in the presence of mixing	-
ξ_{12}	Diffuser effectiveness between Stations 1 and 2	-
ρ	Density	lbm per cu ft
σ	Stefan-Boltzmann constant	Btu per sq ft-(deg R) ⁴ -hr
τ	Film-cooling effectiveness	-
τ	Transmittance	-

PRECEDING PAGE BLANK NOT FILMED.

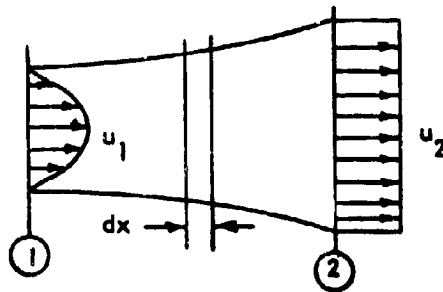
APPENDICES

APPENDIX I

IDEAL PRESSURE-RECOVERY COEFFICIENT IN A DIFFUSER
WITH NONUNIFORM INLET VELOCITY PROFILE

Governing Equations

Consider the incompressible flow in a diffusing passage; it is assumed that the velocity profile is nonuniform at the inlet, and mixes to a uniform profile at the outlet as indicated in the sketch.



The equations of continuity and momentum for an elemental control volume of length dx can be written as

$$\frac{d}{dx} (\rho \bar{u}_s A) = 0 \quad (1-1)$$

$$\frac{dp}{dx} = - \frac{1}{g_0 A} \frac{d}{dx} (\rho \bar{u}_s \bar{u}_m A) \quad (1-2)$$

Equation 1-1 can be integrated to yield

$$\rho \bar{u}_s A = \rho \frac{\bar{u}_m}{\beta} A = \dot{m} \quad (1-3)$$

where \dot{m} is the mass flow in the passage. Combining Equations 1-3 and 1-2 yields

$$\frac{dp}{dx} = - \frac{\dot{m}^2}{\rho g_0 A} \frac{d}{dx} \left(\frac{\beta}{A} \right) \quad (1-4)$$

This is the equation which expresses the static pressure as a function of the passage area and the uniformity of the velocity profile. It is to be noted that for a uniform profile $\beta = 1$, while for a nonuniform profile $\beta > 1$.

Solution for Maximum Possible Pressure Recovery

To obtain a solution for the maximum possible pressure recovery, it is first necessary to determine the form of $\beta(x)$ which yields the maximum value of the function

$$I = \int_{x_1}^{x_2} \left[-\frac{1}{A} \frac{d}{dx} \left(\frac{\beta}{A} \right) dx \right] \quad (1-5)$$

This expression can be integrated by parts to obtain

$$I = \left(\frac{\beta}{A^2} \right)_1 - \left(\frac{\beta}{A^2} \right)_2 - \int_{A_1}^{A_2} \frac{\beta}{A^3} dA \quad (1-6)$$

The maximum value of I will accordingly be obtained when the last term in Equation 1-6 is a minimum; this is obviously achieved by having β reach its minimum value instantaneously at Station 1. Hence, the maximum possible pressure recovery is achieved by instantaneous mixing at Station 1, i.e.,

$$\beta = \beta_1 \text{ at } x = x_1$$

$$\beta = 1 \text{ at } x > x_1$$

The solution of Equation 1-4 for maximum pressure recovery is then

$$p_2 - p_1 = \frac{\dot{m}^2}{\rho g_0} I = \frac{\dot{m}^2}{\rho g_0} \left[\frac{\beta_1}{A_1^2} - \frac{1}{A_2^2} - \frac{1}{2A_1^2} + \frac{1}{2A_2^2} \right]$$

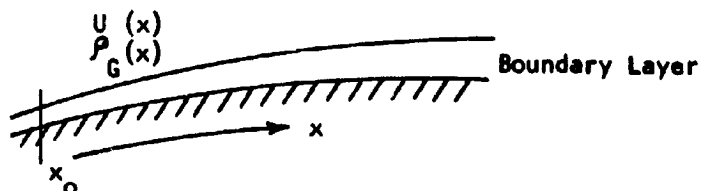
or, from Equation 1-3:

$$\frac{p_2 - p_1}{\bar{q}_1} = \frac{1}{\beta_1^2} \left[2(\beta_1 - 1) + 1 - \frac{1}{AR^2} \right] \quad (1-5)$$

APPENDIX II

BOUNDARY-LAYER MOMENTUM THICKNESSIntroduction

In the present streamtube method, a relationship is required between the boundary-layer momentum thickness along the walls of the diffuser and the local flow variables. The situation considered is indicated in the following sketch:



The method used herein is a modification of standard integral treatments of the turbulent boundary layer (see Ref 76, Chapter XXII) to account for compressibility effects. The integral momentum equation for compressible flow is (see Equation 1-23 of Kutateladze and Leont'ev, Ref 77):

$$\frac{d\theta}{dx} + \frac{\theta}{U} (H + 2) \frac{dU}{dx} + \frac{\theta}{\rho_G} \frac{d\rho_G}{dx} = \frac{\tau_0}{\rho_G U^2} \quad (2-1)$$

where ρ_G = density in free stream

$$\theta = \int_0^{\infty} \frac{\rho_u}{\rho_G U} \left(1 - \frac{u}{U}\right) dy \quad (2-2)$$

If it is assumed that H is constant and that τ_0 , the shear stress at the wall, is given by

$$\frac{\tau_0}{\rho_G U^2} = \frac{\alpha}{(U\delta/v)^{1/n}}$$

where n and α are constants and ν is assumed to be constant, then

Equation 2-1 may be integrated to give:

$$\theta_x \left(\frac{u_x \theta_x}{\nu} \right)^{1/n} = \rho_x^{-1} u_x^{-b} \left[c_1 + a \int_{x_0}^x u^b \rho^{1/n + 1} dx \right] \quad (2-3)$$

where $a = \frac{n+1}{n} \alpha$

$$b = \frac{n+1}{n} (H+2) - \frac{1}{n}$$

c_1 = constant of integration

Taking values of $n = 6$ and $\alpha = 0.0065$ (Ref 76), and assuming a mean value of $H = 11/7$, then 2-3 becomes:

$$\theta_x \left(\frac{u_x \theta_x}{\nu} \right)^{1/6} = \frac{1}{\rho_x^{7/6} u_x^4} \left[c_1 + 0.0076 \int_{x_0}^x u^4 \rho^{7/6} dx \right] \quad (2-4)$$

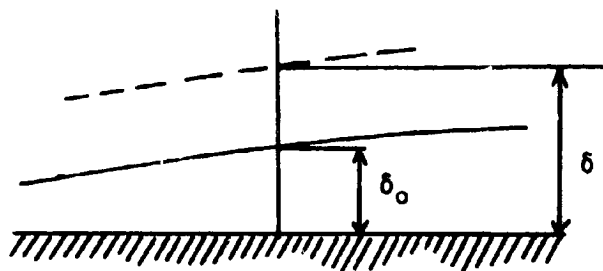
$$\theta_x = \left[\theta_0^{7/6} \left(\frac{u_0}{u_x} \right)^{25/6} \left(\frac{\rho_0}{\rho_x} \right)^{7/6} + \frac{0.0076 \nu^{1/6}}{\rho_x^{7/6} u_x^{25/6}} \int_{x_0}^x u^4 \rho^{7/6} dx \right]^{6/7} \quad (2-5)$$

Equation 2-5 is used in the computer program to calculate θ ; a constant value of $\nu^{1/6} = 0.23$ (sq ft per sec)^{1/6} is assumed.

APPENDIX III

NEW ESTIMATE OF BOUNDARY-LAYER
DISPLACEMENT THICKNESS

This appendix describes the technique used to obtain convergence in the iteration on boundary-layer thickness.



Consider any section where the present value of displacement thickness is δ_0 and the predicted value is δ . The correct value lies between δ_0 and δ since, as δ_0 is increased, the flow velocities increase and δ is reduced. The best estimate, δ^1 , to use as a starting value for the next iteration is such that, as δ_0 is increased to δ^1 , δ is reduced to δ^1 . Let

$$\Delta\delta_0 = \delta^1 - \delta_0$$

At any section, from Equation 2-4:

$$\theta \propto \frac{1}{u^{24/7}}$$

$$\frac{\Delta\theta}{\theta} = -\frac{24}{7} \frac{\Delta u}{u} \quad (3-1)$$

From the continuity equation for two-dimensional flow:

$$\frac{\Delta u}{u} = \frac{\Delta\delta_{o1} + \Delta\delta_{o2}}{EA} \quad (3-2)$$

where EA is the flow area and subscripts 1 and 2 refer to inner and outer walls, respectively.

By definition:

$$\begin{aligned}\delta &= H\theta \\ \delta^1 &= (H + \Delta H)(\theta + \Delta\theta) \\ \delta^1 &= \delta \left[1 + \frac{\Delta H}{H} + \frac{\Delta\theta}{\theta} \right] \quad (3-3)\end{aligned}$$

From Equation 3-6:

$$\begin{aligned}\Delta H &= 70 \cdot (H_o - 1.05) \Delta \left(\frac{d\theta}{dx} \right) \\ \frac{\Delta H}{H} &= 70 \cdot \frac{(H_o - 1.05)}{H} \cdot \frac{(\Delta\theta_i - \Delta\theta_{i-1})}{(x_i - x_{i-1})} \quad (3-4)\end{aligned}$$

Combining Equations 3-1, 3-2, 3-3, and 3-4:

$$\begin{aligned}\delta^1 &= \delta \left[1 - \left(240 \cdot \frac{(H_o - 1.05)}{H} \cdot \frac{\theta}{x_i - x_{i-1}} + 24/7 \right) \left(\frac{\Delta\delta_{o1} + \Delta\delta_{o2}}{FA} \right) \right. \\ &\quad \left. - \frac{70(H_o - 1.05)}{H} \cdot \frac{\Delta\theta_{i-1}}{x_i - x_{i-1}} \right] \quad (3-5)\end{aligned}$$

i.e., for walls 1 and 2

$$\delta_1 \left[1 - \psi_1 \right] + \psi_1 (\delta_{o1} + \delta_{o2}) = (\psi_1 + 1)\delta_1^1 + \psi_1 \cdot \delta_2^1 \quad (3-6)$$

$$\delta_2 \left[1 - \psi_2 \right] + \psi_2 (\delta_{o1} + \delta_{o2}) = \psi_2 \cdot \delta_1^1 + (\psi_2 + 1)\delta_2^1 \quad (3-7)$$

where $\Delta\delta_{o1} = \delta^1 - \delta_o$

$$\psi = \frac{\delta}{EA} \left(240 \cdot \frac{(H_o - 1.05)}{H} \cdot \frac{\theta}{x_i - x_{i-1}} + 24/7 \right)$$

$$\varphi = 70 \frac{(H_0 - 1.05)}{H} \cdot \frac{\Delta\theta_{i-1}}{x_i - x_{i-1}}$$

Solution of Equations 3-6 and 3-7 provides a new estimate of the boundary-layer displacement thickness; experience has indicated, however, that this estimate will not in general yield convergence and hence the actual estimate used is a weighted average of δ_0 and δ^1 as indicated in the text (Equation 37).

APPENDIX IV

ESTIMATES OF BOUNDARY-LAYER SHAPE FACTORS

As inputs to the streamtube method of diffuser analysis, boundary-layer displacement thicknesses and shape factors on the two walls are normally provided. If, however, momentum thicknesses or shape factors are not available, they may be easily calculated, assuming the boundary layer has built up as on a flat plate.

The equation for the shape factor at inlet, H_1 , is derived as follows. Hama (Ref 78), from experiments with boundary layers on various types of flat surfaces, produced the following correlation:

$$H_1 = \frac{1}{1 - 0.78 R_x^{-1/14}} \quad (4-1)$$

where $R_x = \frac{U \cdot x}{\nu}$

x = length of flat plate

U = free stream velocity

ν = kinematic viscosity

For flat plates Equations 2-1 and 2-3 give:

$$\frac{dR_\theta}{dR_x} = \frac{\alpha}{(R_\theta)^{1/n}} \quad (4-2)$$

where $R_\theta = \frac{U \cdot \theta}{\nu} = \frac{U}{\nu} \cdot \frac{\delta}{H}$

Integrating Equation 4-2:

$$\frac{n}{n+1} R_\theta^{\frac{n+1}{n}} = \alpha \cdot R_x \quad (4-3)$$

Using values of $\alpha = 0.0065$ and $n = 6$ (Ref 76), Equations 4-1 and 4-3 give:

$$H_1 = \frac{1}{1 - 0.55 R_0^{-1/12}}$$
$$= \frac{1^*}{1 - 0.55 \left(\frac{U}{\nu} \cdot \frac{\delta}{H_1}\right)^{-1/12}} \quad (4-4)$$

This equation may be solved to obtain H_1 , if the inlet displacement thickness (or boundary-layer blockage) is known.

APPENDIX VDEVELOPMENT OF MIXING EQUATION FOR
INCOMPRESSIBLE FLOWGoverning Equations

The equations governing the incompressible flow in a diffusing passage have been derived in Appendix I; they are:

$$\rho \frac{\bar{u}_m A}{\beta} = \dot{m} \quad (5-1)$$

$$\frac{\rho g_o}{\dot{m}^2} \frac{dp}{dx} = -\frac{1}{A} \frac{d}{dx} \left(\frac{\beta}{A} \right) \quad (5-2)$$

Mixing-Process Assumption

To obtain a solution to Equations 5-1 and 5-2, it is necessary to postulate the form of the mixing process, which is characterized by $\beta(x)$. It is assumed here that mixing will occur in such a way that

$$\frac{A}{\beta - 1} = \text{constant}, K > \beta \quad (5-3)$$

which is merely based on the plausible hypothesis that the mixing rate will be delayed by diffusion. The value of K may be obtained by applying Equation 5-3 at the inlet and exit:

$$K = \frac{\beta_1 - \frac{1}{AR} \beta_2}{1 - \frac{1}{AR}} \quad (5-4)$$

Solution for Pressure-Recovery Coefficient

Substitution of Equation 5-3 into Equation 5-2 yields:

$$\frac{\rho g_0}{\dot{m}^2} dp = K \frac{dA}{A^3}$$

which can be integrated between inlet and exit:

$$\frac{\rho g_0}{\dot{m}^2} (p_2 - p_1) = \frac{K}{2} \left(\frac{1}{A_1^2} - \frac{1}{A_2^2} \right) \quad (5-5)$$

Combining Equations 5-1, 5-4, and 5-5 provides the desired result:

$$\frac{p_2 - p_1}{\bar{q}_1} = \frac{1}{\beta_1^2} \left(1 + \frac{1}{AR} \right) \left(\beta_1 - \frac{1}{AR} \beta_2 \right) \quad (5-6)$$

If the flow mixes to a uniform profile ($\beta_2 = 1$), then:

$$\frac{p_2 - p_1}{\bar{q}_1} = \frac{1}{\beta_1^2} \left(1 + \frac{1}{AR} \right) \left(\beta_1 - \frac{1}{AR} \right) \quad (5-7)$$

APPENDIX VI
PRESSURE DROP ACROSS THE DOME

The total-to-static pressure drop across the dome results from the combined mass-flow rate through the swirler and through holes in the dome:

$$\Delta P_d = f(\dot{m}_d)$$

where \dot{m}_d = total flow through the dome (or snout)
 $= \dot{m}_{dh} + \dot{m}_{sw}$

The mass-flow rate through the dome holes is given by the discharge equation:

$$\dot{m}_{dh} = C_{dh} A_{dh} \sqrt{2 g_o \rho_{ref} \Delta P_d} \quad (6-1)$$

The mass-flow rate through the swirler may be found from the swirler pressure-drop equation:

$$\frac{\Delta P_{sw}}{q_{ref}} = K_{sw} \left(\frac{A_{ref}^2}{A_{sw}^2} \sec^2 \beta - \frac{A_{ref}^2}{A_{ft}^2} \right) \frac{\dot{m}_{sw}^2}{\dot{m}_{ref}^2} \quad (6-2)$$

The reference dynamic pressure is given by:

$$q_{ref} = \frac{\rho_{ref} u_{ref}^2}{2 g_o} = \frac{\dot{m}_{ref}^2}{2 g_o \rho_{ref} A_{ref}^2}$$

This expression is substituted for q_{ref} in Equation 6-2 and the result is solved for the swirler mass-flow rate:

$$\dot{m}_{sw} = \sqrt{\frac{2 g_o \rho_{ref} \Delta P_{sw}}{K_{sw} \left(\frac{\sec^2 \beta_{sw}}{A_{sw}^2} - \frac{1}{A_{ft}^2} \right)}} \quad (6-3)$$

The total flow through the dome may now be found by adding Equations 6-1 and 6-3:

$$\dot{m}_d = C_{dh} A_{dh} \sqrt{2g_o \rho_{ref} \Delta P_d} + \sqrt{\frac{2g_o \rho_{ref} \Delta P_{sw}}{K_{sw} \left(\frac{\sec^2 \beta_{sw}}{A_{sw}^2} - \frac{1}{A_{ft}^2} \right)}} \quad (6-4)$$

Since the pressure drop across the dome holes and the swirler must be equal, this equation may be solved for this pressure drop:

$$\Delta P_d = \frac{\dot{m}_d^2}{2g_o \rho_{ref} \left[A_{dh} C_{dh} + \frac{1}{\sqrt{K_{sw} \left[\frac{\sec^2 \beta_{sw}}{A_{sw}^2} - \frac{1}{A_{ft}^2} \right]}} \right]^2} \quad (6-5)$$

APPENDIX VIIINTEGRATION OF INTEGRAL PRESSURE TERM

The integral pressure term in the annulus momentum equation (Equation 90) may be integrated by parts to yield:

$$\int_{1'}^2 p \frac{dA}{dx} dx = (pA) \Big|_{1'}^2 - \int_{1'}^2 A dp \quad (7-1)$$

An appropriate relation between A and p for mixing has been derived in Appendix V:

$$\frac{\rho g_o}{\dot{m}^2} dp = K \frac{dA}{A^3} \quad (7-2)$$

When Equation 7-2 is substituted into Equation 7-1, the latter may be integrated:

$$\int_{1'}^2 p \frac{dA}{dx} dx = (pA) \Big|_{1'}^2 + \frac{\dot{m}^2 K}{\rho g_o} \left(\frac{1}{A_2} - \frac{1}{A_{1'}} \right) \quad (7-3)$$

Equation 7-2 may be integrated directly:

$$\frac{\rho g_o}{\dot{m}^2} (p_2 - p_{1'}) = -\frac{K}{2} \left(\frac{1}{A_2^2} - \frac{1}{A_{1'}^2} \right) \quad (7-4)$$

The desired result is obtained by eliminating K between Equations 7-3 and 7-4:

$$\int_{1'}^2 p \frac{dA}{dx} dx = (pA)_2 - (pA)_{1'} + 2(p_{1'} - p_2) \left(\frac{1}{A_2} + \frac{1}{A_{1'}} \right) \quad (7-5)$$

END

DATE

FILMED

APR 10 1968